# THE SPATIAL DISPERSION EFFECT IN STRATIFIED METAL-DIELECTRIC METAMATERIAL

**Aunuddin Syabba Vioktalamo**
Department of Physics, Tohoku University, 6-3 Aramaki-aza-Aoba, Sendai, Japan

## I. Introduction

The exotic electromagnetic response in typical metamaterial is attributed to the unusual inhomogeneous electro-magnetic distribution in unit cell at particular frequencies. Therefore, the unit cell should small enough compare to wavelength which replaces the role of atom and molecule in conventional materials. But special unit cell design is not the only way to realize an inhomogeneous electromagnetic distribution.

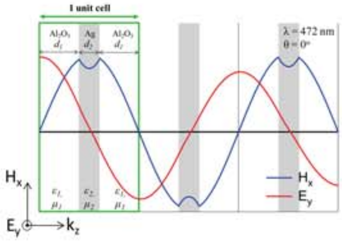


Stratified metal dielectric metamaterial, or SMDM, is an artificial metal dielectric composite that consists of silver (30 nm) sandwiched by identical alumina (60 nm). Usually the optical response in optical frequency range is simply ascribed to the 1-dimensional photonic crystal effect, but we go to one further step to generalize the concept of effective medium to the structure with much larger unit cell size. We regard the artificial structure to be a hypothetical uniform material, which can be described in terms of effective permittivity and effective permeability.

## II. Retrieval Procedure

*The Maxwell Equation in a unit cell:*

$$\oint_C \vec{E}\cdot d\vec{l} = -\frac{\partial}{\partial t}\iint_S \vec{B}\cdot\vec{n}dS$$

$$\oint_C \vec{H}\cdot d\vec{l} = \frac{\partial}{\partial t}\iint_S \vec{D}\cdot\vec{n}dS$$

The Bloch Boundary Condition:

$$\bar{E}_x\left[\left((n+1/2)d\right)\right] = \bar{E}_x\left[d/2\right]e^{i(n\theta+\theta/2)}$$

$$\bar{H}_y\left[(nd)\right] = \bar{H}_y\left[0\right]e^{in\theta}$$

Where θ is the phase advance across one cell

The dispersion equation in SMDM can be described as:

$$\sin(\theta/2) = \omega d\sqrt{\mu\varepsilon}/2$$

The averaging impedance is described as:

$$Z = \sqrt{\frac{\bar{\mu}}{\bar{\varepsilon}}}\cos(\theta/2)$$

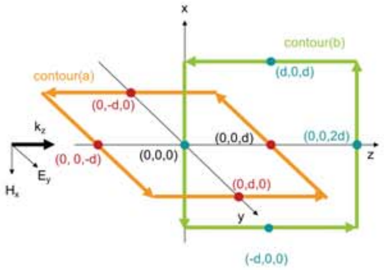


## III. Experimental set-up

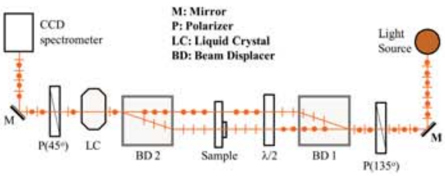


Schematic set up phase measurement. Polarization directions in two arms in the Mach-Zehnder interferometer are indicated by bars (horizontal) and dots (vertical). The second polarizer is set to be orthogonal to the first one. Additional retardation to the reference arm is introduced by liquid crystal variable retarder to recover the cross polarization condition for every wavelength.

## IV. Results and Discussions

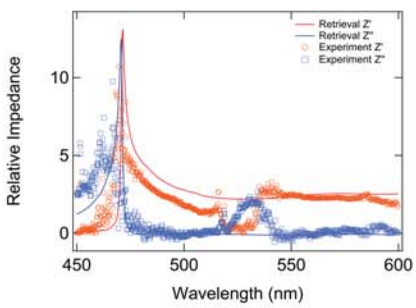


☐ The field distribution graph was calculated for a sample with many unit cells in order to suppress the reflected wave from the interface.

☐ The cusp-like features for H-field at the dielectric-metal interface is explained by Ampere-Maxwell equation with different sign of permittivity in Ag and alumina.

☐ The largest permeability is 17 for the experiment and 20 for the numerical calculation. The origin of permeability is due to inhomogeneity of the field distribution in the unit cell. The condition occurs when the half wavelength of the light in the structure matches to the unit cell size, when the microscopic magnetic field is concentrated in the metal. Interpretation of effective medium is valid as far as the incident wavelength is so long that no diffraction is allowed.

☐ The permittivity and permeability resonance around 520 nm in experimental data is ascribed to the Fabry-Perot interference. Such structure does not show in calculation data unless we introduce inequivalent unit cell.

☐ When we apply Bloch boundary system in our study, the three cases are observed in different wave modes in SMDM. From 460 to 470 nm, the real refractive index is constant. It means the phase advance reach π/2 and the wave is resonant crystal band-gap regime. Above 470 nm, all modes correspond to propagating modes. The evanescent modes cannot be observed in the graph, it occurs in higher wavelength regime. In our case, we limits the observation just in optical regime.

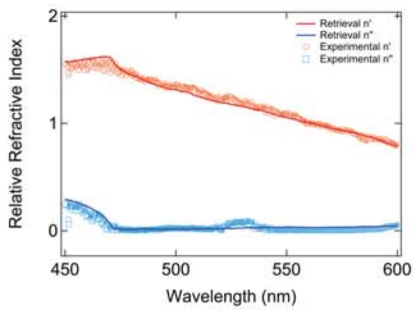


## V. Conclusion

We have investigated an optical response of metal dielectric multilayers with sub-wavelength period. Our calculation predicted enhancement of permeability, while experimental data of three periods SMDM confirmed it. Imperfections in fabrication process responsible to create another resonance correspond with Fabry-Perot interference. There are no ordinary materials exhibiting magnetic response in optical frequency. By combining each layer as SMDM, which has effective μeff, we succeeded to create high fascinate magnetic response in this structure. SMDM is simple but useful and pedagogic example to understand the origin of magnetic response in artificial structure consisting of non-magnetic materials.

## References

[1] R. Liu et. al., PRE 76 026606 (2007).
[2] R. Watanabe et. al., Phys. Status Solidi B 245 2696 (2008).
[3] P. B Johnson et al. PRB 6 4370 (1972)
[4] D. R. Smith et al., PRB 65 195104 (2002)
[5] A. S. Vioktalamo et al., e-print PNFA: 10.1016/j.photonics.2011.08.005

**Contact**: *asvioktalamo@sspp.phys.tohoku.ac.jp*

# Resonance femtosecond stimulated Raman spectroscopy: development and application to vibration of excited state

TOHOKU UNIVERSITY

Kenta Abe (Physics, D3)

## 1. INTRODUCTION

### Primary Process of Photosynthesis

**Light Harvesting (LH) Function**
Efficient use of solar light energy: Ultrafast energy transfer from Carotenoid to Bacteriochlorophyll.

**Photoprotective Function**
Preventing damage to the cell: Carotenoid absorbs strong light energy.

**LH1 Complex**

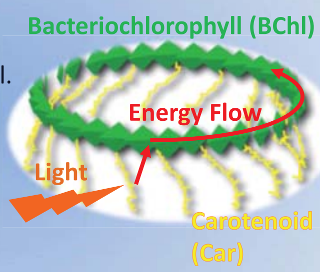


**Main theme:**
**Dynamics of energy transfer in Light Harvesting.**

## 2. OBJECTIVE

### Hot $S_1$ is Relaxed from $S_2$ and Involved with Energy Transfer in LH.

**More efficient** energy transfer than $S_1$. Why does it happens?

What's the hot $S_1$ state?
**Vibrational** state of $S_1$?
**Electronic** state?
($3A_g^-$ or $1B_u^-$)

$S_1$ is **optical forbidden**.
It is not very easy to examine.

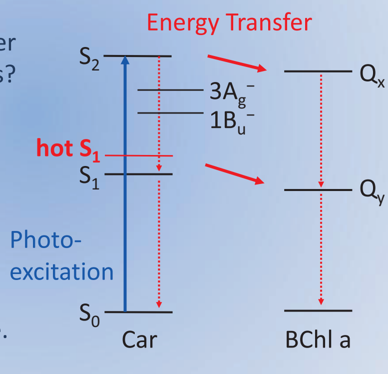


## 3. METHODS

### Femtosecond Stimulated Raman Spectroscopy (FSRS)

Stimulated Raman Spectroscopy
**Detection of Transmittance Change**

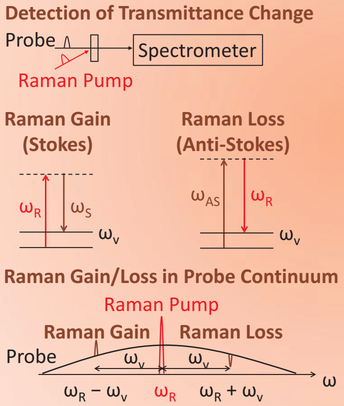


FSRS
**Raman Scattering of Transient State**

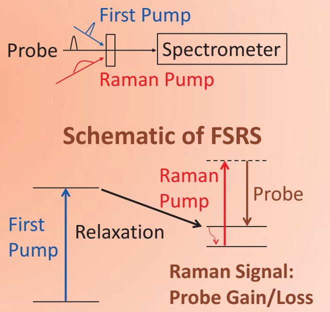


## 4. PERFORMANCE

### FSRS Sensitivity and Spectral Resolution

**kHz Synchronized Detection System**

**Sensitivity:**
**ΔT/T: $10^{-5}$–$10^{-4}$**

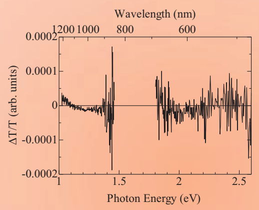


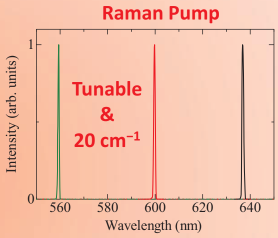


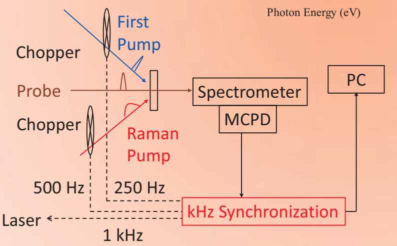


## 5. RESULTS

### FSRS of β-Carotene Resonant to $S_1$

**β-Carotene**

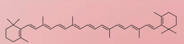

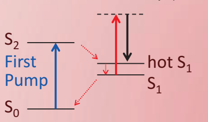


**Lifetime**
$S_2$: ~0.1ps
hot $S_1$: ~0.4ps
$S_1$: 9ps

**Absorption Spectra and Resonance Condition**

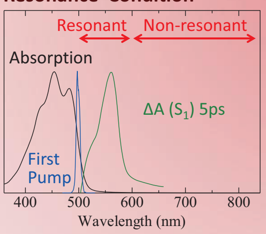


**Stokes Raman Signal**

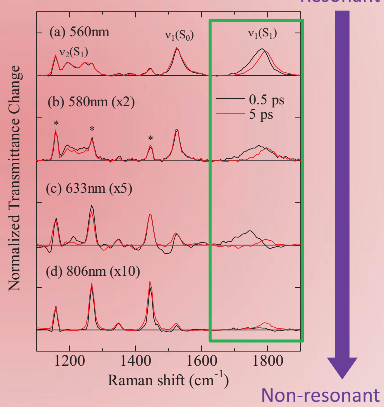


## 6. DISCUSSION

### Simulating Negative Signal of $\nu_1(S_1)$ Mode

Stokes Raman Signal Simulations of Vibrational Ground/Excited State

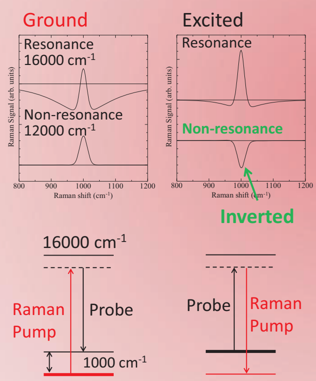


**$\nu_1(S_1)$ Signals of 5ps and 0.5ps after $S_2$ Pump**
Red: $S_1$, Black: hot $S_1$ Stokes Raman Signal

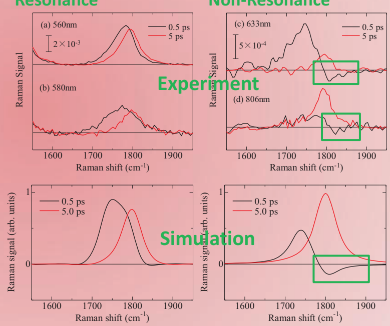


The negative signal **by vibrational state** were reproduced successfully.

**Hot $S_1$ has been confirmed to the $\nu_1$ vibrational state of $S_1$ — not to the other electronic state.**

P-3

# Electronic State and Superconductivity of $CeRhSi_3$

Department of Physics, Tohoku University

Hiroki Iida

## Introduction

Heavy-fermion superconductivity appears in the vicinity of the border of magnetism in which a magnetic transition temperature goes zero. $CeRhIn_5$ is one of the typical heavy-fermion superconductors. The superconducting transition temperature $T_c$ becomes maximum at the pressure where the antiferromagnetic order vanishes. An application of pressure suppresses the antiferromagnetic order and simultaneously induces the superconductivity. The effective mass of the conduction electron diverges at this pressure [1]. Interplay between the emergence of superconductivity and the critical phenomenon of the magnetismis an interesting issue for the heavy-fermion system.

$CeRhSi_3$ is a heavy-fermion superconductor found in 2005 [2]. Although pressure-temperature phase diagram of $CeRhSi_3$ is similar to that of $CeRhIn_5$, a critical behavior has not been observed thus far. In order to verify whether or not the effective mass diverges at a critical pressure, we have measured the electrical resistivity under pressure and magnetic field.

### Pressure-induced heavy-fermion superconductivity

**$CeRhSi_3$**

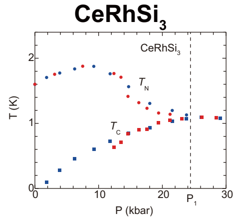


**$CeRhIn_5$**

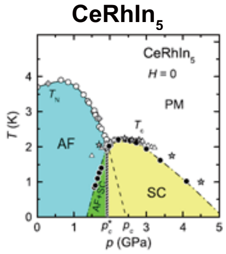


■ Pressure-temperature phase diagram of $CeRhSi_3$ [2] is similar to that of $CeRhIn_5$ [3].

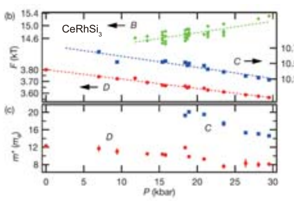


■ No divergence of effective mass [4]

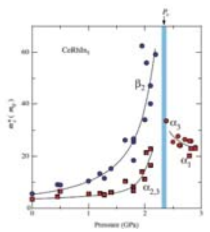


■ Effective mass diverges critical pressure [1]

### References

[1] H. Shishido et al., J. Phys. Soc. Jpn. **74** (2005) 1103.
[2] N. Kimura et al., J. Phys. Soc. Jpn. **76** (2007) 051010.
[3] G. Knebel et al., J. Phys. Soc. Jpn. **77** (2008) 114704.
[4] T. Terashima et al., Phys. Rev. B **76** (2007) 054506.

## Sample and Measurement

### Sample preparation

■ The single crystal of $CeRhSi_3$ was grown by the Czochralski pulling method in a tetra-arc furnace.

■ Residual resistivity ratio (RRR) > 100

### Application of pressure system

■ Clamped piston cylinder cells

■ Pressure transmitting medium
:equal mixture of n- and i-propanol

### Measurement

■ Low ac four-terminal method

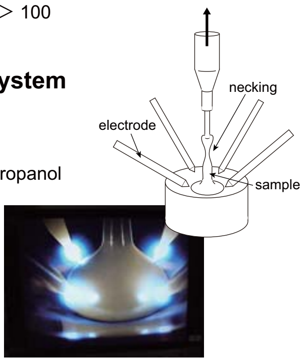


## Resistivity under magnetic field for 1.97, 2.30, 2.41 and 2.61GPa

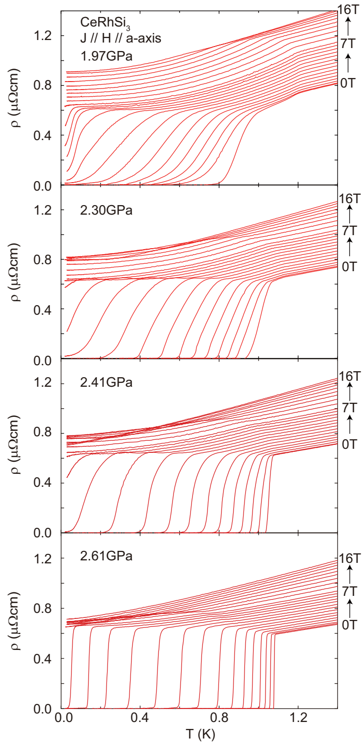


※ρ (T) curves of $CeRhSi_3$ for the magnetic fields every 0.5T from 0T to 7T and every 1T from 7T to 16T each Pressure.

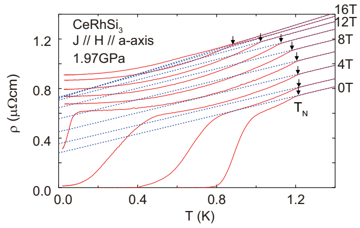


※ρ (T) curves of 1.97GPa for the magnetic fields every 2T from 0T to 16T.

■ In the paramagnetic stat, $\rho_{PM}(T)$ obeys

$$\rho_{PM}(T) = \rho_0 + AT^1 .$$

■ PM state fitting lines indicate that the residual resistivity $\rho_0$ and the coefficient A is change with applied magnetic field.

## Magnetic field dependences of residual resistivity $\rho_0$ and the coefficient A

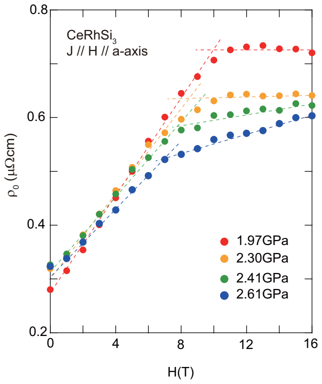


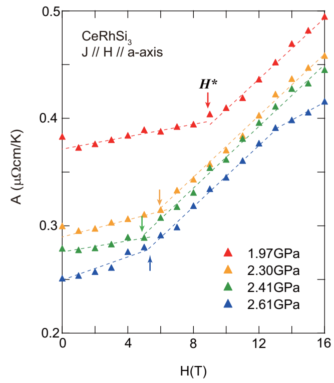


■ The $d\rho_0$ /dH changes at 7~9 T each pressure.

⇒ We suppose that change of the $d\rho_0$ /dH is cused by the valence transition or change of electronic structure.

■ The coefficient A exhibit monotonic increase with applied magnetic field.

⇒ No signatures of quantum criticality !!

## Sammary

1) In the paramagnetic stat of $CeRhSi_3$, $\rho_{PM}(T)$ obeys $\rho_{PM}(T) = \rho_0 + AT^1$ .

2) The coefficient A does not diverges under magnetic field. Therefore critical behavior of $CeRhSi_3$ has not been observed.

3) No critical behavior of $CeRhSi_3$ is consistent with dHvA results.

# Accurate Crystal Structure Analysis of $YTiO_3$ by Synchrotron X-ray Diffraction


Yoshihisa Ishikawa, Terutoshi Sakakura, Takahiro Nakano, Hiroyuki Kimura, Yukio Noda, Yasuyuki Takenaka[1], Syunji Kishimoto[2]

*IMRAM, Tohoku Univ. , Hokkaido University of Education[1], KEK-Photon Factory[2]*


## Introduction

$YTiO_3$ is well known as one of orbital-ordering system materials. The orbital–ordering phenomenon of $YTiO_3$ have many studied the both side of theoretical and experimental method. The crystal structure of $YTiO_3$ belong to a perovskite, Pbnm (Space group No.62 Pnma). The wycoff position of Ti atom is 4a and the site symmetry is -1. Figure shows the crystal structure of yttrium titanate. $YTiO_3$ undergoes the phase transition from paramagnetic to ferromagnetic at Tc=28K.

In the cubic crystal field, one 3*d* electron of the $Ti^{3+}$ ion may occupy the triply degenerate $t_{2g}$ states. The Jahn – Teller distortion of $TiO_6$ octahedron in $YTiO_3$ splits the energy levels of $t_{2g}$ state. In the $t_{2g}$ energy levels of $TiO_6$ octahedron, Ti3d has |yz> and |zx> orbits. The electron of the orbits $c_1$|zx> - $c_2$|yz> and $c_1$|zx> + $c_2$|yz> , where coefficients of $c_1$ and $c_2$ are satisfied $c_1^2 + c_2^2 = 1$. The study to be determined the coefficients $c_1$ and $c_2$ is performed by Polarized neutron diffraction (PND) [1], the resonant X-ray scattering (RXS) [2], NMR [3], and the X-ray Magnetic Diffraction (XMD) [4].

The aim of this experiment is to perform the accurate crystal structure analysis by Synchrotron X-ray Diffraction to obtain the coefficients $c_1$ and $c_2$.

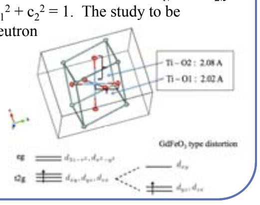



[1] J. Akimitsu, et.al, JPSJ **70**, 3475 (2001), [2] H. Nakao, et.al, PRB **66**, 184419 (2002)
[3] M. Itoh, et.al, JPSJ **68**, 2783 (1999), [4] M. Itoh, et.al, J. Phys. Chem. Solid **65**, 1993 (2004)


## Experiment

X-ray 4-circle Diffractometer @ KEK PF BL-14A (Tsukuba)
- Perpendicular wiggler type x-ray source
- Monochrometer Si (1 1 1) : Wave Length : 0.752Å / 0.850Å
- $2\theta < 122^\circ$ (Q < 1.163)
- Detector : Si – APD [Avalanche PhotoDiode] (*)

Temperature control
- He-gas flow

| Temp | R(F) | meas pt. | used pt. |
|---|---|---|---|
| 23K | 4.9 | 1339 | 1140 |
| 32K | 3.08 | 2750 | 2430 |
| 55K | 3.2 | 268 | 213 |
| 65K | 2.44 | 4833 | 4353 |
| 145K | 2.52 | 1683 | 1919 |
| 293K (RT) | 1.04 | 3198 | 2892 |

*Sample Information*

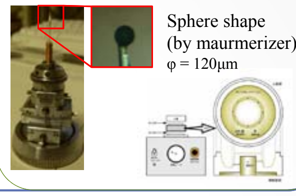

Sphere shape
(by maurmerizer)
$\varphi$ = 120μm


(*) S. Kishimoto, et.al, PRL **85**, 1831 (2000)


## Result

### *Avoidance of Multiple Scattering*

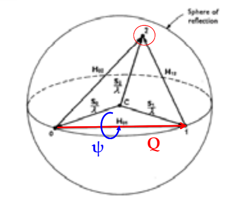


Fig. 1. Geometric representation of simultaneous reflections in the reciprocal lattice. Points 0, 1 and 2 lie on the sphere of reflection. The unit vectors $S_0$, $S_1$ and $S_2$ define the direction of the incident, primary and secondary beams.


R. M. Moon, et.al, Acta Cryst **17**, 805 (1964)
K. Tanaka, et.al, Acta Cryst **A66**, 438 (2010)


Simultaneous reflections means several Bragg peaks ride on the Ewald sphere.

To avoid the simultaneous reflections, the setting angle would be rotated around Q-vector which is called "ψ-axis"

In this measurement, the avoidance of multiple scattering performed the program "*MDC++*" which is coded by Dr. Sakakura.

### *Crystal Structure Analysis*

Lp Correction : Lorentz Corr. = $2\theta$
linear polarization p = 1.

Absorption Correction : program by DABEX

Extinction Correction. : Becker – Coppens, Type Ⅰ, Gaussian Model

$$E_b = \sqrt{1+2x+\frac{(0.58+0.48\cos 2\Theta+0.24\cos^2 2\Theta)x^2}{1+(0.02-0.025\cos 2\Theta)x}}$$

$$x = \frac{7.9406\times10^3 \lambda^3 F_c^2 \bar{t} E_g (\cos 2\Theta_m + \cos^4 2\Theta)}{V_0^2 \sin 2\Theta (\cos 2\Theta_m + \cos^2 2\Theta)}$$


P. Becker & P. Coppens, Acta Cryst A**30**,129 (1974)


### *Multipole Refinement*

$$\rho(\mathbf{r}) = \rho_c^s(r) + \kappa^3 P_v \rho_v^2(\kappa \cdot r) + \sum_{l=0}^{lmax} \kappa'^3 R_l(\kappa' \cdot r) \sum_{m=\pm l} P_{lm} Y_{lm}(\theta,\phi)$$

Core Electron — valence Electron — Radial distribution function — Spherical Harmonic Function

$$R_l(r) = \frac{\xi_l^{n_l+3}}{(n_l+2)!} r^{n_l} e^{-\xi \cdot r}$$

Radial distribution function is based on Slater-like Hartree-Fock-Roothaan algebraic equation. (Clementi Table)


N. K. Hansen & P. Coppens, Acta Cryst A**34**, 909 (1978)
E. Clementi & C. Roetti, ATOMIC DATA AND NUCLEAR DATA TABLES **14**, 177 – 478 (1974)
M. Dusek, et.al, Journal of Physics **226**, 012014 (2010)


### *Framework of Lattice & Octahedron*

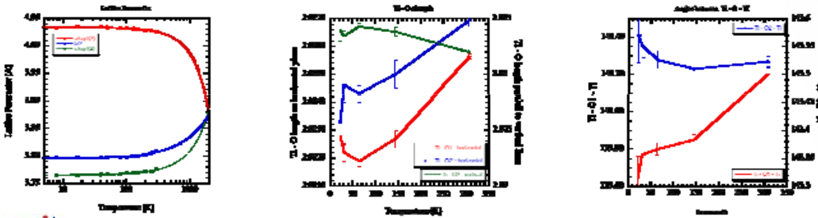


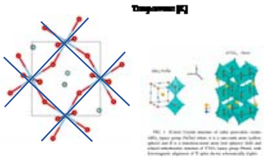

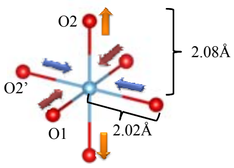


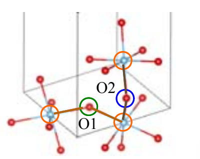



N. N. Kovaleva, et.al, PRB **79**, 045114 (2009)


### *Electron Density*

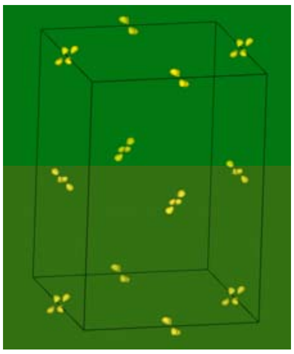

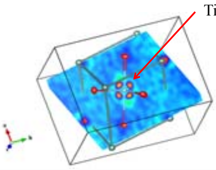


Deformation Density :

$$\Delta\rho_{model}(\mathbf{r}) = \sum_i^{all\ atoms} \Big\{ P_{i,c}\rho_{core}(\mathbf{r}) + P_{i,v}\kappa^3\rho_{valence}(k_i r) + \sum_{i=0}^{l_{max}} \kappa_i'^3 R_{i,l}(\kappa_i' r) \sum_{m=0}^{l} P_{i,lm\pm} d_{lm\pm}(\mathbf{r}/r) \Big\} - \rho_{reference}(\mathbf{r})$$

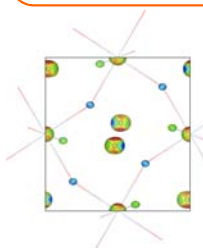

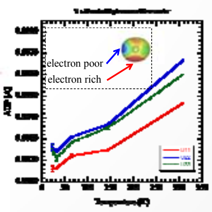


FIGURE.
( Left ) Deformation Density of $YTiO_3$ by multipole refinement at room temperature. And 2-dimensional Differential Fourier Mapping on Ti3d orbital. Electron density level of $0.8e/Å^{-3}$ .
( Right ) Contour valence electron density mapping on observed Fourier transform density $\rho_{obs}$. The Blue and Red color means the poor and rich electron number.

## Discussion

To determine the coefficients $c_1$ and $c_2$, Ti–O vector has a projection onto a local coordinate system. In this case, Ti-O1, Ti-O2', and Ti-O2 is transformed x, y, and z onto a local orthogonal coordinate. The valence electron density of Ti3d orbitals can estimate the position by calculation of center of weight. In the crystal field theory, these 3d1 wave functions is representation of linear combination between |zx> and |yz>. It means the rotation around local z-axis.

Since Ti valence electron density position is tilted 9 degree than dzx = dyz line (45 degree: In the case of dzx = dyz, c1 = √2/2 = 0.71), the coefficients of Ti3d of this experiment evaluates $c_1$=0.81. This result is consistent with NMR measurement.

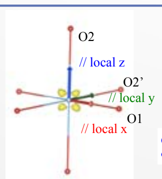


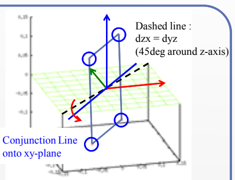


| $c_1$ | *measurement* | *Reference* |
|---|---|---|
| 0.69 | NMR | M.Itoh, JPSJ **68**, 2783 |
| 0.71 | RXS, XMD | H.Nakao, PRB **66**, 184419 |
| 0.77 | PND | J.Akimitsu, JPSJ **70**, 3475 |
| 0.8 | NMR | T.Kiyama, JPSJ **74**, 1123 |
| 0.81 | This Experiment | |
| 0.84 | Magnetic Compton | F.Iga, PRL **93**, 257207 |

## Summary

In the crystal field theory, Ti3d of the octahedron in $YTiO_3$ has the 2 energy levels |dzx> and |dyz>. To determine the coefficients of linear combination $c_1$ and $c_2$, the accurate crystal structure analysis performed by Synchrotron X-ray Diffraction.

Estimation for electron density involved Ti3d $t_{2g}$ orbitals, it succeeds the result for R-Factor within 1% by multipole refinement. And then, the coefficient $c_1$ was obtained 0.81.

In this measurement, the environment of a low temperature was not optimized. In the next step, we try to improve the measurement methods for a low temperature below Tc.

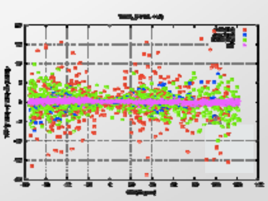

# Terahertz Time Domain Spectroscopy of Dimer Mott Insulator

**K. Itoh[1], H. Nakaya[1], Y. Kawakami[1], T. Fukatsu[1], H. Itoh[1,2], T. Sasaki[3,2], S. Saito[4], and S. Iwai[1,2]**

Department of Physics, Tohoku University[1], JST-CREST[2],
Institute for Materials Research, Tohoku University[3], National Institute of Information and Communications Technology[4]

## Low-Dimensional Organic Conductor $\kappa$-$(ET)_2Cu_2(CN)_3$

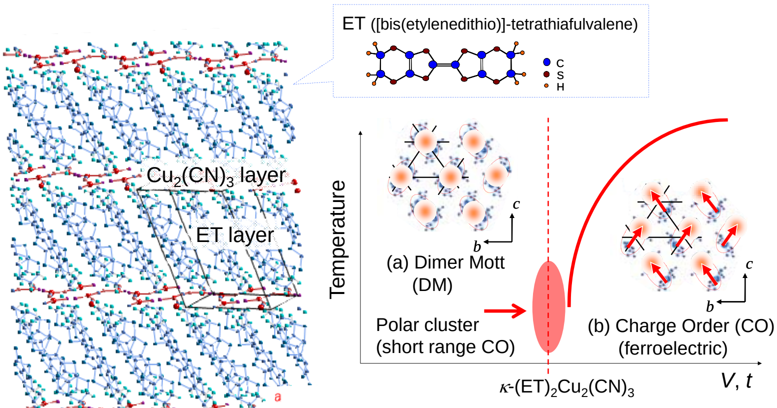


Seo *et al.*, JPSJ **76**, 103701 (2007)
Naka and Ishihara, JPSJ **79**, 063707 (2010)
Hotta, PRB **82**, 241104(R) (2010)

## Dielectric anomaly in $\kappa$-$(ET)_2Cu_2(CN)_3$

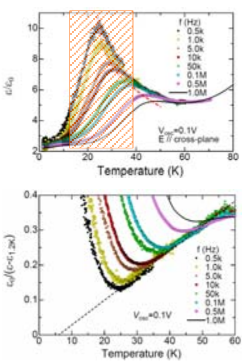


Relaxer-like behavior (dielectric fluctuation)
Abdel-Jawad, Terasaki, Sasaki *et al.*, PRB **82**, 125119 (2010)

**<40 K; Polar Nano Cluster (PNC)**

Charge disproportionation (dimer dipoles) | PNC (dipole glass)

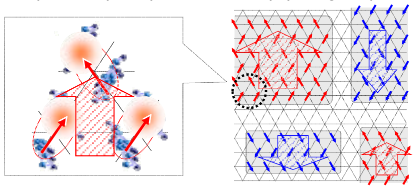

**Objective: Capture of the optical response of PNC**

- Steady state Terahertz (THz) spectrum
- Optical pump THz probe measurements

## Terahertz Time-Domain Spectroscopy (THz-TDS)

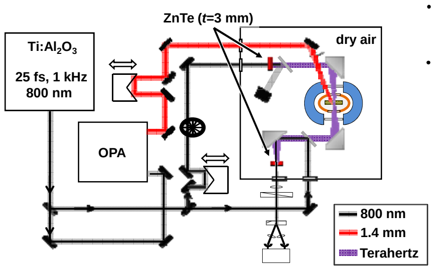


- Steady state TDS
  → THz response of PNR
- Pump Probe TDS
  → Photoinduced effect of PNC

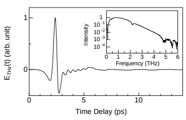

Typical THz waveform
Range: 0.5-4 THz (20-130 cm$^{-1}$)

## Optical Conductivity in the *bc*-plane

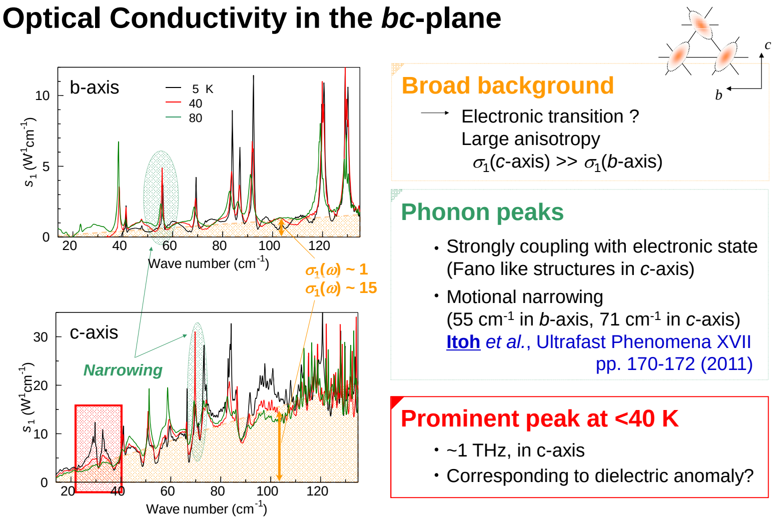


**Broad background**

→ Electronic transition ?
Large anisotropy
$\sigma_1$(*c*-axis) >> $\sigma_1$(*b*-axis)

**Phonon peaks**

- Strongly coupling with electronic state (Fano like structures in *c*-axis)
- Motional narrowing (55 cm$^{-1}$ in *b*-axis, 71 cm$^{-1}$ in *c*-axis)
  **Itoh** *et al.*, Ultrafast Phenomena XVII pp. 170-172 (2011)

**Prominent peak at <40 K**

- ~1 THz, in c-axis
- Corresponding to dielectric anomaly?

## Optical Transition of Polar Nano Cluster

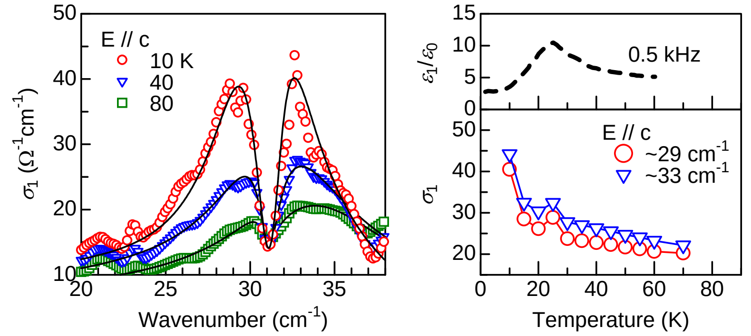


~30 cm$^{-1}$; **Collective excitation in PNC**
(~1 THz) c.f.) Kaisar *et al.*, PRL **105**, 206402 (2010)

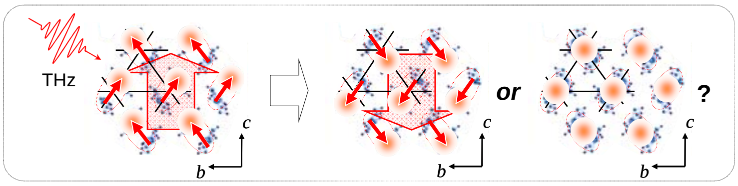


### Fano resonance

Interference { Collective electronic excitation; Phonon }

$$\sigma(\omega) = -\frac{f_\beta}{\pi}\,\mathrm{Im}\left(\frac{\beta}{1-\gamma^2 f_\beta f_\alpha \beta\alpha}\right)$$

- $\gamma$ : Coupling constant
- $\alpha(\omega)$ : Line shape function (phonon)
- $\beta(\omega)$ : (collective excitation)
- $f_{\alpha,\beta}$ : Oscillator strength

Neuhauser et al., PRL **85**, 5304 (2000)

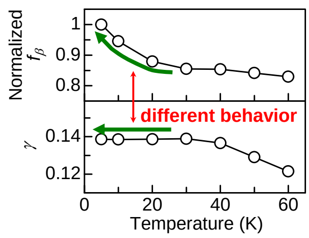


## Photoinduced Proliferation of Polar Nano Cluster

Pump wavelength; 1.4 μm (intra-dimer excitation)

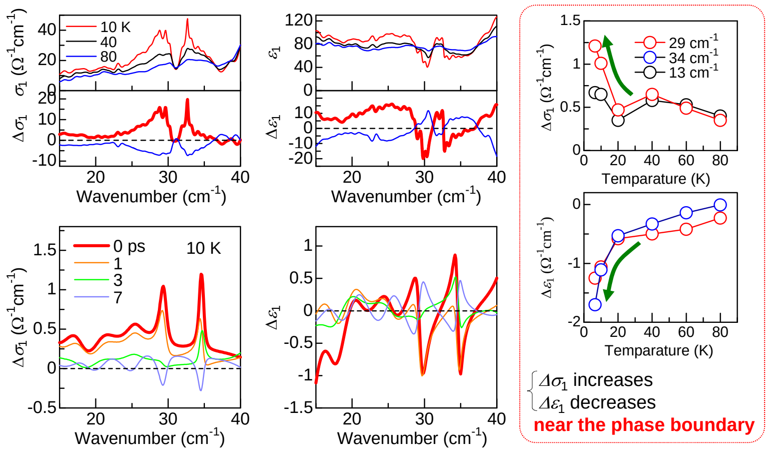


{ $\Delta\sigma_1$ increases; $\Delta\varepsilon_1$ decreases } near the phase boundary

Photoinduced $\{\Delta\sigma_1, \Delta\varepsilon_1\} \cong \{\sigma_1(10\text{ K}) - \sigma_1(40\text{ K}), \varepsilon_1(10\text{ K}) - \varepsilon_1(40\text{ K})\}$

**Optical Growth of Polar Nano Cluster**
**Proliferation is driven by the collapse of dimer Mott phase**

**Summary;**

THz response associated with polar nano clusters or dipole glass state was investigated in organic dimer Mott insulator $\kappa$-$(ET)_2Cu_2(CN)_3$ exhibiting relaxer-like low-frequency dielectric anomaly. Electronic transition at ~1 THz can be assigned to the corrective excitation of the intradimer dipole in the polar nano cluster. Optical pump and THz probe measurement shows that photoinduced increase of this THz response reflecting the proliferation of the polar cluster. Such photoinduced proliferation of polar cluster is discussed in terms of the competition between the dimer Mott phase and the charge ordered ferroelectric phase.

# Periodic decomposition of functions holomorphic in domains containing convex polygons

Takanao Negishi

Let $\mathfrak{E}(\mathbb{C})$ and $\mathfrak{M}(U)$ denote, respectively, the sets of all entire functions and all meromorphic functions on $U \subseteq \mathbb{C}$. Let $\Delta_c$ be the forward difference operator: $\Delta_c f(z) := f(z+c) - f(z)$. The following two results are fundamental in this study.

**Theorem 1.** *(Leont'ev) Let $D$ be a convex polygonal domain with vertices $\gamma_1, \gamma_2, \ldots, \gamma_n \in \mathbb{C}$ and let $\gamma_{n+1} = \gamma_1$. For $1 \le k \le n$, let $c_k = \gamma_{k+1} - \gamma_k$ and let $D_k$ be the open half-plane containing $D$ bounded by the line through $\gamma_k$ and $\gamma_{k+1}$. Then, any function $f$ holomorphic in $D$ has a periodic decomposition of the form*

$$f(z) = P_{c_1}(z) + P_{c_2}(z) + \cdots + P_{c_n}(z) \quad (z \in D),$$

*where each $P_{c_k}$ is holomorphic and $c_k$-periodic in $D_k$.*

**Theorem 2.** *Let $c_1, c_2, \ldots, c_n \in \mathbb{C}$ be pairwise linearly independent over $\mathbb{R}$. Then any function $f \in \mathfrak{M}(\mathbb{C})$ satisfying the difference equation $\Delta_{c_1}\Delta_{c_2}\cdots\Delta_{c_n} f = 0$ has a meromorphic periodic decomposition of the form $f(z) = P_{c_1}(z) + P_{c_2}(z) + \cdots + P_{c_n}(z)$, where each $P_{c_k}(z) \in \mathfrak{M}(\mathbb{C})$ is $c_k$-periodic.*

As an application of these theorems, we can show the following theorem.

**Theorem 3.** *The definitions of $D$, $D_k$, $\gamma_k$, and $c_k$ are same as in Theorem 1. Let $c_1, c_2, \ldots, c_n \in \mathbb{C}$ be pairwise linearly independent over $\mathbb{R}$ ( this assumption implies that $D$ has no parallel sides). Then for any function $f$ holomorphic in $\overline{D}$, the follwing periodic decomposition holds for any $z \in \overline{D} \setminus \{poles\}$:*

$$f(z) = P_{c_1}(z) + P_{c_2}(z) + \cdots + P_{c_n}(z),$$

*where each $P_{c_k}$ is meromorphic and $c_k$-periodic in $D_k$. Furthermore if $n$ is even, $P_{c_k}$ and its first $\frac{n}{2} - 1$ derivatives are continuous in $\partial\overline{D}$; and if $n$ is odd, $P_{c_k}$ and its first $\frac{n-1}{2} - 1$ derivatives are continuous in $\partial\overline{D}$.*

This result is extendable to the periodic decompositions of meromorphic functions on $\overline{D}$. Let $f \in \mathfrak{M}(\overline{D})$. If there are $c_k$-periodic meromorphic functions $Q_{c_k} \in \mathfrak{M}(\mathbb{C})$ $(1 \le k \le n)$ such that $f - (Q_{c_1} + Q_{c_2} + \cdots + Q_{c_n})$ is holomorphic in $\overline{D}$, then Theorem 3 gives a meromorphic periodic decomposition $f - (Q_{c_1} + Q_{c_2} + \cdots + Q_{c_n}) = P_{c_1} + P_{c_2} + \cdots + P_{c_n}$. Thus we have a meromorphic periodic decomposition

$$f = (P_{c_1} + Q_{c_1}) + (P_{c_2} + Q_{c_2}) + \cdots + (P_{c_n} + Q_{c_n}).$$

Let $R_{c_k} = P_{c_k} + Q_{c_k}$. Each $R_{c_k}$ is meromorphic in $D_k$. If we can choose $Q_{c_k}$ as a function that has no poles in $\partial\overline{D_k}$, $R_{c_k}$ is also a $c_k$-periodic meromorphic function in $\overline{D_k}$ that is holomorphic on $\partial\overline{D_k}$. Then what are conditions on $n$ for all meromorphic functions on $\overline{D}$ to have such decompositions? We give some results for $n = 3, 4, 5, 6$ as follows.

**Proposition 1.** *We assume $n = 3$, that is to say, $D$ is a triangle domain. Then any meromorphic function $f$ on $\overline{D}$ has a meromorphic periodic decomposition $f(z) = P_{c_1}(z) + P_{c_2}(z) + P_{c_3}(z)$ $(z \in D \setminus \{poles\})$, where each $P_{c_k}$ is a $c_k$-periodic meromorphic function on $D_k$.*

**Theorem 4.** *We assume $n = 4, 5, 6$. That is to say, $D$ is a convex quadrilateral, pentagonal, or hexagonal domain. Then any meromorphic function $f$ on $\overline{D}$ has a meromorphic periodic decomposition $f(z) = P_{c_1}(z) + P_{c_2}(z) + \cdots + P_{c_n}(z)$, where for each $P_{c_k}$ is meromorphic and $c_k$-periodic in $D_k$ and $(i)(n = 4)$ continuous in $\partial\overline{D_k}$, and $P_{c_k}{}'$ is continuous in $\partial\overline{D_k}$; $(ii)(n = 5)$ continuous in $\partial\overline{D_k}$; or $(iii)(n = 6)$ continuous in $\partial\overline{D_k}$ except at poles, and its first two derivatives are also continuous in $\partial\overline{D_k}$ except at poles.*

We can consider another application of Theorem 1. We give periodic decompositions of functions holomorphic in domains satisfying some conditions. Let $D$ be a domain and let $\gamma_1$ $(= \gamma_{n+1})$, $\gamma_2, \ldots, \gamma_n \in \partial D$ and $c_k = \gamma_{k+1} - \gamma_k$. Consider the following conditions:

(a) The $n$-sided polygon $[\gamma_1\gamma_2\cdots\gamma_n]$ is convex and contained in $D$. Let $E$ be this polygonal domain.

(b) For $1 \le k \le n$, let $E_k$ be the open half-plane containing $E$ bounded by the line through $\gamma_k$ and $\gamma_{k+1}$ and let $G_k = (\mathbb{C} \setminus \overline{E_k}) \cap E_{k-1} \cap E_{k+1} \cap D$. Then $G_k \cap (G_k + \gamma_k) = G_k \cap (G_k - \gamma_k) = \emptyset$.

(c) $\partial G_k \cap \partial E_{k-1} = \{\gamma_k\}$, $\partial G_k \cap \partial E_{k+1} = \{\gamma_{k+1}\}$ $(1 \le k \le n)$.

If the above conditions are satisfied, we call $D = G_1 \cup G_2 \cup \cdots \cup \overline{E} \setminus \{\gamma_1, \ldots, \gamma_n\}$ a *strictly convex polygonal decomposition* of domain $D$.

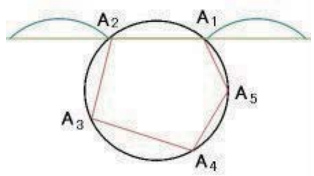


**Theorem 5.** *Let $D$ be a domain that has a strictly convex polygonal decomposition as above and let $D_k = E_k \cup \{\bigcup_{m\in\mathbb{Z}}(D + m\gamma_k)\}$ $(1 \le k \le n)$. Then any function $f$ holomorphic in $D$ has a periodic decomposition $f = P_{c_1} + P_{c_2} + \cdots + P_{c_n}$, where each $P_{c_k}$ is holomorphic and $c_k$-periodic in $D_k$.*

We consider the condition (d) instead of (b), (c):

(d) $D \cap (\mathbb{C} \setminus \overline{E_k}) \cap \{(\mathbb{C} \setminus E_{k-1}) \cup (\mathbb{C} \setminus E_{k+1})\} = \emptyset$ $(1 \le k \le n)$.

If the conditions (a), (d) are satisfied, we call $D = G_1 \cup G_2 \cup \cdots \cup \overline{E} \setminus \{\gamma_1, \ldots, \gamma_n\}$ a *convex polygonal decomposition* of domain $D$. We can think that $G_k + m\gamma_k$ is contained in separate complex planes for each $m \in \mathbb{Z}$. Then $D_k$ is regarded as a Riemann surface that have a $c_k$-periodic shape and satisfy $G_k \cap (G_k + \gamma_k) = G_k \cap (G_k - \gamma_k) = \emptyset$. Then Theorem 5 can be extended to functions holomorphic in domains having convex polygonal decompositions.

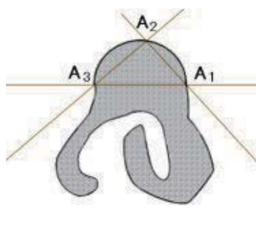

# An ODE-diffusion system modeling regeneration of Hydra

Madoka Nakayama
(Mathematical Institute, Tohoku University)

## What controls a head regeneration of Hydra?

- Activator-inhibitor reaction

Gierer-Meinhardt (1972), MacWilliams (1982)

- Receptor-Ligand reaction

Sherrat, Maini, Jäger & Müller (1995), Marciniak-Czochra (2003, 2006, 2010)

## The idea of a Receptor-Ligand reaction

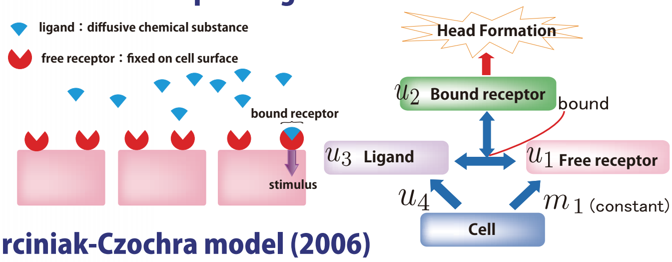


## Marciniak-Czochra model (2006)

$$
\begin{cases}
\tau\dfrac{\partial u_1}{\partial t} = -\mu_1 u_1 - b u_1 u_3 + d u_2 + m_1 & \text{for } x\in\Omega,\ t>0,\\
\tau\dfrac{\partial u_2}{\partial t} = -\mu_2 u_2 + b u_1 u_3 - d u_2 & \text{for } x\in\Omega,\ t>0,\\
\dfrac{\partial u_3}{\partial t} = \dfrac{1}{\gamma}\triangle u_3 - \mu_3 u_3 - b u_1 u_3 + d u_2 + u_4 & \text{for } x\in\Omega,\ t>0,\\
\dfrac{\partial u_4}{\partial t} = -\delta u_4 + \dfrac{m_4 u_3}{1+\sigma u_4^2 - \beta_l u_4} & \text{for } x\in\Omega,\ t>0,\\
u_j(x,0) = \phi_j(x) \quad (j=1,\ldots,4) & \text{for } x\in\Omega.
\end{cases}
$$

$u_1$ : Density of free receptor,
$u_2$ : Density of bound receptor,
$u_3$ : Density of ligand,
$u_4$ : Production rate of ligand,
$\tau,\ \mu_1, \mu_2, \mu_3, m_1, m_4, b, d, \sigma, \alpha, \beta_l, \delta$ : positive constants,
$\partial u_3/\partial\nu = 0$, $\phi_j(x)$ $(j=1,\ldots,4)$ are assumed to be smooth and positive on $\bar\Omega$.

## Boundedness of a solution

There exist positive constants $\rho_j$ $(j=1,\ldots,4)$, depending on the initial functions $(\phi_1, \phi_2, \phi_3, \phi_4)$ s.t.

$$0 < u_j(x,t) \le \rho_j \quad \text{for all } x\in\Omega,\ t\ge 0,$$

for $j = 1, 2, 3, 4$.

## Diffusion-ODE system

$\tau = 0$

$$u(x,t) = u_3(x,t), \quad v(x,t) = u_4(x,t)$$

$$f(u,v) = v - \mu_3 u - \frac{m_1\mu_2 b u}{\mu_1(\mu_2+d)+\mu_2 b u},\quad g(u,v) = -\delta v + \frac{m_4 u}{1+\sigma v^2 - \beta_l v}.$$

$$
\begin{cases}
\dfrac{\partial u}{\partial t} = \dfrac{1}{\gamma}\dfrac{\partial^2 u}{\partial x^2} + f(u,v), \quad \dfrac{\partial v}{\partial t} = g(u,v) & \text{for } 0<x<1,\ t>0,\\
\dfrac{\partial u}{\partial x} = 0 & \text{at } x=0,1,\ t>0,\\
u(x,0) = \phi_3(x),\ v(x,0) = \phi_4(x) & \text{for } 0\le x\le 1
\end{cases}
$$

## Constant stationary solutions

Theorem
Put $I_0 = \{(\phi_3(x), \phi_4(x)) | 0 \le x \le 1\}$.

(i) $^\exists(U_0, V_0) \in W^s$ s.t. $0 < U_0 < U_s$ and $I_0 \subset (U_0,\infty)\times(V_0,\infty)$. Then $(u(x,t), v(x,t)) \to (u_1, v_1)$ as $t\to+\infty$.

(ii) $^\exists(U_0, V_0) \in W^s$ s.t. $0 < U_0 < U_s$ and $I_0 \subset (0,U_0)\times(0,V_0)$. Then $(u(x,t), v(x,t)) \to (u_0, v_0) = (0,0)$ as $t\to\infty$.

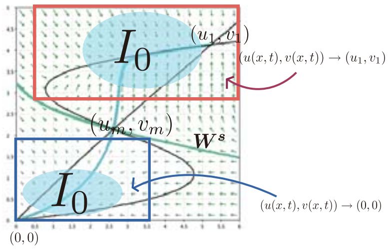


## Monotone increasing stationary solutions

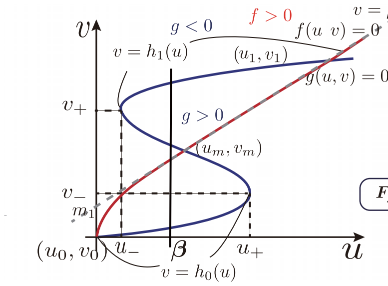


$$v = \begin{cases} h_0(u) & \text{if } u<\beta,\\ h_1(u) & \text{if } u>\beta.\end{cases}$$

$$F_j(u) = f(u, h_j(u))\ (j=0,1)$$

$$
(S)\begin{cases}
\dfrac{d^2u}{dx^2} + \gamma F_0(u) = 0 & \text{for } 0<x<l,\\
\dfrac{d^2u}{dx^2} + \gamma F_1(u) = 0 & \text{for } l<x<1,\\
u_x(0) = u_x(1) = 0, \quad u(l) = \beta.
\end{cases}
$$

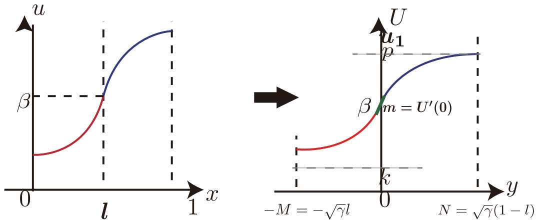


$$\mathfrak{F}_0(u) = \int_{u_0}^{u} F_0(z)dz, \quad \mathfrak{F}_1(u) = \int_{u_1}^{u} F_1(z)dz$$

$^\forall\beta \in (u_-, \min\{u_+, u_1\})$. $^\exists$one-parameter family of solutions

$$(\gamma(\beta,m),\ l(\beta,m),\ u(x;\beta,m)) \in (0,+\infty)\times(0,1)\times C^1[0,1])$$

with $m \in (0, \min\{\sqrt{2|\mathfrak{F}_0(\beta)|}, \sqrt{2|\mathfrak{F}_1(\beta)|}\})$

such that

- $u(l(\beta,m);\beta,m) = \beta$, $\cdot u'(x;\beta,m) > 0$ $(0<x<1)$,
- $u(x;\beta,m)$ solves (S) with $\gamma = \gamma(\beta,m)$.

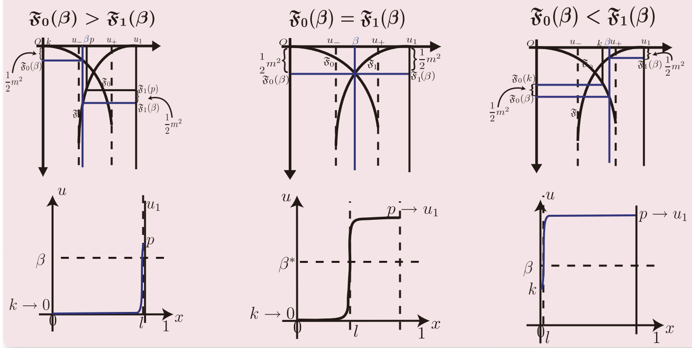


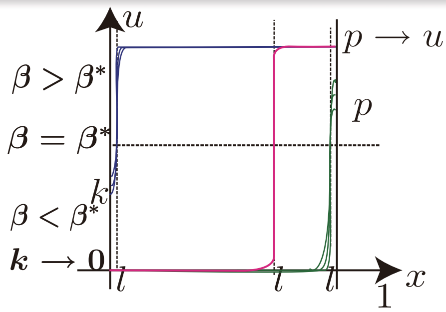

# Network Games with and without Synchroneity

Ahmad Termimi AB GHANI
sa9d12@math.tohoku.ac.jp

## Introduction

In this presentation, we study **mixed Nash equilibria** for stochastic strategies in the **network games**. We then generalize our network game to an **asynchronous game**, where two players repeatedly execute simultaneous games.

## Network Games and Profits

**Definition 1.** *Let $G = (V, E)$ be an undirected graph with no isolated vertices. Fix integer $\alpha$ and $\delta$ with $\alpha, \delta \geq 1$. A network game $\Gamma_{\alpha,\delta}(G) = \langle \mathcal{N}, \mathcal{S} \rangle$ on $G$ is defined as follows:*
*$\mathcal{N} = \mathcal{N}_A \cup \mathcal{N}_D$ is the set of players where*
*$\mathcal{N}_A$ is a finite set of attackers $a_i$, $1 \leq i \leq \alpha$*
*$\mathcal{N}_D$ is a finite set of defenders $d_j$, $1 \leq j \leq \delta$*
*$\mathcal{S} = E^\alpha \times V^\delta$ is the strategy set of $\Gamma_{\alpha,\delta}(G)$*

The individual *profit* of attacker $a_i$, is given by

$$P_{\boldsymbol{s}}(a_i) = \begin{cases} 0 & \text{if } v_j \in e_i \text{ for some } j, 1 \leq j \leq \delta \\ 1 & \text{if } v_j \notin e_i \text{ for all } j, 1 \leq j \leq \delta \end{cases}$$

The individual *profit* of defender $d_j$ is given by

$$P_{\boldsymbol{s}}(d_j) = |\{i : 1 \leq i \leq \alpha, v_j \in e_i\}|$$

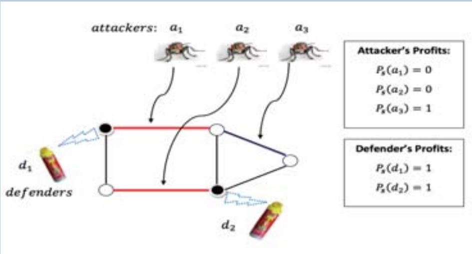


## Asynchronous Games

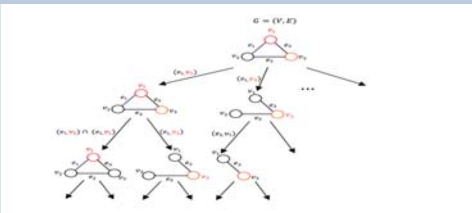


Let $G = (V, E)$ be an undirected graph. The set $\mathcal{P} \subset (E \times V)^{<\mathbb{N}}$ of partial plays is defined recursively as follows:
-Put the empty sequence $\lambda \in \mathcal{P}$ and $E_\lambda = E$ and $V_\lambda = V$.
-Now assume that $\eta \in \mathcal{P}$, and $E_\eta \subset E$ and $V_\eta \subset V$ have been defined. We put $\rho := \eta^\frown\langle(e, v)\rangle$ into $\mathcal{P}$, if $e \in E_\eta$ and $v \in V_\eta$.
Then, we define

$$E_\rho := \begin{cases} E_\eta & \text{if } v \in e \\ E_\eta - \{e\} & \text{if } v \notin e \end{cases}$$

$$V_\rho := V(E_\rho).$$

Finally, let $[\mathcal{P}] = \{w \in (E \times V)^{\mathbb{N}}$ :
each finite initial segment of $w$ belongs to $\mathcal{P}\}$.

## Expected Profits (One-Round)

Given $G :=$ a finite graph and $f : \{G' : G'$ is a proper subgraph of $G\} \to \mathbb{R}$, a state evaluation. We define a function $h : E \times V \to \{$subgraphs of $G\}$ by

$$h(e, v) := \begin{cases} G & \text{if } v \in e \\ G(E \setminus \{e\}) & \text{if } v \notin e \end{cases}$$

**Definition 2.** *Let $\boldsymbol{s} = (\sigma, \tau)$ be a pair of mixed strategies. The expected profit of the attacker with the delay constant c given by*

$$P_{\boldsymbol{s}}(\Gamma(G; f)) := \sum_{v \notin e} \sigma(e)\tau(v)\{1 + f(h(e, v))\}$$
$$+ \sum_{v \in e} \sigma(e)\tau(v) c P_{\boldsymbol{s}}(\Gamma(G; f))$$

## Characterizations of Mixed Nash equilibria

A *mixed strategy* for an attacker (resp. defender) is a probability distribution over edges (resp. vertices) of $G$.

$\sigma_i(e)$ : the probability that attacker $a_i$ chooses edge $e$
$\tau_j(v)$ : the probability that defender $d_j$ chooses vertex $v$.

**Definition 3.** *For each $i \leq \alpha$, $\sigma_i : E \to [0, 1]$ satisfies $\sum_{e \in E} \sigma_i(e) = 1$, and for each $j \leq \delta$, $\tau_j : V \to [0, 1]$ satisfies $\sum_{v \in V} \tau_j(v) = 1$.*

A *mixed profile* $\boldsymbol{s} = \langle \sigma_1, ..., \sigma_\alpha, \tau_1, ..., \tau_\delta \rangle$ is a collection of mixed strategies, one for each player.

**Definition 4.** *The support of a player $r \in \mathcal{N}$ in a profile $\boldsymbol{s}$, denoted by $S_{\boldsymbol{s}}(r)$, is the set of edges or vertices to which $r$ assigns positive probability in $\boldsymbol{s}$. Let $S_{\boldsymbol{s}}(A) = \bigcup_{a_i \in \mathcal{N}_A} S_{\boldsymbol{s}}(a_i)$ and $S_{\boldsymbol{s}}(D) = \bigcup_{d_j \in \mathcal{N}_D} S_{\boldsymbol{s}}(d_j)$.*

Let Save(e) := the event that at least one end $v \in e$ is protected by a defender.
Let $\pi_{\boldsymbol{s}}(\text{Save}(e))$ be the probability of the event Save$(e)$ with respect to $\boldsymbol{s}$.

**Definition 5** (Expected Profits)**.** *For a defender $d_j \in \mathcal{N}_D$,*

$$P_{\boldsymbol{s}}(d_j) = \sum_{\substack{v \in V \\ i \leq \alpha \\ e \in E(v)}} \tau_j(v)\sigma_i(e) = \sum_{v \in V} \tau_j(v) \sum_{\substack{i \\ e \in E(v)}} \sigma_i(e)$$

*For an attacker $a_i \in \mathcal{N}_A$,*

$$P_{\boldsymbol{s}}(a_i) = \sum_{e \in E} \sigma_i(e) \cdot (1 - \pi_{\boldsymbol{s}}(\text{Save}(e)))$$

**Definition 6** (Nash Equilibrium)**.** *A mixed profile $\boldsymbol{s}$ is a mixed Nash equilibrium if for each player $r \in \mathcal{N}$, it maximizes $P_{\boldsymbol{s}}$ over all profiles $\bar{\boldsymbol{s}}$ that differ from $\boldsymbol{s}$ only with respect to the mixed strategy of player $r$.*

Intuitively, no player can gain more by a unilateral change of his strategy. We proceed to study the characterization of a mixed Nash equilibrium.

**Theorem 1.** *In any mixed Nash equilibrium $\boldsymbol{s}$ of $\Gamma_{\alpha,\delta}(G)$, $S_{\boldsymbol{s}}(D)$ is a vertex cover of $G$.*

**Theorem 2.** *In any mixed Nash equilibrium $\boldsymbol{s}$ of $\Gamma_{\alpha,\delta}(G)$, $S_{\boldsymbol{s}}(A)$ is an edge cover of the subgraph of $G$ obtained by restricting to $S_{\boldsymbol{s}}(D)$.*

## Determinacy of Asynchronous Games

**Theorem 3.** *Given a graph $G$ and function $f : \{G' \subsetneq G : G'$ a subgraph$\} \to \mathbb{R}$. Then, the one-round game $\Gamma(G; f)$ is determined with a stable solution.*

*Proof.* Suppose $f : \{G' \subsetneq G\} \to \mathbb{R}$, and $f(G) = x \in \mathbb{R}$ (for the next round with the same $G$) are given. The expected profit according to a profile $(\sigma, \tau)$ is following:

$$P(\sigma, \tau, x) := \sum_{v \notin e} \sigma(e)\tau(v)\{1 + f(h(e, v))\} + \sum_{v \in e} \sigma(e)\tau(v)\frac{1}{2}x.$$

By the mini-max theorem, we have $\max_\sigma \min_\tau P(\sigma, \tau, x) = \min_\tau \max_\sigma P(\sigma, \tau, x)$ for all $x \in \mathbb{R}$. Note that the set of strategy $\sigma$'s (similar for $\tau$'s) is bounded closed convex, and so it is easy to see that $M(x) = \max_\sigma \min_\tau P(\sigma, \tau, x)$ is a continuous function.

Now put $m = 1 + \max f$. Clearly, $M : [0, m] \to [0, m]$. So it has a fixed point $\hat{x}$. Then $M(\hat{x})$ serves as a stable solution. □

Now, we define a function $f : W \to \mathbb{R}$, which plays the role of a natural payoff for the attacker of our asynchronous game. For $w = ((e^1, v^1), (e^2, v^2), (e^3, v^3), ...) \in [\mathcal{P}]$, we set

$$b_i(w) := \begin{cases} 0 & \text{if } v^i \in e^i, \\ 1 & \text{if } v^i \notin e^i. \end{cases}$$

Then we define

$$f(w) = \sum_{i > 0} \frac{b_i(w)}{2^i}$$

**Theorem 4.** *The asynchronous game $\Gamma(G; f)$ is determined.*

*Proof.* (Idea) We show the existence of a stable solution in the game without referring to the Blackwell determinacy and we reduced the infinite game $\Gamma(G; f)$ to a finite-round game. □

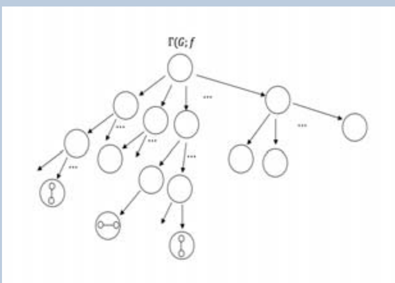


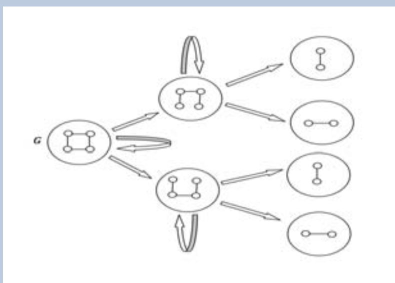

# Asymptotic Behavior of Non-local Feynman-Kac Semigroups

Masakuni MATSUURA*

February 21, 2012

## 1 Feynman-Kac penalization problem

Let $X$ be a symmetric $\alpha$-stable process on $\mathbb{R}^n$ $(n > \alpha)$ and let $A_t^\mu$ be a positive continuous additive functional corresponding with Revuz measure $\mu$. We define $A_t^{\mu,F}$ by

$$A_t^{\mu,F} := A_t^\mu + \sum_{u \le t} F(X_{u-}, X_u),$$

where $F(x,y)$ is a bounded positive symmetric function vanishing on the diagonal. We call the next problems the Feynman-Kac penalization problem.

(1) Does there exist a probability measure $\tilde{\mathbb{P}}_x$ such that

$$\lim_{t\to\infty} \frac{\mathbb{E}_x[e^{A_t^{\mu,F}} 1_\Lambda]}{\mathbb{E}_x[e^{A_t^{\mu,F}}]} = \tilde{\mathbb{P}}_x[\Lambda] \text{ for every } \Lambda \in \mathscr{F}_s?$$

(2) Is the limit distribution $\tilde{\mathbb{P}}_x$ determined by a martingale $M_s$: $d\tilde{\mathbb{P}}_x = M_s d\mathbb{P}_x$?

We first decompose the non-local multiplicative functional $e^{A_t^{\mu,F}}$ as $L_t e^{A_t^{\mu+\mu_{F_1}}}$, where

$$L_t := e^{\sum_{u\le t} F(X_{u-},X_u) - c\int_0^t \int F_1(X_u,y)|X_u-y|^{-(n+\alpha)} dy du}$$

is a martingale and

$$\mu_{F_1}(dx) := c\left(\int F_1(x,y)|x-y|^{-(n+\alpha)} dy\right) dx, F_1 = e^F - 1.$$

$c > 0$ is a constant. We also transform $X$ to $Y$ whose law is $dP_x^L = L_t dP_x$. We then find that the Dirichlet form $\mathscr{E}^Y$ of $Y$ is

$$\mathscr{E}^Y(u,u) = \frac{c}{2}\int (u(x)-u(y))^2 e^{F(x,y)} |x-y|^{-(\alpha+n)} dxdy.$$

Let $\lambda_0 := \inf\{\mathscr{E}^Y(u,u); ||u||_{L^2(\mu+\mu_{F_1})} = 1\}$. Feynman-Kac penalization problem is solved for $\lambda_0 \neq 1$ if $\mu$ and $\mu_{F_1}$ are in the Green-tight Kato class $\mathscr{K}_\infty$. (a) If $\lambda_0 > 1$, then $M_s$ is given by

$$M_s = \frac{e^{A_s^{\mu,F}} h(X_s)}{h(x)}, \quad h(x) := \mathbb{E}_x^M[e^{A_\infty^{\mu+\mu_{F_1}}}].$$

(b) If $\lambda_0 < 1$, then $M_s$ is given by

$$M_s = \frac{e^{-\theta_0 s + A_s^{\mu,F}} h(X_s)}{h(x)},$$

where $\theta_0 > 0$ is the constant such that $\inf\{\mathscr{E}_{\theta_0}^Y(u,u); ||u||_{L^2(\mu+\mu_{F_1})} = 1\} = 1$. $h$ is the ground state of Schrödinger type operator $\mathscr{L}^Y - (\mu + \mu_{F_1})$. Here, $\mathscr{L}^Y$ is the generator of $Y$: $\mathscr{E}^Y(u,u) = (\mathscr{L}^Y u, u)$.

(c) If $\lambda_0 = 1$, then $M_s$ is given by

$$M_s = \frac{e^{A_s^{\mu,F}} h(X_s)}{h(x)}$$

only if $\mu$ and $\mu_{F_1}$ are in the special Kato class $\mathscr{K}_s (\subset \mathscr{K}_\infty)$. Here, $h$ is the ground state as in the case of (b).

*Mathematical institute, Tohoku University. Mail : sa9d10@math.tohoku.ac.jp

## 2 Examples of jumping functions

We give examples of jumping functions with full support such that $\mu_F \in \mathscr{K}_\infty$

$$F(x,y) := (1 \wedge |x-y|^p)\langle x\rangle^{-q}\langle y\rangle^{-q} \text{ for } p > \alpha \text{ and } q > n.$$

Here, $\langle\cdot\rangle := \sqrt{1+|\cdot|^2}$. If we further assume $q > 2n-\alpha$, then $\mu_F \in \mathscr{K}_s$.

## 3 Asymptotic behavior of non-local Feynman-Kac semigroups

We also see asymptotic behavior of non-local Feynman-Kac semigroups. Let

$$P_t^{\mu,F} f(x) := \mathbb{E}_x[e^{A_t^{\mu,F}} f(X_t)], \quad \text{for } f \in L^2 \cap \mathscr{B}_b.$$

We then obtain

$$P_t^{\mu,F} 1(x) \begin{cases} \sim \mathbb{E}_x[e^{A_\infty^{\mu,F}}] & \text{if } \lambda_0 > 1 \\ \sim (h(x)\int_{\mathbb{R}^n} h(x)dx)\, e^{\theta_0 t} & \text{if } \lambda_0 < 1 \\ \sim (h(x)\int_{\mathbb{R}^n} h(x)d(\mu+\mu_{F_1}))\, t & \text{if } \lambda_0 = 1, n > 2\alpha \\ = o(t) & \text{if } \lambda_0 = 1, \alpha < n \le 2\alpha \end{cases}$$

as $t \to \infty$.

We further compute the growth of $L^p$-spectral bounds due to Tawara ([2, Example 5.3]). Let $l_p := \lim_{t\to\infty}(-1/t)\log||P_t^{\mu,F}||_{p,p}$ $(1 \le p \le \infty)$. We then see

$$l_p = \begin{cases} 0 & \text{if } \lambda_0 \ge 1 \\ -\theta_0 & \text{if } \lambda_0 < 1. \end{cases}$$

## References

[1] Matsuura, M., *Feynman-Kac Penalization Problem for Additive Functionals with Jumping Functions*, in preparation.

[2] Tawara, Y., *$L^p$-independence of Growth Bounds of Generalized Feynman-Kac Semigroups*, Doctor Thesis, Tohoku University, 2008.

# The characterization of a pinned polymer

**NISHIMORI Yasuhito**
**(Mathematical Institute Tohoku University)**

## Introduction

We consider a polymer which given in the form of the Brownian motion $(B_t,\ P_0)$. Let $L_{0,t} = \int_0^t \delta_0(B_s)ds$ denote the energy of the polymer and set

$$\begin{aligned} P_{\beta,t}(d\omega) &= Z_{0,t,\beta}^{-1}\exp(\beta L_{0,t})P_0(d\omega), \\ Z_{0,t,\beta} &= E_0[\exp(\beta L_{0,t})]. \end{aligned} \tag{1}$$

Where a parameter $\beta > 0$ means the inverse temperature. K. S. Alexander and V. Sidoravicius[1] introduced the *pinned polymer*. That is, for given $\beta$, there exists $\delta > 0$ such that $\lim_{t\to\infty} P_{\beta,t}(L_t/t > \delta) = 1$. Our aim is to give the condition the pinning occurs under the general situation.

## 1 Preliminaries

Let $\mathbb{M}^\alpha = (P_x, X_t)$ be a symmetric $\alpha$-stable process on $\mathbb{R}^d$ with $0 < \alpha \le 2$ and $d \le 2\alpha$ (in particular, the case of $\alpha = 2$ means the Brownian motions). For a positive Radon measure $\mu$ belongs to Green tight Kato class (in notation $\mu \in \mathcal{K}_{d,\alpha}^\infty$), let $A_t^\mu$ be the positive continuous additive functional under the Revus correspondence. Where the above functional $A_t^\mu$ is a extension of $L_{0,t}$. And we define a Gibbs measure $P_{\beta,t}^\mu$ same as (1) by the $A_t^\mu$ and the law of $\alpha$-stable process.

From the large deviation principle, we can estimate the asymptotic behavior of $A_t^\nu/t$: for any $\kappa > 0$,

$$P_{\beta,t}^\mu\left(\frac{A_t^\nu}{t} > \kappa\right) \sim \exp\Big\{-t\inf_{z>\kappa} C_{\beta,N}^*(z)\Big\}, \quad \text{as } t\to\infty. \tag{2}$$

Where a function $C_{\beta,N}^*$ is a Fenchel-Legendre transform of $C_{\beta,N}(\lambda)$: $C_{\beta,N}^*(z) = \sup\{\lambda z - C_{\beta,N}(\lambda) | \lambda \in \mathbb{R}\}$

$$\begin{aligned} C_\beta(\lambda) &:= \lim_{t\to\infty}\frac{1}{t}\log E_x\left[\exp\{\beta A_t^\mu + \lambda A_t^\nu\}\right], \\ C_{\beta,N}(\lambda) &:= C_\beta(\lambda) - C_\beta(0). \end{aligned} \tag{3}$$

We set

$$\begin{aligned} \lambda_0(\beta) &= \sup\{\lambda\in\mathbb{R} | C_\beta(\lambda) = 0\}, \\ \beta_{cr} &= \sup\{\beta > 0 | C_\beta(0) = 0\}, \end{aligned}$$

and

$$z_0(\beta) = \frac{d}{d\lambda}C_\beta(\lambda)\Big|_{\lambda=0}.$$

The function $C_\beta(\lambda)$ is differentiable for every $\lambda$. So we can define this. The logarithmic moment generating function $C_\beta(\lambda)$ is called a rate function of the large deviation principle, and it coinside with the spectral bottom of Schrödinger operator $\mathcal{H}_{\mu,\nu}$[2]:

$$\begin{aligned} \mathcal{H}_{\mu,\nu}(\beta,\lambda) &= \frac{1}{2}(-\Delta)^{\frac{\alpha}{2}} - \beta\mu - \lambda\nu, \\ C_\beta(\lambda) &= -\inf\{\sigma(\mathcal{H}_{\mu,\nu}(\beta,\lambda))\}. \end{aligned}$$

In the case of the 1-dimensional Brownian motion and $\mu = \nu = \delta_0$, we can compute the rate function:

$$C_{\beta,N}(\lambda) = \begin{cases} \frac{1}{2}(\lambda^2 + 2\beta\lambda), & \lambda \ge -\beta \\ -\frac{1}{2}\beta^2, & \lambda < -\beta \end{cases}$$

and

$$C_{\beta,N}^*(z) = \begin{cases} \frac{1}{2}(z-\beta)^2, & z > 0 \\ \frac{1}{2}\beta^2, & z = 0 \\ \infty, & z < 0. \end{cases} \tag{4}$$

Therefore, polymer is pinned, for any $\beta > 0$. And $z_0(\beta) = \beta$, $\lambda_0(\beta) = -\beta$, $\beta_{cr} = 0$.

## 2 Main theorem

In this section, we fix measures $\mu, \nu \in \mathcal{K}_{d,\alpha}^\infty$.

**Theorem 2.1.** *If $\beta > \beta_{cr}$, then for any $0 < \kappa < z_0(\beta)$,*

$$\lim_{t\to\infty} P_{\beta,t}^\mu\left(\frac{A_t^\nu}{t} > \kappa\right) = 1. \tag{5}$$

*But for $0 < \beta \le \beta_{cr}$ and any $\kappa > 0$, the limit of (5) is not one.*

**Skech of the proof.**
By the (2), we see that the polymer is pinned if and only if a null set of $C_{\beta,N}^*$ is in $\mathbb{R}_+$. Note the null set as $\mathcal{N} = \{z > 0 | C_{\beta,N}^*(z) = 0\}$. In fact, $C_{\beta,N}(\lambda)$ is strictly increasing on $\{\lambda \ge \lambda_0(\beta)\}$ but $C_{\beta,N} \equiv 0$ otherwise, for each $\beta > 0$. This is a key point, and it implies following lemma.

**Lemma 2.1.** *For each $\beta$,*

$$\begin{aligned} \lambda_0(\beta) < 0 &\Longleftrightarrow \mathcal{N} = \{z_0(\beta)\}, \\ \lambda_0(\beta) \ge 0 &\Longleftrightarrow \mathcal{N} = \emptyset. \end{aligned}$$

Intuitively, the function $z_0(\beta)$ is increasing by the definition (3). Thus $z_0(\beta) > 0$ if $\beta$ is large enough. Precisely,

**Lemma 2.2.**

$$\begin{aligned} 0 < \beta \le \beta_{cr} &\iff \lambda_0(\beta) \ge 0, \\ \beta > \beta_{cr} &\iff \lambda_0(\beta) < 0. \end{aligned}$$

So we have the conclusion above.

**Remark 2.1.** *In general, if an underlying process is transient, then $\lambda_0(0) > 0$, otherwise $\lambda_0(0) = 0$. Thus in the recurrent case, $\beta_{cr} = 0$. That is, for any $\beta > 0$, the polymer is pinned when the recurrent case(The d-dimensional Brownian motion is recurrent if $d = 1, 2$, but transient $d \ge 3$). Because $\alpha$-stable process on $\mathbb{R}^2$ with $\alpha < 2$ is transient, so we can chose $\beta_{cr} > 0$.*

## References

[1] K. S. Alexander, V. Sidoravicius, Pinning polymers and interfaces by random potentials, Ann. Appl. Probab., **16**, no. 2, 636-669, 2006.

[2] M. Takeda, Asymptotic properties of generalized Feynman-Kac functionals, *Potential Analysis* **9** 261-291, 1998.

# On some orbit spaces of prehomogenous vector spaces

Kazuaki Tajima
(Mathmatical Institute, Tohoku University, D3)
sa7m19@math.tohoku.ac.jp

## 1 What is Prehomogenous vector space?

Let $k$ be an arbitrary field. Let $G$ be a connected reductive group, $V$ a representation of $G$, and $\chi$ a non-trivial rational character of $G$, all defined over $k$.

**Definition 1.1** (M.Sato)**.** A triple $(G, V, \chi)$ is called a **prehomogenous vector space (PV)** if the following two conditions are satisfied:

(1) There exists a Zariski open orbit.

(2) There exists a polynomial $\Delta \in k[V]$ such that $\Delta(gx) = \chi(g)^a \Delta(x)$ for some positive integer $a$.

If $V$ is irreducible, we may use the notation $(G, V)$ instead of $(G, V, \chi)$, because of the choice of $\chi$ is essentially unique. Furthermore, the set $V^{\mathrm{ss}} = \{x \in V; \Delta(x) \neq 0\}$ is well–defined (Where "ss" means "semi stable"). **Roughly speaking, a PV is a representation space of an algebraic group with a polynomial, so called relative invariant polynomial.**

**Example 1.2.** Put $G = \mathrm{GL}(1) \times \mathrm{GL}(2)$ and $V =$(the space of binary quadratic forms). For $g = (t, g_1) \in G, x = x(v) \in V$, we define $gx = tx(vg_1)$. Then the couple $(G, V)$ is a PV. Now we identitfy $V$ with $k^3$ via $k^3 \ni x = (x_0, x_1, x_2) \mapsto F_x(v) = x_0 v_1^2 + x_1 v_1 v_2 + x_2 v_2^2 \in V$. Under this identification, $gx$ is given by $F_{gx}(v) = tF_x(vg_1)$ for $g = (t, g_1) \in G, x \in V$. If we denote this representation by $\rho : G \to \mathrm{GL}(V)$, we have

(1) $T = \ker \rho = \{(t^{-2}, \left(\begin{smallmatrix} t & 0 \\ 0 & t \end{smallmatrix}\right)); t \in \mathrm{GL}(1)\}$,

(2) $P(gx) = \chi(g)P(x)$, where $P(x) = x_1^2 - 4x_0x_2$ and $\chi(g) = t^2(\det g_1)^2$.

## 2 Parametrization of fields

If $(G, V)$ be a (regular irreducible) PV, then $V_{\overline{k}}$ is a single $G_{\overline{k}}$–orbit in general. But $V_k$ is not necessarily a single $G_k$–orbit, and it is difficult and interesting problem to describe the orbit space $G_k \backslash V_k$ explicitly. In this section, we consider an arithmetical meaning of the orbit space of PV's.

In the rest of this section, we will assume $(G, V)$ as in Example 1.2. For $x \in V$, $k(x)$ denotes the splitting field of $F_x(v)$. Note that $F_x$ is separable over $k$ if and only if $x \in V_k^{\mathrm{ss}}$.

**Proposition 2.1** (Gauss)**.** For $x, y \in V_k^{\mathrm{ss}}, G_k x = G_k y$ if and only if $k(x) = k(y)$. Therefore, the map

$$\begin{array}{ccc} G_k \backslash V_k^{\mathrm{ss}} & \to & \{\text{separable extension of } k \text{ with deg} \leq 2\} \\ \cup & & \cup \\ G_k x & \mapsto & k(x) \end{array}$$

is well–defined and bijective.

*Proof.* Since "if" part is obvious, we only prove "only if" part.

(i) $k(x) = k$: Put $w = (0, 1, 0)$. Since $F_x$ splits in $k$ and $x \in V_k^{\mathrm{ss}}$, there exist $t, a, b, c, d \in k$ such that

$$F_x(v) = t(av_1 + cv_2)(bv_1 + dv_2), \quad t \neq 0, ad - bc \neq 0.$$

Therefore $x = (t, \left(\begin{smallmatrix} a & b \\ c & d \end{smallmatrix}\right))w$.

(ii) $[k(x) : k] = 2$ : We can assume $x_0 = y_0 = 1$. If $F_x$ and $F_y$ split in $k^{\mathrm{sep}}$ as

$$F_x(v) = (v_1 + \alpha_1 v_2)(v_1 + \alpha_2 v_2), \quad F_y(v) = (v_1 + \beta_1 v_2)(v_1 + \beta_2 v_2),$$

then $k(x) = k(\alpha_1), k(y) = k(\beta_1)$. So we have $k(\alpha_1) = k(\beta_1)$. Therefore, there exist $p \in k^\times, q \in k$ such that $\beta_1 = p\alpha_1 + q$. Since $v_1 + \beta_1 v_2 = (v_1\, v_2)\left(\begin{smallmatrix} 1 \\ \beta_1 \end{smallmatrix}\right) = (v_1\, v_2)\left(\begin{smallmatrix} 1 & 0 \\ q & p \end{smallmatrix}\right)\left(\begin{smallmatrix} 1 \\ \alpha_1 \end{smallmatrix}\right)$ and this conjugation is equal to $(v_1\, v_2)\left(\begin{smallmatrix} 1 \\ \beta_2 \end{smallmatrix}\right) = (v_1\, v_2)\left(\begin{smallmatrix} 1 & 0 \\ q & p \end{smallmatrix}\right)\left(\begin{smallmatrix} 1 \\ \alpha_2 \end{smallmatrix}\right)$, we have $y = (1, \left(\begin{smallmatrix} 1 & 0 \\ q & p \end{smallmatrix}\right))x$. This prove the proposition. □

Next we describe the structure of the stabilizer. For $x \in V_k^{\mathrm{ss}}$, $G_x^\circ$ denotes the identity component of $G_x$.

**Proposition 2.2.** (1) $[G_x : G_x^\circ] = 2$

(2) $G_x^\circ \cong \begin{cases} \mathrm{GL}(1) \times \mathrm{GL}(1) & \text{if} \quad k(x) = k \\ \mathfrak{R}_{k(x)/k}(\mathrm{GL}(1)) & \text{if} \quad [k(x) : k] = 2 \end{cases}$

Note that the "tamagawa number" of $G_x^\circ / T$ is constant multiple of $h_{k(x)} R_{k(x)}$ if $[k(x) : k] = 2$.

## 3 Application

The following type theorem is so called **density theorems**:

**Theorem 3.1** (Goldfeld–Hoffstein 1986)**.**

$$\lim_{X \to \infty} \frac{1}{X^{3/2}} \sum_{\substack{[F:\mathbb{Q}]=2 \\ 0 < -D_F < X}} h_F R_F = \frac{\pi}{36} \prod_p (1 - p^{-2} - p^{-3} + p^{-4})$$

$$\lim_{X \to \infty} \frac{1}{X^{3/2}} \sum_{\substack{[F:\mathbb{Q}]=2 \\ 0 < D_F < X}} h_F R_F = \frac{\pi^2}{36} \prod_p (1 - p^{-2} - p^{-3} + p^{-4})$$

The above theorem was first proved by using Eisenstein series of half–integral weight. In 1993, Datskovsky gave another proof based on the "zeta function" for the space of binary quadratic forms.

## References

[1] A.Yukie, Rational orbit decomposition of prehomogenous vector spaces (Lecture note), Available from http://www.math.tohoku.ac.jp/~yukie

**Weak Determinacy of Infinite Games and Corresponding Hierarchy of Inductive Definitions, Keisuke Yoshii, (D1)**

### The PURPOSE of this research is . . .

to investigate the logical strength of weak determinacy of infinite game from the standpoint of reverse mathematics.

### In Other Words . . .

How strong axiom is exactly needed to compute the winning strategy for certain game?

**What is the axiom $X$?!**

$X \vdash$ A winning strategy exists for game $G$.

•$\vdash$: "$T \vdash \varphi$" menas "$\varphi$ is provable from $T$."

**Reverse Mathematics Program:** a program to answer the next questions: *What set existence axioms are needed to prove the theorems of ordinary mathematics?*

### Examples of Axioms of $Z_2$ and equivalent Theorems

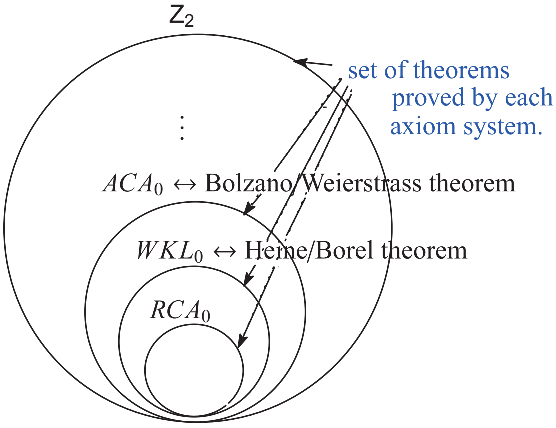


•$RCA_0, WKL, ACA, \dots, Z_2$: axiom systems of second order arithmetic, from weaker to stronger.
•$Z_2$: strongest axiom system.
• ↔: logical equivalence relation.

### Determinacy of Infinite Games

(i)Let $C \subseteq \mathbb{N}^{\mathbb{N}}$. Fix $A \in C$, set of infinite sequences of $\mathbb{N}$.
(ii)Player I and II alternately choose natural numbers as follows:

| | | | | | |
|---|---|---|---|---|---|
| I | $n_0$ | | $n_2$ | | . . . |
| II | | $n_1$ | | . . . | |

• player I wins if $n_0, n_1, n_2, \dots \in A$. (II wins o.w.)
•$C$-Game $G_A$ is determinate (det.) if one of the players has a winning strategy for $G_A$.

### Mathematical Meanings of game determinacy?

"A game is determinate" = "Some real number with some complexity exists"!

Indeed, each axiom in $Z_2$, g.e. $RCA_0, WKL, \dots$, also insists an existence of set of real number with some complexity.

### Some well-known facts on Det. of Games

⋆$Z_2 \nvdash$Borel($\Delta^1_1$) game is determinate.
⋆ZFC $\vdash$ Borel game is determinate.
⋆ZF+AD$\vdash$ any set of real numbers are Lebesgue measurable.
⋆ZFC + AD $\vdash 1 = 0$ (contradiction).

•$\nvdash$: "$T \nvdash \varphi$" menas "$\varphi$ is Not provable from $T$."
•ZFC: Zermelo/Fraenkle set theory+Axiom of Choice.
•When $A$ is a Borel set, $G_A$ is called Borel game.
•AD (axiom of determinacy): For any $A \subseteq \mathbb{N}^{\mathbb{N}}$, $G_A$ is determinate.

### Weak Determinacy of Games in $Z_2$

We consider "How strong axioms are needed to prove the det. of the following classes?" e.g. when $A \in \Sigma^0_1$,

$$?? \vdash \text{Game } G_A \text{ is determinate, (written as } \Sigma^0_1\text{-Det)}$$

Class on $\mathbb{N}^{\mathbb{N}}$ : $\Delta^0_1, \Sigma^0_1, \Sigma^0_2, \Sigma^0_2 \wedge \Pi^0_2, \dots$
⟶ (more complex)

### Inductive Definitions

**Definition 0.1.** $\Sigma^1_1$-ID asserts that for any $\Sigma^1_1$-operator $\Gamma$, there exists a pre-well-ordering set $W \subset \mathbb{N} \times \mathbb{N}$ on its field $F$ s.t.
(i)$\forall x \in F \quad W_x = \Gamma(W_{<x}) \cup W_{<x}$,
(ii)$\Gamma(F) \subset F$.

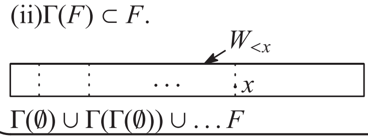


Following variations of inductive definitions have been considered.

**Definition 0.2.** $\Sigma^1_1$-IDTR:=transfinite iterations of $\Sigma^1_1$-ID.
$[\Sigma]^k$-ID:=$\Sigma^1_1$-ID with $k$-operators.
$[\Sigma^1_1]^k$-IDTR:=trans. iterat. of $\Sigma^1_1$-ID with $k$-operators.

### I.D. v.s. Det. of Games

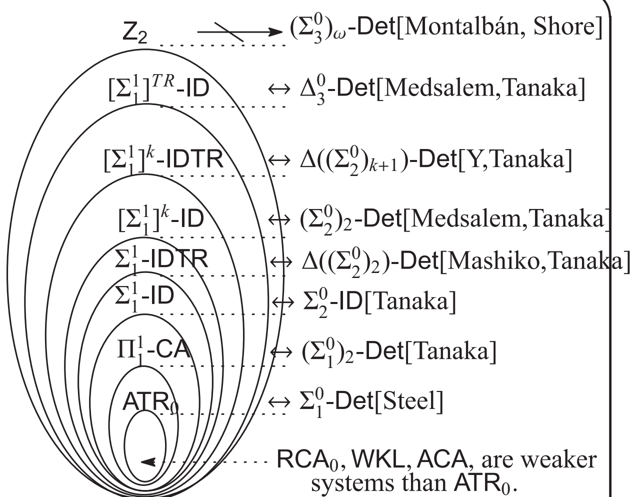

# Location of the concentration point in the ground-state solution of a reaction-diffusion equation in a heterogeneous medium

**Hiroko Yamamoto**

Mathematical Institute, Tohoku University

## 1 Introduction

Consider the Neumann problem for a semilinear elliptic equation:

$$\begin{cases} \varepsilon^2 \Delta u - a(x)u + b(x)u^p = 0 & \text{in } \Omega, \\ u(x) > 0 & \text{in } \Omega, \\ \dfrac{\partial u}{\partial \nu}\Big|_{\partial\Omega} = 0, \end{cases} \tag{1}$$

where $\Omega \subset\subset \mathbb{R}^n$, $\partial\Omega \in C^\infty$, and $\nu$ denotes the unit outward normal to $\partial\Omega$; $\varepsilon > 0$, $\Delta = \sum_{i=1}^n \partial^2/\partial x_i^2$; $a$, $b \in C^\alpha(\overline{\Omega})$; $\min_{x\in\overline{\Omega}} a(x)$, $\min_{x\in\overline{\Omega}} b(x) > 0$. Let the exponent $p$ satisfy $1 < p < (n+2)/(n-2)$ if $n \geq 3$, $1 < p < \infty$ if $n = 1, 2$.

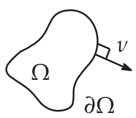


**Definition 1.** *An energy functional of* (1) *:*

$$J_\varepsilon(u) := \frac{1}{2}\int_\Omega \{\varepsilon^2 |\nabla u(x)|^2 + a(x)u(x)^2\}\,dx - \frac{1}{p+1}\int_\Omega b(x)u_+(x)^{p+1}\,dx$$

*where* $u_+(x) := \max\{u(x), 0\}$.

By the Mountain Pass Lemma, there exists a critical value $c_\varepsilon$ of $I_\varepsilon$. Let $u_\varepsilon \in H^1(\Omega)$ be a critical point for $c_\varepsilon$ (i.e. $c_\varepsilon = I_\varepsilon(u_\varepsilon)$). We call $u_\varepsilon$ a **ground-state solution** of (1).

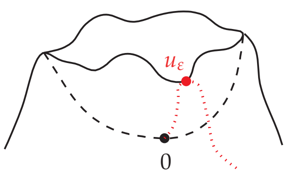


**Definition 2.** *A family of ground-state solutions* $\{u_\varepsilon\}_{\varepsilon>0}$ **concentrates at** $P_0 \in \overline{\Omega}$.

$\overset{\text{def}}{\Leftrightarrow}$ $^\exists\{\varepsilon_j\}_{j\in\mathbb{N}}$ $(\varepsilon_j > 0)$, $^\exists\{P_j\}_{j\in\mathbb{N}} \subset \overline{\Omega}$ *s.t.*

(1) $\varepsilon_j \to 0$, $P_j \to P_0$,

(2) $\max_{x\in\overline{\Omega}} u_{\varepsilon_j}(x) = u_{\varepsilon_j}(P_j)$,

(3) $I_{\varepsilon_j}(u_{\varepsilon_j}) = O(\varepsilon_j^n)$.

| **Known Results** | $a(x)$, $b(x)$ | Concentration Point |
|---|---|---|
| W.-M. Ni & I. Takagi ([1]) | $a(x) \equiv b(x) \equiv 1$, | Maximum Point of Mean Curvature of $\partial\Omega$. |
| X. Ren ([2]) | $a \equiv 1$,<br>$b \in C^\alpha(\overline{\Omega})$, $b(x) > 0$, | • $\max_\Omega b(x) > 2^{\frac{p-1}{2}} \max_{\partial\Omega} b(x)$<br>$\Rightarrow$ Max. Pt. of $b(x)$ in $\Omega$.<br>• $\max_\Omega b(x) < 2^{\frac{p-1}{2}} \max_{\partial\Omega} b(x)$<br>$\Rightarrow$ Max. Pt. of $b(x)$ on $\partial\Omega$. |

## 2 Main Results

**Theorem 3.** *A function* $\Phi$ *is given by*

$$\Phi(x) := a(x)^{\frac{2}{p-1}+1-\frac{n}{2}}\, b(x)^{-\frac{2}{p-1}}.$$

*Assume* $u_{\varepsilon_j}(P_j) = \max_{x\in\overline{\Omega}} u_{\varepsilon_j}(x)$, $P_j \to P_0$ *as* $\varepsilon_j \downarrow 0$. *Then:*

(i) $\min_{x\in\overline{\Omega}} \Phi(x) > \dfrac{1}{2}\min_{x\in\partial\Omega}\Phi(x) \Rightarrow P_0 \in \partial\Omega$, $\Phi(P_0) = \min_{x\in\Omega}\Phi(x)$.

(ii) $\min_{x\in\overline{\Omega}} \Phi(x) < \dfrac{1}{2}\min_{x\in\partial\Omega}\Phi(x) \Rightarrow P_0 \in \Omega$, $\Phi(P_0) = \min_{x\in\overline{\Omega}}\Phi(x)$.

**Quiz 4.** *Where on* $[0,1]$ *do you think* $u_\varepsilon$ *concentrates in the following case?* $(n = 1, p = 2)$

$$\begin{cases} a(x) = x + 0.03, \\ b(x) = x + 0.01. \end{cases}$$

$$\Rightarrow \Phi(x)^2 = a(x)^5 b(x)^{-4}.$$

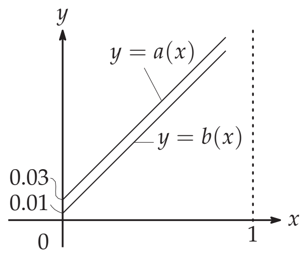


## 3 Background

A. Gierer and H. Meinhardt proposed the following reaction-diffusion system comprised of an activator $A = A(x,t)$ and an inhibitor $H = H(x,t)$ as the morphogenetic model of organisms:

$$\begin{cases} \dfrac{\partial A}{\partial t} = \varepsilon^2 \Delta A - \mu_a(x)A + \rho_a(x)\dfrac{A^p}{H^q} + \sigma_0(x) & \text{in } \Omega, \\ \tau\dfrac{\partial H}{\partial t} = D\Delta H - \mu_h(x)H + \rho_h(x)\dfrac{A^r}{H^s} & \text{in } \Omega. \end{cases} \tag{GM}$$

Change in cells begin at the place of higher activator concentration. Stationary solutions of the shadow system ($D = +\infty$, $\sigma_0 \equiv 0$) are given by $(A(x), H(x)) \equiv (\xi^{q/(p-1)}u(x), \xi)$, where $u$ solves

$$\varepsilon^2 \Delta u - \mu_a(x)u + \rho_a(x)u^p = 0.$$

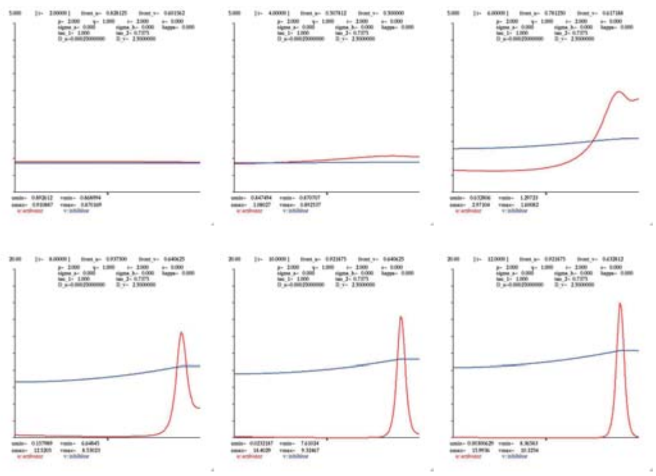

## References

[1] W.-M. Ni and I. Takagi, *Locating the peaks of least-energy solutions to a semilinear Neumann problem*, Duke Math. J. **67** (1993), 247–281.

[2] X. Ren, *Least-energy solutions to a non-autonomous semilinear problem with small diffusion coefficient*, Electron. J. Differential Equations **1993** (1993), No. 05, 1–21 (electronic only).

# Heat kernel estimates for Markov processes associated with perturbed Dirichlet forms

Masaki Wada*

February 20, 2012

## 1 Notations and definitions

- $(\mathscr{E},\mathscr{D}(\mathscr{E}))$: Dirichlet form on $L^2(\mathbb{R}^d)$ as follows:
  $\mathscr{E}(u,u)=\iint_{\mathbb{R}^d\times\mathbb{R}^d}(u(y)-u(x))^2J(x,y)dxdy$,
  $\mathscr{D}(\mathscr{E})=\{u\in L^2(\mathbb{R}^d)\ :\ \mathscr{E}(u,u)<\infty\}$
  $\frac{c_1}{|x-y|^d\phi(|x-y|)}\le J(x,y)=J(y,x)\le\frac{c_2}{|x-y|^d\phi(|x-y|)}$ for some positive constants $c_1$ and $c_2$.
  $\phi(r)=r^\alpha$ or $r^\alpha\exp(mr)\quad(0<\alpha<2,\ m>0)$
- $\mathscr{D}_e(\mathscr{E})$: extended Dirichlet space of $\mathscr{D}(\mathscr{E})$
- $\{P_t\}_{t\ge0}$: semigroup associated with $(\mathscr{E},\mathscr{D}(\mathscr{E}))$
- $\{X_t\}_{t\ge0}$: Hunt process associated with $(\mathscr{E},\mathscr{D}(\mathscr{E}))$
- $p(t,x,y)$: transition density function of $\{X_t\}$ or equivalently, the integral kernel of $\{P_t\}$.
- $G(x,y)=\int_0^\infty p(t,x,y)dt$.
- $\mu$: positive Radon smooth measure on $\mathbb{R}^d$
- $A_t^\mu$: positive continuous additive functional corresponding to $\mu$.
- $\mathscr{K}$: the set of Kato class measure

**Assumption 1.** *Dirichlet form $(\mathscr{E},\mathscr{D}(\mathscr{E}))$ is transient, that is, $G(x,y)<\infty$ for $x\ne y$.*

**Definition 2.** *Let $\mu$ be the positive Radon smooth measure. The measure $\mu$ belongs to $\mathscr{K}_\infty$ if $\mu\in\mathscr{K}$ and for arbitrary $\varepsilon>0$, there exist positive constant $\delta>0$ and compact set $K$ such that*
$\sup_{x\in\mathbb{R}^d}\int_{K^c\cup B}G(x,y)\mu(dy)<\varepsilon$
*where $B$ is an arbitrary set that satisfies $B\subset K$ and $\mu(B)<\delta$.*

In the sequel we consider $\mu\in\mathscr{K}_\infty$.

**Assumption 3.** *(i) The extended Dirichlet space $\mathscr{D}_e(\mathscr{E})$ is compactly embedded into $L^2(\mu)$.*

*(ii) $\iint_{\mathbb{R}^d\times\mathbb{R}^d}G(x,y)\mu(dx)\mu(dy)<\infty$.*

**Remark 4.** *From [8] it is known that (i) of Assumption 3 holds when $\phi(r)=r^\alpha$.*

## 2 Main result

Chen and the coauthors gave the two sided estimates of the transition density function $p(t,x,y)$ in [2, 3]. Here, we consider the Schrödinger form as follows:
$\mathscr{E}^\mu(u,u):=\mathscr{E}(u,u)-\int_{\mathbb{R}^d}u^2d\mu$
Denote the semigroup associated with $\mathscr{E}^\mu$ by $\{P_t^\mu\}$. Then, it is known that $\{P_t^\mu\}$ admits the integral kernel $p^\mu(t,x,y)$ defined on $(0,\infty)\times\mathbb{R}^d\times\mathbb{R}^d$ by [1]. We are going to consider the sufficient condition for $p^\mu(t,x,y)$ to have the same estimates as $p(t,x,y)$ does.

**Definition 5.** *The measure $\mu$ is called gaugeable if it holds that $\sup_{x\in\mathbb{R}^d}\mathbb{E}^x[\exp(A_\infty^\mu)]<\infty$.*

Set $h(x)=\mathbb{E}^x[\exp(A_\infty^\mu)]$. Since $h$ is $P_t^\mu$-excessive function, we can define $h$-transformed semigroup $\{P_t^{\mu,h}\}$ on $L^2(h^2dx)$. Moreover, following the arguments of [4, 7], we can describe the corresponding Dirichlet form $(\mathscr{E}^{\mu,h},\mathscr{D}(\mathscr{E}^{\mu,h}))$ as follows:
$\mathscr{E}^{\mu,h}(u,u)=\iint_{\mathbb{R}^d\times\mathbb{R}^d}(u(y)-u(x))^2J(x,y)h(x)h(y)dxdy$
$\mathscr{D}(\mathscr{E}^{\mu,h})=\mathscr{D}(\mathscr{E})$
Noting that $1\le h(x)\le c_3$ for some positive constant $c_3$, we can obtain the main result.

**Theorem 6.** *Suppose $\mu\in\mathscr{K}_\infty$ be gaugeable. Under Assumptions 1 and 3, $p^\mu(t,x,y)$ has the same two-sided estimates as $p(t,x,y)$ does.*

## References


[1] S. Albeverio, P. Blanchard, Z.-M. Ma: *Feynman-Kac semigroups in terms of signed smooth measures,* Inter. Series of Num. Math. 102, 1-31, (1991).

[2] Z.-Q. Chen, T. Kumagai: *Heat kernel estimates for jump processes of mixed types on metric measure spaces,* Probab. Theory Relat. Fields 140, 277-317, (2008).

[3] Z.-Q. Chen, P. Kim, T. Kumagai: *Global heat kernel estimates for symmetric jump processes,* Trans. Amer. Math. Soc. 363, 5021-5055, (2011).

[4] Z.-Q. Chen, T.-S. Zhang: *Girsanov and Feynman-Kac type transformations for symmetric Markov processes,* Ann. I. H. Poincarè -PR38, 475-505, (2002)

[5] M. Fukushima, Y. Oshima, M. Takeda: *Dirichlet forms and symmetric Markov processes,* De Gryuter Studies in Mathematics 19, second edition, (2011).

[6] M. Takeda: *Conditional gaugeability and subcriticality of generalized Schrödinger operators,* Journal of Funct. Analy. 191, 343-376, (2002).

[7] M. Takeda: *Gaugeability for Feynman-Kac functionals with applications to symmetric $\alpha$-stable processes,* Proc. Amer. Math. Soc. 134, 2729-2738, (2006).

[8] M. Takeda, K. Tsuchida: *Differentiability of spectral functions for symmetric $\alpha$-stable processes,* Trans. Amer. Math. Soc. 359, 4031-4054, (2007).


*Mathematical institute, Tohoku University. Mail : sb1d14@math.tohoku.ac.jp

# On the enhancements to the Milnor numbers of a class of mixed polynomials

**Kazumasa Inaba**

**(Mathematical Institute, Tohoku University, Sendai, Japan)**

sb0d02@math.tohoku.ac.jp

The enhancement to the Milnor number $\lambda(K)$ is an invariant of a fibered link $K$ on the 3-sphere $S^3$ defined via a vector field $\xi(K)$ on $S^3$ [1].

### Construction of $\xi(K)$

- On $N(K)$, it is homotopic to $r(\frac{\partial}{\partial\theta}) + (1-r^2)\frac{\partial}{\partial\phi}$ , where $N(K)$ is a tubular neighborhood of $K$ with coordinates $(r,\theta,\phi)$.
- On $E(K) := S^3 \setminus \mathrm{Int}N(K)$, it is a transverse field to the fiber surfaces of the fibration.
- On $K$, it is the tangent field of $K$.

### Definition of $\lambda(K)$

$$\lambda(K) := \mathrm{link}(\Delta^+(K), \Delta^-(K)) \in \mathbb{Z}$$

where $\Delta^{\pm}(K) = \{x \in S^3 \mid \xi(K)(x) = \pm t\psi(x), \quad t > 0\}$ and $\psi$ is a vector field which is homotopic to the tangent vector field of the Hopf fibration.

Remark.

We assume that $\xi(K)$ and $\psi$ are vector fields in general position, so $\Delta^{\pm}(K)$ are 1-manifolds in $S^3$.

In this poster, we study the following type of mixed polynomials

$$f(z,\bar{z}) := \prod_{j=1}^{m_+}(z_1^p + \alpha_j z_2^q)\prod_{j=m_++1}^{m_++m_-}\overline{(z_1^p + \alpha_j z_2^q)},$$

where $m_+ > m_-, \alpha_j \neq \alpha_{j'}$ $(j \neq j')$ and $\overline{z_1^p + \alpha_j z_2^q}$ represents the complex conjugate of $z_1^p + \alpha_j z_2^q$.

$f(\mathbf{z},\bar{\mathbf{z}})$ satisfies the strong non-degeneracy condition. M. Oka showed the existence of the Milnor's fibration under this condition [2]. Remark that $f(\mathbf{z},\bar{\mathbf{z}})$ is a special case of forms $(f\bar{g}, O)$ studied by A. Pichon and J. Seade [3, 4].

Thus $K_f := S^3_\varepsilon \cap f^{-1}(0)$ is an oriented fibered link in $S^3_\varepsilon$ centered at the origin $O \in \mathbb{C}^2$ of radius $\varepsilon$.

The main theorem is the following:

> **Main Theorem** For any $k \in \mathbb{Z}$, there exists a mixed polynomial $f(\mathbf{z},\bar{\mathbf{z}})$ whose Milnor fibration $f/|f| : S^3_\varepsilon \setminus K_f \to S^1$ satisfies $\lambda(K_f) = k$.

### The sketch of the proof

The proof of Main Theorem consists of the following two steps.

### [1] Construction of $\xi(K_f)$

The fibration is produced by the $S^1$-action on $S^3_\varepsilon$ given by $(z_1, z_2) \mapsto (s^q z_1, s^p z_2)$ with parameter $s \in S^1$.

Let $B$ be the orbit space of $S^3_\varepsilon$ under the $S^1$-action. To construct $\xi(K_f)$, we prepare a vector field $\eta(K_f)$ on $B$ as follows.

- The North and South poles are repellor points.
- There exist $m_+ + m_-$ mutually disjoint disks on $B$ and, on each disk, $\eta(K_f)$ has exactly one attractor point and one saddle point.
- $\eta(K_f)$ has no zero outside these disks, $N$ and $S$.

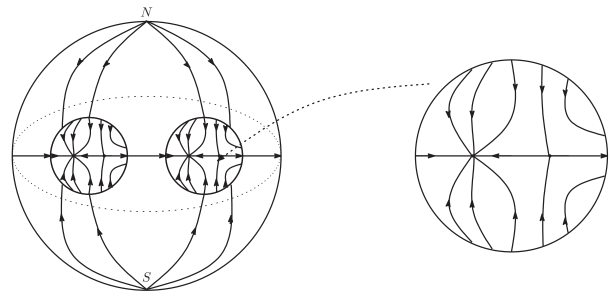


Figure 1: The vector field $\eta(K_f)$ and a 2-disk which has one attractor and one saddle point

Now we construct $\xi(K_f)$ as follows. On $N(K_f)$, set $\xi(K_f)$ such that it satisfies the following properties:

- The image of $N(K_f)$ by the orbit map is a union of disjoint 2-disks $D_1^2, \ldots, D^2_{m_++m_-}$ each of which has only one attractor point.
- The image of $\xi(K_f)$ by the orbit map is $\eta(K_f)$ on $D_1^2, \ldots, D^2_{m_++m_-}$.

On $E(K_f)$, $\xi(K_f)$ is constructed by a perturbation of $\psi$ such that it is transverse to the fiber surfaces and its image by the orbit map is $\eta(K_f)$ on $B \setminus \bigcup_{j=1}^{m_++m_-} D_j^2$.

### [2] Calculation of $\lambda(K_f)$

By the construction of $\xi(K_f)$, $\Delta^+(K_f)$ and $\Delta^-(K_f)$ are the preimages of zero points of $\eta(K_f)$.

We set

$\Delta_N^+, \Delta_S^+, \Delta^+_{\mathrm{saddle}}$ : the link components of $\Delta^+(K_f)$ corresponding to $N, S$ and the saddle points.

$K^+, K^-$ : the link corresponding to the holomorphic (resp. anti-holomorphic) factors of $f(\mathbf{z},\bar{\mathbf{z}})$.

Then $\Delta^+(K_f) = \Delta_N^+ \cup \Delta_S^+ \cup \Delta_{\mathrm{saddle}} \cup K^+$ and $\Delta^-(K_f) = -K^-$. Thus $\lambda(K_f)$ can be calculated as follows:

$$\begin{aligned}\lambda(K_f) &= \mathrm{link}(\Delta_N^+ \cup \Delta_S^+ \cup \Delta^+_{\mathrm{saddle}} \cup K^+, -K^-)\\ &= pm_- + qm_- - pq(m_+ + m_-)m_- + pqm_+m_-\\ &= (-pqm_- + p + q)m_-.\end{aligned}$$

We can check that $\lambda(K_f)$ realize all integers less than 2. The remaining integers can be realized by the mirror images of $K_f$.

## References

[1] W. Neumann and L. Rudolph, Difference index of vectorfields and the enhanced Milnor number, Topology, **29** (1990), 83–100.

[2] M. Oka, Non-degenerate mixed functions, Kodai Math. J., **33** (2010), 1–62.

[3] A. Pichon Real analytic germs $f\bar{g}$ and open-book decompositions of the 3-sphere, Internat. J. Math., **16** (2005), 1–12.

[4] A. Pichon and J. Seade, Fibered multilinks and real singularities $f\bar{g}$, Math. Ann., **324** (2008), 487–514.

# On the formal group of the Jacobian

Tomonori Nakayama
Mathematical Institute, Tohoku University

## Formal Group

Let $R$ be a commutative ring with the identity.
Let $X = (x_1, x_2, ..., x_g)$ and $R[[X]]$ be the ring of formal power series with coefficients in $R$.

$$F(X,Y) = (F_1(X,Y), ..., F_g(X,Y)), F_i(X,Y) \in R[[X,Y]]$$

is a formal group (or a group law) over $R$ if it satisfies (1) and (2).

$$(1) \quad F(Z,0) = F(0,Z) = Z$$
$$(2) \quad F(F(X,Y),Z) = F(X,F(Y,Z))$$

## Examples of (a one-parameter) Formal Group

The additive formal group:

$$\mathbb{G}_a(x,y) = x + y$$

The multiplicative formal group:

$$\mathbb{G}_m(x,y) = (x+1)(y+1) - 1$$

For $f(x) \in R[[x]]$ such that $f(x) = ex + \cdots$ ($e$ is a unit in $R$), $F(x,y) = f^{-1}(f(x) + f(y)) \in R[[x,y]]$ is a formal group over $R$.

## Elliptic Curve

An elliptic curve $E$ over a field $K$ is a nonsingular projective cubic curve, defined over $K$, with a $K$-rational point. $P = (x_1, \cdots, x_n)$ is a $K$-rational point if $\forall i, x_i \in K$. We write $P \in E(K)$ if $E(P) = 0$.
An elliptic curve over $\mathbb{Q}$ can be expressed in Weierstrass form $\acute{E}$:

$$\acute{E} : y^2 + a_1xy + a_3y = x^3 + a_2x^2 + a_4x + a_6 (a_i \in \mathbb{Q})$$

and by taking the minimal model of $\acute{E}$, $a_i$ will be in $\mathbb{Z}$.
In general, a line through $E$ meets $E$ at $3$ points. By using this fact, we can define an addition on an elliptic curve and the points on $E$ form a group. This addition can be expressed as a formal group.

## Honda's Theorem(1968)

Let $E$ be an elliptic curve over $\mathbb{Q}$, $E_w$ be the Weierstrass minimal model of $E$, $E_p = E_w \mod p$ for a prime number $p$, and $E(x,y)$ be the formal group(A) given by the group law of $E$. For each prime number $p$, $L_p$ is defined as:

$$L_p = \begin{cases} (1 - a_p p^{-s} + p^{1-2s})^{-1} & \text{if } E_p \text{ is of genus one;} \\ (1 - \varepsilon_p p^{-s})^{-1} & \text{if } E_p \text{ has an ordinary double point;} \\ 1 & \text{if } E_p \text{ has a cusp.} \end{cases}$$

where $a_p = p + 1 - \#E(\mathbb{F}_p)$, and $\varepsilon_p = 1$ if the tangents at the double point are rational over $\mathbb{F}_p$ and $\varepsilon_p = -1$ if not. $a_n$, $l(x)$, $L(x,y)$ are defined as:

$$\sum_{n=1}^{\infty} a_n n^{-s} = \prod_{p \in S} L_p(s)$$

$$l(x) = \sum_{n=1}^{\infty} n^{-1} a_n x^n$$

$$L(x,y) = l^{-1}(l(x) + l(y))$$

Let $S$ be any set of prime numbers which does not contain $2$ (resp. $3$) if $E_2$ (resp. $E_3$) has genus one with $a_2 = \pm 2$ (resp. $a_3 = \pm 3$), and $\mathbb{Z}_S = \bigcap_{p \in S}(\mathbb{Z}_p \cap \mathbb{Q})$. Then

$$L(x,y) \text{ is a formal group(B) over } \mathbb{Z}$$

$$L(x,y) \cong E(x,y) \quad \text{over } \mathbb{Z}_S$$

*The restriction about $S$ is removed by his paper in 1970.
In this theorem, there are two ways of the construction of a formal group; (A) and (B).

## Hyperelliptic Curve

Let $K$ be a field, $g \geq 1$ be an integer and let $h(x)$ and $f(x)$ be polynomials with coefficients in $K$ such that $\deg f = 2g + 1$ and $\deg h \leq g$. Assume $f$ is monic. The curve $C$ given by the equation

$$C : y^2 + h(x)y = f(x)$$

is a hyperelliptic curve of genus $g$ if it is nonsingular for all $x, y \in K$.
If $g = 1$, $C$ is an elliptic curve. So the hyperelliptic curve is a generalisation of the elliptic curve.
If $g \geq 2$, a line meets $C$ at more than $3$ points, so we cannot define the addition on $C$ like an elliptic curve. Instead, we use the divisor.

## Jacobian Variety

Let $C$ be a hyperelliptic curve defined over a field $K$. For each point $P \in C(\bar{K})$, define a formal symbol $[P]$. A divisor $D$ on $C$ is a finite linear combination of such symbols with integer coefficients:

$$D = \sum_j a_j [P_j], \quad a_j \in \mathbb{Z}$$

Let $f$ be a function on $C$. We define the degree of a divisor and the divisor of $f$ by

$$\deg(\sum_j a_j[P_j]) = \sum_j a_j (\in \mathbb{Z})$$

$$div(f) = \sum_{P \in C(\bar{K})} ord_P(f)[P]$$

The divisor of a function on $C$ is called a principal divisor. It is known that the degree of a principal divisor is always zero.

The group of divisors of degree $0$ modulo principal divisors is called the Jacobian variety $J$ of $C$.

## Generalisation of Honda's Theorem (Freije (1993), Sairaiji (2010))

Let $C$ be a complete nonsingular algebraic curve of genus $g$ over a field $K$ of $ch(K) = 0$. Assume $P$ is a $K$-rational point on $C$ which is not a Weierstrass point. Choose a basis $\eta_1, \cdots, \eta_g$ for the space of the holomorphic differentials of $C$ such that the $K$-expansion of $\eta_i$ with respect to the parameter $t$ satisfies

$$\eta_i \equiv (-t)^{i-1} \quad \text{mod } t^g dt$$

Let $l_i(t) = \int \eta_i$ satisfying $l_i(0) = 0 (1 \leq i \leq g)$ and let $S(X) = (s_1(X), \cdots, s_g(X))$ where $s_i(X)$ is the $i$th symmetric function on $g$ letters. Define $L(X) = (L_1(X), \cdots, L_g(X))$ by

$$L_i(S(T)) = l_i(t_1) + \cdots + l_i(t_g)$$

Then the formal group of $J$, $\hat{J}$, is:

$$\hat{J} = L^{-1}(L(X) + L(Y))$$

Freije showed that the formal group of $J$ can be constructed by using the expansion of a holomorphic differential of $J$ by a local parameter at the zero. This is a generalisation of a formal group(B) of Honda's theorem. She also proved that $\hat{J}_i(X,Y) \in \mathbb{Z}_p[[X,Y]]$ for all primes $p \notin S$, where $S$ is some finite set of primes, in the case of the modular curve $X_0(l)$ ($l$ a prime).

In his 2010 paper, Sairaiji constructed a formal group $\hat{J}$ by expanding the addition formula of $J$ by a system of local parameters at the zero of $J \times J$ in the case of the hyperelliptic curve and showed that the ring generated by the coefficients of $\hat{J}$ is essentially generated over $\mathbb{Z}$ by the coefficients of $C$. This is a generalisation of a formal group(A) of Honda's theorem.

# On the density of some sequences of integers

**Rena Tateda**
Mathematical Institute, Tohoku University

February 21, 2012

## 1 Notation and Definition of Density

Let $n = p_1^{\alpha_1} \cdots p_r^{\alpha_r}$ be the prime factorization of a positive integer $n$.

**Def 1.1.** Define the **excess** of $n$ be $(\alpha_1 - 1) + \cdots + (\alpha_r - 1)$.
An integer with excess 0 is said to be **square-free**.

Let $A$ denote $\mathbb{Z}$ or $\mathbb{F}_q[x]$ for some prime power $q = p^e$ and $K$ denote the fraction field of $A$. Define

$$\begin{aligned} \mathrm{Box} &= \mathrm{Box}(B_1, ..., B_l) \\ &:= \{(a_1, ..., a_l) \in A^l; |a_i| \le B_i \text{ for all } i\}. \end{aligned}$$

For $E \subseteq A^l$, define that the density of $E$ is the limit (if it exists)

$$\mu(E) := \lim_{B_1,...,B_l \to \infty} \frac{\#(E \cap \mathrm{Box})}{\#\mathrm{Box}}.$$

Also, define the density in weaker sense,

$$\mu_l(E) := \lim_{B_1,...,B_{n-1} \to \infty} \lim_{B_l \to \infty} \frac{\#(E \cap \mathrm{Box})}{\#\mathrm{Box}}.$$

This has the effect of considering only boxes in which the $l$th dimension is large relative to the others.

## 2 Density of $E_k \subset \mathbb{Z}$

Let $E_k$ denote a set of positive integers with excess $k$.
If $A = \mathbb{Z}$, the density of $E_k \subset \mathbb{Z}$ is the limit (if it exists)

$$\mu(E_k) = \lim_{n \to \infty} \frac{\#(E_k \cap \{1, 2, ..., n\})}{n},$$

which is the limiting "probability" that an integer from 1 to $n$ is in $E_k$.

**Thm 2.1.** (Rényi) *The set $E_k$ has a density $d_k$ and that the generating function of the sequence $\{d_k\}$ is given by*

$$\sum_{k=0}^{\infty} d_k z^k = \prod_{p:\text{prime}} \left(1 - \frac{1}{p}\right)\left(1 + \frac{1}{p - z}\right). \tag{1}$$

Substituring $z = 0$ into (1), we obtain the special case

$$d_0 = \prod_p \left(1 - \frac{1}{p^2}\right) = \frac{1}{\zeta(2)} = \frac{6}{\pi^2}, \tag{2}$$

which is well-known result that the density of square-free integers. Substituring $z = 1$ into (1), one sees that $\sum_k d_k = 1$, so that $d_k$ can be considered as elements of a probability distibution.

## 3 The analogue of Rényi's result

Let $f = \pi_1^{\alpha_1} \cdots \pi_l^{\alpha_l}$ be a monic polynomial with prime factorization, and define the excess of $f$ to be $(\alpha_1 - 1) + \cdots + (\alpha_r - 1)$, just as integers. Let $e_{l,k}$ be the number of monic polynomials of degree $l$ and excess $k$. Define $d_{l,k} = e_{l,k}/q^l$, which is the probability that a monic polynomial of degree $l$ has excess $k$. Then define the analogue of the density to be the limiting "probability" as

$$d_k = \lim_{l \to \infty} d_{l,k}. \tag{3}$$

Let $Nf = q^{\deg f}$ be the norm of $f$, which is the cardinality of the residue ring $\mathbb{F}_q[x]/(f)$.

**Thm 3.1.** (Morrison) *The generating function $D(z)$ of the sequence $\{d_k\}$ has a factorization over the prime polynomials given by*

$$\begin{aligned} D(z) &= \sum_{k=0}^{\infty} d_k z^k \\ &= \prod_{\pi:\text{prime}} \left(1 - \frac{1}{N\pi}\right)\left(1 + \frac{1}{N\pi - z}\right). \end{aligned} \tag{4}$$

## 4 Square-free Values over $A$

Now suppose $f(x) \in \mathbb{Z}[x]$ is a polynomial and let $E = E_0$ be the set of $n \in \mathbb{Z}_{\ge 0}$ for which $f(n)$ is square-free. Then one guesses that

$$\mu(E) = \prod_{p:\text{prime}} \left(1 - \frac{c_p}{p^2}\right), \text{ where } c_p := \#\{n \in [0, p^2 - 1] \ ; \ p^2 | f(n)\}$$

When $\deg f \le 3$, this guess is corrent. For general $f$ with $\deg f \ge 4$, it's unknown whether this is corrent. But Granville and Poonen showed the following theorems.

**Thm 4.1.** (Square-free values over $\mathbb{Z}$) *Assume the abc-conjecture. Let $f \in \mathbb{Z}[x_1, ..., x_l]$ be a polynomial that square-free as an element of $\mathbb{Q}[x_1, ..., x_l]$ and suppose that $x_l$ appears in $f$. For each prime $p$, let*

$$E_f := \{a \in \mathbb{Z}^l \ ; \ f(a) \text{ is square-free}\},$$

$$c_p := \#\{x \in (\mathbb{Z}/p^2)^l \ ; \ f(x) = 0 \text{ in } \mathbb{Z}/p^2\}.$$

*Then the density of $E_f$ is*

$$\mu_l(E_f) = \prod_p \left(1 - \frac{c_p}{p^{2l}}\right). \tag{5}$$

**Remark** This time the *abc*-conjecture is used to bound the number of polynomial values divisible by the square of a large prime.

**Thm 4.2.** (Square-free values over $\mathbb{F}_q[t]$) *Let $A = \mathbb{F}_q[t]$. Let $f \in A[x_1, ..., x_l]$ be a polynomial that square-free as an element of $K[x_1, ..., x_l]$. For each non-zero prime $\mathfrak{p} \subset A$, let*

$$E_f := \{a \in A^l \ ; \ f(a) \text{ is square-free}\},$$

$$c_{\mathfrak{p}} := \#\{x \in (A/\mathfrak{p}^2)^l \ ; \ f(x) = 0 \text{ in } A/\mathfrak{p}^2\}.$$

*Then the density of $E_f$ is*

$$\mu(E_f) = \prod_{\mathfrak{p}} \left(1 - \frac{c_{\mathfrak{p}}}{|\mathfrak{p}|^{2l}}\right). \tag{6}$$

## 5 Square-free Values over function fields

**Thm 5.1.** (Square-free Values over other rings of functions) *Let $S$ be a finite nonempty set of closed points of smooth, projective, geometrically integral curve $X$ over $\mathbb{F}_q$. Define the affine curve $U := X \backslash S$, and let $A$ be the ring of regular functions on $U$. Then there is the analogous result of* Thm4.2.

The proof of Thm5.1 is the analogue of the proof of Thm4.2.

### References

1. B. Poonen. Squarefree values of multivariable polynomials, Duke Math. J. 118(2003), no.2, 353-373.

2. K. E. Morrison. The polynomial analogue of a theorem of Rényi, Amer. Math. Sci. 133(2005), no.10, 2897-2902.

# Homogeneous Reinhardt domains of Stein in the comlex n-space

**Kouichi Kimura**

**Mathematical Institute,Tohoku University**

## Algebraic isomorphisms

An analytic automorphism $(z_i) \longmapsto (w_i)$ of $(\mathbb{C}^*)^n$ is called an algebraic automorphism, if whose components are given by Laurent monomials, that is, of the form

$$w_i = \alpha_i \, z_i{}^{a_{i1}} \cdots z_n{}^{a_{in}} \qquad (1 \leq i \leq n)$$

where $(a_{ij}) \in GL(n, \mathbb{Z})$ and $(\alpha_i) \in (\mathbb{C}^*)^n$.

Suppose $D_1$ and $D_2$ are domains in $\mathbb{C}^n$ and an analytic isomorphism $\varphi : D_1 \longmapsto D_2$ is induced by an algebraic automorphism. Then the isomorphism $\varphi$ is said to be an algebraic isomorphism, and two domains $D_1$, $D_2$ are called algebraically equivalent.

## Bounded Reihardt domains

A domain in $\mathbb{C}^n$ is called a Reinhardt domain, if it is stable under rtations around the coodinate axis. As is well known, Poincaré showed that there is no analytic isomorphism of the polydisc to the unitball in $\mathbb{C}^2$. By the way, both of them are Reinhardt domains. This is sharp contrast to the Riemann mapping theorem in $\mathbb{C}$, i.e. analytic isomorphisms of several complex variables are considered to be high rigid. Sunada and Shimizu generalized by far over the Poincaré example:

**Theorem 1. (Shimizu)** Two bouded Reinhardt domains in $\mathbb{C}^n$ are holomorphically equivalent, if and only if they are algebracally equivalent.

## Homogeneous Reinhardt domains

Unfortunately it is difficult to generalize Theorem 1 in unbounded Reinhardt domains, because in such a case we cannot use the classical Cartan theorem. And so, extending algebraically equivalence to unbounded cases, we want to classify homogeneous Rreinhardt domains of Stein. This classification is conjectured to be as follows:

**Conjecture 1.** For a homogeneous Reinhardt domain $D$ to be Stein in $\mathbb{C}^n$, there exist integers $n_1, \cdots, n_k$ and non-negative integers $l, m$ with $n_1 + \cdots + n_k + l + m = n$ such that

$$D \overset{alg}{\cong} B_{n_1} \times \cdots \times B_{n_k} \times \mathbb{C}^l \times (\mathbb{C}^*)^m,$$

where $B_{n_i}$ is the comlex $n_i$-unit ball.

Shimizu proved this conjecture in the case of which $D$ is bounded, but in the unbounded case it is still remains. The next result in my master's thesis is a partial solution of the problem in the latter case. I announced it in Several Complex Variables Winter Seminar 2011 at Hiroshima.

**Theorem 2.** If a Reinhardt domain $D$ in $(\mathbb{C}^*)^n$ is homogeneous and Stein, then the domain $D$ is identified with $(\mathbb{C}^*)^n$.

## Future study

Now I shall reseach on Conjecture 1 under the opposite condition to it of Theorem 2, that is, assume a domain contains the origin. In addition, for the sake of simplicity, let the complex dimension be equal to 3:

**Conjecture 2.** For a homogeneous Reinhardt domain $D$ in $\mathbb{C}^3$ that is Stein and contains the origin, there exist non-negative integers $n_1$, $n_2$, $n_3$ and $m$ with $n_1+n_2+n_3++m = 3$ such that

$$D \overset{alg}{\cong} B_{n_1} \times B_{n_2} \times B_{n_3} \times \mathbb{C}^m$$

where $B_{n_i}$ is the comlex $n_i$-unit ball.

I think the notion of Liouville foliation, which was introduced by Shimizu in order to analize tube domains, would play a key role in a solution.

**Definition 1.** Let $M$ be a complex manifold. A collection $\{\Sigma_\alpha\}_{\alpha \in A}$ of subsets of $M$ is called a Liouville foliation on $M$ if the following conditions are satisfied:

(L1) If $\alpha_1 \neq \alpha_2$ , then $\Sigma_{\alpha_1} \cap \Sigma_{\alpha_2} = \phi$;

(L2) $\underset{\alpha \in A}{\cup} \Sigma_\alpha = M$;

(L3) For each $\Sigma_\alpha$, any bounded holomorphic function on $M$ takes a constant value on $\Sigma_\alpha$;

(L4) $\alpha_1, \alpha_2 \in A$ with $\alpha_1 \neq \alpha_2$, there exists a bounded holomorphic function $h$ on $M$ such that the constant values of $h$ on $\Sigma_{\alpha_1}$ and $\Sigma_{\alpha_2}$ are different.

In the above definition, if we exchange 'holomorphic' for 'plurisubharmonic', then a Liouville foliation is said to be a plurisubhamonic Liouville foliation. Furthermore, we can fuse these tow notions for the foliations on $M$: Suppose a mapping $h = (f_1, \cdots, f_p, g_1, \cdots, g_q) : M \to \mathbb{C}^p \times \mathbb{R}^q$ satisfies following conditions:

(1) $f_i : M \to \mathbb{C}$ is a bounded holomorphic function,

(2) $g_j : M \to \mathbb{R}$ is a bounded plurisubharmonic function.

Then h is called a Liouville mapping of type $(p, q)$. By this, we can think of Liouville foliation with type $(p, q)$ in the same way.

# Calibrated Submanifolds

Kotaro Kawai
Mathematical Institute, Tohoku University

## SYZ Conjecture

Mirror symmetry is a mysterious relationship between pairs of Calabi-Yau 3-folds $X, \hat{X}$. It was discovered by physicists working in string theory.

SYZ Conjecture explains mirror symmetry in terms of dual fibrations $f : X \to B, \hat{f} : \hat{X} \to B$ with special Lagrangian fibers.

Similar statement also holds for pairs of $G_2$ manifolds in terms of dual coassociative fibrations.

## Calibrated Geometry

**Definition .** *Let $(M, g)$ be an $m$-dim Riemannian manifold and $\varphi$ be the closed $k$-form on $M$ ($1 \leq k \leq m$).*

*We say $\varphi$ is calibration on $M$ if for any $p \in M$ and any oriented $k$-dim subspace of $T_pM$ we have*

$$\varphi|_V \leq \mathrm{vol}_V.$$

*Let $N$ be the $k$-dim oriented submanifold of $M$. We say $N$ is a calibrated submanifold($\varphi$-submanifold) of $M$ if*

$$\varphi|_N = \mathrm{vol}_N.$$

**Examples**

| Hol($g$) ($\subset$) | U($m$) | SU($m$) | $G_2$ |
|---|---|---|---|
| $(M, g)$ | Kähler | Calabi-Yau | $G_2$ |
| $\varphi$ | $\omega^k/k!$ ($\omega$:Kähler form) | Re($\Omega$) ($\Omega$:hol. vol. form) | $\varphi \in \Omega^3$ $*\varphi \in \Omega^4$ ($\varphi$:$G_2$-structure) |
| $\varphi$-sub manifolds | $k$-dim complex submfds | special Lagrangian submfds | (co)associative submfds |

## Construction of Calibrated Submfds

We forus on that of SL submfds.

**Fact .** *Let $(M, J, \omega, \Omega)$ be an $m$-dim CY mfd and $L$ be a real $m$-dim oriented submfd of $M$.Then,*
*$L$ is a SL submfd of $M$ $\Leftrightarrow$ $\omega|_L = 0$ $(i.e.\ L : Lagrangian)$, $\mathrm{Im}\Omega|_L = 0$.*

From this fact, we know SL submfds are characterized by vanishing of forms. This fact is very useful for the construction.

◆Graph in $\mathbb{C}^m$

For any $f \in C^\infty(\mathbb{R}^m)$, $graph(df) \subset T^*\mathbb{R}^m = \mathbb{C}^m$ is a Lagrangian submfd.

Solving a second order elliptic PDE, we get SL submfds.

◆Evolution Equations in $\mathbb{C}^m$

Re($\Omega$) is "maximal" on SL submfds.

Let $P \subset \mathbb{C}^m$ be an $(m-1)$-dim submfd.

Solving ODE for $\{\phi_t : P \to \mathbb{C}^m\}_{t \in \mathbb{R}}$ to flow $\phi_t(P)$ in the direction in which Re($\Omega$) is "largest", we get SL submfds.

◆SL submanifolds with Large symmetry

Assume that a compact Lie group $G$ acts on a CY mfd $M$ preserving CY structure and there exists a moment map $\mu$ for the $G$-action.

Connected $G$-invariant Lagrangian submfds must be in the level set of $\mu$.

Find $G$-inv. SL submfds in the level set of $\mu$.

When $G = T^{m-1}$ and M is simply connected, there exists a $T^{m-1}$-inv. function $f \in C^\infty(M)$ and

$$(\mu, f) : M \to U \overset{open}{\subset} (\mathfrak{t}^m)^* \times \mathbb{R}$$

is a SL fibration.

**Remark .** *Similar methods can be considered for coassociative submfds from the following fact.*

**Fact .** *Let $(Y.\varphi)$ be a torsion-free $G_2$ mfd and $L$ be a 4-dim oriented submfd of $Y$. Then,*
*$L$ is a coassociative submfd of $M \Leftrightarrow \varphi|_L = 0$.*

**References**

[1] R. Harvey and H. B. Lawson : Calibrated geometries, Acta Mathematica 148 (1982),47-157.

[2] M. Ionel and M. Min-Oo : Cohomogeneity one special Lagrangian 3-folds in the deformed and the resolved conifolds. Illinois J. Math. 52 (2008), no. 3, 839-865.

[3] K. Kawai : Torus invariant special Lagrangian submanifolds in the canonical bundle of toric positive Kahler Einstein manifolds. Kodai Math. J. 34 (2011), no. 3, 519-535.

[4] A. Strominger, S.-T. Yau, and E. Zaslow : Mirror symmetry is T -duality, Nuclear Physics B479 (1996), no.1-2, 243-259.

# On Legendrian minimal submanifolds in Sasakian manifolds

Toru Kajigaya
Department of Mathematics, Tohoku University
email: sa9m09@math.tohoku.ac.jp

## Introduction

In 1990's, Y.-G.Oh introduced the notion of *Hamiltonian-minimal* (*H-minimal*) Lagrangian submanifolds in Kähler manifolds ([2]). This is a nice extension of the notion of *minimal* submanifold, and has been studied by many researchers. One of the main concern is H-stablity of an H-minimal Lagrangian submanifold in a specific Kähler manifold.

On the other hand, there is a notion of *Sasakian manifolds* which is an odd-dimensional counterpart of Kähler manifolds. In Sasakian manifolds, we consider *Legendrian-minimal* (*L-minimal*) Legendrian submanifolds which corresponds to H-minimal Lagrangian manifolds in Kähler manifolds. We call L-minimal Legendrian submanifolds *Legendrian-stable* (*L-stable*) if the second variation is non-negative for any Legendrian deformations. In this presentation, we mention some results for the construction and the L-stability of L-minimal Legendrian sumanifolds in specific Sasakian manifolds.

## Definition

An odd-dimensional Riemannian manifold $(M^{2n+1}, g)$ is called *Sasakian manifold* if its metric cone $(M \times \mathbf{R}_{>0}, r^2g + dr^2)$ admits a Kähler structure. A Sasakian manifold is a contact manifold with the contact structure $(\phi, \xi, \eta, g)$, where $\eta$ is a contact 1-form, $\xi$ is the characteristic vector field, $\phi$ is an $(1, 1)$-tensor.

**Definition 1.** *Let $(M^{2n+1}, \phi, \xi, \eta, g)$ be a Sasakian manifold, and $L^n$ a n-dimensional manifold.*

*(1) An immersion $\iota : L^n \to M^{2n+1}$ is called Legendrian $:\Longleftrightarrow \iota^*\eta = 0$.*

*(2) An Legendrian immersion $\iota$ is called L-minimal $:\Longleftrightarrow \mathrm{div}\phi H = 0$, where $H$ is the mean curvature vector of $\iota$.*

**Remark 1.** A deformation $\{\iota_t\}$ of $\iota$ is called *Legendrian deformation* if it preserves the Legendrian condition, *i.e.*, ${\iota_t}^*\eta = 0$. The L-minimal Legendrian immersion is a critical point of the volume functional under the Legendrian deformation. Thus the L-minimal immersion is an extension of minimal immersion.

A compact L-minimal immersion $\iota$ is called *Legendrian stable (L-stable)* if the second variation is non-negative for any Legendrian deformations.

## L-minimal immersion into $\mathbf{R}^{2n+1}(-3)$

The odd-dimensional Euclidean space admits the standard Sasakian structure. We denote this $\mathbf{R}^{2n+1}(-3)$.

**Theorem 1** ([1]). *Let $\iota : L^n \to \mathbf{R}^{2n+1}(-3)$ be a Legendrian immersion. Assume that $L^n$ lies in a cylinder*

$$N^{2n}_{\mathbf{x}_0}(r) := \{\mathbf{x} \in \mathbf{R}^{2n+1} | g(\mathbf{x} - \mathbf{x_0}, \mathbf{x} - \mathbf{x_0}) - \eta(\mathbf{x} - \mathbf{x_0})^2 = r^2\},$$

*where $\mathbf{x}_0 := (x^1_0, \cdots, x^n_0, y^1_0, \cdots, y^n_0, z_0)$ is a constant vector in $\mathbf{R}^{2n+1}$ and $r$ is a constant. If $\iota$ has the parallel mean curvature in $N^{2n}_{\mathbf{x}_0}$, then $\iota$ is L-minimal in $\mathbf{R}^{2n+1}(-3)$.*

In the case of $n = 1$, L-minimal Legendrian curve in $\mathbf{R}^3(-3)$ is the only the geodesic or the curve which is minimal in the cylinder. In general, an immersion into $\mathbf{R}^{2n+1}(-3)$ which lies in some cylinders and minimal in the cylinder is called *1-type*. By Theorem 1, we have

**Corollary 1.** *An 1-type Legendrian immersion is L-minimal.*

**Remark 2.** Similar result of Theorem 1 for H-minimal Lagrangian submanifolds in $\mathbf{C}^n$ was obtained by Y.-G.Oh in [2].

## L-minimal curves in 3-dim Sasakian space forms

A Sasakian manifold is called *Sasakian space form* if it has constant $\phi$-sectional curvature $(= c)$. We denote Sasakian space form $M^{2n+1}(c)$.

**Theorem 2** ([1]). *Let $\gamma$ be a compact L-minimal Legendrian curve in a 3-dimensional Sasakian space form $M^3(c)$. Then $\gamma$ is L-stable if and only if it satisfies $\lambda_1 \geq c + 3 + h^2$, where $\lambda_1$ is the first eigenvalue of the Laplace-Beltrami operator $\Delta$ acting on $C^\infty(\gamma)$, and $h$ is the curvature of $\gamma$.*

**Example 1** ([1]). (1) The 3-dimensional unit sphere $S^3(1)$ : All of closed L-minimal Legendrian curves in $S^3(1)$ are obtained by Schoen-Wolfson and Iriyeh:

$$\gamma(s) = \frac{1}{\sqrt{p+q}}\Big(\sqrt{q}e^{\sqrt{-1}\sqrt{\frac{p}{q}}s}, \sqrt{-1}\sqrt{p}e^{-\sqrt{-1}\sqrt{\frac{q}{p}}s}\Big), \ \ s \in [0, 2\pi\sqrt{pq}],$$

where $(p, q)$ is a pair of relatively prime positive number. They are torus knots of type $(p, q)$, and in the case of $(p, q) = (1, 1)$, it is minimal. By Theorem 2, *these curves are all L-unstable*.

(2) $\mathbf{R}^3(-3)$ : An L-minimal Legendrian curve in $\mathbf{R}^3(-3)$ is the only the geodesic $(h = 0)$ or the following:

$$\gamma(s) = \mathbf{x}_0 + \Big(\frac{2}{h}\cos hs, \frac{2}{h}\sin hs, -\frac{2}{h}s + \frac{1}{h^2}\sin 2hs + \frac{2y_0}{h}\cos hs\Big),$$

where $\mathbf{x}_0 = (x_0, y_0, z_0)$ and $s$ is the arc-length parameter. These curves are *helices*, and so *not periodic*. If we cut the curve with the length $l$, by Theorem 2, L-minimal curve in $\mathbf{R}^3(-3)$ is L-stable if and only if $0 \leq h \leq \pi/l$.

(3) The special linear group $SL(2, \mathbf{R}) = M^3(-7)$ : We choose a global coordinate $(x, y, \theta) \in \mathbf{R} \times \mathbf{R}^+ \times S^1$ of $SL(2, \mathbf{R})$ by the Iwasawa decomposition. Then L-minimal curves in $SL(2, \mathbf{R})$ are given by:

$$\gamma(s) = \Big(r\sin\mu(s) + x_0,\ r\Big(\frac{h}{2} - \cos\mu(s)\Big), \frac{\mu(s)}{2} - \frac{h}{2}s + \theta_0\Big),$$

where $r \in \mathbf{R}^+$ is a positive constant, $h$ is the curvature of $\gamma$, and the smooth function $\mu : \mathbf{R} \to \mathbf{R}$ is a solution of the ODE $\dot{\mu}(s) = h - 2\cos\mu(s)$. The above curve is closed if and only if $h = 2/\sqrt{1 - (m/k)^2}$ for some relatively positive integers $m, k \in \mathbf{Z}^+$ with $m/k < 1$. By Theorem 2, the closed curve is L-minimal if and only if $h = 2/\sqrt{1 - (1/k)^2}$. Thus *there exist an closed L-stable L-minimal curves in* $SL(2, \mathbf{R})$.

## Some relations between H-minimal Lagrangian submanifold and L-minimal Legendrian submanifold

The notion of L-minmal Legendrian submanifold is closely related to the notion of H-minimal Lagrangian submanifold. The following facts are known.

**Fact 1.** *Let $\pi : S^{2n+1}(1) \to \mathbf{C}P^n$ be the Hopf fibration, and $\bar{\iota} : \overline{L}^n \to \mathbf{C}P^n$ a Lagrangian submanifold. Then we have a Legendrian immersion $\iota : L^n \to S^{2n+1}(1)$ as the lift of $\bar{\iota}$. Moreover, $\iota$ is L-minimal if and only if $\bar{\iota}$ is H-minimal.*

**Fact 2.** *Let $\iota : L^n \to S^{2n+1}(1)$ be a Legendrian submanifold. Then the cone $C(L) := L^n \times \mathbf{R}_{>0}$ of $L^n$ is Lagrangian submanifold in $S^{2n+1} \times \mathbf{R}_{>0}$. Moreover $L$ is L-minimal if and only if $C(L)$ is H-minimal.*

**Remark 3.** We can generalize Fact 1 for the *canonical fibration* $\pi : M^{2n+1} \to \overline{M}^{2n}$. For example, $\pi : \mathbf{R}^{2n+1}(-3) \to \mathbf{C}^n$. We can generalize Fact 2 for any Sasakian manifolds.

## L-unstability Theorem for L-minimal immersion into the unit sphere

In $\mathbf{C}P^n$, it is known that there *exist* an compact *H-stable* H-minimal Lagrangian submanifold. For example, the Clifford torus and the parallel Lagrangian submanifold (which means Lagrangian submanifold with the parallel second fundamental form) are all H-stable. In contrast to this fact, we have the following theorem for L-minimal immersion into $S^{2n+1}(1)$:

**Theorem 3.** *There are no compact L-stable L-minimal Legendrian immersion into the unit sphere $S^{2n+1}(1)$.*

**Remark 4.** For the case of *minimal* Legendrian submanifolds in $S^{2n+1}(1)$, L-unstability theorem has been proven by H.Ono. The case of $n = 1$ follows from Theorem 2.

To prove Theorem 3, we find a Legendrian vector field along $\iota$ which gives the Legendrian deformation $\{\iota_t\}$ with $\frac{d^2}{dt^2}\mathrm{Vol}(\iota_t) < 0$.

## References

[1] T. Kajigaya, *Second variation formula and the stability of Legendrian minimal submanifolds in Sasakian manifolds*, preprint.

[2] Y. G. Oh, *Volume minimization of Lagrangian submanifolds under Hamiltonian deformations*, Math. Zeit. 212(1993), 175-192

# On elliptic surfaces related to Beilinson' s Tate conjecture

## $K_2(U)^{(2)}_{\mathbb{Q}_p}$ and $H^2_{\acute{e}t}(U_{\bar{k}}, \mathbb{Q}_p(2))^{G_k}$ are very important objects over a variety U !!

We consider the case that U is an open subscheme of an elliptic surface $\pi : E \to C$. Assume that $P_1, \dots, P_s \in C$ give all fibers of split type of $\pi : E \to C$. Put $D_i = \pi^{-1}(P_i)$, $D = \sum_{i=1}^{s} D_i$ and $U = E \setminus D$.

$$K_2(U)^{(2)}_{\mathbb{Q}_p} \xrightarrow{\ \partial_{\mathbb{Q}_p}\ } \bigoplus_{i=1}^{s} \mathbb{Q}_p[D_i]$$

$$K_2(U)^{(2)}_{\mathbb{Q}_p} \xrightarrow{\ c\ } H^2_{\acute{e}t}(U_{\bar{k}}, \mathbb{Q}_p(2))^{G_k} \xrightarrow{\ \partial_{\acute{e}t}\ } \bigoplus_{i=1}^{s} \mathbb{Q}_p[D_i].$$

The surjectivity of c is called "Beilinson' s Tate conjecture"

The surjectivity of c follows from the surjectivity of $\partial$

Considering the relation between them is a historical problem.

We present examples of an elliptic surface over a field k whose open subscheme U satisfies Beilinson' s Tate conjecture but the surjectivity of $\partial_{\mathbb{Q}}$ !!!

## Main Theorem

**Theorem** Let F be a field and ch(F) the characteristic of F. Set k = F(S), where S is an indeterminate element. Consider the rational elliptic surfaces defined by the Weierstrass forms over k(t)

$$E_1 : y^2 = x^3 + x^2 + tx + t(1 - S^2), \quad \text{if} \quad ch(F) \neq 2, 3$$

$$E_2 : y^2 = x^3 + (S^2 - 1)t^2x^2 + t^3(t - 1), \quad \text{if} \quad ch(F) = 3$$

$$E_3 : y^2 + xy = x^3 + S^2x^2 + t^2(S - t), \quad \text{if} \quad ch(F) = 2.$$

Then the map $\partial_{\mathbb{Q}} : K_2(U)^{(2)}_{\mathbb{Q}} \to \bigoplus_{i=1}^{s} \mathbb{Q}[D_i]$ is not surjective for the above rational elliptic surfaces.

Mariko OHARA : Department of Mathematics, Tohoku University
E-mail : sa9m08@math.tohoku.ac.jp

# The Law of the Iterated Logarithm (LIL) for $G$-Brownian Motion

Emi Osuka
Mathematical Institute, Tohoku University
(e-mail: sa9m06@math.tohoku.ac.jp)

Motivated by volatility uncertainty problems in finance, S. Peng introduced the notion of $G$-Brownian motion. Intuitively, $G$-Brownian motion is a Brownian motion whose variance is uncertain. The purpose of this study is a quasi-sure analysis of paths of $G$-Brownian motion.

**Notation**

- $\Omega := C_0([0,\infty);\mathbb{R})$
- $B$ : the canonical process of $\Omega$

A nonlinear heat equation

$$\frac{\partial u}{\partial t} - \frac{1}{2}\sup_{\gamma\in[\sigma_0,\sigma_1]}\left\{\gamma^2\frac{\partial^2 u}{\partial x^2}\right\} = 0 \quad \text{in } (0,\infty)\times\mathbb{R},$$

is called $G$-heat equation. Here $[\sigma_0,\sigma_1]$ is a given subset of $[0,\infty)$.

Using the viscosity solutions of $G$-heat equation, Peng [4] constructed a sublinear expectation, called $G$-expectation, under which $B$ becomes a $G$-Brownian motion; the given subset $[\sigma_0,\sigma_1]$ expresses the volatility uncertainty of $G$-Brownian motion.

Denis–Hu–Peng [1] proved that $G$-expectation can be represented as the supremum of the linear expectations with respect to martingale measures. The precise claim is as follows:

Let

$W$ : B.m. on a prob. sp. $(\Omega,\mathcal{F},P)$

$\mathcal{A}$ : the set of all $[\sigma_0,\sigma_1]$-valued prog. m'ble proc. on $[0,\infty)$

$P_\theta$ : the law of $\int_0^{\cdot}\theta_s\,dW_s,\quad \theta\in\mathcal{A}$

**Theorem.** (Denis–Hu–Peng [1])

$$\mathbb{E}[X] = \sup_{\theta\in\mathcal{A}} E_{P_\theta}[X]$$

Define a pair of capacities $(V,v)$ by

$$V(A) := \sup_{\theta\in\mathcal{A}} P_\theta(A),\quad v(A) := \inf_{\theta\in\mathcal{A}} P_\theta(A)\quad \text{for } A\in\mathcal{B}(\Omega).$$

A proposition holds quasi-surely if it holds outside a set $N$ with $v(N^c)=1$.

$\leadsto$ It becomes possible to investigate pathwise properties of $G$-Brownian motion.

## LIL for $G$-Brownian motion (Hariya–O. [3])

$$\sigma_0 \leqslant \limsup_{t\to\infty}\frac{B_t}{\sqrt{2t\log\log t}} \leqslant \sigma_1 \quad \text{quasi-surely.}$$

(The idea of the proof in [3])

**Time-change formula**

$\exists$ B.m. $\beta$ on $(\Omega,\mathcal{F},P)$ s.t.

$$\int_0^t\theta_s\,dW_s = \beta\left(\int_0^t\theta_s^2\,ds\right),\quad \forall t\geqslant 0,\ P\text{-a.s.}$$

Combining this with LIL for $\beta$, we have

$$P_\theta\left(\sigma_0\leqslant\limsup_{t\to\infty}\frac{B_t}{\sqrt{2t\log\log t}}\leqslant\sigma_1\right) = 1,\quad \forall\theta\in\mathcal{A}.$$

(Another proof)

LDP of Schilder's type for $G$-B.m.:

- upper bound of LDP for $\{V(\varepsilon B\in\cdot),\varepsilon>0\}$ (Gao–Jiang [2])
- lower bound of LDP for $\{v(\varepsilon B\in\cdot),\varepsilon>0\}$

⇓

Invariance principle of $G$-B.m. for LIL (Wu–Chen [5])

⇓

LIL for $G$-B.m.

## References

[1] L. Denis, M. Hu and S. Peng. Function spaces and capacity related to a sublinear expectation: Application to $G$-Brownian motion paths. *Potential Anal.*, 34:139–161, 2011.

[2] F. Gao and H. Jiang. Large deviations for stochastic differential equations driven by $G$-Brownian motion. *Stochastic Process. Appl.*, 120:2212–2240, 2010.

[3] Y. Hariya and E. Osuka. Pathwise properties of $G$-Brownian motion. *Preprint.*

[4] S. Peng. $G$-expectation, $G$-Brownian motion and related stochastic calculus of Itô type. *Stoch. Anal. Appl., Abel Symp.*, 2:541–567, 2007.

[5] P. Wu and Z. Chen. An invariance principle of G-Brownian motion for the law of the iterated logarithm under G-expectation. arXiv:1105.0135v1 [math.PR] 1 May 2011, 2011.

# Modified wave operator for the 2d nonlinear Schrödinger system with mass resonance


Kota Uriya
**Mathematical Institute, Tohoku University, Japan**
sa9m05@math.tohoku.ac.jp


## 1 Introduction

We study the asymptotic behavior of the solution to the following nonlinear Schrödinger system:

$$\text{(2-NLS)} \quad \begin{cases} i\partial_t u_1 + \dfrac{1}{2m_1}\Delta u_1 = \overline{u}_1 u_2, & t \in \mathbb{R},\ x \in \mathbb{R}^2, \\ i\partial_t u_2 + \dfrac{1}{2m_2}\Delta u_2 = u_1^2, & t \in \mathbb{R},\ x \in \mathbb{R}^2. \end{cases}$$

where $u_1(t,x),\ u_2(t,x) : \mathbb{R} \times \mathbb{R}^2 \to \mathbb{C}$ ; unknown complex valued functions. $m_1,\ m_2$ ; positive constants.

Weighted Sobolev spaces Let $s, m \in \mathbb{R}$,

$$H^{s,m} := \left\{ \psi \in \mathcal{S}' ; \|(1+|x|^2)^{m/2}(1-\Delta)^{s/2}\psi\|_{L^2} < \infty \right\}.$$

## 2 Known results (Single case)

Nonlinear Schrödinger equation:

$$\text{(NLS)} \qquad i\partial_t u + \frac{1}{2m}\Delta u = f(u), \quad t \in \mathbb{R},\ x \in \mathbb{R}^2.$$

- $f(u) = |u|^{p-1}u$ $\quad p > 2 : u(t) \sim e^{\frac{i}{2m}t\Delta}u_+$,
  $p \le 2 : u(t) \not\sim e^{\frac{i}{2m}t\Delta}u_+$.
  Barab ('84), Y. Tsutsumi-Yajima ('84).
- $f(u) = |u|u$ $\quad u(t) \sim e^{iS(t)}e^{\frac{i}{2m}t\Delta}u_+$,
  $S(t) := -m|\hat{u}_+(mx/t)|\log t$.
  Ozawa ('91), Ginibre-Ozawa ('93).
- $f(u) = u^2$ or $\overline{u}^2$ $\quad u(t) \sim e^{\frac{i}{2m}t\Delta}u_+$.
  Moriyama-Tonegawa-Y. Tsutsumi ('03).
- $f(u) = |u|^2$ $\quad u(t) \not\sim e^{\frac{i}{2m}t\Delta}u_+$.
  Shimomura ('05),
  Shimomura-Y. Tsutsumi ('06).

## 3 Results

**Theorem 1.** *Let $2m_1 = m_2$, $1 < \alpha < 2$. Then there exists $\varepsilon > 0$ with the following property:*
*For any $u_{1+}, u_{2+} \in H^{0,\alpha}$ with $|\hat{u}_{1+}(\xi)| = \sqrt{2}|\hat{u}_{2+}(\xi)|$ ($^\forall \xi \in \mathbb{R}^2$) and $\|\hat{u}_{1+}\|_{H^\alpha} + \|\hat{u}_{2+}\|_{H^\alpha} \le \varepsilon$, (2-NLS) has a unique global solution $(u_1(t), u_2(t)) \in (C([0,\infty); L^2))^2$ which satisfies the estimates*

$$\left\| u_1(t) + e^{\frac{it}{2m_1}\Delta}\widetilde{S}_1(t)u_{1+} \right\|_{L^2} + \left\| u_2(t) + e^{\frac{it}{2m_2}\Delta}\widetilde{S}_2(t)u_{2+} \right\|_{L^2} \le Ct^{-b}$$

*for all $t \ge 0$, where $\frac{1}{2} < b < 1$,*

$$\widetilde{S}_1(t) = \mathcal{F}^{-1}D(m_1)e^{\frac{1}{2}(\theta_0(\xi)+\sqrt{2}|\hat{u}_{1+}(\xi)|\log t)}\mathcal{F},$$
$$\widetilde{S}_2(t) = \mathcal{F}^{-1}D(m_2)e^{(\pi-\theta_0(\xi)+2|\hat{u}_{2+}(\xi)|\log t)}\mathcal{F}$$

*and $\theta_0(\xi) = -\arg \hat{u}_{1+}(\xi) + \frac{1}{2}\arg \hat{u}_{2+}(\xi)$.*

**Remark**. Hayashi-Li-Naumkin [1] constructed the modified wave operator with the special assumptions on both amplitude and argument of two scattering states. Theorem 1 shows that we are able to construct the modified wave operator without no restrictions on the argument of two scattering states. We introduce a new angular modification to show the result.

## 4 Free evolution operator

We introduce decomposition of the free evolution operator.

$$e^{\frac{it}{2m}\Delta} = M_m(t)D_m(t)\mathcal{F}M_m(t),$$

where $M_m(t)$ is the multiplication operator and $D_m(t)$ is the dilation operator defined as follows:

$$M_m(t)\phi(x) = e^{\frac{im|x|^2}{2t}}\phi(x),\ D_m(t)\phi(x) = \frac{m}{it}\phi\left(\frac{mx}{t}\right).$$

We have formal asymptotics of free Schrödinger equation:

$$e^{\frac{it}{2m}\Delta}\phi \sim M_m(t)D_m(t)\mathcal{F}\phi.$$

## 5 Outline of the proof

We prove

$$\Phi_1(u) = -i\int_t^\infty e^{\frac{i(t-\tau)}{2m_1}\Delta}\left(\overline{u}_1 u_2 - \overline{w_1}w_2\right)d\tau + \text{h.o.t.}$$

and

$$\Phi_2(u) = -i\int_t^\infty e^{\frac{i(t-\tau)}{2m_2}\Delta}\left(u_1^2 - (w_1)^2\right)d\tau + \text{h.o.t.}$$

are contraction mapping on

$$X := \left\{ \phi = (\phi_1, \phi_2) \in \left(C([T,\infty); L^2)\right)^2 ; \|\phi - w\|_X < \infty \right\}$$

with

$$(w_1, w_2) = (M_{m_1}(t)D_{m_1}(t)\mathcal{F}\widetilde{S}_1(t)u_{1+}, M_{m_2}(t)D_{m_2}(t)\mathcal{F}\widetilde{S}_2(t)u_{2+})$$

and

$$\|\phi\|_X := \sum_{j=1}^{2}\sup_{t\in[T,\infty)}\left( t^{\frac{\beta}{2}+\mu}\|\phi_j(t)\|_{L^2} + t^\mu \||J_{m_j}|^\beta \phi_j(t)\|_{L^2} \right),$$

where $1 < \beta < \alpha < 2$, $\alpha - \beta > \mu > 0$ and

$$|J_{m_j}|^\beta(t)\phi = e^{\frac{it}{2m_j}\Delta}|x|^\beta e^{-\frac{it}{2m_j}\Delta}\phi.$$

## References


[1] N. Hayashi, C. Li, P. I. Naumkin, *Modified wave operator for a system of nonlinear Schrödinger equations in 2d*, preprint.

# Leaf-wise intersections in coisotropic submanifolds

Satoshi Ueki

Department of Mathematics, Tohoku University

## Introduction

J. Moser defined the leaf-wise intersection which is motivated by perturbation theory of Hamiltonian systems. Perturbation theory is used to find an approximate solution to a problem which cannot solved exactly.

In this poster, we consider the existence of leaf-wise intersections.

## Definitions

$(P^{2n}, \omega)$ is called a *symplectic manifold* if $\omega$ is a nondegenerate closed 2-form on a $2n$-dimensional manifold $P$. A submanifold $M$ of $P$ is said to be *coisotropic* if $(T_pM)^\omega \subset T_pM$ holds for each $p \in M$, and is said to be *Lagrangian* if $(T_pM)^\omega = T_pM$. Here, $(T_pM)^\omega := \{v \in T_pP \mid \omega(v,w) = 0\ ({}^\forall w \in T_pM)\}$. For a function $H : P \to \mathbb{R}$, we define the *Hamiltonian vector field* $X_H$ by $i(X_H)\omega = dH$ and denote the flow of $X_H$ by $\phi_H^t$. A diffeomorphism $\psi : P \to P$ is called *Hamiltonian* if $\psi = \phi_H^1$ for some $H$ and we denote the set of Hamiltonian diffeomorphisms by $\mathrm{Ham}(P,\omega)$.

Let $M$ be a coisotropic submanifold of $P$ whose codimension is $r$. Then $(TM)^\omega \subset TM$ is a completely integrable distribution on $M$ of rank $r$. Therefore $(TM)^\omega$ defines a foliation on $M$ which is called the *characteristic foliation*. We denote the *leaf* of $(TM)^\omega$ through $p$ by $L_p$, namely $L_p$ is the maximal $r$-dimensional submanifold of $M$ through $p$ which is tangent to $(TM)^\omega$. Then $p \in M$ is called a *leaf-wise intersection* of $\psi \in \mathrm{Ham}(P,\omega)$ if $\psi(p) \in L_p$.

## Examples

1. $P = \mathbb{R}^{2n}$ with a 2-form $\omega_0 = \sum dx_j \wedge dy_j$ is a symplectic manifold. In this case, the orbits of a Hamiltonian vector field $X_H$ are nothing but the solutions of the Hamilton-Jacobi equations: $\dot{y} = -\frac{\partial H}{\partial x}, \dot{x} = \frac{\partial H}{\partial y}$.

2. Let $(P, \omega, H)$ be a Hamiltonian system and $(P, \omega, \tilde{H})$ be a perturbed system, namely $H$ and $\tilde{H}$ are very close to each other with their derivatives. We assume that the regular level set $M := H^{-1}(0)$ is compact and the orbits of $X_H$ on $M$ are all periodic with period $T > 0$. If $p \in M$ is a leaf-wise intersection of certain Hamiltonian diffeomorphism, then the orbit of $X_{\tilde{H}}$ through $p$ is periodic. Therefore, the existence of a leaf-wise intersection guarantees the existence of a periodic orbit for the perturbed system.

## The first existence theorem

Moser showed the following theorem for the existence of the leaf-wise intersections:

**Theorem 1** (Moser, 1978)**.** *Let $(P, \omega = d\lambda)$ be a simply connected exact symplectic manifold and $M$ be a compact coisotropic submanifold of $P$. If $\psi \in \mathrm{Ham}(P,\omega)$ is $C^1$-close to the identity $\mathrm{id}_P : P \to P$, then $\psi$ has at least $\mathrm{cat}(M)$ leaf-wise intersections. Here, $\mathrm{cat}(M)$ is the Lusternik-Schnirelmann category of $M$.*

We remark that the simply connectivity assumption can be replaced by the condition that $H^1(P,\mathbb{R}) = 0$.

## Main Theorem

We considered the another approach to the existence using a theorem by A. Weinstein and obtained the following:

**Theorem 2** (Main theorem)**.** *Let $(P,\omega)$ be a symplectic manifold and $M$ be a coisotropic submanifold of $P$. If $\psi \in \mathrm{Ham}(P,\omega)$ is $C^1$-close to the identity $\mathrm{id}_P : P \to P$, then there exist a closed 1-form $\Gamma$ on $M$ and an embedding $G : M \to P \times P$ so that $\mathrm{pr}_1 \circ G(p)$ is a leaf-wise intersection of $\psi$ for each $p \in \mathrm{Zero}(\Gamma)$. In particular, if $M$ is compact and $H^1(M,\mathbb{R}) = 0$, then $\psi$ has at least $\mathrm{cat}(M)$ leaf-wise intersections.*

Actually, it is sufficient that $\psi$ is defined on a neighborhood of $M$. So the assumptions on the ambient manifold $P$ are not essential. In this meaning, $H^1(M,\mathbb{R}) = 0$ is more rational assumption than $H^1(P,\mathbb{R}) = 0$.

## Further results

H. Hofer introduced the norm on the space of compactly supported Hamiltonian diffeomorphisms. For a compactly supported smooth function $H : P \to \mathbb{R}$, we define $||H|| := \max H - \min H$. Then, define the norm of a compactly supported Hamiltonian diffeomorphism $\psi \in \mathrm{Ham}_c(P,\omega)$ by $||\psi|| := \inf\{||H|| \mid \psi = \phi_H^1\}$.

**Theorem 3** (Hofer, 1990)**.** *Let $M$ be a restricted contact type hypersurface in $\mathbb{R}^{2n}$ with the standard symplectic structure. Assume that $M$ bounds an open bounded domain $U$. Then there exist a constant $c(M) > 0$ such that for any $\psi \in \mathrm{Ham}_c(P,\omega)$ with $||\psi|| \leq c(M)$ has a leaf-wise intersection.*

Here, a coisotropic submanifold $M^{2n-r}$ is of (restricted) contact type if there exist 1-forms $\alpha_1, \ldots, \alpha_r$ on $M$ (on $P$) such that $d\alpha_j = \omega$ on $M$ (on $P$) and $\alpha_1 \wedge \cdots \wedge \alpha_r \wedge \omega^{n-r} \neq 0$ on $M$. We note that all hypersurfaces are coisotropic. We remark that $c(M)$ in the theorem is a symplectic capacity.

The other results are listed in the following table.

| authors | assumptions on $P$ and $M$ | conclusion |
|---|---|---|
| D.L. Dragnev (2008) | $P = \mathbb{R}^{2n}$, $M$ is a compact and contact type coisotropic submanifold | If $\lVert\psi\rVert \leq c(M)$, then $\psi$ has a leaf-wise intersection |
| V.L. Ginzburg (2007) | $P$ is a subcritical Stein manifold, $M$ is a closed connected restricted contact type hypersurface | If $\lVert\psi\rVert \leq c(M)$, then $\psi$ has a leaf-wise intersection |
| P. Albers, U.Frauenfelder (2010) | $P$ is convex at infinity, $M$ is a closed restricted contact type hypersurface | If $\lVert\psi\rVert \leq c(M)$, then $\psi$ has $\sum b_i(M,\mathbb{Z}_2)$ leaf-wise intersections |
| B.Z. Gürel (2010) | $P$ is geometrically bounded and wide, $M$ is restricted contact type coisotropic submanifold | If $\lVert\psi\rVert \leq c(M)$, then $\psi$ has a leaf-wise intersection |
| F. Ziltener (2010) | $P$ is geometrically bounded, $M$ is a closed coisotropic submanifold, the characteristic foliation is a fibration | If $\lVert\psi\rVert \leq c(M)$, then $\psi$ has $\sum b_i(M,\mathbb{Z}_2)$ leaf-wise intersections |

# The origin of low-luminosity AGN/AGN-like activity in red early-type galaxies

Takayuki Maebayashi, Hitomi Yachi, Hidetomo Honma, Takashi Murayama.
(Graduate School of Science, Astronomical Institute of Tohoku University)

The 4th GCOE International Symposium
02.20-22,2012 @Tohoku University

## 1. Abstract

**Primary Aim:** We focus on the ionizing mechanism of low-luminosity AGNs(LL-AGNs, especially a class of LINER) in order to construct LL-AGN picture.
**Sample:** We reconstructed morphologically selected early-type galaxy sample from the SpecObj catalog of the Sloan Digital Sky Survey(SDSS).
**Analyses:** We examined emission-line properties and their relations to host stellar mass and u'-r' color.
**Results:** We obtained two main results: (1)The emission-line ratios of LINERs show the concentrated distribution on the diagnostic diagrams.
(2)The host galaxies of these LINERs always have red color and not always have large stellar mass.
**Discussion: The host color suggests that photoionization from old stellar population(possibly post-AGB stars) is promising ionizing mechanism of LINERs and photoionization from LL-AGN is also possible if host stellar age correlates with mass accretion rate onto its super massive black hole(SMBH).**

## 2. Introduction

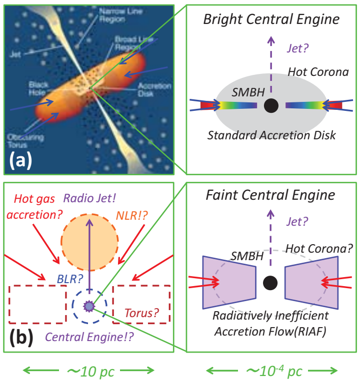


### Active Galactic Nuclei(AGN) pictures.

***Bright AGN(Fig.a):*** When matter accrete onto SMBH, they release their gravitational energy. This energy is transformed efficiently into radiative energy in accretion disk. This radiation ionizes ambient gases. As a result, ionized gases radiate prominent emission lines.

***Faint AGN(Fig.b):*** When accretion rate decreases, accretion disk state changes into RIAF. Therefore, central region and emission lines become faint. **However, faint AGN picture is still under discussion because these weak activities can also be explained by many other models.**

Fig.a: Urry & Padovani 1995, PASP 107, 803

## 3. Sample

### Flux limited sample of nearby bright, morphologically selected, 34497 ETGs.

**Data set:**
- SDSS DR7 SpecObj catalog
- the MPA-JHU DR7 release of spectrum measurements

**Selection criteria:**
fracDeV_g', r', i' > 0.95,
Spectroscopic S/N_g', r', i' > 10,
0.05 < z < 0.1, r' < 16.8.

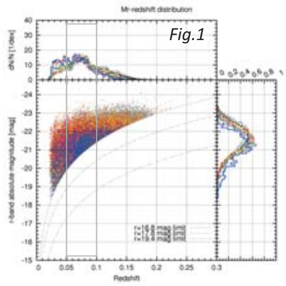


Fig.1: The distribution of our galaxy sample in r-band absolute magnitude vs. redshift plane.

## 4. Analyses & Results

### 4-1. Emission-line diagnostic diagrams

Hβ, [OIII]λ 5007, Hα, [NII]λ 6584 > 3σ → **Active ETGs**,
1~3 these emission lines > 3σ → **Semi-Active ETGs**,
Hβ, [OIII]λ 5007, Hα, [NII]λ 6584 < 3σ → **Quiescent ETGs**.

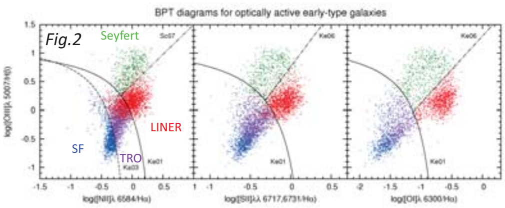


***After classification:***
- 830 SF
- 1576 TRO
- 637 Seyfert
- 1897 LINER
- 12444 Semi-Active
- 17113 Quiescent

Fig.2: Result of our classification. From fig.2, we recognized clump of the distribution in LINER region. To investigate correlation to other properties of these LINERs, we also plotted the diagrams with the coloring according to its host stellar mass or color.

**Ka03:** Kauffmann et al. 2003, MNRAS 346, 1055, **Ke01:** Kewley et al. 2001, ApJ 556, 121,
**Ke06:** Kewley et al. 2006, MNRAS 372, 961, **Sc07:** Schawinski et al. 2007, MNRAS 382, 1415
**SF:** Star Forming
**TRO:** Transition Region Object
**LINER:** Low-Ionization Emission-Line Region

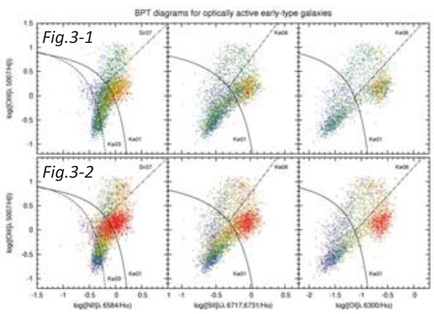


***Color definition***

$\log(M_*/M_\odot) < 10.4$,
$10.4 < \log(M_*/M_\odot) < 10.7$,
$10.7 < \log(M_*/M_\odot) < 11.0$,
$11.0 < \log(M_*/M_\odot) < 11.3$,
$11.3 < \log(M_*/M_\odot)$

$u'-r' < 1.9$,
$1.9 < u'-r' < 2.2$,
$2.2 < u'-r' < 2.5$,
$2.5 < u'-r' < 2.8$,
$2.8 < u'-r'$

Figs.3: The diagnostic diagrams with the coloring defined above. These diagrams show that **massive or red active ETGs tend to concentrate into the LINER region**. Because host stellar mass correlates with its color, however, it is possible that we see just the same ETGs. So next, we plotted the active ETGs separately.

### 4-2. Color-Mass & Diagnostic diagrams

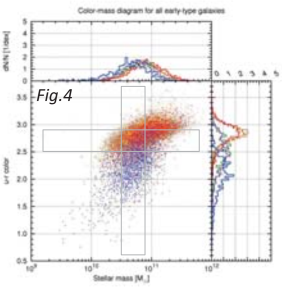


Fig.4: Color-mass diagram for our classified ETGs. We intended to show our separation range in these panels(gray square).
***Case (i) : $10.5 < \log(M_*/M_\odot) < 10.9$***
***Case (ii): $2.5 < u'-r' < 2.9$***

The diagnostic diagrams for each subsample are showed in figs.5 – 6. [Note that figs.5-0 & 6-0 show total plots of the case (i) & (ii)]

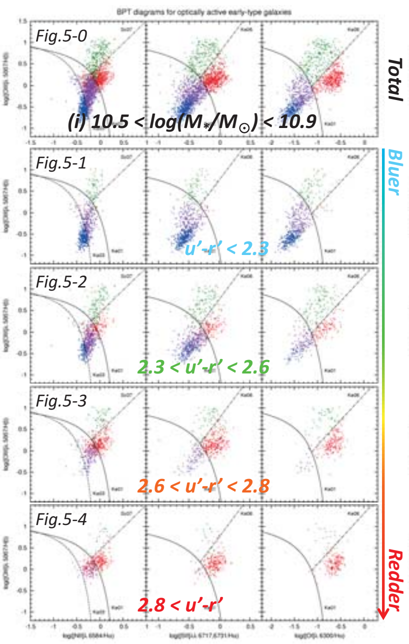


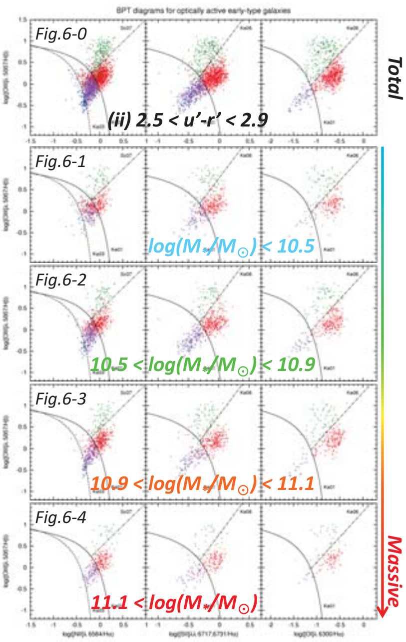


**(i)** In figs.5-1 – 5-4, each subsample shows very different distributions in the sense that **redder subsample concentrates into the LINER region**.
**(ii)** In figs.6-1 – 6-4, **this distribution dose not vary across subsamples**.

## 5. Discussion

A number of the ionizing mechanisms reproducing LINER(-like) emission-line properties have been proposed. These mechanisms fall roughly into four categories: (A)photoionization by LL-AGN, (B)fast shock, (C)photoionization by post-AGB stars(pAGBs), (D)interaction between warm and hot inter-stellar medium. If we adopt (A), we speculate that (1)as the old stellar population dominates in host galaxy, mass accretion rate onto its SMBH decreases, (2)accretion state varies from the standard accretion disk to radiatively inefficient accretion flow(RIAF), (3)the ionization parameter decreases with maintaining the hardness of ionizing spectrum, (4)as a result, such galaxies become LINERs. If we adopt (C), it suggests that the pAGBs spreading over host galaxy provide ionizing photons. In (B) and (D), because these can not simply explain the host properties presented here, we think it is not likely that these mechanisms are primary in the clump LINERs.

# Path Integral Analysis of Bianchi type I spacetime in Loop Quantum Cosmology

Kazuya Fujio
Department of Physics, Tohoku University

Loop quantum gravity ( LQG ) is the best candidate for quantum gravity.
Cosmology based on LQG is called Loop quantum cosmology ( LQC ).

Although the full analysis is very complex even in toy model.
we can use the path integral formulation to investigate the brief behavior.

In this presentation,
path integral analysis of Bianchi type I spacetime with a massless scalar field and cosmological constant will be reported.

## Bianchi type I spacetime

Bianchi type I spacetime is homogeneous but anisotropic model.
There are three directional scale factors. However their values have no physical meaning directly, only ratios $a_i(\tau)/a_i(\tau_0)$ have.

$$ds^2 = a_1^2 dx_1^2 + a_2^2 dx_2^2 + a_3^2 dx_3^2$$

$$a_i = ae^{\theta_i}, a = (a_1 a_2 a_3)^{\frac{1}{3}} \qquad H_i = \frac{\dot{a}_i}{a_i}$$ Directional Habble parameter (directional expansion rate)

Note that $\dot{\theta}_i \propto \frac{1}{a^3}$ In classical general relativity

Anisotropy of spacetime is defined as $\Sigma = \frac{1}{18}\left[(H_1 - H_2)^2 + (H_2 - H_3)^2 + (H_3 - H_1)^2\right]$

$$= \frac{1}{6}\left(\dot{\theta}_1^2 + \dot{\theta}_2^2 + \dot{\theta}_3^2\right) \propto \frac{1}{a^6}$$ In classical general relativity

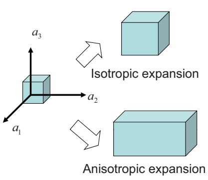


Friedmann equation is written as

$$H^2 = \frac{8\pi G}{3}\rho + \Sigma + \frac{\Lambda}{3}$$

## Effective action of Bianchi I model

We investigate Bianchi I spacetime with avmassless scalar field $\phi$ and cosmological constant $\Lambda$. The effective action is given as;

$$S_{BianchiI} = \int d\tau \left( p_\phi \dot{\phi} - \frac{\beta_1}{2}\dot{\lambda}_1 - \frac{\beta_2}{2}\dot{\lambda}_2 - \frac{b}{2}\dot{v} + \alpha\left[ p_\phi^2 + \frac{\pi G}{4l^2}\left[v^2 P(\lambda, v, \beta, b) + 2\hbar l v Q(\lambda, v, \beta)\right] + \pi G \Lambda v^2 \right] \right)$$

$\lambda_i \propto \sqrt{a_j a_k}$ (i,j,k cyclic) $p_\phi, \beta_i$ and b are momenta to $\phi, \lambda_i$ and volume respectively

$l = \gamma\sqrt{4\sqrt{3}\pi G \hbar l_P^2}$, $\gamma$ is Barbero-Immirizi parameter ~0.2735

$$P, Q = \cos\left[\frac{l}{\sqrt{v(v+2\hbar l)}}(\beta_1\lambda_1 - \beta_2\lambda_2)\right] + \ldots\ldots$$

We can obtain first order approximation equations from this action.
These equations reproduce the general relativity in large scale,
but there is non-trivial departure from classical theory in small scale.

We can show that $\beta_i\lambda_i$ are constant and they represent anisotropy.
Therefore if we set $\beta_i = 0$, this model becomes the isotropic one.

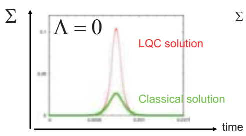


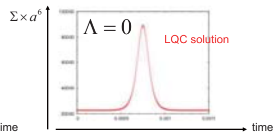


The anisotropy $\Sigma$ is larger than classical one in small scale.
However in $\Lambda > 0$ case have contrary result. The anisotropy in LQC is smaller than classical one.

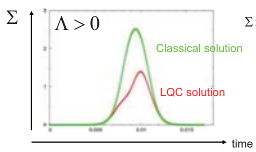


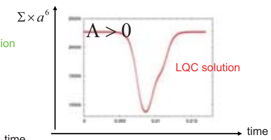


This is because the anisotropy $\Sigma$ has upper limit $\Sigma_{max} \sim 1.85$ in LQC.
Therefore we summrize as

- LQC anisotropy is larger than classical one if clasiical anisotropy is smaller than $\Sigma_{max} \sim 1.85$
- LQC anisotropy is smaller than classical one if classical anisotropy is larger than $\Sigma_{max} \sim 1.85$

Note that in both case the anisotropy in large scale is conserved under the big bounce.

## Loop Quantum Cosmology

Cosmology based on Loop Quantum Gravity ( LQG ) is called Loop Quantum Cosmology ( LQC ).

- LQC has NOT *differential* equation but ***difference*** equation.
  This is caused by discreteness of geometrical values.

$$(\hat{C}_{grav} + \hat{C}_{mat})\Psi(v) = f_+(v)\Psi(v+4) + f_0\Psi(v) + f_-\Psi(v-4) + \hat{C}_{mat}\Psi(v) = 0$$

$v$ : volume of the Universe

- Expectation value of volume has initial bounce.
  This means that the quantum effect causes the repulsive force to avoid the singularity.

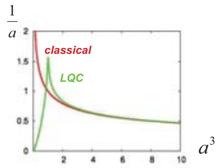


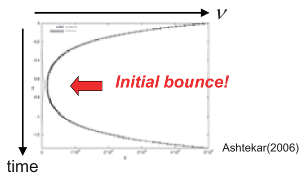


## Path integral formulation

Although we play with simple toy models, whether analytic or numerical, full Hamiltonian analysis of LQC is very complicated.
Ashtekar followed the Feynman's original path integral formulation.
We can obtain <u>*effective action*</u> which contain ***quantum correction***.

$$\langle v_f, \phi_f | v_i, \phi_i \rangle = \delta_{v_f, v_i}\delta(\phi_f - \phi_i) \qquad A(v_f, \phi_f; v_i, \phi_i) \equiv \int d\alpha \langle v_f, \phi_f | e^{\frac{i}{\hbar}\alpha\hat{C}} | v_i, \phi_i \rangle$$

$$(\Phi_{phys}, \Psi_{phys}) \equiv \langle \Phi_{kin} | \int d\alpha\, e^{\frac{i}{\hbar}\alpha\hat{C}} | \Psi_{kin} \rangle = \sum_{v, v'} \int d\phi d\phi' \bar{\Phi}_{kin}(v, \phi) A(v, \phi; v', \phi') \Psi_{kin}(v', \phi')$$

$$\langle v_f, \phi_f | e^{\frac{i}{\hbar}\alpha\hat{C}} | v_i, \phi_i \rangle = \sum_{v_{N-1} \ldots v_1} \int d\phi_{N-1} \ldots d\phi_1 \langle v_N, \phi_N | e^{\frac{i}{\hbar}\frac{\alpha}{N}\hat{C}} | v_i, \phi_i \rangle \ldots \langle v_1, \phi_1 | e^{\frac{i}{\hbar}\frac{\alpha}{N}\hat{C}} | v_0, \phi_0 \rangle$$

$$A(v_f, \phi_f; v_i, \phi_i) = \int d\alpha \int [Dv(\tau)][Db(\tau)][D\phi(\tau)][Dp(\tau)]\, e^{\frac{i}{\hbar}S}$$

$$S = \int_0^1 d\tau \left( p\dot{\phi} - \frac{1}{2}b\dot{v} - \alpha\left(p^2 - 3\pi G v^2 \sin^2 b\right) \right)$$ Flat FRW + massless scalar field model ( Ashtekar's original paper )

## Results

We compute the solution of first order approximation equations.
At first we consider $\Lambda = 0$ case.

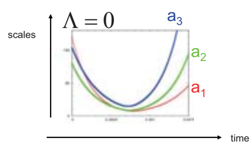


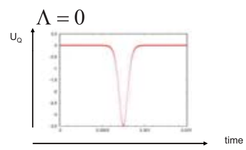


Scale factors are bouncing in small scale as isotropic one.
We can write the quantum effect $U_Q \equiv H^2 - \frac{8\pi G}{3}\rho - \Sigma - \frac{\Lambda}{3}$ i.e. departure from classical Friedmann eq.
In large scale $U_Q$~0 but becomes large with negative sign in small scale.
This shows that quantum effect causes the repulsive force to avoid the initial singularity.

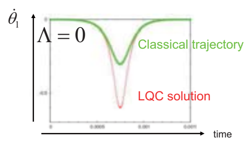


$\dot{\theta}_i \propto \frac{1}{a^3}$ In classical theory.

However this relation is invalid because of quantum effect.
Also

$\Sigma = \frac{1}{6}\left(\dot{\theta}_1^2 + \dot{\theta}_2^2 + \dot{\theta}_3^2\right) \propto \frac{1}{a^6}$ Is invalid in LQC.

## Summary

- The effective action of Bianchi I spacetime with a massless scalar field and cosmological constant is constructed.
  We obtain approximation equations which contain quantum correction.
  And these equation has isotropic solution as special case.

- In large scale, equations reproduce the classical general relativity.
  Even if there is anisotropy, the quantum effect cause the repulsive force in small scale to avoid the Big Bang singularity as we expected.

- The anisotropy has interesting behavior in small scale.
  Because the anisotropy has upper limit in LQC,
  If classical anisotropy is larger (smaller) than this upper limit,
  LQC anisotropy is smaller (larger) than classical one.
  The anisotropy in large scale is conserved under the big bounce.
  Note that results are depending on matter configuration.
  If we consider matter content which has anisotropic stress
  ( e.g. magnetic field ), the results maybe change.

# Consistency Relation for Multi Field Inflation Scenario

Naonori Sugiyama


## Abstract

**While it is well-known that the universe began from a very hot and dense state called "Big Bang", many cosmologists now think that there was a period even before the "Big Bang". It is called "inflation". In this "inflation period", the universe has expanded more rapidly than it does today, and this is the reason for its name "inflation". Unfortunately, we have not yet obtained a satisfactory physical description of inflation because we do not have cosmological observation accurate enough to reach it. Indeed, lack of such observations allows theorists invent many inflation models different from each other when comparing those in various aspects. In short, "The number of inflation models is being inflated".**

**In this work, we derived a quite general inequality among observable quantities by considering a concept called "Non-Gaussianity". This inequality should be satisfied by almost all inflation models considered today. If future observation suggests that our inequality does not hold in our universe, our inequality can rule out almost all models subject to it.**


## The universe began from "Big Bang"!!

Big Bang

A huge explosion

A much hot and dense state

"Big Bang" is not a huge explosion. It is a much hotter and denser state of the universe than today. In the early universe, there are just elemental matters, for example electron, newtorino, and photon. The universe have been expanding and cooling ever now.

The universe began from "Big Bang"!!

The universe was a hotter and denser state called "Big Bang"!!

## There was a period called "inflation" before "Big Bang"!!

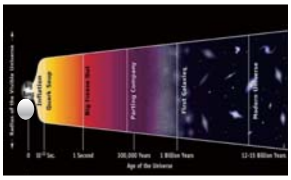

Many cosmologists think that the universe was expanding much more rapidly before "Big Bang" than it does today.
We call the period "inflation".
Inflation theory is just a theoretical demand, it is not yet verified from observation. Furthermore nobody understand the detail of physics during inflation period.
The verification of inflation theory is one of the most important topic in cosmology.

How do we verify the inflation theory ?

## Cosmic Microwave Background radiation (CMB)

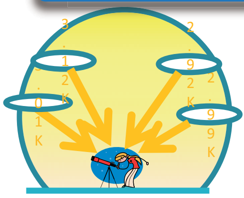

There is the light called "Cosmic Microwave Background radiation" in the universe. Its temperature is 2.725 K (Kelvin). It is the oldest light that we can observe. To be precise, the temperature of the CMB is different in each direction it comes. The distribution for the difference of the temperature is nearly "Gaussian distribution". Recently, it has been found that CMB has a little departure from Gaussian distribution. It is called "Non-Gaussianity of the perturbation of the CMB temperature". Many cosmologists think that inflation scenario explain how the Non-Gaussianity is created. So we have information of the inflation period by researching the CMB Non-Gaussianity.

In order to characterize amount of the Non-Gaussianity,
we often use the below parameters, called "Non-linear parameter",

$$\tau_{NL} \quad f_{NL}$$

## The way of theoretical research for inflation

We have not yet understand inflation physics in detail.
Each researcher makes their own models for inflation and predict s different non-linear parameters.

There are inflation models which predict a small non-linear parameter: $f_{NL} \approx O(10^{-2})$

While, a large non-linear parameter is also predicted in other models: $f_{NL} \approx O(10)$

The observational value of non-Gaussian parameters

$$f_{NL} = 32 \pm 21 (65\% CL)$$

$\tau_{NL}$ is not yet observed.

We do not have observational values enough to constrain theoretical Inflation models. So we can not rule out almost all inflation models. As the result,
the number of Inflation models have been increasing.

## result!!

It is difficult to verify huge number of inflation models one by one.
We should have a more general discussion.

$$\tau_{NL} \geq \left( \frac{6}{5} f_{NL} \right)^2$$

**We have discovered above inequality between non-linear parameters.**
**This inequality is satisfied in a large class of inflation models called "multi-field inflation".**
**If the new experimental data such as Plank (which is a satellite for observation of CMB) detect fNL but do not see tauNL large enough to satisfy the above inequality, then almost all inflation models may be ruled out.**

## Conclusion!!

**We have discovered the general inequality (A) between non-linear parameters. The most interesting case would be the observation of a complete violation of the inequality, i.e.,**

$$\tau_{NL} << \left( \frac{6}{5} f_{NL} \right)^2$$

**which implies that inflation cannot be responsible for generating the observed Non-Gaussianity. We may not be so far away from testing this prediction. Our result provide a strong science case for measuring the local-form tri-spectrum of the cosmic microwave background .**

# The star formation in the SSA22 protocluster at z=3.09

**2012/2/20-22 GCOE symposium**
**Mariko Kubo, (D1 Astronomical institute)**
Yuka.Uchimoto, Toru Yamada, Masayuki Akiyama, Tomoki Hayashino(Tohoku university), Yuichi Matsuda(Dahram university),
Masaru Kajisawa(Ehime university), MOIRCS Group

## 1. Overview; K-selected galaxies in the SSA22 protocluster

The SSA22 z=3.09 protocluster is a known high density region at high redshift which identified with the density excess of the Lyα Emitters(LAEs), Lyman break Galaxies(LBGs) at z~3.1.

In this work, we selected the candidate of the protocluster galaxies based on stellar mass with MOIRCS JHK band deep imagings at the highest density region of LAEs in the SSA22 protocluster. And then analysed the star formation and stellar populations in the protocluster using Spitzer IRAC, MIPS 24um (Webb+2008). We selected the galaxies with $K_{AB}<24$ at $z_{phot}$=2.6-3.6 by using photometric redshift estimated from Spectral Energy Distribution(SED) fitting with UBVRi'zJHK, IRAC 3.6,4.5, 5.8, 8.0um. The photometric redshift error at z~3 is ~0.5. We selected the galaxies with stellar mass ~ $10^{9-11}M_{sun}$

The sky distribution of the K-selected galaxies is Fig.1. They are concentrated around the density peak of the LAEs at z=3.09. The surface number density of the K-selected galaxies is 1.6 times larger than that in the GOODS-North field at same redshift range(Fig. 2).

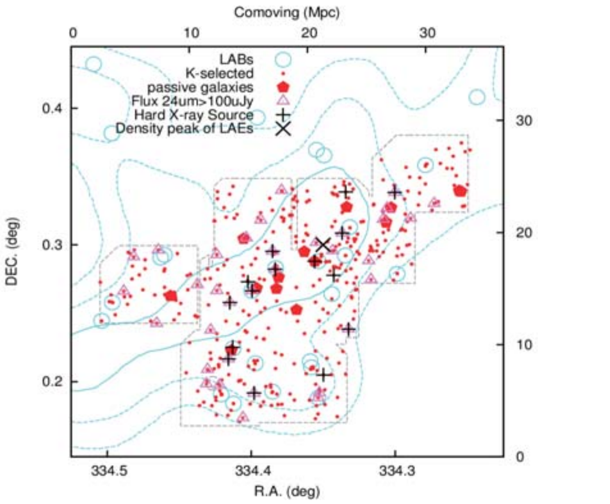


Figure. 1; The sky distribution of the K-selected galaxies ( $K_{AB}<24$ and $2.6<z_{phot}<3.6$ )(redcircles). The large X is the density peak of the LAEs. The light blue circles are Lyα Blobs(LABs). Big red pentagons are the passive galaxies selected with I'-K>3.0 and K-4.5 um <0.5. The 24um detected(pink triangles), X-ray detected(Lehmer+2009, black crosses) are marked.

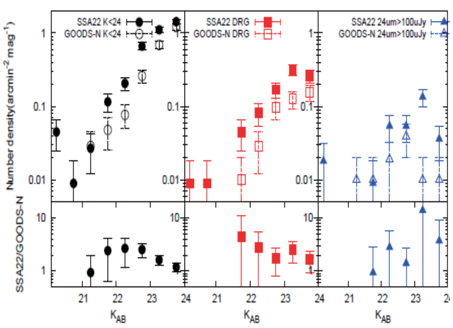


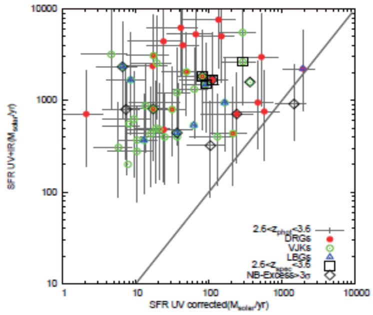


Figure. 2; The comparison of the differential surface number density of the K-selected galaxies(left), those classifeid as DRGs(middle), MIPS24um detected (right) in the SSA22 protocluster(filled) and in the GOODS-North field(Kajisawa et al.2009) (unfilled). Bottom panels are the ratio of the number density in the SSA22 to that in the GOODS-N.

Figure.3; The $SFR_{UV+IR}$ v.s. $SFR_{UVcorrected}$ of the 24um sources. K-selected galaxies selected as DRGs(red), VJKs(green, BzK galaxies at z~3), LBGs(blue) are marked. Black squares are those at z_spec=2.6-3.6, black diamonds are those with NB-excess>3σ.

## 2. The excess obscured starbursts in the protocluster

There are further density excess of some K-selected galaxies; which selected as Distant Red Galaxies(DRGs; $J-K_{AB}>1.4$ ) are 2.2 times, which detected with 24μm are 3.4 times numerous (Fig.2).

Fig.3 is the $SFR_{UV+IR}$ and $SFR_{UVcorrected}$ of the 24um detected galaxies. $SFR_{UV+IR}$ are estimated from unobscured UV light and dust obscured star formation re-emitted at IR. $SFR_{UVcorrected}$ are estimated from the UV light corrected of the extinction.

They have SFR~ $1000M_{sun}/yr$ . Most of them are too faint at rest-UV to be selected as LBGs, LAEs, but be selected as DRGs.

Thus NIR survey have revealed not only the stellar mass but also the obscured starburst in the protocluster.

## 3. The passive galaxies

Furthermore, we found the passively evolving galaxies in the protocluster.

Though, the detection limit of 24μm is too large, we used rest-UV to NIR color to see the properties of the galaxies. Fig.4 is the I'-K v.s. K-4.5um color diagram. 24μm detected galaxies have color consisted with dusty starburst. On the other hand, there are the galaxies which have color like the single burst >0.5Gyr, those would be passively evolving galaxies.

Top panel of the Fig. 4 is the K-4.5um color distribution of the DRGs in the SSA22 protocluster and in the GOODS-North field at z=2.6-3.6. There are the excess of the K-4.5 um bluer DRGs, or passive galaxies in the protocluster. Sky distribution of the passive galaxies(in Fig.1) show strong clustering around the highest density region of the LAEs. The x-ray detected, 24 μm detected galaxies show similar sky distributions.

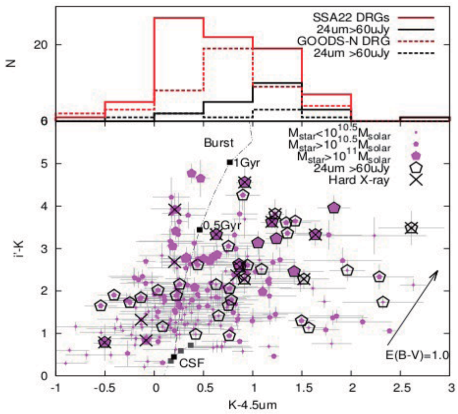


Figure.4; The bottom panel is I'-K v.s. K-4.5 um color distribution of the K-selected galaxies(pink pentagons). 24 um detected galaxies are marked with black pnetagons. Black dashed line is the age evolution track of the single burst star formation model at z~3. The grey line is same but of the constant star formation model.

Top panel of Figure.5 is the K-4.5um color distribution of the DRGs(red) at $2.6<z_{phot}<3.6$ and those detected with 24um (black) in the SSA22 proto-cluster(solid lines) and in the GOODS-North field (dashed lines).

## 4.Discussion and Future works

There are the density excess of the K-selected galaxies detected with 24um. They have very high SFR and they would rapidly evolve into the massive ellipticals in the center of the present cluster. Furtheremore the sky and color distribution of the X-ray detected galaxies suggest the correlation of the nuclear activities and the formation of the massive galaxies.

Are the passive galaxies already like the local massive ellipticals? The stellar mass of these are as large as $10^{10.5-11}M_{sun}$ . Fig.5 are the resolved image of 24um source(top) and the passive galaxy selected with I'-K>3.0 and K-4.5um >0.5(bottom). At least this passive galaxy is massive spheroid like system.

Thus, at the center of the z=3.1 protocluster, the massive galaxies are dramatically being formed but some mature systems may already exist.

Future works, the NIR spectroscopies of the K-selected galaxies are required to confirm their redshift, though there are large uncertainties about photometric redshifts.

Morphological analysis of these are also important to understand the formation and evolution of the massive ellipticals.

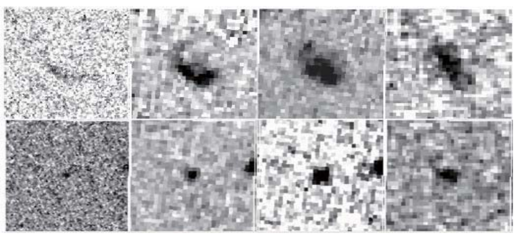

Fig.5 The HST ACS F814(PI Chapman ID 10405), WFC3 F110W, F160W(PI Siana ID 11636), and MOIRCS K images of the K-selected galaxies.
Top; 24um detected galaxy. Bottom; passive galaxy with I'-K>3 and K-4.5um<0.5

# Quasinormal modes of charged anti-de Sitter black holes

Nami Uchikata and Shijun Yoshida (*Astronomical Institute, Tohoku University*)

**Abstract**

It is well known that rotating and/or charged black holes in asymptotically flat spacetime become unstable via superradiant scattering. Superradiance is a phenomenon that an impinging wave can be amplified by a rotating and/or charged black hole when the wave satisfies a certain condition.

For the black holes in asymptotically anti-de Sitter (AdS) spacetime, it has been known that the rotating AdS black holes also become unstable if their quasi-normal modes satisfy the superradiance condition when the black holes' radii are sufficiently smaller than the AdS scale. However, it is not well studied for the charged AdS black holes. Thus, we have investigated the quasinormal modes of the charged AdS black holes analytically and numerically in the small black hole limit, and showed that the charged AdS black holes become unstable against scalar perturbations if their quasinormal modes satisfy the superradiance condition.

## Introduction

### [What is an anti-de Sitter (AdS) black hole ?]

AdS is the spacetime whose boundary behaves as an effective wall at spatial infinity. We refer to this characteristic size of the AdS spacetime as an AdS scale (L).

AdS black holes are black holes which exist in such spacetime.

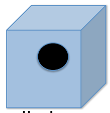

### [What are quasinormal modes?]

Every objects have their characteristic oscillations, called normal modes. For black holes, the oscillations usually decay (or amplify) with time, so we say *quasi*normal modes.

(Vishveshwara 1970; Chandrasekhar & Detweiler 1975, Leaver 1985)

Since the AdS boundary behaves as a wall, the wave scattered by the black hole will reflect at the AdS boundary. Thus, the waves having decaying (growing) modes are stable (unstable). Instability occurs only for rotating and/or charged black holes. And this unstable phenomenon is called superradiance.

(Zel'dovich 1971; Misner 1972; Starobinsky 1973)

### [Example]

The quasinormal modes of rotating AdS black holes have unstable modes when their radii are sufficiently smaller than the AdS scale.

(Cardoso & Dias 2004; Cardoso et al. 2004; Cardoso et al. 2006; Uchikata et al. 2009 )

We focus on the quasinormal modes of charged AdS black holes and investigate whether the system is stable or not.

## Calculation methods

We consider the perturbations of the charged scalar field on the charged AdS black holes.

### [Metric of charged AdS black holes]

$$ds^2 = -f(r)dt^2 + f(r)^{-1}dr^2 + r^2(d\theta^2 + \sin\theta^2 d\phi^2)$$

$$f(r) = \frac{r^2}{L^2} + 1 - \frac{2M}{r} + \frac{Q^2}{r^2}$$

M : the black hole mass Q : the charge of the black hole

$L^2$ : the inverse of a cosmological constant (Λ)

### [Equations of perturbations]

Quasinormal modes have complex ω. If we decompose the wave function Φ as, $\Phi(r,\theta,\phi,t) = R(r)Y_{\ell m}(\theta,\phi)e^{-i\omega t}$,

then Φ∝exp(-i Re(ω) t) exp(-Im(ω) t). ($Y_{lm}$ is the spherical harmonics.)

•Re(ω) represents frequency of the oscillation.

•Im(ω) represents the damping timescale of the oscillation.

Thus, if Im(ω)>0, Φ grows exponentially with time.

→The wave is amplified as it scattered off by the black hole. Thus the system is unstable.

◆the basic equation (radial part)

$$\frac{d}{dr}\left(r^2 f(r)\frac{dR(r)}{dr}\right) + \left[\frac{(\omega r - eQ)^2}{f(r)} - \ell(\ell+1)\right]R(r) = 0$$

e: the charge of the scalar field

## Results

### [Analytical calculation]

We find that

$$\mathrm{Im}(\omega) \propto -\left(\mathrm{Re}(\omega) - e\,Q/r_+\right),$$

for small black holes. (The black hole radius, r+, is sufficiently smaller than the AdS scale, r+<<L.) Thus, if the condition ω-eQ/r+<0 is satisfied, the black hole becomes unstable. The instability condition can also be written as

$$\frac{Q}{Q_C} > \frac{3}{eL},$$

for the fundamental mode, where Qc is the maximum of Q.

### [Numerical calculation]

It is verified Im(ω)>0 when ω-eQ/r+<0 for small black holes.

Fig.1

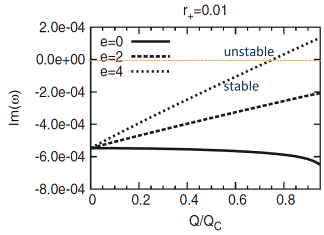


Fig.2

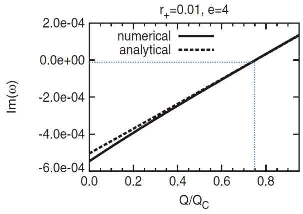


(Uchikata & Yoshida 2011)

Both figures are the results of the imaginary part of the frequency for the black hole with its radius r+=0.01L. Fig.1 shows that for the scalar field with eL<4, the black hole is stable but for the scalar field with eL=4, the black hole becomes unstable when the black hole charge, Q, is larger than 0.75Qc. Fig.2 shows that numerical results agree with analytical calculations.

## Conclusions

- We have studied the scalar perturbations of the charged AdS black holes whose radii are sufficiently smaller than the AdS scale.
- From both analytical and numerical calculations, we have showed that the instability condition can be expressed as ω-eQ/r+<0 , or
$$\frac{Q}{Q_C} > \frac{3}{eL}.$$
For example, when the scalar field has a charge eL=4, the black hole becomes unstable when the black hole charge is Q>0.75Qc.
- It is also interesting to examine whether this instability condition stands for the large AdS black holes, i.e. for black holes having r+>L. This will be the future problem.

# Scanning tunneling microscopy of electronic properties of bulk and layered $MoS_2$

A. Vakhshouri[1],K. Hashimoto[1, 2], Y. Hirayama[1, 2]

[1]Tohoku University, [2]JST-ERATO

## INTRODUCTION

Reaching to dimensional limit of the metal-oxide semiconductors, finding other alternatives is crucial. The suitable substitute should diminish the size of the semiconductor and possess the required characteristics of the semiconductors such as band gap.

### ➢Low dimensional electron systems

Low dimensional electron systems can reduce the size of the electronic circuits significantly. The well known two dimensional system, graphene, could be a appropriate choice, however it has no intrinsic band gap which is necessary for logic devices. However a single layer of molybdenum disulfide ($MoS_2$) has an intrinsic band gap, $E_g$=1.8eV. This enabled to fabricate $MoS_2$-based logic device recently[1].

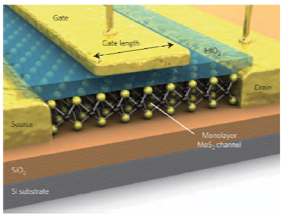


Fabrication of $MoS_2$ monolayer transistors [1].

A single crystal of $MoS_2$ (bulk), likewise graphite, is composed of vertically stack layers, held by weak Van der Waals force.

### ➢Molybdenum disulfide (Bulk)

- ✓ Forms in nature as mineral ore in the form of bulk.
- ✓ The appearance is black solid (Similar to graphite).
- ✓ Weak van der Waals interaction between the layers.
- ✓ Used as lubricant.
- ✓ Large indirect band gap, $E_g$=1.2eV.

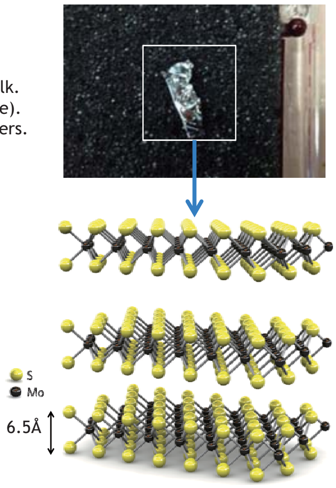


### ➢Molybdenum disulfide (single layer)

- ✓ Single layer has the thickness of 6.5Å.
- ✓ Direct band gap semiconductor with $E_g$=1.8eV.

In this work, we observed the surface of the bulk $MoS_2$ and visualized the distinct step structures using scanning tunneling microscopy (STM). We then examined the band gap of the bulk $MoS_2$ by scanning tunneling spectroscopy (STS).

## EXPERIMENT

✓Omicron STM in ambient condition.
✓Active damping system for mechanical isolation.
✓Mechanically sharpened Ir/Pt tip.
✓The modulation frequency and the modulation voltage are 1.7KHz and is 15mV for STS measurements.

## RESULTS

### ➢STM and STS results on bulk $MoS_2$.

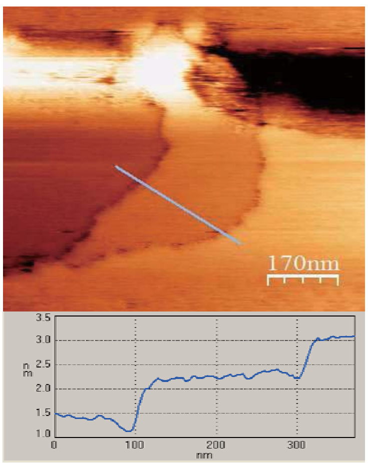


Fig.1: 850x850nm² STM image of bulk $MoS_2$.

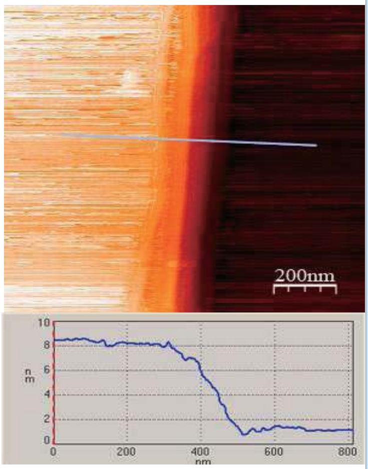


Fig.3: 1x1μm² STM image of bulk $MoS_2$ .

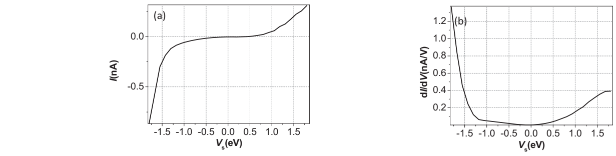


Fig.2: Average *I-V* and d*I*/d*V* curves detected on the area shown in figure 1.

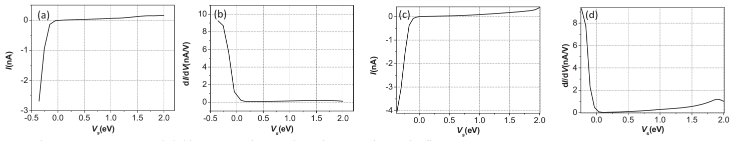


Fig.4: Average *I-V* and d*I*/d*V* curves detected on the area shown in figure 3.

## RESULTS

✓In figure 1 we applied positive sample bias voltage, $V_s$=+6.0V and tunnel current, $I_t$=0.1nA. The bottom panel of figure 1 shows the corrugation across the light blue line from which the step height is estimated to be about 6.5Å. This is the thickness of a single layer of $MoS_2$.

✓Figure 2 (a) shows the average *I_V* curve taken on the different area shown in figure 1. $I_t$ varies between -0.9nA and 0.3nA while $V_s$ ranges between -1.8V and 1.8V.

✓In the figure 3, the top panel shows the STM image is taken by applying negative sample bias voltage, $V_s$=-0.1V and tunnel current $I_t$=0.04nA. The bottom panel shows a 7nm thick layer of $MoS_2$ across the light blue profile line. This thick layer is composed of approximately 10 single layers of $MoS_2$.

✓Figure 4 shows the *I_V* and d*I*/d*V* curves detected on the area shown on figure 3 with the set points $V_s$=+1.5V and $I_t$=0.1nA for (a),(b) and $I_t$=0.2nA for (c),(d).

✓The I-V curves in figure 2 and 4 are asymmetric. It seems in negative sample bias regime the absolute value of $I_t$ increases drastically unlike the positive $V_s$ regime.

## DISCUSSION

✓In figure 2_(b) the d*I*/d*V* curve shows a band gap, $E_g$≈0.7eV which is close to the calculated indirect band gap $E_g$≈1.06eV [2].

✓A shift in offset of *I-V* curves can caused by tip oxidization or tip contamination. Since the Ir/Pt tip is robust against oxidization it is more likely that an object was attached to the tip apex. it is reported that the a likely tip contaminant is sulfur because of an excess of S at the $MoS_2$ cleavage surface[4]. However this contaminated apex can lead to clear and correct topographic image but not necessarily a real LDOS.

✓The curves in figure 4 (b) and (d) in positive $V_s$ regime show different behavior. For $V_s$ > 0.0eV, curve (b) does not change so much, but curve (d) starts to raise for $V_s$ > 0.5eV. This behavior should be canceled out after normalizing by dividing them by *I*/*V* curves, however this is not our case (the normalized curves are not shown here). The origin of this behavior is not clear but one possible reason can be tip contamination which can also lead to energy shift as mentioned before.

## CONCLUSION

✓The topographic image of single layer and multilayer of bulk $MoS_2$ was obtained in ambient condition.
✓A band gap, $E_g$≈0.7eV is detected for bulk $MoS_2$.
✓A shift in offset of *I-V* curves and the asymmetric behavior of d*I*/d*V* curves can be due to contaminated tip.

## PROSPECTIVE

✓Detecting a few layers as well as single layer of $MoS_2$ using atomic force microscope (AFM) (fig.5)

✓Studying the electronic properties of bulk and single layer of MoS2 at low temperature in the presence of high magnetic field using STM/STS.

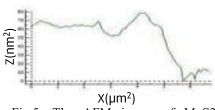



Fig.5: The AFM image of MoS2 flakes. The left panel shows the corrugated surface across the blue line.

## REFERENCES

[1] B. Radisavljevic et. al., *nature nanotechnology* ,**6**, 147 (2011)
[2] H.S.S R.Matte et. al., *Angew. Chem.*, **122**, 4153, (2010)
[3] A. Enyahsin et. al., *Eur. Phys. J. Special topics*, **149**,103, 2007.
[4] J. S. Zahinski et. al., Mat. Res. Soc. Symp. Proc., 140, 239, (1989).

# Porting Linux to MoGURA Frontend Electronics

XU, Benda
Research Center for Neutrino Science, Tohoku University, Japan

## KamLAND and MoGURA

- KamLAND is a low energy neutrino and anti-neutrino detector
  - **1000ton** of liquid scintillator in $\phi$**13m** sphere
  - ultra clean and low background
  - converted to a Xenon double beta decay searcher as *KamLAND-Zen*
  - major challenge for DAQ:
    energetic cosmic $\mu$ overwhelms DAQ with exceeding events
- MoGURA: Module for General-Use Rapid-Application
  - new DAQ system operating in parallel for KamLAND
  - integrates 1GSPS flash ADC and Spartan 3E FPGA from Xilinx
  - large ring buffer holding **10us** waveform

## MoGURA System Overview

trigger board

Trigger Logic FPGA: Spartan 3E x 1
Trigger System FPGA: Spartan 3E x 1

main board

Front End FPGA: Spartan 3E x 6
System FPGA: Spartan 3 x 1
User FPGA: Virtex 2 Pro x 1

- FPGA: field-programmable gate array
  - integrated circuit is loaded from flash memory when power on
  - flash memory are reprogrammable
    flexibility in developing and debugging
- Features: to catch the most useful data
  - trigger system
  - zero suppression
  - mode switch by occupancy of buffer
    normal, almost full, full

illustration of the whole

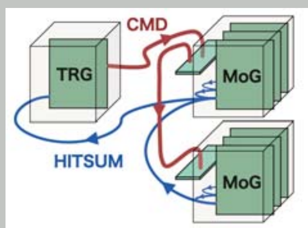


## Development and Debug with VHDL

- VHDL: VHSIC hardware description language
  - VHSIC: very-high-speed integrated circuits
  - call for dedicated hardware skills to master (e.g. hardware constraints)
  - too deep learning curve to be an auxiliary tool for physics
  - present systems (front end FPGA, system FPGA) are complex

## Problems in Present Working Flow

- it is hard to describe and reproduce the bug
  - without understanding VHDL
  - without a compatible software simulator
  - by only observing
- it is hard to make sure the bug really gets fixed without a test-bench
- it is slow to get bugs fixed
  - when the application is dedicated to physics and not general
  - when the engineer do not have the same physics environment to reproduce the bug
  - when the physicists can only tune limited registers to play with the bug

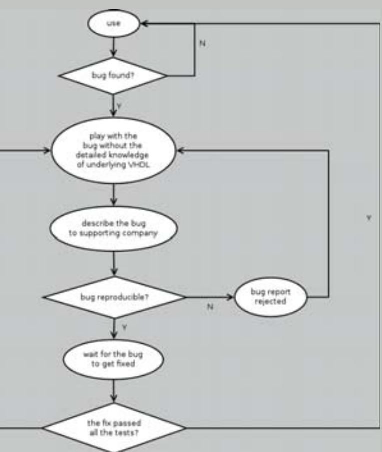


## Linux on FPGA SoC

- SoC: system on a chip
  - CPU and system memory on a single integrated circuit
  - powerful enough to run an operating system
- features are implemented in software include OS
  - easy to learn, easy to develop and debug
  - CPU is general purpose, which runs much slower than present register-transfer level implementation
- try Linux in order to make a balance with present RTL design
  - Linux is a portable open-source operating system kernel
  - there are ongoing efforts to run Linux on Virtex 2 pro and spartan 3(E) FPGAs

## Results: Linux on Virtex 2 Pro

| | |
|---|---|
| ISE | 10.1 |
| Linux | 3.0 |
| toolchain | compiled |
| gcc | 4.5.3 |
| binutils | 2.22 |
| glibc | 2.12 |
| rootfs | nfs |
| CPU | PowerPC405 |
| clock | 100Mhz |
| console | RS232 |

- user FPGA on main board
  - software level on board control
  - read data from system FPGA via board circuit and push out by Ethernets
- preliminary speed test
  - 100Mbps on board connected to 1Gbps host
  - standard FTP protocol
  - 629 KB/s, bottleneck being CPU

## Results: Linux on Spartan 3E

| | |
|---|---|
| ISE | 13.2 |
| Linux | 3.0 |
| toolchain | downloaded |
| gcc | 4.1.2 |
| binutils | 2.16.1 |
| glibc | 2.3.6 |
| rootfs | ramdisk |
| CPU | MicroBlaze |
| clock | 50Mhz |
| console | RS232 |

- system/front-end FPGA on main board
  - replace non time critical and complex housekeeping function with software
- trigger logic/system FPGA on trigger board
  - implement smart trigger logic (e.g. FFT, DWT) with software

## Conclusions and Prospects

- we are able to run Linux on FPGAs on MoGURA, both hard core (powerpc) and soft core (microblaze)
- our goal of developing and debugging MoGURA firmware independent of supporting company is far from complete
  - software alone is too slow, RTL alone is too hard to master
  - somewhere in between would be the final scheme
- possibilities includes
  - hybrid: CPU architecture with software optimized by hardware accelerator
    wrap present RTL into accelerators
  - hybrid: independent Linux and RTL for different tasks and communicated via a bus
    minimal change, only new features in software
  - C-to-RTL: generates VHDL from C syntax and libraries, easy to simulate
    e.g. No-Instruction-Set-Computer
  - myHDL: generates VHDL from python, easy to simulate
  - any mixture of the above



http://www.awa.tohoku.ac.jp/~benda
benda@awa.tohoku.ac.jp

# MAGNETIC PROPERTIES OF POTASSIUM DOPED POLYACENE: ANTHRACENE, TETRACENE, PENTACENE

Quynh Phan, Satoshi Heguri, Katsumi Tanigaki
Department of Physics, Graduate School of Science, Tohoku University

## Motivation

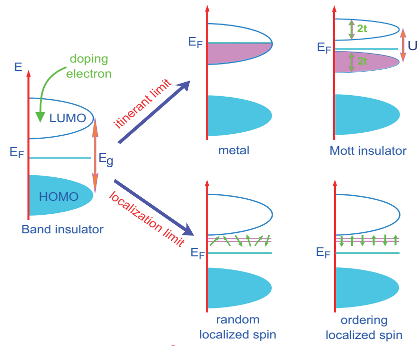


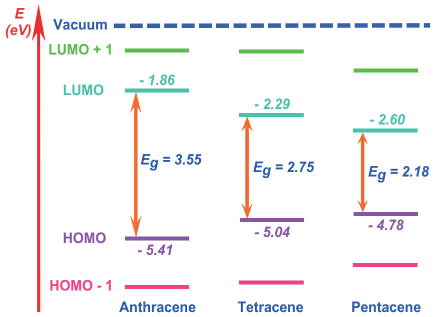


- Searching for synthetic technique induce high homogeneity alkali metal doped organic semiconductor
- Investigating electronic states of intercalation compounds between anthracene, tetracene, penrtacene and potassium

## Experiment

### Synthesis

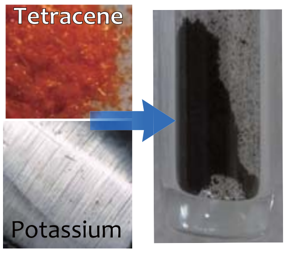


Annealing in glycerin bath, He atmosphere

- Anthracene: 70°C
- Tetracene: 180°C
- Pentacene: 180°C

### Crystal Structure & XRD measurement

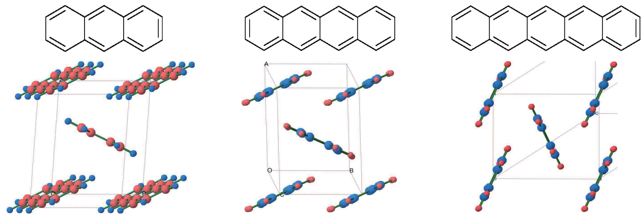

| Anthracene | Tetracene | Pentacene |
|---|---|---|
| Monoclinic | Triclinic | Triclinic |
| $P2_1/a$ | P1 | P1 |

- Packed in capillary
- Condition: Ar gas
- Measured at SPring-8

### SQUID measurement

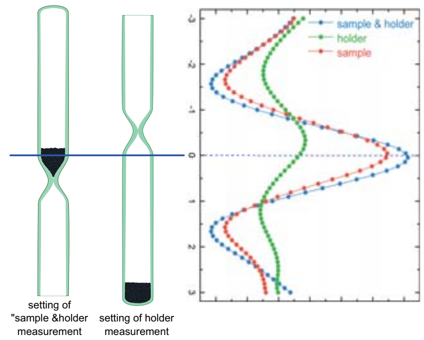


Subtract signal of quartz tube from one of sample in tube

## Result & Discussion

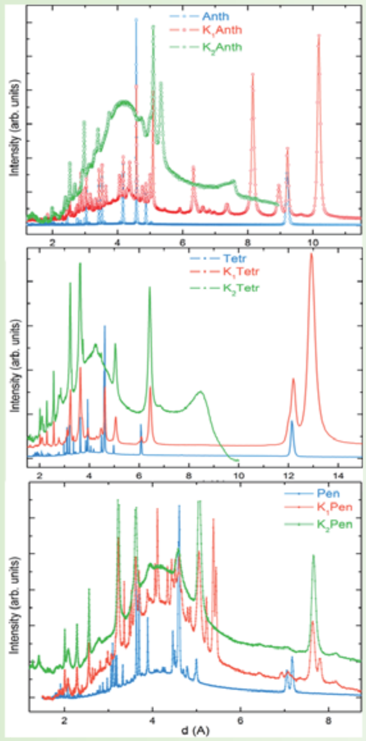


- $K_1$Anth, $K_1$Tetr, $K_1$Pen: remain pristine diffraction peaks
- $K_2$Anth, $K_2$Tetrn: pristine peaks disappear.
- All $K_1$ samples exist different peaks from $K_2$ samples.

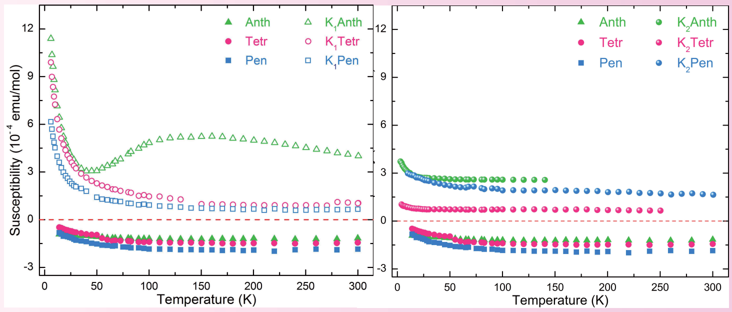


- $K_1$Anth show a hump $K_2$Anth large magnetization
- $K_1$Tetr & $K_2$Tetr: same magnetization at high T range
- $K_1$Pen: magnetization less than $K_2$Pen

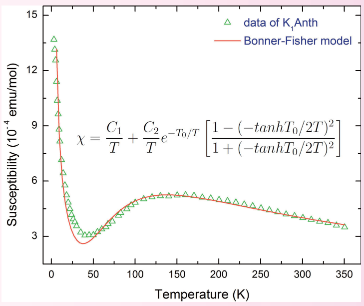


Antiferromagnetic interaction
Ising chain model

Doped spin number:
*n = 0.44 spin/molecule*

Interacting energy:
*J = 8.3 meV*

## Summary & Future work

### Summary

- K doped samples with nominal composition 1 include pristine & $K_2$ phase beside $K_1$ phase.
- $K_1$Anth is stable while $K_1$Tetr & $K_1$Pen are not.
- Antiferromagnetic interaction only exist in $K_1$Anth

### Future work

Synthesizing intercalation compound of other polycyclic aromatic hydrocarbons
➡ Investigating effects of molecule structure & crystal structure to electronic state

# A Test for Uniformity of BGO Crystals to be Used For an EM Calorimeter

**Qinghua HE, Ryuji YAMAZAKI, Shinichi MASUMOTO**
Research Center for Electron Photon Science, Tohoku University

## Abstract

We are constructing a 4π BGO electromagnetic (EM) calorimeter named BGOegg. It consists of 1320 BGO crystals, which are shaped as tapered blocks to make up an egg-shaped EM calorimeter. The scintillation lights of each BGO crystal will be read out through the back surface with a photomultiplier tube (PMT). If the light collection from every point along the path of interacting particles is not uniform, the whole crystal will give different responses depending not only on the energy deposit but also on the position of the light release. In other words, the amount of scintillation lights reaching PMT is affected by the shape of the BGO crystal. In general, the position dependence of light output could be attributed to the optical properties of tapered crystals and reflectors with which the crystals are wrapped. The surface treatment by an etching method can make an improvement on the uniformity. In the present test, we are measuring the effect on the uniformity due to different surface treatments and wrapping reflectors for BGO crystals. Three different surface treatments and three kind of wrapping reflectors have been tested. In this presentation, we report the results of longitudinal uniformity for each combination of surface treatment and reflector for BGO crystals.

## BGOegg

The left part of figure 1 shows the overall geometry of the BGOegg covering the polar angle from 24° to 156°. This egg- shaped BGOegg consists of 1320 BGO crystals which are shaped as tapered blocks. The plot on the right side of figure 1 displays the arrangement of BGO crystals between 24° - 90° polar angle and the shape parameters for each crystal. The horizontal axis z is along the incident gamma beam as shown in the picture on the left side of figure 1 while the vertical axis represents the distance to the axis z.

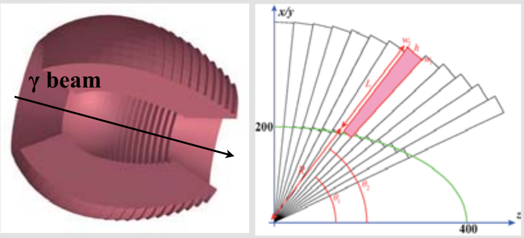


Fig. 1 The overall geometry of BGOegg (left) and the arrangement of the BGO crystals(right).

## BGO Crystal

Three kinds of surface treating methods are used in order to change the optical properties. These methods are named Main, Etched and Polished respectively. More details about each method are described in the following table. Figure 2 shows the 00F BGO crystal processed with Main, Etched and Polished surface treating methods respectively. For the purpose of improving light reflection on the surfaces of the crystal, three kinds of reflectors (ESR, Al foil and Tyvek) are applied as a wrapping reflector for BGO crystal as shown in figure 3.

| Surface treatment | |
|---|---|
| 1.Main | Both front and back surfaces polished while the lateral surfaces etched |
| 2.Etched | Only back surface polished while other surfaces etched |
| 3.Polished | All surfaces polished |

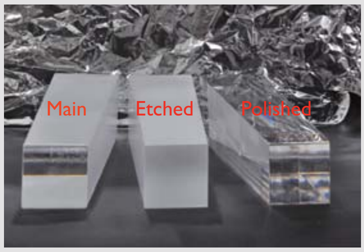


Fig. 2 Surface treatments.


Fig. 3 wrapping reflectors.

## Experimental Setup

As shown in figure 4, the experimental setup mainly consists of a photomultiplier tube, a BGO crystal, a collimator, a $^{137}C_s$ gamma source (Eγ=661.7 keV) and several light shielding equipments. The collimator is made of two lead blocks (50×100×200 mm) with nine holes of 6 mm in diameter, which is placed at about 120 mm far from the BGO crystal. The distance between two adjacent holes is 25 mm and the depth of the hole is 50 mm. The gamma source is placed at the entrance of one of the these nine holes in order to change the measuring point on BGO crystal. A circuit diagram of DAQ system is displayed in figure 5.


Fig. 4. An photograph of the experiment setup.

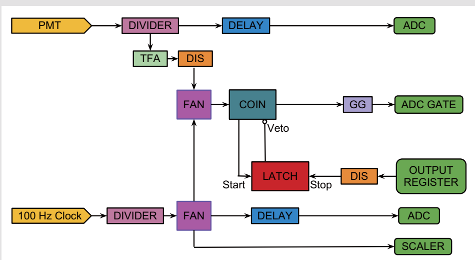


Fig. 5. Electrical data acquisition system.

## Results

In this section, we report the results of the test of the effect on the uniformity of BGO crystal due to different surface treatments and wrapping reflectors. Figure 6 displays the light output as a function of the distance from PMT. Figure 7 shows the distance dependence of the resolution. The non-uniformity is plotted versus the distance in figure 8. These results show that the Main surface treatment have the best uniformity while the Polished one the worst and the ESR reflector have the largest light output , better energy resolution and an improvement on the uniformity. Based on these ideas, it can be concluded that a BGO crystal with Main surface treatment and ESR reflector has an optimal performance compared with other combinations of surface treatment and reflector.

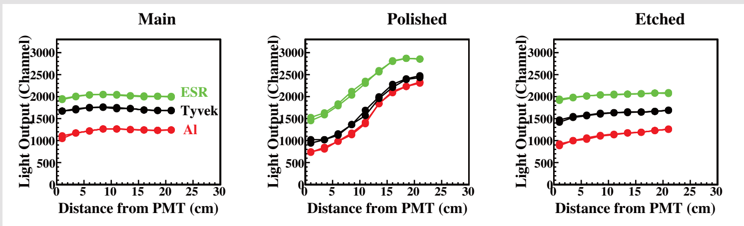


Fig. 6. Light output are plotted as a function of the distance from PMT.

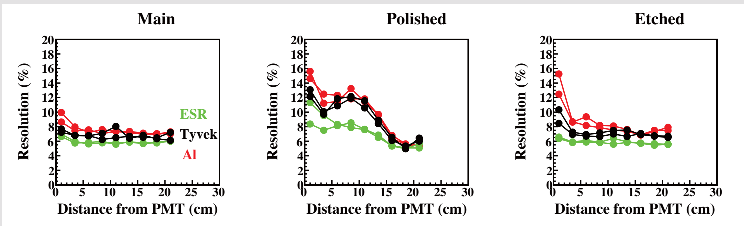


Fig. 7. Resolution is plotted versus the distance from PMT.

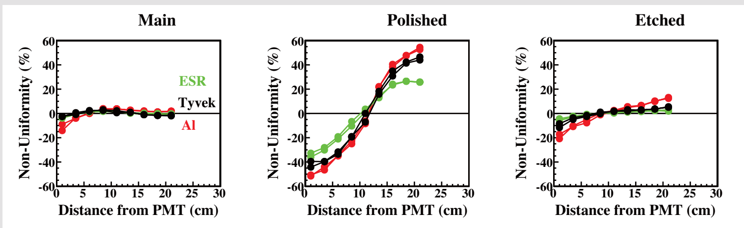


Fig. 8. Non-uniformity is plotted as a function of the distance from PMT.

A living body system uses an amphipathic molecule etc. as a fundamental component

S.FUKAYA
Department of Physics, Tohoku univ., Sendai, Japan

## Vesicles has 'strange' form

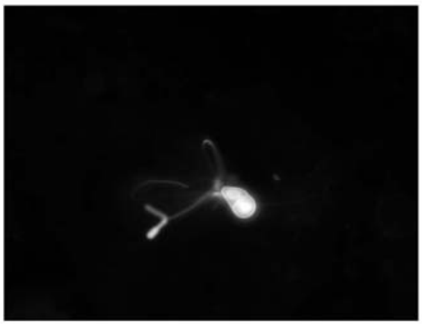

## Time variation of vesicle

- NaOH solution was dropped

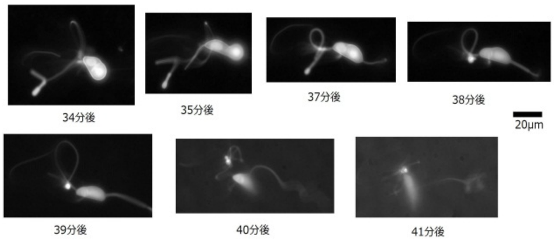


## What is a Vesicle

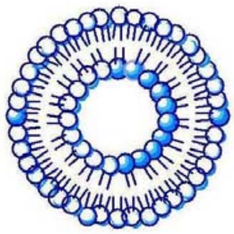

- Sphelical lipid bilayer membrare

## effect of changes in pH

- nomal

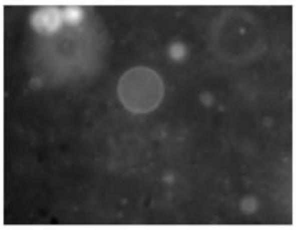

- NaOHaq dropped

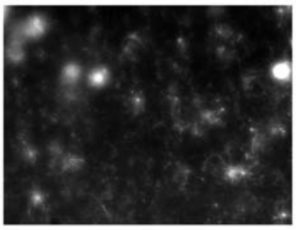

## effect of changes in pH(graph)

- In pH12

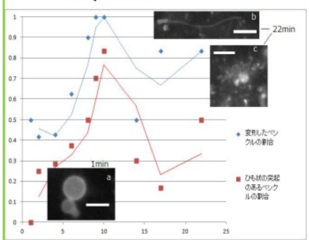


- In various pH

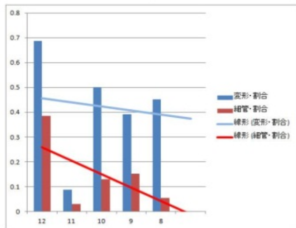

## How does form of a vesicle change?

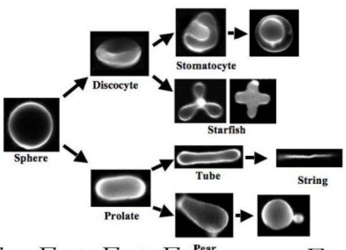


- Area Difference Elasticity model

$$F = F_b + F_l + F_A$$

$$F_a = \frac{\langle \kappa_r \rangle}{2Ad^2}(\Delta A - \Delta A_0)^2$$

$$F_b = \int \left(\frac{1}{2}\kappa(2H)^2 + \bar{\kappa} K\right) dA$$

$$F_l = \sum_i \sigma \oint dl^{(i)}$$

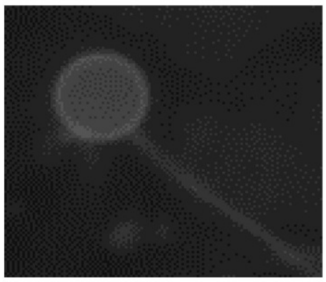

...but
Tubuler formation has not been exprained completly!

# CRYSTAL GROWTH OF NEW TARGET SYSTEMS FOR HIGH-ENERGY NEUTRON-SCATTERING MEASUREMENTS AT J-PARC


K. Tsutsumi[1], M. Enoki[1], K. Sato[1], Y. Ai[1] M. Matsuura[2], K. Yamada[3], and M. Fujita[2]

[1]*Department of Physics, Tohoku University, Sendai, Japan*

[2]*Institute for Materials Research, Tohoku University, Sendai, Japan*

[3]*World Premier International Research Center, Tohoku University, Sendai, Japan*


## Introduction

Magnetism on doped CuO2 plane is considered to play a key role for the emergency of high-Tc superconductivity. Therefore, the observation of spin fluctuations is important. However, huge amount of crystal is required for the neutron scattering measurement due to the low flux.


~10cc

## Motivation

Except for few examples, growth of large single crystal of high-Tc cuprate is difficult. To overcome difficulties in the crystal growth, and to obtain sufficiently large crystal for the neutron scattering measurement. we have attempted improved floating-zone method for a couple of systems Also, we have prepared high-quality but tiny crystals and assembled them to gain the effective sample volume.

## Method

### Floating-Zone method

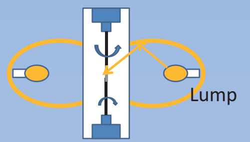


**Merit**
Large and impurity-free crystal can be available.

**Demerit**
Difficulty in finding out the growth condition

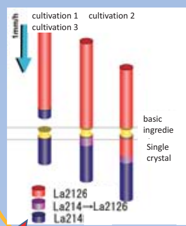


We used a feed rod with a concentration-gradient. The crystal growth was started from a part for which the growth is rather easy and continuously proceeded with changing conditions.

## Crystal Growth

### $La_{2-x}Ca_{1+x}Cu_2O_6$

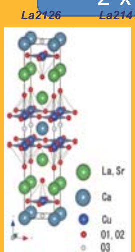


| basic ingredient | La2126-System | La214-System |
|---|---|---|
| Solvent composition | $La_{1.9}Ca_{1.1}Cu_2O_8$ | $La_{1.88}CSr_{0.12}Cu_5O_{8+\delta}$ |
| Solvent quantity | 200-270mg | 200mg |
| Air | Oxygen flow | Oxygen flow |
| Feed | 1.00mm/h | 1.00m/h |
| Rotation | 25rpm | 10rpm |
| Lump power | 160-170W×2 | 200W×2 |

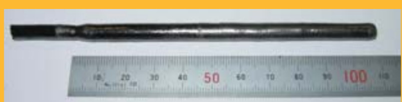

### $Bi_{2+x}Sr_{2-x}CuO_{6+\delta}$

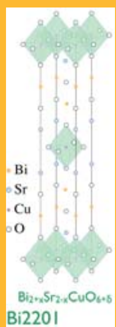


| basic ingredient | Bi2201-System |
|---|---|
| Solvent composition | None |
| Air | Oxygen flow |
| Feed | 0.60mm/h |
| Rotation | |
| Lump power | 150W×2 |

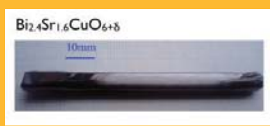


### $YBa_2Cu_3O_{6+\delta}$

$YBa_2Cu_3O_7$

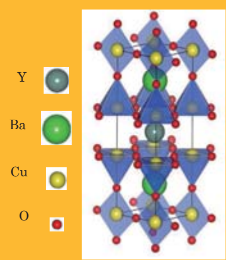



3.0×3.0×0.3[mm]

10pieces～100mg

Large single crystals for neutron scattering measurement have been successfully obtained.

Several tiny crystals were assembled.

## Results of Preliminary Neutron Scattering measurement

Elastic neutron scattering @AKANE JRR-3

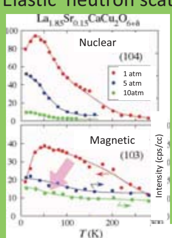


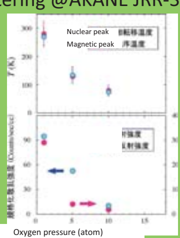


With increasing the oxygen pressure during the crystal growth, intensity of both nuclear and magnetic peaks are reduced.

Close relation between crystal structure and magnetic order

The first observation of spin fluctuation in Bi2201

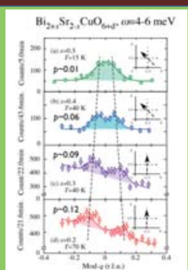

Incommensurate spin fluctuations exist and the peak-splitting increases upon doping, similar to the case of LSCO

Possible universality of spin correlation in single-layer system

annealed in $N_2$ gas flow @530° C

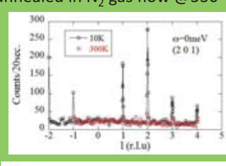


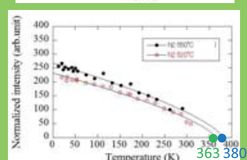


Magnetic order and its doping-dependence were confirmed

## Summary

Utilizing an improved growth technique, we have succeeded in growing large single crystal of new target systems for neutron scattering measurement. Preliminary measurements have been done at triple-axis spectrometer and we observed magnetic response in the new samples. Based on these results, we are going to study high-energy spin dynamics by using a newly constructed high-flux neutron beam facility, J-PARC

# Simple model for rupture process of pressure-sensitive adhesives


Shinobu Sekine

Tohoku University,Department of physics


2012/02/20



## Abstract:


Pressure-sensitive adhesives (PSA) are very useful in our ordinary life, which is a thin layer applied, for example, on the surface of tape film. Typical materials of PSA are made of block copolymers such as acrylates or styrene-isoprene-styrene (SIS) triblocks. They are usually very soft and highly dissipative, and can stick on a variety of surfaces under low pressure in short time without any solvent evaporation, heating process or chemical reactions.
We propose a simple mechanical model describing viscoelasticity and cavitation during the crack propagation process in pressure-sensitive adhesive. This model is originally proposed by Yamaguchi et,al,. They applied this model for probe-tack test, but their model is not applicable to the final rupture process. We extended this model to treat this rupture process, and applied to the situation of peel test.
In this presentation, we will report our extended model and calculation results.




## PSA debonding process

PSA=Pressure Sensitive Adhesives.
Example of PSA is the viscoelastic surface layer of packing tape.

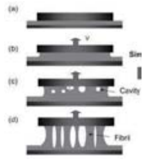


Figure: Schematics of PSA debonding process

The debonding process of PSA [a]:

- Initial state
- Uniform deformation
- Cavity expansion
- fibrillation
- fracture of fibrils or debonding from the probe

[a] T.Yamaguchi et al:Eur.Phys.J.E 20,7-17(2006)



## Rupture block model

Our model is extended from Yamaguchi's model [1]. Original Yamaguchi's model is not treated in the final rupture process.

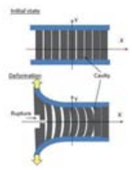


Figure: Schematics of PSA rupture block model model

Major features of this model:

1. the adhesive layer is divided into $N_b$ rectangular blocks of equal size
2. the flow of films is assumed to be superposition of slippage and parabolic deformation of the block
3. cavity is assumed to described by the gap between adjacent blocks
4. cavitation dynamics is described by the Rayleigh-Plesset equation
5. If the elongation ratio is over the limitation conditon,this block is divided into half.

[1] T.Yamaguchi et al:Eur.Phys.J.E 20,7-17(2006)



## Deformation of one block

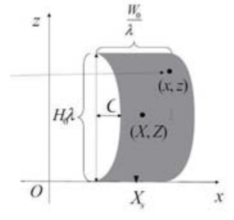


Figure: Coordinate system to describe the block motion and deformation

- (X,Z):Coordinates of the center of gravity,
- $X_s$:Coordinate of the central position of the surface.
- $C$:Parameter characterizing the parabola $\propto$ curvature of the side surface
- $H_0$:Initial thickness
- $W_0$:Initial width of one block
- $\lambda(t)$:Elongation ratio



## Constitutive equation

**The upper-convected Maxwell fluid model**

$$\frac{\partial \sigma_{ij}}{\partial t} = -\frac{1}{\tau}\sigma_{ij} + \left(\frac{\partial v_k}{\partial x_i}\right)^T \cdot \sigma_{kj} + \sigma_{ik} \cdot \left(\frac{\partial v_k}{\partial x_j}\right) + \left(\frac{\partial v_j}{\partial x_i} + \left(\frac{\partial v_j}{\partial x_i}\right)^T\right) \quad (1)$$

- With a single relaxation time $\tau = \frac{\eta}{G}$
- Generalization of Newtonian fluid to satisfy principle of material objectivity.

**Principle of material objectivity**

Physical properties,such as angle,length, are unchanged by any parallel displacement and rotation as a whole in any manner in space[2]

[2] T.Kyoya:Continuum Mechanics(in Japanese),Morikita,2008



## Surface tension and rupture process.

Surface tension is acting on upper side of blocks because of the deformation.

$$\eta \dot{z}_j = \gamma \frac{(z_{j+1} + z_{j-1} - 2z_j)}{w_0^2}, \quad z_j(t) = H_0\lambda_j(t)$$

$$\therefore \dot{\lambda}_j = \frac{\gamma}{\eta w_0^2}(\lambda_{j+1} + \lambda_{j-1} - 2\lambda_j) \quad (2)$$

$$\eta : viscosity, \gamma : surfaceenergy \quad (3)$$

R.H.S. is assumption of curvature elasticity.
To describe rupture process,we introduce the forming rupture condition:

$$\lambda(t)_j > \lambda_{limit} = 2.0 \quad (4)$$

If one of these block's elongation ratio is over this limitation,this block is ruptured at the center point. After this rupture process,the under surface of this block, which is created this process newly,has same motion under surface tension describe above.



## Parameter

The typical set of parameters.

| Parameter | Unit | Value | Comment [3] |
|---|---|---|---|
| PSA thickness $H_0$ | m | $1.0 \times 10^{-4}$ | |
| PSA width $L_0$ | m | $5.0 \times 10^{-3}$ | |
| Separation speed $V_z$ | m/s | $1.0 \times 10^{-4}$ | $\dot{\lambda} = 0.1$ |
| Atmospheric pressure $P_0$ | Pa | $1.0 \times 10^{5}$ | |
| Viscosity $\eta$ | Pa s | $2.0 \times 10^{5}$ | $water 1.0 \times 10^{-3}$ |
| Elastic modulus $G$ | Pa | $2.0 \times 10^{3}$ | $Au 2.7 \times 10^{10}$ |
| PSA surface energy $\gamma$ | $J/m^2$ | $30.0 \times 10^{-3}$ | $water 70.0 \times 10^{-3}$ |
| Friction coefficient $\mu$ | Pa s/m | $2.0 \times 10^{9}$ | |
| Initial cavity radius $R_0$ | m | $1.0 \times 10^{-6}$ | |
| Number of blocks $N_{block}$ | | 100 | |
| Rupture condition $\lambda_{limit}$ | | 2.0 | |

$$Relaxation\ time\ \tau = \frac{\eta}{G} = 100[s]$$

[3] material properties are referenced by Rika Nenpyo



## Snap shots of deformation

For the symmetry of the model system,these images are drawed on

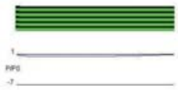

STEP0:Initial stage

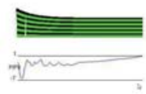

STEP3:Generation of cavity

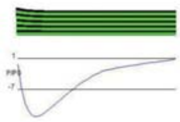

STEP2:Early state of deformation

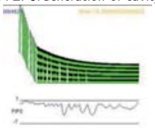

STEP4:Beginning of Rupture



## Effect of cavity

To consider the effect of cavity,we compare CASE1,which is cavity existed,and CASE2, no cavity existed.

| case | cavity |
|---|---|
| CASE1 | exist |
| CASE2 | not exist |

Cavity has very important effect for rupture process to weak the stress of the adhesive layer.

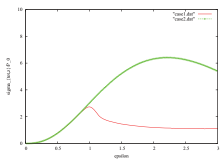


Figure: The stress-strain (S-S)curves for the effect of cavity



## Effect of thickness(1/2)

| case | $H_0[m]$ | $H_0/L_0$ |
|---|---|---|
| CASE1 | $1.0 \times 10^{-4}$ | 0.02 |
| CASE3 | $2.0 \times 10^{-4}$ | 0.04 |
| CASE4 | $5.0 \times 10^{-5}$ | 0.01 |

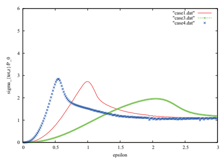


Figure: The S-S curves for various thickness

1. Initial stage is strongly affected by the thickness of the adhesives.
2. The stress at the peak decreases as the thickness of the adhesives increases.
3. The peak position is dependent of the film thickness.



## Effect of thickness(2/2)

### Origin of these results

From the detail calculation of upper convected Maxwell model (1), we get the following result:

$$\frac{\partial \sigma_{s,j}}{\partial t} = -\frac{\sigma_{s,j}}{\tau} + \frac{4\dot{C}_j}{H_0\lambda}(\sigma_{zz,j} + G)$$

In the initial stage, $\sigma_{s,i} = 0$:

$$\frac{\partial \sigma_{s,j}}{\partial t} \simeq \frac{4\dot{C}_j}{H_0\lambda}(\sigma_{zz,j} + G)$$

where $\sigma_s$:shear stress at the surface.
R.H.S shows that thinner the thickness of the adhesives $H_0$, larger the rate of stress increases.



## Effect of separation speed(1/2)

**Deborah number**

$$D_e = \frac{\tau\dot{\lambda}L_0}{H_0} = \frac{stress\ relaxation\ time}{time\ scale\ of\ observation} \quad (5)$$

At higher $D_e$,fluid property changes viscosity to elasticity.

The peak stress value increases as the separation speed $\dot{\lambda}$ goes up.

| case | $\dot{\lambda}$ | $D_e$ |
|---|---|---|
| CASE1 | 0.1 | 500 |
| CASE5 | 0.5 | 2500 |
| CASE6 | 0.02 | 100 |

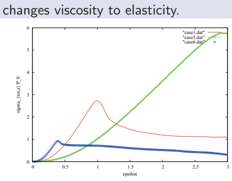


Figure: S-S curves for various $\dot{\lambda}$



## Effect of separation speed(2/2)

### Origin of these results

- Higher separation rate causes larger shear stress and larger resistance for the cavity expansion,leading to the larger negative pressure (6).

$$\dot{R}_j = \frac{R_j}{2\eta}(P_{cav,j} - P_j) - \frac{\gamma}{2\eta}$$

$$\therefore P_j = P_{cav,j} - \underbrace{\left(\underbrace{\frac{2\eta\dot{R}_j}{R_j}}_{dissipation} + \underbrace{\frac{\gamma}{R_j}}_{surface\ tension}\right)}_{Lead\ to\ large\ negative\ pressure} \quad (6)$$



## Effect of friction coefficient

The stress decreases with the decrease of $\mu$ since slippage at the surface reduces the negative pressure.

| case | $\mu$ |
|---|---|
| CASE1 | $2.0 \times 10^{9}$ |
| CASE7 | $2.0 \times 10^{8}$ |
| CASE8 | $2.0 \times 10^{10}$ |

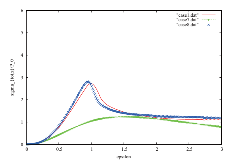


Figure: S-S curves for various friction coefficients



## Conclusion

- We extended Yamaguchi's block model to treat rupture process.
- In qualitative view point,our results are good agreement of experimental data.
- Cavity has very important effect for rupture process to weak the stress of the adhesive layer.As can be seen from this result,to compare simulation results and experiments quantitativery,we would need more detailed modeling,for examples,shape and position of cavity,stress concentration around cavity.
- The slip velocity is proportional to the shear stress at the interface. $\mu\dot{X}_{si} = \sigma_{si}$ Though such model is standard for simple liquid, non-linearity and memory effect will be important for adhesives.
- The constitutive model is the viscoelastic fluid one, while the commercial PSA is viscoelastic solid because it is actually weakly cross-linked.

# An investigation of the photo induced production of strangeness in the threshold energy range.


## B. Beckford for NKS2 collaboration, Dept. of Physics, Tohoku University


## Introduction

### Strangeness photoproduction

Strangeness production on a nucleon or a nucleus by the electromagnetic interaction provides invaluable information on the strangeness production mechanism and strengths of meson-hadron coupling constant.. Kaon photoproduction can be a good probe to find missing resonance states.

NKS2 experiment aims to explore the strangeness photoproduction on the deuteron by measuring neutral kaons and Λ hyperons with tagged photon beams of $E_\gamma$ = 0.8-1.1 GeV.

### $n(\gamma, \Lambda)K^0$ reaction in the threshold region

$n(\gamma, K^0)\Lambda$ process has unique features in the investigation of kaon production process by electromagnetic interaction as follows,

- no charge in initial and final state
  - → t-channel Born term does not contribute
- isospin symmetry to $p(\gamma, K^+)\Lambda$ process
  - → sign of coupling constant in u-channel is opposite
  - $g(K^0\Sigma^0 n) = -g(K^+\Sigma^0 p)$
- the electromagnetic coupling constants of resonances in the s- and t-channels
  - → It' s different from $K^+$ process : e.g., $g(N^* n\gamma)$ and $g(K^* K^0\gamma)$

Due to these characteristics, the interference among the diagrams in the $K^0$ production process is quite different from that in the $K^+$ process. For the elementary reaction of $\gamma n \rightarrow K^0\Lambda$, photon energy dependence and angular distribution at Eγ = 1.05 GeV are calculated using Kaon-MAID model and Saclay Lyon model(SLA). These two isobar models agree well in their predictions of the $\gamma p \rightarrow K^+\Lambda$ process, however they are significantly different for the $\gamma n \rightarrow K^0\Lambda$ process.

*Total cross section for 6 isospin channels of kaon photo-production*

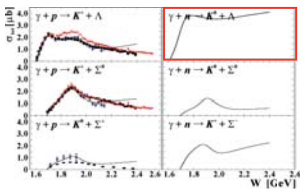


solid lines : Kaon-MAID [T. Mart and C. Bennhold, Phys. Rev. C 61 012201(R) (1999)]
data : SAPHIR(98) [M. Q. Tran et al., Phys. Lett B445, 20 (1998)] [S. Goers et al., Phys. Lett B445, 20 (1998)]
SAPHIR(04) [K. -H. Glander et al., Eur. Phys. J. A 19, 251 (2004)] [R. Lawall et al., Eur. Phys. J. A 24, 275 (2005)]
CLAS [R. Bradford et al.(CLAS Collaboration), Phys. Rev. C 73, 035202 (2006)]

*Feynman Diagrams for isobar model*

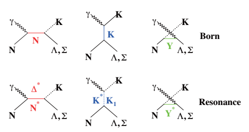


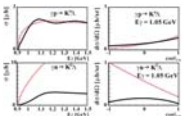

- $n(\gamma, \Lambda)K^0$ reaction
  - $K^0_S : K^0_L$ = 1 : 1
- Λ decay channel
  - Λ (cτ = 7.89 cm)
  - : $p\pi^-$ (63.9 ± 0.5 %)
  - $n\pi^0$ (35.8 ± 0.5 %)

- Total Cross Section Incident Photon Energy Dependence
  - Kaon-MAID and SLA Isobar Models

Total Cross Section of Inclusive Λ Measurement

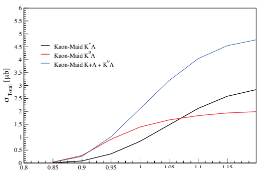


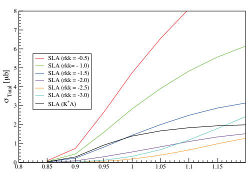


- Angular distribution
- Using RPR (Regge Plus Resonance)

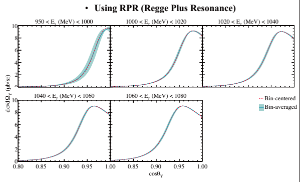

Angular distribution in lab frame, forward peak is suggested

## Experimental Apparatus

### Tagged photon beam

NKS2 was installed at Laboratory of Nuclear Science, Tohoku (LNS-Tohoku).

The photon beam is generated via bremsstrahlung and the scattered electron's energy is tagged by STB-Tagger system.

- Energy Region: 0.8 - 1.1 GeV
  - $n(\gamma, K^0)\Lambda$ threshold (915 MeV)
- Energy Resolution: 10 MeV
- Beam Intensity: $2 \times 10^6$ Hz
- Duty Factor: 35 - 85 %

**Schematic view of the experimental hall in ELPH**

**STB Tagger System**

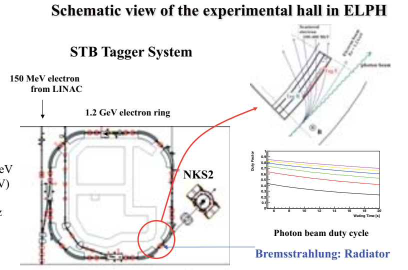


### NKS2 Upgrade Setup

Λ are measured with Neutral Kaon Spectrometer (NKS2) by detecting the $\Lambda \rightarrow p\,\pi^-$ decay channel .

NKS2 is a spectrometer dedicated to measure the $n(\gamma, \Lambda)K^0$ reaction in the threshold region. It consists of a dipole magnet and two types of drift chamber, TOF counter. The liquid deuterium target is located at the center of NKS2.

*Schematic view of NKS2*

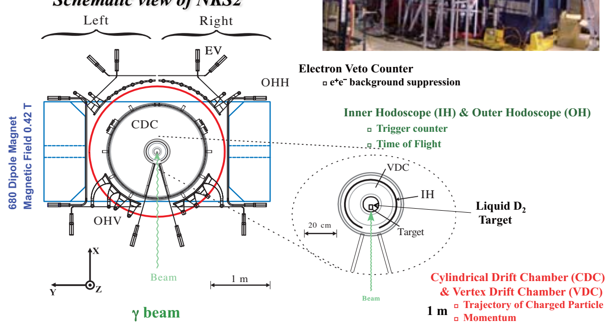


## $p\pi^-$ Event Distribution

*Particle Identification (PID)*

PID capability of two charged particle track events

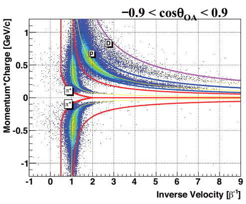


The correspondence particles the between the square of the particles' mass and momentum.

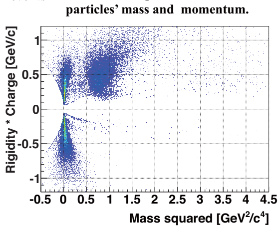


The figure above presents the correspondence particles the between momentum and inverse velocity. The red, blue and magenta line represents the pion, proton and deuteron designated regions.

The figure at the right is the kaon missing mass in the MMx (γN->(pπ⁻)X measurement

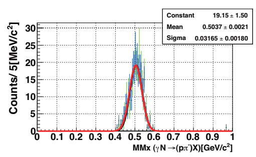


*Invariant Mass Distribution*

This figures presents the invariant mass distribution of $p\pi^-$ each energy bins. The $p\pi^-$ invariant mass is shown with the missing mass region of region of $MM_{\pi+\pi-}$>0.40 GeV/c$^2$ . The green line shown in the fit represents the estimated background.

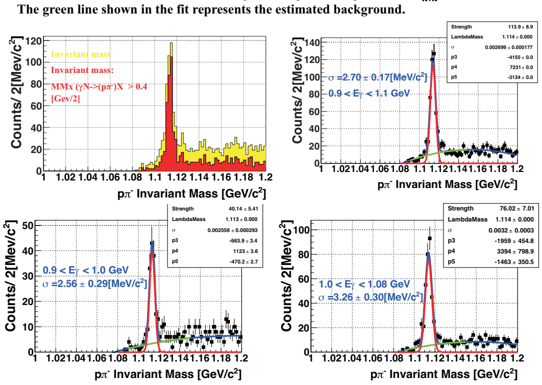


*Momentum and Angular Distribution*

Simulated momentum and angular distributions

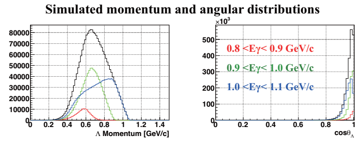


The Lambda particle was generated isotropically in the laboratory frame. The distribution are shown for the energy range of 0.8-1.0 , 0.8 - 0.9, 0.9-1.0, 1.0-1.1 GeV as black, red, green and blue lines respectively.

Measured momentum and angular distributions

The background is estimated from the side bands in the invariant mass distribution is shown as the red and blue solid squares.

Background is attributed to miscombinations of $p\pi^-$

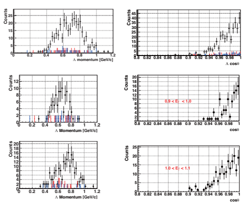

## Detector Acceptance

Λ Acceptance

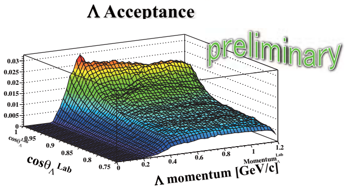


Simulation Condition :

Generated Λ isotropically in Lab frame,

$0 < p_\Lambda < 1.2$ GeV, $0.75 < \cos\theta_\Lambda^{Lab} < 1.0$

Use the same analyzer for the experimental data.

## Total Cross Section

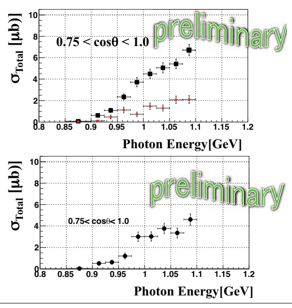


## Momentum Spectra

After acceptance correction

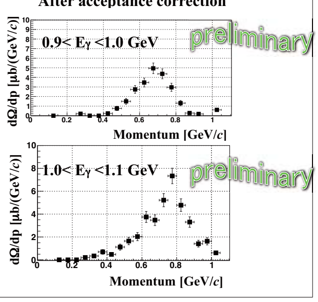


## Summary

- The $\gamma + n \rightarrow K^0 + \Lambda$ process plays a unique role in the investigation of photoproduction mechanism
- We have successfully the upgrade of Neutral Kaon Spectrometer (NKS2) The experiment in the photoproduction of strangeness on a deuteron target was accomplished using a tagged photon beam at the ELPH research facility
- The invariant mass spectrum of $p\pi^-$ was obtained and the resolution of the spectrums have been detailed
- The momentum distribution was obtained for two photon energy region, 0.9 to 1.0 GeV and 1.0 to 1.1 GeV.
- Preliminary results have been reported.

# Research of Transmission-line STJ Detector for Terahertz Band

Kenta TAKAHASHI[a,b], Seiichiro ARIYOSHI[a], Takashi NOGUCHI[c], Masahiko KURAKADO[a,d], Kensuke KOGA[a,b], Noboru FURUKAWA[a], Chiko OTANI[a,b]

[a] RIKEN , [b] Tohoku University , [c] National Astronomical Observatory of Japan , [d] Techno X Co.,Ltd.

**Abstract**

We have proposed and demonstrated a new broadband and high efficiency THz wave detector using a superconducting tunnel junction (STJ). The detector uses by Cooper-pair Braking(CPB) process. The detector consists of two log-periodic antenna wings connected with an impedance transformer and two long (micro-stripline) STJs. The detector utilizes the excess tunneling current caused by the Cooper pair breaking due to the radiation whose photon energy is greater than the energy gap of the used superconductor (around 0.7 THz for niobium). We have fabricated the device and performed the experiments for confirming the principle of this detector. We have succeeded the detection for the first time.

## 0.Introduction

Terahertz (THz) waves are electromagnetic waves with frequencies between high-frequency edge of the microwave band and the long-wavelength edge of far-infrared light. THz waves were non-development from difficulty of the generation and the detection, but a study of THz band advances in late years, THz band attracts attention in the field of industry and research.

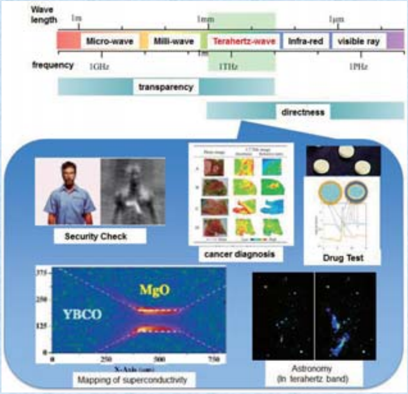


## 1.Desin of Micro-stripline Detectors

### Mechanism of STJ detector

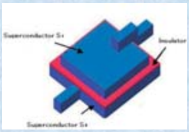

There are two detection processes to the STJ detector. One is the Cooper-pair Braking(CPB). The other is the Photon Assisted Tunneling(PAT) process. They are separate by the gap frequency of the superconductor.

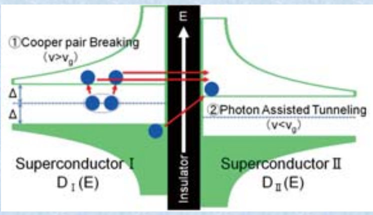


**Density of the state of the STJ**

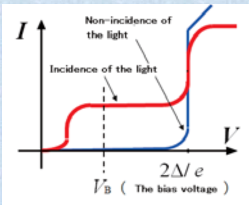


**I-V curve of the STJ**

### Transmission-line STJ Detector

If the length of STJ is enough long compared with the mean free path of the emergent quasiparticles (~10 μm for niobium), the energy of THz waves is absorbed by the STJ behaves as a transmission line and we detect it.

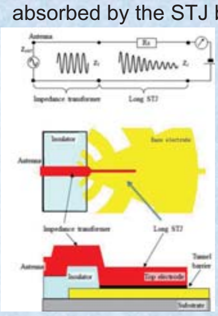

①Length of STJ $L_j$

A:Amplitude of THz wave after through STJ

$$A = \exp(-\alpha L_j) \approx \exp\left(-\frac{\frac{R_s L_j}{Z_j} + \frac{Z_j}{R_n}}{2}\right) \quad (1)$$

$\alpha$: Decay constant $L_j$: Length of STJ
$Z_j$: Impedance of STJ $R_s$: Surface resistance of Nb $R_n$: Normal resistance of STJ

| Length of STJ $L_j$[μm] | 2.9 | 6.7 | 26.7 | 50 |
|---|---|---|---|---|
| Power $\lvert A\rvert^2$ | 1/e | 1/10 | 1/10000 | <10⁸ |

②Width of STJ $W_j$

Impedance matching

$$Z_t = \sqrt{Z_{ant} \times Z_j} \quad (2)$$

Relation between impedance and width

$$Z_j \propto \frac{Z_0}{W}, Z_t \propto \frac{Z_0}{W} \quad (3)$$

$Z_{ant}$: Impedance of Antenna $Z_t$: Impedance of Transformer $Z_j$: Impedance of STJ

## 2.Fabrication of STJ

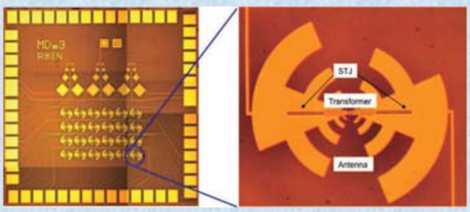


We have fabricated the STJ detector in RIKEN clean room. The left photograph is the general view and magnification image.

Lj:4kinds × Wj:3kinds = 12 kinds of combinations of length and width

## 3.Current-Voltage measurements

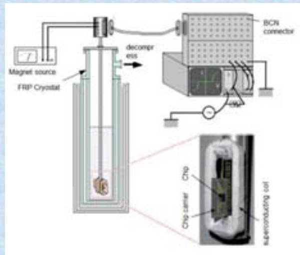

We measure the performance of the element by current voltage measurement. An important point is a value of the subgap leak currents of 4.2K and 1.5K. Because the decline of the leak current means the decline of the noise.

### 4μm×27μm-STJ detector

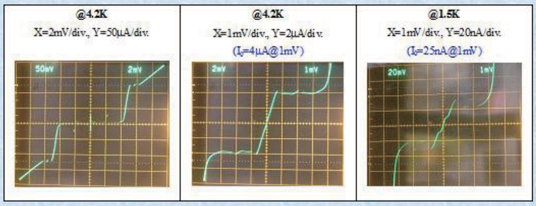


This STJ has good I-V curve in the subgap leak current. The current of 1.5K becomes one hundredth in comparison with the current of 4.2K.

## 4.Optical measurements (FT-IR)

### Fourier transform infrared spectrometer and 0.3K cryostat

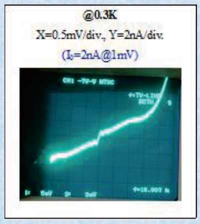


We measured optical properties with Fourier transform infrared spectrometer. We measured in 0.3K so that the leak current reduce enough.

### 4μm×27μm-STJ detector

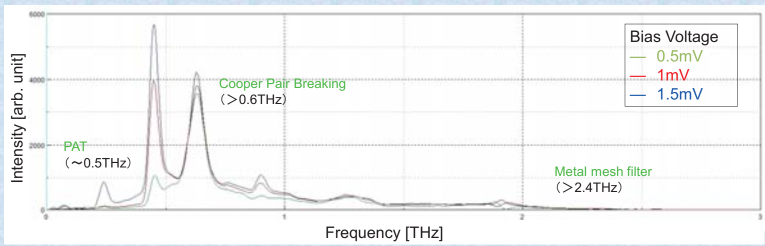


- CBP process detection is seen in more than 0.6THz.
- As bias voltage increases, PAT process detection increases.
- More than 0.7 THz detection is disturbed by the niobium antenna.

## 5.Summary

1.We have proposed a new THz wave detector using two long micro-stripline STJs.
2.We fabricated the device and performed the experiments for confirming its detection principle.
3.We have succeeded the detection of THz wave for the first time.

References:
1. T. Noguchi, T. Suzuki, 10th Workshop on Submillimeter-Wave Receiver Technologies in Eastern Asia (2009).
2. K. Takahashi, Master Thesis (in Japanese) (2011).
3. S. Ariyoshi et al., EUCAS2011 (2011).

4th GCOE SYMPOSIUM , February 20th - 22th 2012

# Evidence for Quantum Magnetotransport of Dirac Cone States in $Ba(FeAs)_2$

K. K. Huynh [a,*], Y. Tanabe [b,*], T. Urata [a], R. Nouchi [b], N. Mitoma [a], S. Heguri [a], J. Xu [b], G. Mu [a], H. Nojiri [c], K. Tanigaki [b,*]

[a] Department of Physics, Graduate School of Science, [b] WPI-Advanced Institute of Materials Research, [c] IMR,
Tohoku University, Aoba, Aramaki, Aoba-ku, Sendai, 980-8578, Japan

## Introductions and motivations

A Dirac Cone State (DCS) is a quantum state with a linear dispersion relation between energy (E) and momentum (k).

**Parabolic band**

$$E = \frac{\hbar^2 k^2}{2m^*}$$

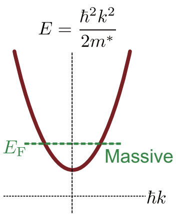


Usual metals and semiconductors.

**Dirac cone state**

$$E = \pm v_F \hbar |k|$$

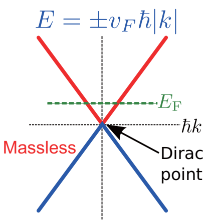


Graphene, Topol. Insulators, α-$(BEDT\text{-}TTF)_2I_3$, and **Iron Pnictide materials.**

❶ **Landau level (LL) splitting in magnetic field *B*:**

$$E_n = \pm v_F \sqrt{2\hbar e B |n|}$$

Distinguished energy scale
→ large LL splitting in a small B.

Intriguing quantum magnetotransport phenomena
(e.g. Quantum Hall Effects at room temperature)

❷ **Very light mass:**
high mobility carriers.

### $Ba(FeAs)_2$ material

DCS is theoretically predicted and experimentally observed (ARPES) in Ba(FeAs)2. In this material, the DCS's appear as SDW gap nodes.

High T tetragonal phase

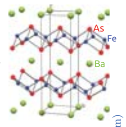


Low T Orthorhombic phase

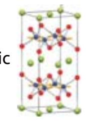

Interesting Transport properties

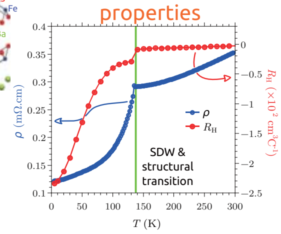


DCS (by ARPES)

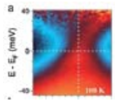

P. Richard *et al.*, PRL 104 137001 (2010)

DCS's are due to the SDW band folding at 138 K.

❶ Effects of DCS's on transport properties of $Ba(FeAs)_2$ ?
❷ Possible quantum transport of DCS's ?

## Experimental Results

Transport properties, including Resistivity ($\rho$), Magnetoresistance (MR), and Hall coefficient ($R_H$) of $Ba(FeAs)_2$ single crystal were measured and analyzed in order to understand of the transport properties of the DCS's.

### Experimental setup

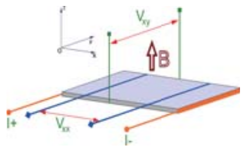


- Single crystal grown out from FeAs flux.
- $\rho$, MR, and $R_H$ were measured using PPMS.
- High-B (B ≤ 17.5 T) MR were measured at High Field LAB, Tohoku University.

### Interesting magnetotransport property

**MR is linear.**

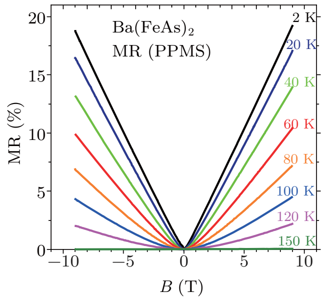


dMR/dB demonstrate clearly the *B*-linear dependence.

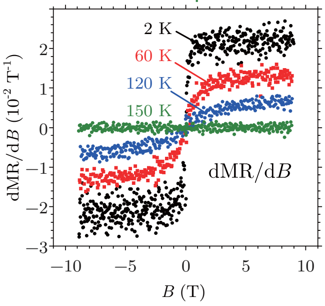


Linear MR persists up to $B \leq 17.5$ T

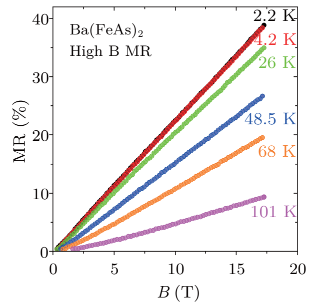


For an usual semimetal, MR is $B^2$-dependent. The *B*-linear MR indicates a distinct and new transport phenomenon.

## Analyses and Discussions

A detailed investigation of the *B*-dependent MR and dMR/d*B* reveals that the magnetotransport is composed of two regimes: **the semiclassical one at low *B*** and **the quantum regime at higher *B*.**

**Two transport regimes**

### Low *B*-region: Semiclassical transport

Two-carrier-type semiclassical model:

$$\rho(0) = \frac{1}{e\,(n_T \bar{\mu} + p_T \bar{\nu})}$$

$$\mathrm{MR} = \frac{\rho(B) - \rho(0)}{\rho(0)} = \frac{n_T p_T \bar{\mu}\bar{\nu}\,(\bar{\mu} + \bar{\nu})^2}{(n_T \bar{\mu} + p_T \bar{\nu})^2} B^2$$

$$R_H = \frac{-n_T \bar{\mu}^2 + p_T \bar{\nu}^2}{e\,(n_T \bar{\mu} + p_T \bar{\nu})^2}$$

Total numbers ( $n_T$ & $p_T$ ) and effective mobilities ( $\bar{\mu}$ & $\bar{\nu}$ ) of electron and hole can be estimated.

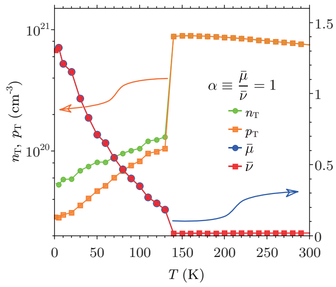


Carrier numbers drop down by 90% whereas mobilities of both electrons and holes jump up by 10 times at the SDW transition.

**Both electron-like and hole-like DCS's.**

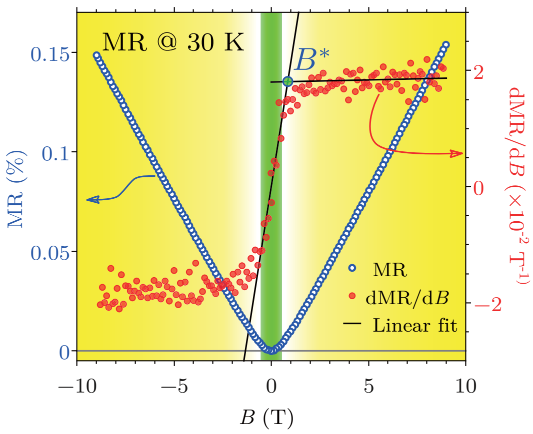


The semiclassical transport regime (MR ∝ $B^2$) crossovers to the quantum MR regime (MR ∝ *B*) at $B^*$ .

**The 1st LL splitting equals to $E_F$ and $k_BT$ at $B^*$:**

$$B^* = \left(1/2e\hbar v_F^2\right)\left(k_B T + E_F\right)^2$$

Estimations of $E_F$ and $v_F$

$$E_F = 1 \pm 5\ \mathrm{meV} \quad v_F \approx 1.88 \times 10^5\ \mathrm{ms}^{-1}$$

### High *B*-region: Quantum transport

Splitting between the 0th and the 1st LL's:

$$\Delta_1 = |E_{\pm 1} - E_0| = \pm v_F \sqrt{2\hbar e B}$$

A. A. Abrikosov, PRB 58 2788 (1998)

When $\Delta_1$ is larger than both Fermi and thermal energies, only the 0th LL is occupied.

$$\begin{cases} \Delta_1 > E_F \\ \Delta_1 > k_B T \end{cases}$$

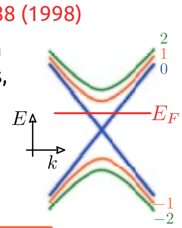


$\mathrm{MR} \propto \left(N_i / e n_D^2\right) \times B$ ($N_i$: impurity)

**Linear MR is the transport at the limit of 0th LL in DCS's.**

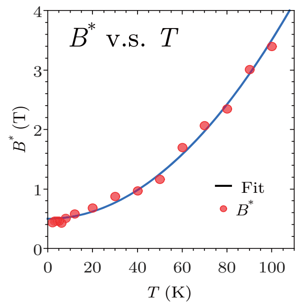


## Conclusions

❶ Below the SDW transition, transport properties of $Ba(FeAs)_2$ are dominated by the DCS's.
❷ The coexistence of electron-like and hole-like DCS's were observed. These two DCS's may reside at different $k_z$ positions.
❸ Quantum transport of the 0th LL in the DCS's are observed and confirmed by using the linear MR and the Abrikosov's model.

**Journal Ref.:** Khuong K. Huynh, Y. Tanabe, K. Tanigaki, *Phys. Rev. Lett.* 106, 217004 (2011)

# Double Chooz: A Search for the Neutrino Mixing Angle $\theta_{13}$


**Thiago J. C. Bezerra**
**on Behalf of the Double Chooz Colaboration**
thiago@awa.tohoku.ac.jp
**Research Center for Neutrino Science**
**Tohoku University**


## Purpose and Motivation

The main purpose of the Double Chooz Experiment is to determine the last unknown Neutrino Mixing Angle, $\theta_{13}$. It is important to know this parameter since it will let to the determination of the $\delta_{CP}$ in the neutrino sector and mass hierarchy.

$$P(\bar{\nu}_e \rightarrow \bar{\nu}_e) \cong 1 - \sin^2 2\theta_{13} \sin^2\left(\frac{\Delta m_{13}^2 L}{4E}\right) + O(10^{-3})$$

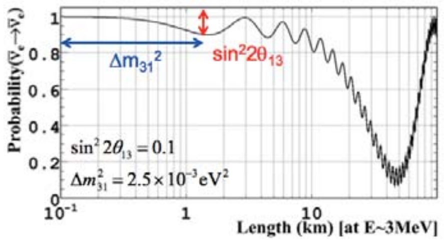


## Method

To obtain the $\theta_{13}$ value, the experiment will use two identical detectors, in order to cancel the systematics uncertainties (neutrino flux, interaction cross-section, number of target and efficiency).

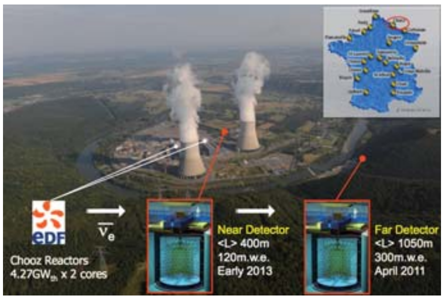


## Expected Antineutrino Rate and Detection Principle

Electron antineutrinos are produced in nuclear reactors through beta decays from the fission fragments. The two Chooz commercial reactors are used as source of antineutrinos and the expected number of events can be predicted using the following relation:

$$N_{\nu}^{\exp}(E,t) = \frac{N_p\,\varepsilon}{4\pi L^2} \times \frac{P_{th}(t)}{\langle E_f \rangle} \times \langle \sigma_f \rangle$$

where $N_p$ is the number of protons in the detector, $P_{th}$ is the reactor thermal power, $\langle E_f \rangle$is the mean energy released per fission and $\langle \sigma_f \rangle$ is the mean cross section per fission.

At the detector, these antineutrinos will interact with the protons of the liquid scintillator, through the reaction:

$$\bar{\nu}_e + p \rightarrow e^+ + n$$

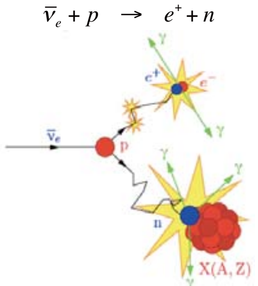


The positron annihilation and the neutron capture give the signature of a antineutrino interaction.

## Detector Design

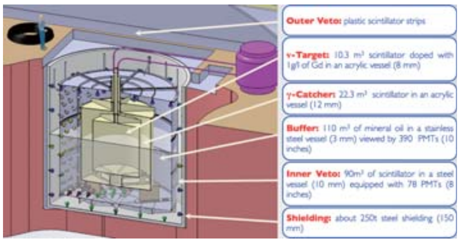


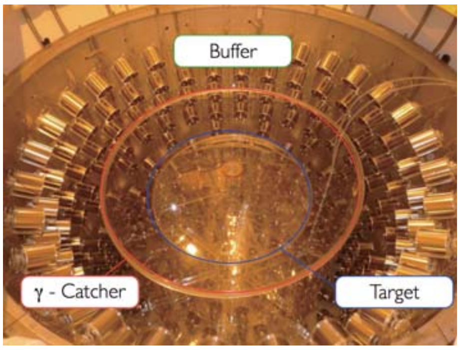


## Data Taking and Event Selection

Since mid-April of 2011, the Double Chooz Far Detector is operational and getting data continuously. Its average total efficiency for physics runs, i.e. not considering calibration periods, is 77.5% of the time. For the first result, a total run time of 101.523 days were used, corresponding to a live time of 96.823 days, due to 1 ms of muon veto.

The main sources of background can be suppressed by a delayed coincidence selection:

Prompt signal: positron energy ($0.7 < E_P < 12$ MeV)

Delayed signal: gamma emission when a neutron is absorbed by the gadolinium ($6 < E_D < 12$ MeV)

Time correlation: τ ~ 30 μs (2 < τ < 100 μs)

In addition, some qualities cuts are also applied.

**$E_{prompt}$ vs $E_{delayed}$**

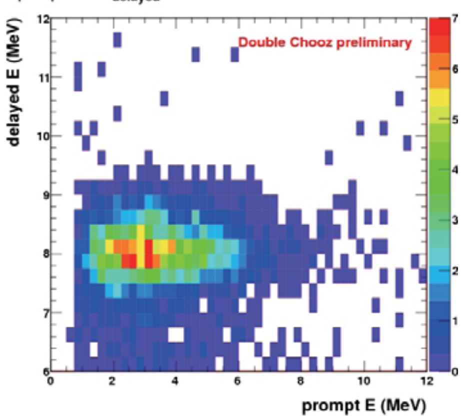


**Neutrino candidates rate (background not subtracted)**

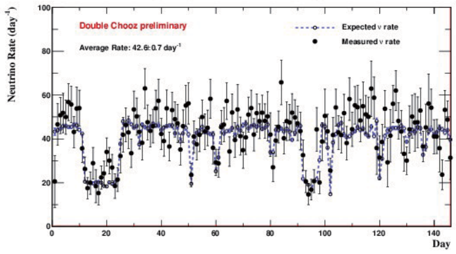


## Backgrounds

The backgrounds can be divided in two types:

I) Accidental: environmental gamma-ray (prompt like) and muon induced neutrons (delayed). It can be estimated by off-time method.

II) Correlated: caused by fast n or $^{9}Li/^{8}He$. Fast n will recoil a proton (prompt like) and, after thermalized, will be captured on Gd. $^{9}Li/^{8}He$ are beta-n emitters, produced by muon-induced spallation. It cannot veto due to long lifetime.

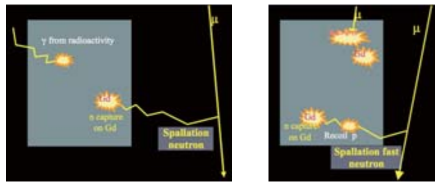


## First Result

To extract the value of $\theta_{13}$, a expected simulated spectrum was compared with the measured one, using the following $\chi^2$ function:

$$\chi^2 = \left(N_i - \left(\sum_R^{\mathrm{Reactors}} N_i^{\nu,R} + \sum_b^{Bkgs} N_i^b(P_b)\right)\right) \times \left(M_{ij}^{signal} + M_{ij}^{\mathrm{detector}} + M_{ij}^{stat} + \sum_b^{Bkgs} M_{ij}^b\right)$$
$$\times \left(N_j - \left(\sum_R^{\mathrm{Reactors}} N_j^{\nu,R} + \sum_b^{Bkgs} N_j^b(P_b)\right)\right)^T + \sum_R^{\mathrm{Reactors}} \frac{(P_R)^2}{\sigma_R^2} + \sum_b^{Bkgs} \frac{(P_b)^2}{\sigma_b^2}$$

which led to the result:

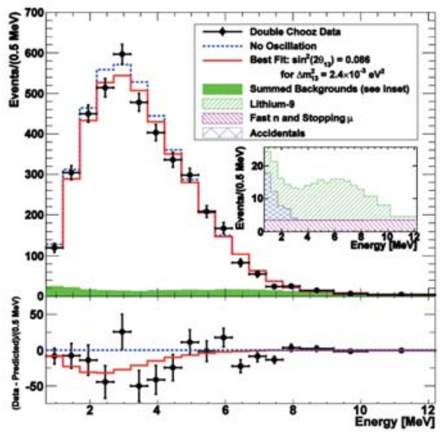


The final fit and first Double Chooz result is, therefore:

Rate Only fit: **$\sin^2 2\theta_{13}$ = 0.104 ± 0.030 (stat.) ± 0.076 (sys.)**

Rate & Shape fit: **$\sin^2 2\theta_{13}$ = 0.086 ± 0.041 (stat.) ± 0.030 (sys.)**

with no oscillation possibility excluded at **94.6%**

P-40

The 4th GCOE International Symposium on "Weaving Science Web beyond Particle-Matter Hierarchy"

# High energy-resolution EELS and SXES studies on characteristic chemical shifts and charge transfer in Al-Si-Mn and Zn-Mg-Zr alloys

S. Koshiya (*Physics, D3*)

EELS: Electron energy-loss spectroscopy
SXES: Soft-X-ray emission spectroscopy

February 21 (Tue.), 2011.

## Introduction

In recent years, Hume-Rothery mechanism, which predicts a existence of a pseudogap around the Fermi level $E_F$, is accepted as a major reason for the stabilization of **quasicrystals**. The presences of pseudogap in quasicrystals were confirmed by X-ray photoemission spectroscopy and electron energy-loss spectroscopy (EELS). EELS experiments also pointed out **characteristic chemical shifts** in Al L-shell excitation spectra of Al-based quasicrystals, which suggested **a decrease of valence electron charge** at Al sites. Recently, **a covalent bonding nature in quasicrystals** was reported by MEM/Rietveld analysis. Thus, it is interesting to investigate the relation between a chemical shift and bonding nature of the quasicrystals.

## Background1: Quasicrystals & approximant crystal

Quasicrystal
D. Shechtman *et al.*, *Phys. Rev. Lett.* 53 (1984) 1951.


Approximant crystal
- Local structure is similar with a QC
- Characterized by **degree of approximation**
1/0→1/1→1/2→2/3→···→1/τ (τ = (1+√5)/2)

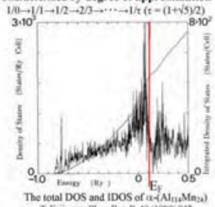

The total DOS and IDOS of α-(Al$_{114}$Mn$_{24}$)
T. Fujiwara, *Phys. Rev. B*, 40 (1989) 942.

QC's anomalous properties
- Luck translation symmetry
- High electronic resistance
- Hard and brittle

Quasicrystal and approximant crystal
→Presence of pseudogap near the $E_F$
→Complicated structure was stabilized??

## Background2: EELS studies of Al-based quasicrystals

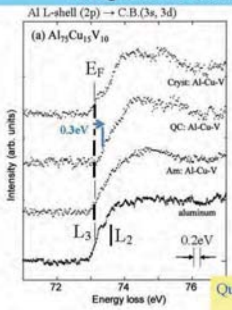


M. Terauchi *et al.*, *Philos. Mag.*, 87 (2009) 2947.

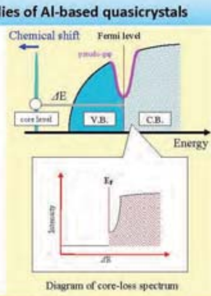


Quasicrystal shows chemical shift
→ Decrease of valence electron charge
→ Presence of covalency ??

## Background3: MEM/Rietveld analysis

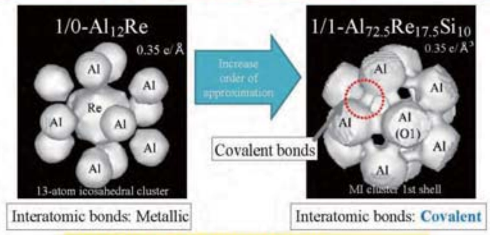


K. Kirihara *et al.*, *Phys. Rev. B*, 64 (2001) 212201.

Covalent bonds between Al atoms
→ Decrease of valence electron charge ??
⟷ Chemical shift (EELS)

## Purpose of this study

The chemical shifts of $Al_{53}Si_{27}Mn_{20}$ alloys and Zn-Mg-Zr alloys were measured by using EELS and SXES.

- Investigate the relation between **chemical shifts and crystalline order** of $Al_{53}Si_{27}Mn_{20}$ alloys.
- Investigate the relation between chemical shift and bonding nature of the Zn-Mg-Zr (**non-Al based**) alloys.
- Those chemical shifts are compared with those of pure materials or their oxides.

## High resolution EELS-TEM instrument


HR-EELS TEM
Acc. Volt.: 60kV, 100kV
Analyzed area: ~1nmφ
Energy resolution: 0.1eV
Monochromator: Wien-filter
Analyzer: Ω-filter
Detector: IP (pixcel size: 25μm)

M. Mukai *et al.*, *Microsc. Microanal.*, 12 (Suppl. 2) (2006) 1206.

## High resolution SXES-TEM instrument

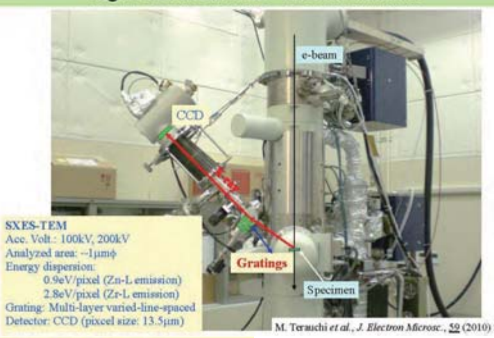


SXES-TEM
Acc. Volt.: 100kV, 200kV
Analyzed area: ~1μmφ
Energy dispersion:
0.9eV/pixel (Zn-L emission)
2.8eV/pixel (Zr-L emission)
Grating: Multi-layer varied-line-spaced
Detector: CCD (pixcel size: 13.5μm)

M. Terauchi *et al.*, *J. Electron Microsc.*, 59 (2010) 251.

## $Al_{53}Si_{27}Mn_{20}$ alloy (sample)

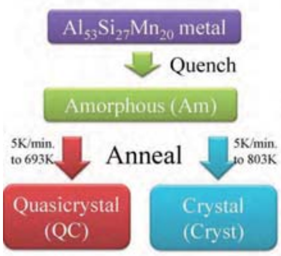


A.P. Tsai *et al.*, *Phys. Rev. B*, 49 (1994) 3569.
S. Koshiya *et al.*, *Philos. Mag.*, 91 (2011) 2309.

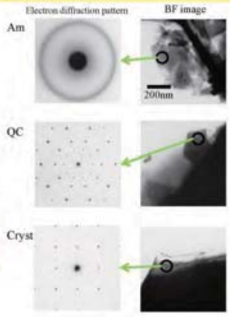


## $Al_{53}Si_{27}Mn_{20}$ alloy (EELS & SXES spectra)

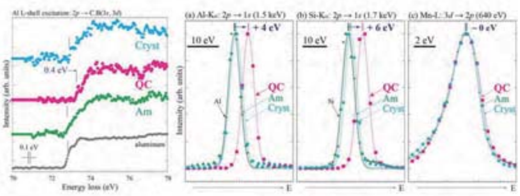


- **Only QC alloy shows an apparent chemical shift** to larger energy side.
  Imply decrease of valence electron charge
- The value of chemical shifts of Al-$K_\alpha$ and Si-$K_\alpha$ are comparable with **oxides**.
  *ex*) 4eV in $Al_2O_3$ (by XES)

## Zn-Mg-Zr alloy (composition & diffraction)

Primitive icosahedral quasicrystal (**P-QC**): $Zn_{83.5}Mg_{9.5}Zr_7$

Face-centered icosahedral quasicrystal (**F-QC**): $Zn_{75}Mg_{18}Zr_6$

1/1-approximant (**1/1-AP**) of F-QC quasicrystal: $Zn_{77}Mg_{19}Zr_4$

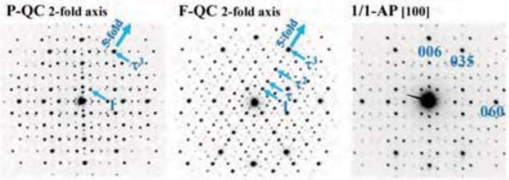


S. Ohhashi *et al.*, *Acta Mater.*, 57 (2009) 4727.

## Zn-Mg-Zr alloy (EELS spectra)

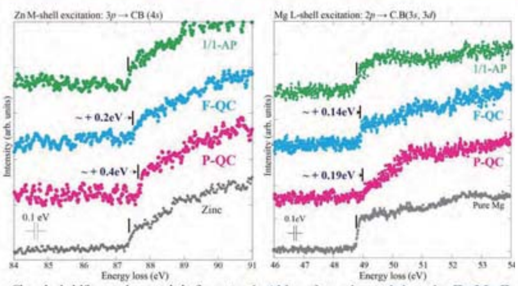


- Chemical shifts are characteristic for not only Al-based quasicrystals but also Zn-Mg-Zr quasicrystals.

## Zn-Mg-Zr alloy (SXES spectra)

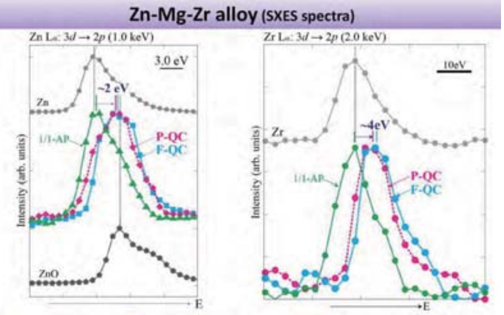


- All constituent atoms of quasicrystal show chemical shifts to larger binding energy side.
- The value of chemical shifts for quasicrystalline alloy comparable to their oxides.

## Summary

The chemical shift of $Al_{53}Si_{27}Mn_{20}$ and Zn-Mg-Zr alloys were investigated by using EELS and SXES.

- **Chemical shifts are characteristic for quascrystalline materials of Al-based and Zn-Mg-Zr alloy.**
  → Chemical shift is intrinsic for quasicrystalline state?
- **All chemical shifts of quasicrystalline materials imply the decrease of valence electron charge.**
  → Strongly suggest an increase of covalency in quasicrystalline states.
- **The amount of shifts comparable to their oxides**
  → Decreased valence electrons of quasicrystal are almost same to oxide?

# Theory of Coherent Phonon Oscillations in Carbon Nanotubes and Nanoribbons

**Ahmad-Ridwan Tresna NUGRAHA and Riichiro SAITO**
*Department of Physics, Tohoku University, Sendai, 980-8578*
E-mail: nugraha@flex.phys.tohoku.ac.jp Web: http://flex.phys.tohoku.ac.jp/~nugraha

## Introduction to coherent phonon spectroscopy

### Pump-probe spectroscopy

Either transmittance or reflectivity change can be measured

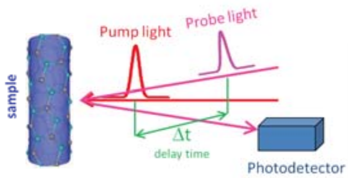


Typical reflectivity change of Si (001)

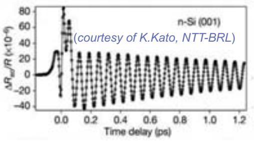


### Coherent phonons in carbon nanotubes

G. D. Sanders et al., PRB 79, 205434 (2009)

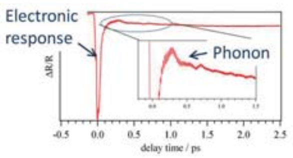


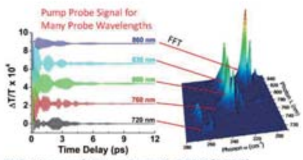


Y. S. Lim et al, Nano Lett. 6, 2696 (2006)

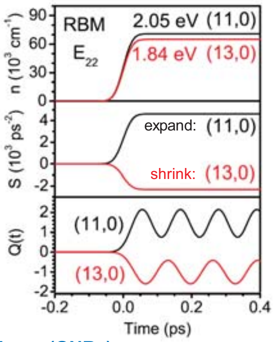


### Coherent phonons in graphene nanoribbons (GNRs)

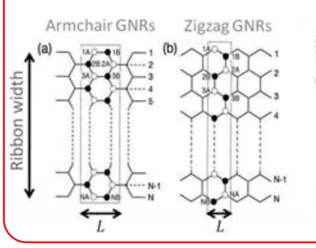


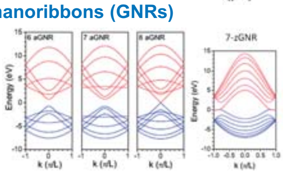


*RBLM phonons* "to shrink" or "to expand"?


### Mechanism of coherent phonons

to find a general mechanism of coherent phonon generation in carbon nanotubes/nanoribbons

$$\frac{\partial^2 Q(t)}{\partial t^2} + \omega^2 Q(t) = S(t)$$

- What is an appropriate driving force for coherent phonons in carbon nanotubes?
- Why different nanotubes start coherent vibrations by uniquely expanding or shrinking their diameters?
- Role of electron-phonon and exciton-phonon interactions?

## Purposes of the work

### Map of initial lattice response

We can predict how a particular (n,m) nanotube/nanoribbons would respond to ultrafast excitation (shrink/expand)

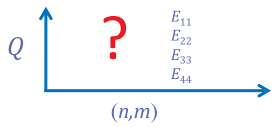


## Calculation method

G. D. Sanders et al., PRB 79, 205434 (2009)

$$\frac{\partial^2 Q_\beta(t)}{\partial t^2} + \omega_\beta^2 Q_\beta(t) = S_\beta(t)\ ; \qquad S_\beta(t) = -\frac{2\omega_\beta}{\hbar}\sum_{s\mu k} M^\beta_{s\mu}(k)[f_{s\mu}(k,t) - f^0_{s\mu}(k)]$$

Q → CP amplitude; Driving force; el-ph interaction; Carrier distribution; Carrier density

Ultrafast Optical Excitation

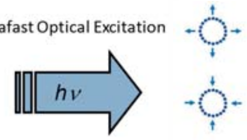


Generation of the coherent phonons:

Excitation by laser pulse → Photo-excited carriers → Electron-phonon interaction → Lattice Vibrations

Coherent phonon driving function

$$S(t) = \sum_{n,k} S_n(k)\left(f_n(k,t) - f_n^0(k)\right)$$

Driving function kernel; Photoexcited carriers; Equilibrium distribution

Driving function kernel

$$S^\beta_\mu(k) = -\frac{2\omega_\beta}{\hbar}[M^\beta_{c\mu}(k) - M^\beta_{v\mu}(k)]$$

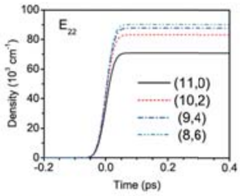


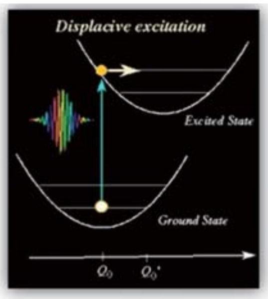


Carrier density is obtained by solving Boltzmann equation

$$\left.\frac{\partial f_{s\mu}(k)}{\partial t}\right|_{\rm gen} = \frac{8\pi^2 e^2 u(t)}{\hbar n_g^2(\hbar\omega)^2}\left(\frac{\hbar^2}{m_0}\right)\sum_{s'} |P^\mu_{ss'}(k)|^2[f_{s'\mu}(k,t) - f_{s\mu}(k,t)]\delta(\Delta E^\mu_{ss'}(k) - \hbar\omega)$$

## Results and Discussion

### Excitation dependence (nanotubes)

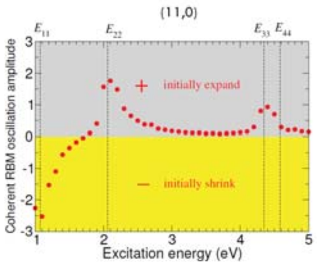


"to expand" $M_{\text{el-ph}} < 0 \rightarrow S(t) > 0 \rightarrow Q(t) > 0$

"to shrink" $M_{\text{el-ph}} < 0 \rightarrow S(t) < 0 \rightarrow Q(t) < 0$

$$\frac{\partial^2 Q_\beta(t)}{\partial t^2} + \omega_\beta^2 Q_\beta(t) = S_\beta(t)$$

$$S_\beta(t) = \sum_{\mu k} S^\beta_\mu(k)[f_{c\mu}(k) - f^0_{c\mu}(k)]$$

contains $M_{op}$

$$S^\beta_\mu(k) = -\frac{2\omega_\beta}{\hbar}[M^\beta_{c\mu}(k) - M^\beta_{v\mu}(k)]$$

Magnitude of oscillations: $|Q| \propto |M_{el-ph}||M_{op}|$

### Eff. Mass theory: *k*-dependent el-ph interaction (nanotubes)

K. Sasaki et al., PRB 78, 235405 (2008)

ART Nugraha et al., PRB 84, 174302 (2011)

**For zigzag tubes:**

$$M_{\text{el-ph}} = \frac{A_Q}{d_t}\left(-2g_{\text{off}}\cos\Theta(\mathbf{k})\right)$$

**For chiral tubes:**

$$M_{\text{el-ph}} = \frac{A_Q}{d_t}\left(-2g_{\text{off}}\cos[\Theta(\mathbf{k}) + 3\theta]\right)$$

- to the *right* of the K-point $M_{\text{el-ph}} < 0$ (expand)
- to the *left* of the K-point $M_{\text{el-ph}} > 0$ (shrink)

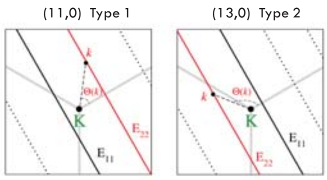


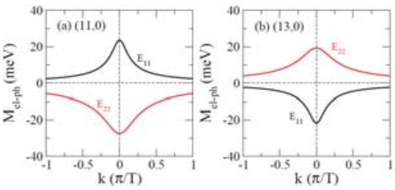


### Semiconducting armchair GNRs: mod 0 and mod 1

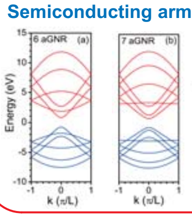


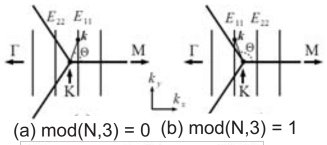


(a) mod(N,3) = 0 (b) mod(N,3) = 1

$$M_{\rm ep} = u_{\rm arm}\left(-2g_{\rm off}\cos\Theta(\mathbf{k})\right)$$

GD Sanders, ART Nugraha et al., submitted to PRB (2012) arXiv:1201.5339

| Type | E11 | E22 |
|---|---|---|
| mod 0 | ex | sh |
| mod 1 | sh | ex |

### Chirality dependence and map of lattice response (nanotubes)

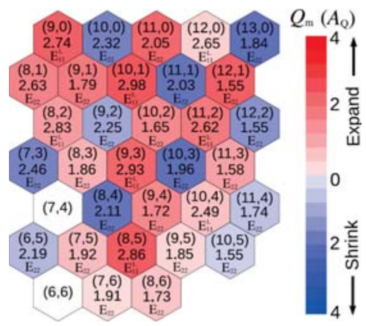


ART Nugraha et al., PRB 84, 174302 (2011)

Deviated results from basic rules: (7,6), (9,5), (10,5) → **near-armchair**

**Excitonic effects** should also be considered in the near future.

Armchair nanotubes have a small coherent amplitude because of **trigonal warping effect**, where the density of states is split into lower and higher branches so that the two contributions cancel to each other.

### Map of nanoribbon lattice response (armchair GNRs)

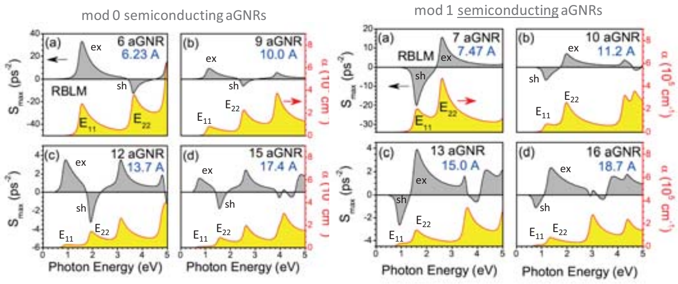


mod 2 metallic aGNRs

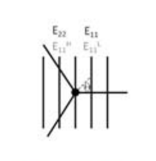

| Type | E11 | E22 |
|---|---|---|
| mod 0 | ex | sh |
| mod 1 | sh | ex |
| mod 2 | ex | ex/sh |

## Summary and Conclusions

- Coherent RBM (nanotube) and RBLM (nanoribbon) phonon starts by expanding or shrinking, depending on excitation energy and type/family
- Type dependence and excitation dependence of coherent phonon amplitudes originate from the *k*-dependent el-ph interactions

# Laser Raman Spectroscopy and the *D* Band of Graphene

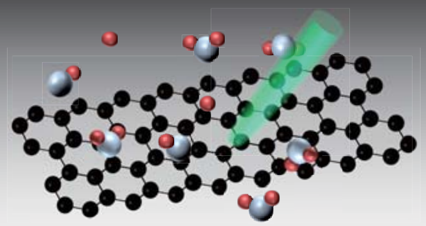

N. Mitoma[1], R. Nouchi[2] and K. Tanigaki[1,2]
E-mail: mitoma@sspns.phys.tohoku.ac.jp
2-1-1 Katahira, Aoba-ku, Sendai 980-8577, Japan
Department of Physics, Tohoku University[1]
WPI-Advanced Institute for Materials Research (WPI-AIMR), Tohoku University[2]

## What is graphene?

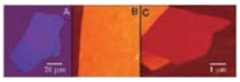

Optical microscope & AFM images


Nobel prize in physics 2010

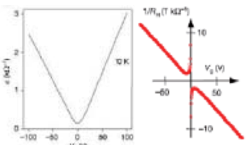

Carrier transport properties

K. S. Novoselov *et al.*, *Science* **306**, 666 (2004).
K. S. Novoselov *et al.*, *Nature* **438**, 197 (2005).

## Energy band structure of graphene

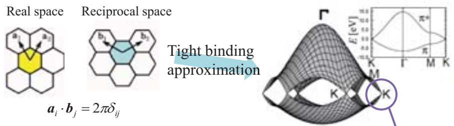


$a_i \cdot b_j = 2\pi\delta_{ij}$

The expectation value of the energy

$$H\Psi = E\Psi.$$
$$\Rightarrow \det(H - EI) = 0$$
$$\therefore E = \hbar v_F |\boldsymbol{k}|.$$

$$H \approx \hbar v_F \begin{pmatrix} 0 & k_x - ik_y \\ k_x + ik_y & 0 \end{pmatrix}$$

Hamiltonian near K point

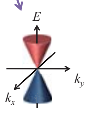

•Effective mass is zero.
-High mobility (~200000 cm$^2$ V$^{-1}$ s$^{-1}$) has been observed at LT.

K. I. Bolotin *et al.*, *Solid State Commun.* **146**, 351 (2008).

## Background

Towards device application


S. Bae *et al.*, *Nat. Nanotechnol.* **5**, 574 (2010).

•Graphene's useful properties.
-Atomically thin (~0.34 nm), i.e., transparent and flexible material.
-High charge-carrier mobility due to its characteristic energy band.
-Eco-friendly material, because all of it is constructed from carbon atoms.

•Problems for device application.
-Graphene cannot be applied as a switching device due to its no band gap…

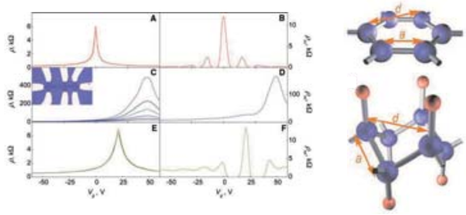

D. C. Elias *et al.*, *Science* **323**, 610 (2009).

## Raman spectroscopy

சந்திரசேகர வெங்கடராமன்

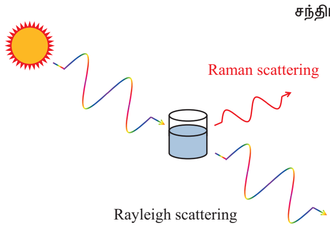


C. V. Raman and K. S. Krishnan, *Nature* **121**, 501 (1928).

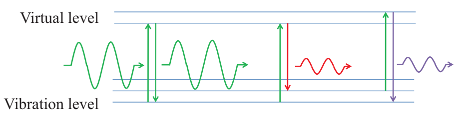


**Water molecules are found to exhibit nonnegligible reactivity with graphene under strong light irradiation. The reaction is triggered by laser Raman spectroscopy measurement itself, and the *D* band (*ca.* 1340 cm$^{-1}$) becomes larger as the laser irradiation is prolonged. The electronic transport properties of the graphene derivative are also measured and the mobility is found to be reduced. These results could originate from modification of graphene with hydrogen.**

•Raman reactive modes


This vibration mode is forbidden on a "perfect" graphene lattice.

Can be seen on all Graphene-related materials.

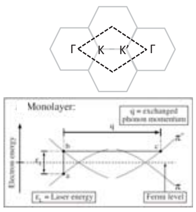


Double resonant Raman process, the origin of the 2*D* band.

A. C. Ferrari *et al.*, *Phys. Rev. Lett.* **97**, 187401 (2006).

•Time evolution of the *D* bands from 3 types of samples.

$$I_{Raman}(D) \propto n_{defects}$$

$$n_{defects} = N\{1 - \exp[-\eta_{H_2O}\sigma ft]\}$$

Reaction cross section    Incident photon flux

-Graphene on a dry substrate exhibited a low reactivity.
-The reaction probability is expressed by the number of water molecules, reaction cross section, and incident photon flux. These are the experimental parameters.
-The reaction probability of graphene on a wet substrate converged to similar value compared to that of on a dry substrate.
-The negative slope appeared on a Au-deposited graphene sample implies that the material went into the amorphousization trajectory.

•Why the reaction is triggered by laser irradiation?

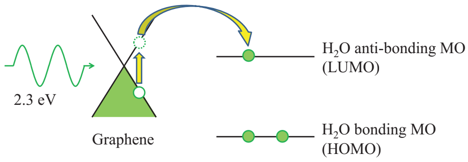


Decomposition of water molecules is accelerated by the photoradiation.

•Charge-carrier transport property
-Charge-carrier mobility reduced after the light irradiation. This is thought to be the result of hydrogenation of the graphene plane.
-The resistivity at Dirac point slightly increased after the irradiation.

**Keywords:**

**Graphene,**

**Raman spectroscopy,**

**Photochemical reaction,**

**Charge-carrier mobility**

## Summary & Future tasks

- **We observed the enlargement of the *D* band as the laser irradiation was prolonged.**
- **The peak position shifts of the *D*, *G*, and 2*D* are also observed. These indicate the carrier doping to the graphene plane.**
- **A study on electronic transport properties is still lacking. We need to measure at a variety of temperatures to clarify the carrier scattering mechanism.**
- **A study on the photochemical reactivity of multi-layer graphene is needed.**

# Spectral-Function Sum Rules in Supersymmetry Breaking Models

Mistutoshi Nakamura

Collaborated with Ryuichiro Kitano, Masafumi Kurachi, and Naoto Yokoi

arXiv:1111.5712 [hep-ph]

## Abstract:

If supersymmetry is realized in nature, it must be spontaneously broken. We derive relations among physical quantites as a consequence of supersymmetry, which generally appries in models of dynamical supersymmetry breaking.

## Symmetry

Symmetry is a field transformation which does not change action.

$$\phi \to \phi + \delta\phi$$
$$S[\phi] \to S[\phi + \delta\phi] = S[\phi]$$

## Supersymmetry

Supersymmetry is symmetry that transforms from boson to fermion and vice versa.

$$\delta_Q(\text{boson}) = \text{fermion}$$
$$\delta_Q(\text{fermion}) = \text{boson}$$

## Spontaneous Symmetry Breaking

$\langle \delta\left(\mathcal{O}_1 ...\right)\rangle = 0$

corresponds to unbroken symmetry

→ Conservation of charge

$\langle \delta\left(\mathcal{O}_1 ...\right)\rangle \neq 0$

corresponds to broken symmetry

→ Massless Nambu-Goldstone particle

## Sum rules

S. Weinberg, (1967).

$$\frac{\langle \mathcal{O}\rangle}{q^n} \sim \langle \delta\left(\mathcal{O}_1\mathcal{O}_2\right)\rangle \neq 0$$

Spectral function

$$= -\int_0^\infty d\sigma^2 \frac{\rho(\sigma^2)}{q^2 - \sigma^2 + i\epsilon}$$

$$= \frac{c_1}{q^2} + ... + \frac{c_{n/2}}{q^n} + ...$$

$= 0 \; ...$

$$c_n = \int_0^\infty d\sigma^2 \rho(\sigma^2)\sigma^{2(n-1)}$$

One can derive sum rules wich do not depend on details of underlying model.

This n is determined by the dimension of $\mathcal{O}$. We denote this dimension as $d$.

→ We apply sum rule to supersymmetry breaking model.

## Gauge Mediation

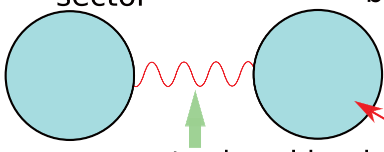


M. Dine, W. Fischler, and M. Srednicki,(1981).
S. Dimopoulos and S. Raby,(1981).
M. Dine, A.E. Nelson, and Y. Shirman,(1995).
M. Dine, A.E. Nelson, Y. Nir, and Y. Shirman,(1996).

Supersymmetry breaking is mediated by gauge interaction.

There exists SM current operators model independently.

Breaking sector particles

| | mass | decay constant |
|---|---|---|
| Spin-0 | $m_0$ | $f_0$ |
| Spin-1/2 | $m_{1/2}$ | $f_{1/2}$ |
| Spin-1 | $m_1$ | $f_1$ |

By taking $\mathcal{O}_1, \mathcal{O}_2$ as currents of SM gauge group, we obtain

$$f_0 = f_{1/2} = f_1 \equiv f_h.$$

By using this scalar and gaugino mass are computed to be

$$m_s^2 = \frac{g^4 c_2 f_h^2}{(4\pi)^2}\log\frac{m_0^2 m_1^6}{m_{1/2}^8} \qquad m_\lambda = \frac{g^2 f_h^2}{m_{1/2}}$$

↓ More generally there exists supercurrent operator.

## Supercurrent

Supercurrent is a current corresponding to supersymmetry.

→ We take supercurrent as $\mathcal{O}_1, \mathcal{O}_2$ .

| | mass | decay constant |
|---|---|---|
| Scalar | | $f_\phi \quad c_\phi$ |
| Pseudoscalar | | $f_\pi \quad c_\pi$ |
| Masless spin-1/2 | $0$ | $f \quad f'$ |
| Massive spin-1/2 | $m_\chi$ | $f_\chi$ |
| Massive spin-1 | $m_v$ | $f_v$ |
| Massive sipin-3/2 | $m_\psi$ | $f_\psi$ |
| Massive spin-2 | $m_h$ | $m_{\mathrm{P}}$ |

Sum rule for $d_0 = 3$ and $4$

$$|f'|^2 + |f_\chi|^2 + \frac{2}{3}|f_\psi|^2 = f_\phi^2 + \frac{8}{3}m_{\mathrm{P}}^2,$$

$$f_\phi^2 + \frac{8}{3}m_{\mathrm{P}}^2 = f_\pi^2 + f_v^2,$$

Sum rule for $d_2 = 4$

$$f^2 f' = m_\psi f_\psi^2 = -\frac{3}{4}m_\chi f_\chi^2,$$

$$f_\phi c_\phi^2 = 0, \quad f_\pi c_\pi^2 = 0,$$

# Terahertz pulse shaping via difference frequency mixing of shaped optical pulses

Koji Uematsu[a,b] and Chiko Otani[a,b]

Department of Physics, Tohoku University [a]  Terahertz Sensing and Imaging Laboratory, RIKEN [b]

*The 4th GCOE International Symposium on "Weaving Science Web beyond Particle-Matter Hierarchy"*

## Abstract

Femtosecond pulse shaping techniques which exist in wavelength range from visible to mid-infrared have been developed for various applications, such as coherent control of matter and chemical reactions. In terahertz (THz) region, the use of intense sub-picosecond THz pulses provides tools in non-linear and time-domain THz spectroscopy, but no efficient way for THz pulse shaping exists. Complex and precise control techniques of THz temporal waveforms are desirable for those applications.

In this poster, we propose and demonstrate a novel method of arbitrary pulse shaping. It is based on spectral phase transfer to THz pulses by a difference-frequency generation technique.

## Principle – difference-frequency generation (DFG)

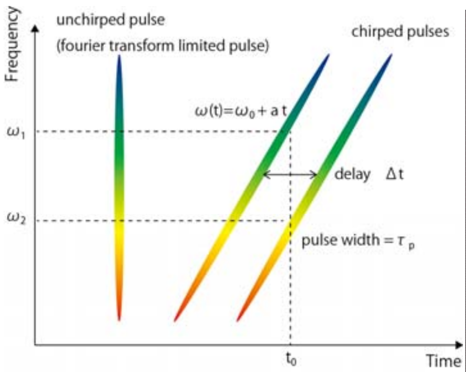


Fig.1. schemed of chirped-pulse DFG

- Electric field of linearly chirped pulses

$$E_1(t)=E_2(t+\Delta t)$$
$$=E_0\exp\left(-4\ln 2\left(t/\tau_p\right)^2\right)\exp\left(-i\omega t-iat^2\right)$$

- Difference frequency : $\omega_{DFG}=a\Delta t$
- Phase of the DFG signal

$$\phi(\omega_{DFG})=\phi(\omega_{NIR1})-\phi(\omega_{NIR2})$$
$$(\omega_{DFG}=\omega_{NIR1}-\omega_{NIR2})$$

- Taylor expansion

$$\phi(\omega)=\phi_0+\phi_1*(\omega-\omega_0)$$
$$+\phi_2*\frac{(\omega-\omega_0)^2}{2}+\phi_3*\frac{(\omega-\omega_0)^3}{6}+......$$

## Experimental setup

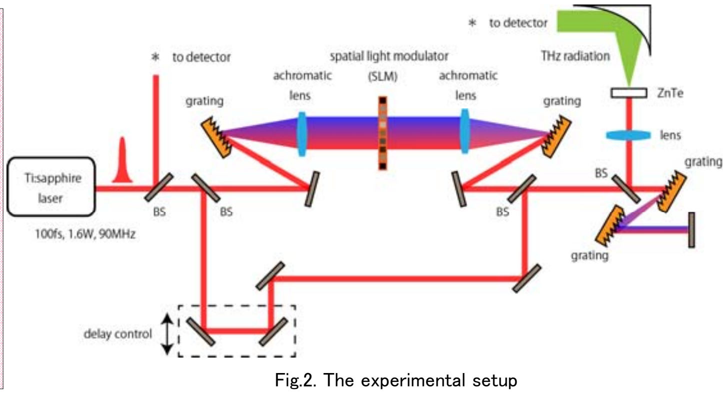


Fig.2. The experimental setup

## Experiments and Results

he phase measurement of a shaped ultrashort optical pulse : patial pectral nterferometry ( )

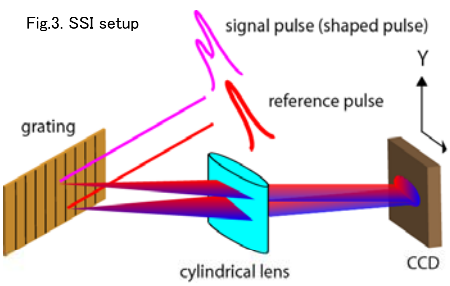


Fig.3. SSI setup

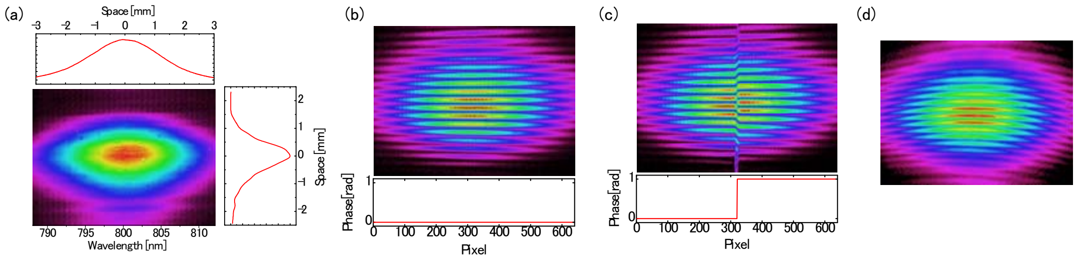


Fig.4. (a) eam profile of the reference pulse measured by a CCD and SSI fringe pattern with (b) no modulation (c) phase change of at pixel 320 (d) second-order chirp.

Signal : $I_{sig}(r,t)=E_{sig}(r)\exp\left[i\left(k_{sig}\cdot r+\phi_{sig}(r)-\omega t\right)\right]$

Reference : $I_{ref}(\mathbf{r},t)=E_{ref}(\mathbf{r})\exp\left[i\left(\mathbf{k}_{ref}\cdot\mathbf{r}+\phi_{ref}(\mathbf{r})-\omega t\right)\right]$

The fringe pattern on the CCD plane

$$I(x,y)=\left|I_{ref}(x,y,t)+I_{sig}(x,y,t)\right|^2=E_{ref}^2(x,y)+E_{sig}^2(x,y)$$
$$+2E_{ref}(x,y)E_{sig}(x,y)\cos\left[2ky\sin\theta+\left(\phi_{ref}(x,y)-\phi_{sig}(x,y)\right)\right]$$

hase transfer to z pulses

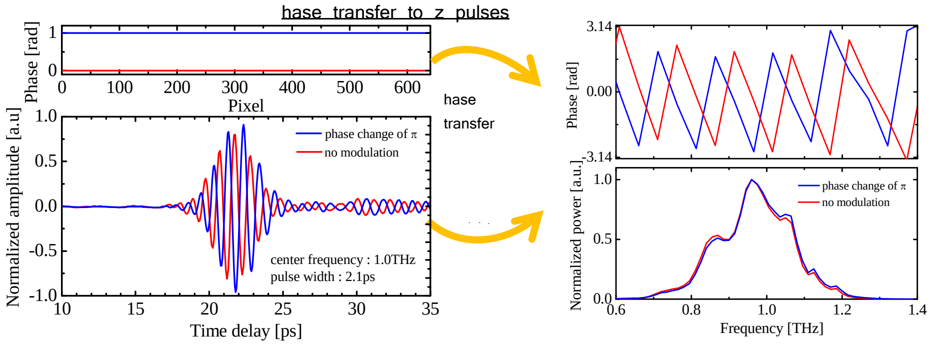


Fig.6. (left) THz waveforms for no modulation and phase change of at S M (right) phase and frequency spectra of the radiation.

z waveforms for chirped- pulse

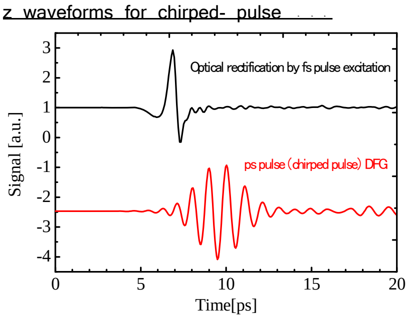


Fig.5. THz waveforms for femtsecond pulse excitation (blac ) and chirped pulse DFG (red).

- Femtsecond pulse width 100fs
- Group delay dispersion of chirped pulse −0.2ps²

\ pulse — Spectral phase control at S M — z pulses

$$\phi(\omega)=\phi_0+\phi_1*(\omega-\omega_0)+\phi_2*\frac{(\omega-\omega_0)^2}{2}+\phi_3*\frac{(\omega-\omega_0)^3}{6}+......$$

→ Tailored THz waveforms for various applications

## Summary

- I have demonstrated that the phase profile of a shaped pulse in the near-infrared is transferred to a pulse in the terahertz via a difference frequency mixing (DFM) process.
- This phenomenon will allow THz waveform shaping by manipulating the high-order dispersion of chirped pulse.
- The THz pulse shaper can be applied to the study of intermolecular vibrations, structure of large molecules and molecular rotational level and the control of the coherent phonons, anitiferromagnetic spin waves and chemical reactions.

# On the development of resonant inelastic x-ray scattering for high-pressure experiments

M. Yoshida
Dept. of Phys. Tohoku Univ. / JAEA SPring-8

## Background

Pressure is one of the most important external parameters along with temperature and magnetic field. By inducing pressure to a material, we can control its physical properties through shrinkage of the crystal lattice. While investigating the electronic structure is central to the understanding of physical properties, such studies are still hardly carried out due to the stringent conditions imposed by the use of high-pressure cells.

## Why RIXS?

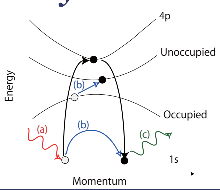


<advantages>

- momentum dependence
- bulk sensitivity
- element sensitivity
- **photon-in-photon-out spectroscopy**

**Applied to high-pressure experiments**

## DAC

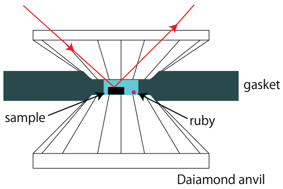


- diamond-in-diamond-out configuration
- diamond size
  h1 = 1 mm, h2 = 1.5 mm
  (asymmetry thickness)
  C1 = 1 mm (for large sample volume)

- sample size 400×250×70 μm$^3$
- fluorinert
- SUS301
- pressure determination for ruby fluorescence

**Intensity is reduced due to diamond, about two or three hundredth parts.**

## Experiments

✓ We performed RIXS experiments at BL11XU, SPring-8

**< beamline layout >**

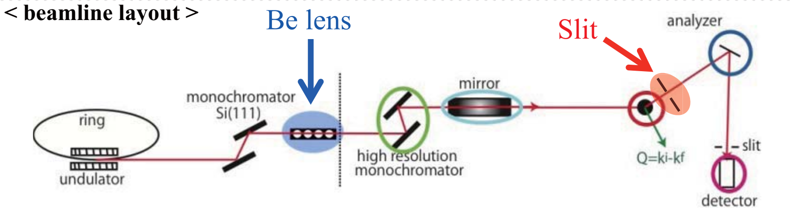


✓ We introduced two optical components for high-pressure RIXS.

- **Be lens**
  For focusing x-rays along vertical direction
- Slit located after sample
  For removing the scattering x-ray from diamond

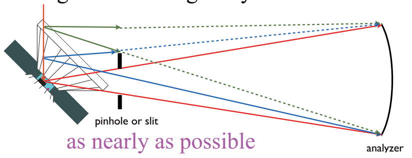


as nearly as possible

## Estimation of two optical components

### < Be lens >

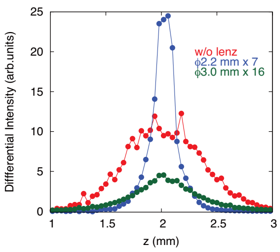


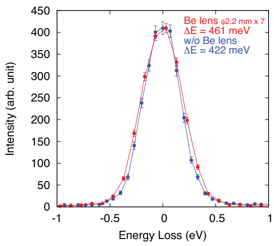


-Using φ2.2 mm × 7, vertical beam size reduce by half but peak height become twice and energy resolution does not change so mach.

### < Slit located after sample>

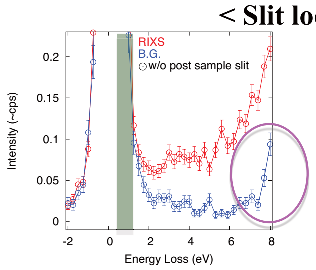


(scattering from diamond)

- asymmetry of elastic scattering
- some excitation around 8 eV

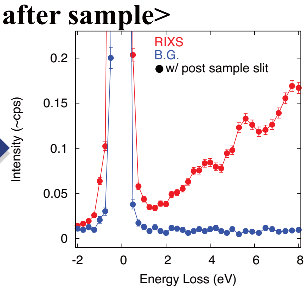


Suppress scattering from diamond !!

## Results

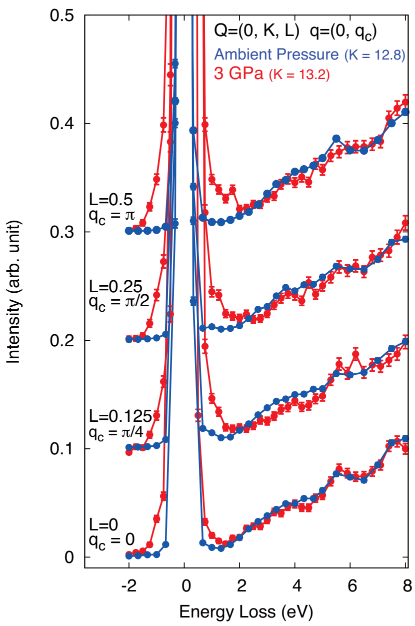


focus on intraband region

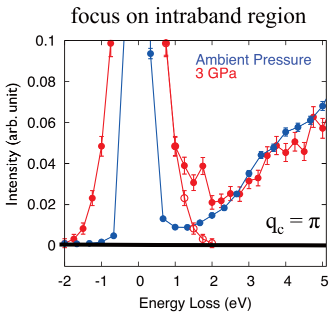


cf. doping dependence

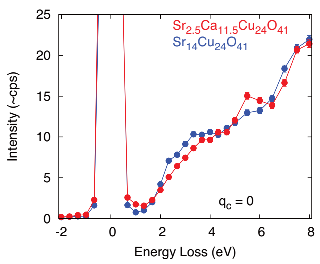


✓ In order to compare the data measured at ambient pressure, we normalize them using the integrated intensity between 5 – 8 eV. (scale factor : ~ 1/160)

**We have succeeded to obtain Q-resolved RIXS spectra under high pressure for the first time** though intensity become very weak.

- crossover around 2 eV energy loss
  → Similar behavior have shown in doping dependence.
- large enhancement of the intensity in the intraband region
  → It is considered that a number of holes in the ladders increases.

## Summary

✓ We succeeded to develop RIXS method for high-pressure experiments due to the introduction of Be lens and a slit located after sample.

✓ We obtained Q-resolved RIXS spectra under high pressure for the first time and observed the change of them in pressure.

✓ In order to understand the effect of physical pressure in detail, we have to measure RIXS spectra under several pressure.

## Acknowledgements

**This work was supported by the follows. I would like to thank them.**

K. Ishii, I. Jarrige, T. Watanuki, K. Ohwada, K. Tsutsui, J. Mizuki, (JAEA, SPring-8), Y. Murakami (IMSS, KEK), N. Hiraoka, H. Ishii, K. D. Tsuei (NSRRC), A. Q Baron (RIKEN), T. Tohyama (YITP, Kyoto Univ.), S. Maekawa (ASRC, JAEA), K. Kudo (Okayam Univ.), Y. Koike (Tohoku Univ). K. Kumagai (Hokkaido Univ.), Y. Endoh (IIAS)

P-34

# Magnetic properties of lightly electron doped $LaCoO_3$

Tohoku Univ., KEK[A]

M. Watahiki, K. Tomiyasu, K. Iwasa, H. Nakao[A]

## 1. Introduction

### Perovskite-type cobalt oxide $LaCoO_3$

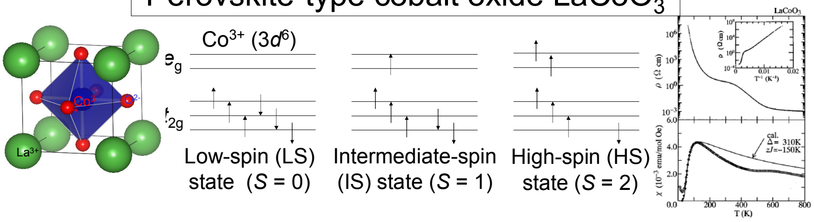


・Pseudo-cubic crystal structure.

・The $Co^{3+}$ ion exhibits spin-state degree of freedom: LS state, IS state, and HS state.

・Below 100 K, non-magnetic insulator state appears with LS state [1].

### Hole doped system $La_{1-x}Sr_xCoO_3$

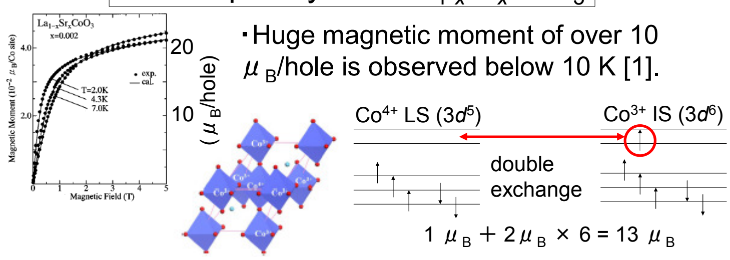


・Huge magnetic moment of over 10 $\mu_B$/hole is observed below 10 K [1].

・To explain the huge magnetic moment, spin-state polaron model comprising seven Co ions was proposed [2, 3].

・The origin of spin polaron is considered to be double exchange interaction between $e_g$ orbitals [4].

### Electron doped $LaCoO_3$

1. $La_{1-x}Ce_xCoO_3$ ($Ce^{4+}$)

・Above x > 0.05, single-phase sample is difficult to synthesize [5].

・Few data have been reported.

2. $La_{1-x}Te_xCoO_3$ recently reported ($Te^{4+}$ [6] or $Te^{6+}$)

・It is easy to synthesize up to $x$ = 0.25 [6].

Which is correct, $Te^{4+}$ or $Te^{6+}$ ?

## 2. Purposes

・Determination of the valence number of doped Te ion.

・Experimental examination of the spin-state polaron in electron-doped system.

## 3. Experiments

・Polycrystalline samples $La_{1-x}Te_xCoO_3$ (x = 0.01, 0.05) were synthesized. (1050 ℃ for 24 h and 1050℃ for 75 h)

・X-ray fluorescence (XRF) analysis method at PF BL-4C, Tsukuba, Japan. The fluorescence energy range from 3.6 to 4.2 keV was selected in energy dispersive XRF spectrum. We used $TeO_2$ and $Te(OH)_6$ as reference compounds of $Te^{4+}$ and $Te^{6+}$, respectively.

・Magnetization measurements down to 1.8 K in magnetic field up to 7 T at Center for Low Temperature Science, IMR, Sendai, Japan.

## 4. Results

### Fluorescence spectra around Te-$L_I$ edge

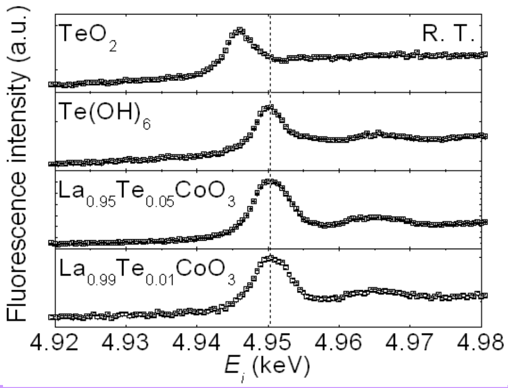


・It is considered that the valence number of doped Te ion is six.

### Magnetization of $La_{1-x}Te_xCoO_3$

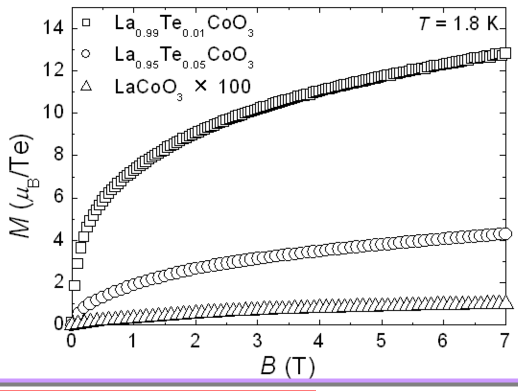


・Magnetization of $La_{0.99}Te_{0.01}CoO_3$ reaches 13 $\mu_B$/Te at 7 T.

## 5. Discussion

・The valence number of doped Te ion: $Te^{6+}$

Each Te ion introduces three electrons.

13 $\mu_B$/Te → 4.3 $\mu_B$/electron consistent with the Kanamori theory [7].

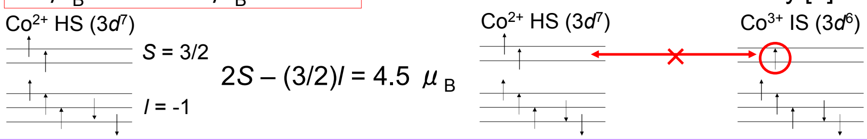


## 6. Summary

・The valence number of doped Te ion: $Te^{6+}$

・It is considered that the spin-state polaron does not realize in the lightly Te-doped $LaCoO_3$.

## 7. Future

・Growth of single crystalline $La_{1-x}Te_xCoO_3$

・Construction of a Te concentration $x$ – $T$ phase diagram

・Investigation of thermoelectric properties

## References

[1] S. Yamaguchi *et al*., Phys. Rev. B **53**, R2926 (1996).
[2] D. Phelan *et al*., Phys. Rev. Lett. **97**, 235501 (2006).
[3] A. Podlesnyak *et al*., Phys. Rev. Lett. **101**, 247603 (2008).
[4] D. Louca *et al*., Phys. Rev. Lett. **91**, 155501 (2003).
[5] J. Kirchnerova *et al*., Appl. Catal. A:Gen **231**, 65 (2002).
[6] G. H. Zheng *et al*., J. Appl. Phys. **103**, 013906 (2008).
[7] J. Kanamori, Prog. Theor. Phys. **17**, 177 (1957).

P-no 33

# Laser cooling of GaAs/AlGaAs cantilever by exciton related GaAs optical absorption

Takayuki Watanabe

## Background

Vibration control with carrier induced optomechanical coupling
→Large amplification occur at bandgap absorption
→This technique is sensitive to the spectrum of bandedge structure
↓
In order to characterize fine absorption spectrum with our technique, we used a GaAs/AlGaAs heterostructured cantilever which have sharp bandedge absorption.

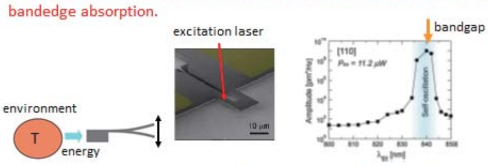


H. Okamoto *et al*, Phys, Rev, B **84** (2011) 014305

## Sample structure and mechanism

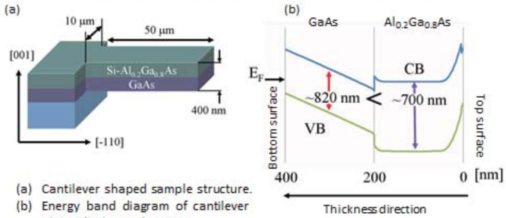


(a) Cantilever shaped sample structure.
(b) Energy band diagram of cantilever along thickness direction.

Resonance frequency of a cantilever is ~114 kHz. Quality factor is ~1300 at 10 K.

## Measurement setup

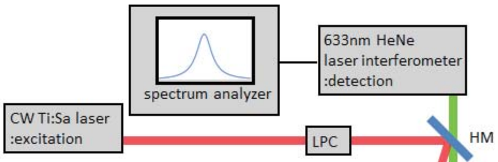


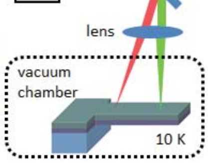


Schematic illustration of a cantilever and the measurement setup. CW Ti:Sa laser is used as an excitation light source and its spot size on samples are about 6 μm. The laser power is controlled by laser power controller (LPC). HeNe Doppler interferometer is used to detect motion of cantilevers. HeNe laser diameter is about 1 μm.

## Experiment 1
## optical absorption measurement of GaAs around exciton state with micro-scale mechanical cantilever

## Cantilever's PSD with excitation laser

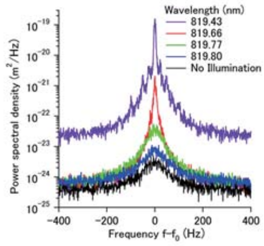


Excitation laser's wavelength dependence of cantilever's power spectral density (PSD) shows strong interaction when the wavelength is just below of the GaAs bandgap at 10 K.
The resonance peak becomes sharper and larger when the excitation laser wavelength is slightly reduced.

## Wavelength dependence of cantilever's amplitude

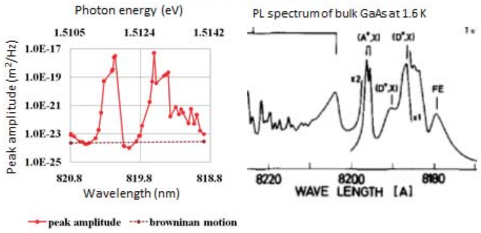


Peaks which appear in the wavelength dependence of cantilever's peak amplitude shows good agreement to the typical PL peak of bulk GaAs.

## Experiment 2
## mechanical mode cooling of cantilever with cavity-free opt-electro-mechanical coupling

## Sample structure

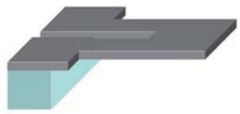

Cantilever structure (sample2)
20um long , 14 um width, 400 nm thickness (including 4um wide and 10um long legs) and [110]-oriented
Resonance property at 10K
Rf~ 383.1k Hz
Q~ 10000

Measurement setup is the same of experiment1.

## Laser power dependence of mechanical response

Wavelength dependence of flat noise added mechanical vibration was measured in detail.
The added flat noise level was 18uVrms/rtHz.

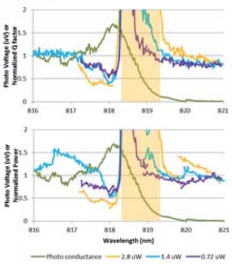


Cooling like effect was observed around 818 nm.

## Laser power dependence of mechanical response

Wavelength dependence of flat noise added mechanical vibration was measured in detail.
The added flat noise level was 18uVrms/rtHz.

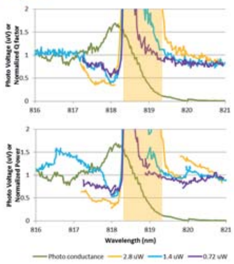


Cooling like effect was observed around 818 nm.

## Mechanical resonance peak de-amplification ( flat noise is added for actuation)

Wavelength 818.50 nm

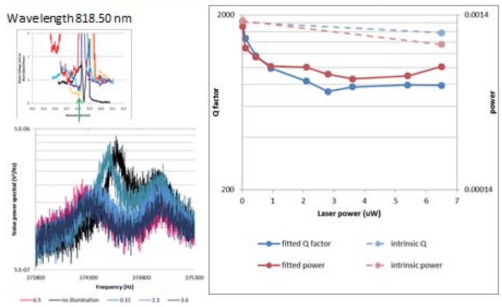


## Summary

- We measured the excitation laser wavelength dependence of thermo-mechanical vibration of GaAs/AlGaAs cantilever.
- A sensitive wavelength dependence of thermal vibration was observed.
- A significant vibration amplification was confirmed around exciton-related PL peaks.
- A mechanical mode cooling is observed around GaAs exciton peak.

# Role of non-collective excitations in heavy-ion reaction around the Coulomb barrier

Shusaku Yusa
Department of Physics, Tohoku University

## Introduction

heavy-ion reaction

nucleus is composed of protons and neutrons

➡ excitation during the collision

⬇

important in reactions near the Coulomb barrier

⬑ quantum tunneling amplify the effect

e.g. large enhancement of fusion cross sections at sub-barrier energies

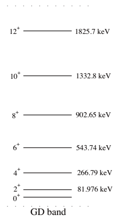


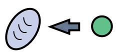

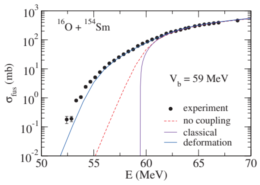


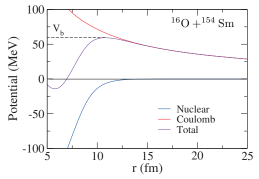


## Coupled-channels method

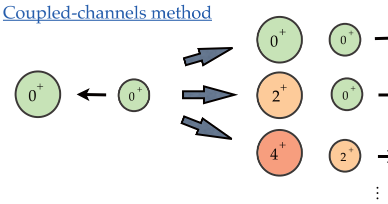


Quantum theory which takes into account nuclear excitations

conventionally, a few low-lying collective excitations (rotation, vibration) are taken into account

⬇

successfully accounted for heavy-ion fusion reaction and quasi-elastic scattering(sum of elastic, inelastic and transfer reaction) experiments

## $^{16}O + {}^{208}Pb$

fusion reaction(barrier distribution)

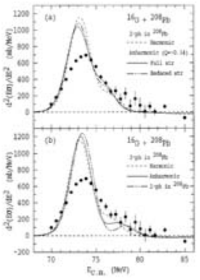

C. R. Morton *et al.*, PRC60, 044608(1999)

failed to account for the data by the C.C. analysis with only collective excitations

quasi-elastic scattering $\theta_{lab} = 163^\circ$ (Q-value distribution)

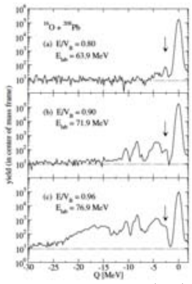

M. Ever *et al.* PRC**78**(2008)034614

increasing contribution from higher energy region(non-collective excitations)

➡ Can non-collective excitations improve the agreement ?

## Nuclear excited states

| | collective states | non-collective states |
|---|---|---|
| number of nucleons | many nucleons | a few nucleons |
| appearance of energy levels | low-lying, regular and high -lying(giant resonances) | relatively high excitation energy, irregular |
| transition strength | dozens of times larger than single-particle transition | comparable to single-particle transition |

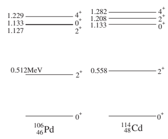

vibrational spectrum (collective states)

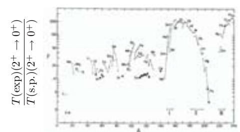

L. Grozins, Phys. Lett., **2**, 88(1962)

E2 transition probabilities

## Coupled-Channels method

coupled-channels equations (in the isocentrifugal approximation):

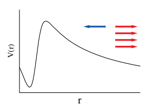

$$\left[\frac{d^2}{dr^2} + k^2 - \frac{J(J+1)}{r^2} - \frac{2\mu}{\hbar^2}\left(V_C(r) + V_N(r) + \epsilon_n\right)\right] u_n^J(r) = \sum_m \frac{2\mu}{\hbar^2} V_{nm}(r) u_m^J(r)$$

$k = \sqrt{\frac{2\mu E}{\hbar^2}}$ $\epsilon_n$ : excitation energy for the $n$-th channel

$V_{nm}(r)$ : coupling matrix element(induce excitations)

collective excitations

$^{208}$Pb : 3⁻ : 2.615 MeV, $\beta_3 = 0.122$

5⁻ : 3.198 MeV, $\beta_5 = 0.058$

2⁺ : 4.085 MeV, $\beta_2 = 0.058$

$^{16}$O : 3⁻ : 6.13 MeV, $\beta_3 = 0.733$

non-collective excitations

70 states in $^{208}$Pb up to 7.382MeV

⬆ deformation parameter $\beta_\lambda$, excitation energy $\epsilon^*$

$^{208}$Pb : high precision proton inelastic scattering experiment

(W.T.Wagner, *et al.* PRC**12** 757(1975))

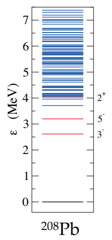


## Results

$^{16}O + {}^{208}Pb$ effect of non-coll. excitations

$$D_{qel} = -\frac{d}{dE}\left(\frac{\sigma_{qel}(E,\pi)}{\sigma_R(E,\pi)}\right)$$

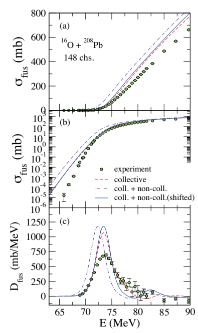


← fusion reaction

quasi-elastic scattering →

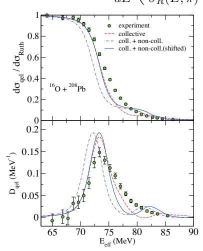


✓ lower part of the barrier distribution remains almost the same

✓ higher energy part(76MeV ~ 80MeV) of the barrier distribution is smeared

✓ fusion cross sections are not much altered(only shift in energy)

✓ agreement with the data is not improved (large difference in main peak)

## $^{16}O + {}^{208}Pb$ Q-value distribution for quasi-elastic scattering

Energy dependence of Q-value distribution ($\theta = 170°$)

red - collective channels, blue - non-coll. channels

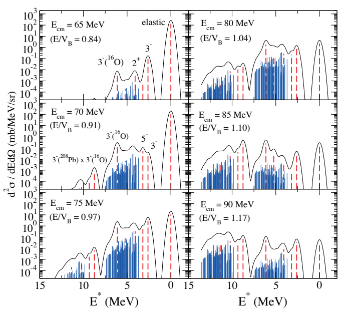


✓ for lower incident energy, collective channels are dominant

✓ as the incident energy increases, non-collective excitations become important

✓ energy dependence is consistent with the experimental Q-value distribution

## Summary

heavy-ion reaction with non-collective excitations → application to $^{16}$O+$^{208}$Pb system

✓ information for non-collective excitations of $^{208}$Pb has been obtained from high resolution proton-inelastic scattering experiment

✓ higher part of the barrier distribution is smeared due to the non-collective excitations (both fusion and quasi-elastic scattering)

✓ agreement with the experiment is not improved

✓ energy dependence of the Q-value distribution is consistent with the experiment

**Future perspectives**

- application to $^{20}$Ne + $^{90,92}$Zr systems (importance of non-coll. excitations is suggested)
- description non-collective excitations with random matrix theory(for the purpose of application to the system whose information for non-coll. states is absent)

# No.31 Improvement of the detector systems for Neutral Kaon Spectrometer 2

Physics D1 Fumiya Yamamoto

## ✓Introduction

- Measurement of meson photoproduction with Neutral Kaon Spectrometer 2 (NKS2)
  - Elementary photoproduction of strangeness : $\gamma n \rightarrow K^0\Lambda$
  - Non-quasi-free photoproduction on the deuteron : $\gamma d \rightarrow \pi^+\pi^- pn$ ($\gamma d \rightarrow \Delta^{++}\Delta^-$)
    * a consistent cross section at wide photon energy range 0.54 - 1.25 GeV (Fig.1).

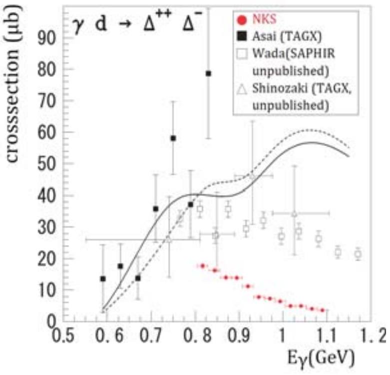


Fig.1: The Cross section for the $\gamma d \rightarrow \Delta^{++}\Delta^-$.
Ref. K. Hirose, *et al.*, Phys. Lett. B 674 (2009) 17.

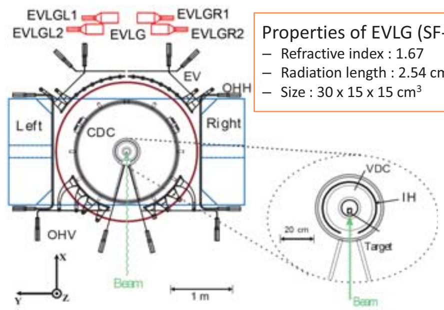


Properties of EVLG (SF-5)
- Refractive index : 1.67
- Radiation length : 2.54 cm
- Size : 30 x 15 x 15 cm$^3$

Fig.2: NKS2 scheme and position and properties of EVLG. NKS2 consists of dipole magnet (a diameter 80 cm, a gap 68 cm), hodoscopes , drift chamber and liquid deuterium target on center of magnet. EVLG located on beam plane, 3 m from center of magnet.

- Improvement of NKS2
  - Lead glass Cherenkov counter (EVLG, FIg2).
    * Decrease trigger rate of $e^+e^-$ background → High beam intensity.
  - Vertex Drift Chamber (VDC, Fig3).
    * Vertex resolution → Higher the momentum and angler resolution.
    * Acceptance (Fig.4) : $K^0$ 3 times, $\Lambda$ 1.5 times, $K^0\Lambda$ 8 times.
    * Elimination of a Fermi motion correction of neutron in deuteron by coincidence $K^0\Lambda$.
  - Development of new tagger with MPPC.
    * Photon energy range : 0.54 - 1.1 GeV → 0.54 - 1.25 GeV.
    * Photon energy resolution : 6 MeV → 3 MeV.

- Report in this poster
  - Evaluation of a quality of trigger level $e^+e^-$ background reduction with ADC of EVLG.
  - Evaluation of DAQ efficiency before and after incorporating EVLG as veto in the trigger.

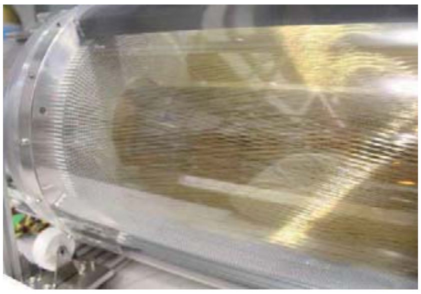

Fig.3 : Photograph of VDC. This counter located close to a target. The number of channel is 626. Three dimensional analyses are possible by wire having tilt for z-axis.

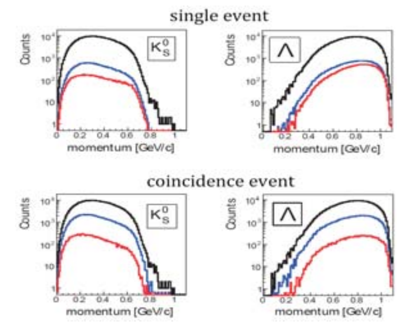


Fig.4 : Compare of a single event $K^0$ and $\Lambda$ and a coincidence event $K^0\Lambda$ with / without VDC by Monte-Carlo simulation. Black line : Total event. Red line : Acceptance of NKS2 without VDC. Blue line : Acceptance of NKS2 with VDC.

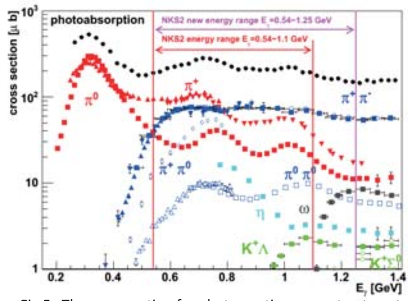


Fig.5 : The cross section for photoreaction on proton target.
Red line : previous tagged photon energy range 0.54-1.1 GeV.
Purple line : new tagged photon energy range 0.54-1.25 GeV.

## ✓Particle identification

- Particle selection by its mass :
  $$m^2 = p^2(\beta^{-2} - 1)$$
  m : mass
  p : momentum
  β : velocity
- Condition of π selection :
  $$-0.5 < m^2 < 0.5$$
  $$|p| > (0.144/(\beta^{-1}-0.2)-0.8)$$

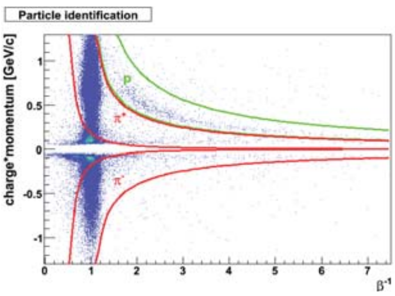


Fig.6 : Particle identification, β inverse vs momentum. Green line : proton. Red line : $\pi^+$ and $\pi^-$.

## ✓Results

- Electron reduction : $\{N_{threshold}(\text{without}) - N_{threshold}(\text{with})\} / \{N_{all}(\text{without}) - N_{all}(\text{with})\}$
  π loss : $N_{threshold}(\text{with}) / N_{all}(\text{with})$
- Effect of EVLG veto.
  DAQ efficiency : Improvement about 10% at beam rate 1.5 MHz.
  Beam intensity : Improvement about 30% at DAQ efficiency 0.8.

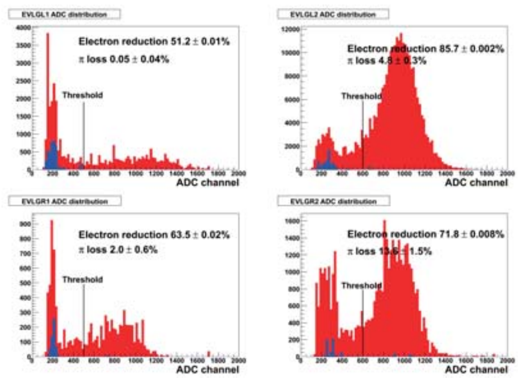


Fig.7 : EVLGL2 ADC distribution. Blue fill : With π selection. Red fill : Without π selection. Threshold : setting value at experiment. $N_{all}$ (with/without) : All number of EVLG ADC with / without π selection. $N_{threshold}$ (with/without): Number above threshold. Statistics error Only.

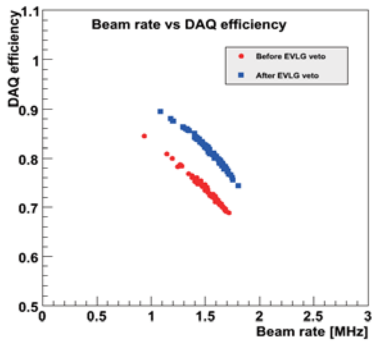


Fig.8 : Beam rate vs DAQ efficiency.
Red circle : before EVLG veto. Blue cube : after EVLG veto.

## ✓Summary

- Measurement of meson photoproduction with NKS2.
  - Elementary photoproduction on strangeness : $\gamma n \rightarrow K^0\Lambda$.
  - A consistent cross section for $\gamma d \rightarrow \pi^+\pi^- pn$ at wide energy range.
- We are improving NKS2.
  - Installation EVLG and VDC , and development tagger system.
- From EVLG ADC, number of $e^+e^-$ background hitting this counter decreased to about 51% - 85%.
- Loss of π in one segment of EVLG is about 13% at the most.
- DAQ efficiency and beam intensity increased about 10% and 30% after incorporating EVLG as veto in the trigger, respectively.
- EVLG is effective in $e^+e^-$ background reduction at trigger level.

# Theory of Superconductivity in fullerides by the repulsive interaction model

**Satoshi Yamazaki** **Yoshio Kuramoto**
Department of Physics, Tohoku University

## Introduction

$A_3C_{60}$ $A$=K, Rb, Cs

- 3D crystal structure (bcc, fcc)
- Degenerate $t_{1u}$ molecular orbitals (3 fold degeneracy)

$Cs_3C_{60}$

- Mott insulator at ambient pressure
- Superconducting (SC) state under applied pressure

Phase diagram

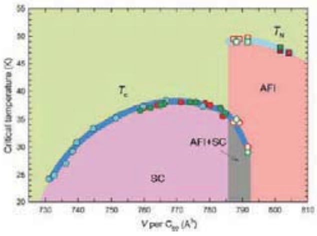


Y. Takabayashi, *et al.* Science **323**, 1585 (2009)

The Coulomb repulsion plays a significant role.

## Purpose

- Effect of the Coulomb repulsion for the SC state

⟶ Weak coupling approach
S. Rague, *et al*, Phys. Rev. B. **81** (2010) 224511.
S. Graser, *et al*, New J. Phys. **11**, 025016 2009.

- Effect of the crystal structure in $A_3C_{60}$

⟶ 3 dimensionality (bcc, fcc), orbitaly degeneracy

- Symmetry of superconductivity in $A_3C_{60}$

⟶ Point group $T_h$ ⟶ $A_g$, $E_g$, $T_g$

## Result

$U = U' = W = 0.5\text{eV},\ J = K = 0$

bcc model — SC state with $T_g$ symmetry

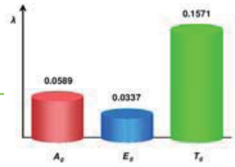


The SC state with $A_g$ and $E_g$ have the smaller value of λ .

Brillouin zone ($k_z$=0)

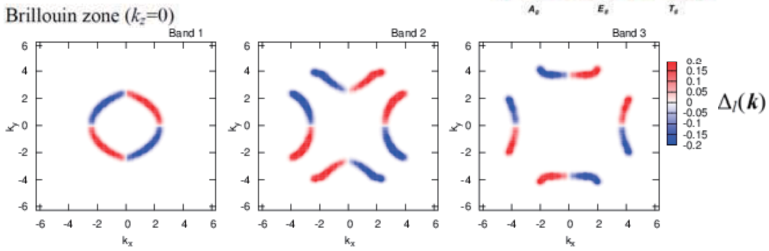


fcc model — SC state with $E_g$ symmetry

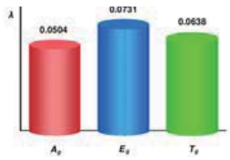


The value of λ with $A_g$ and $T_g$ are comparable.

Brillouin zone ($k_z$=0)

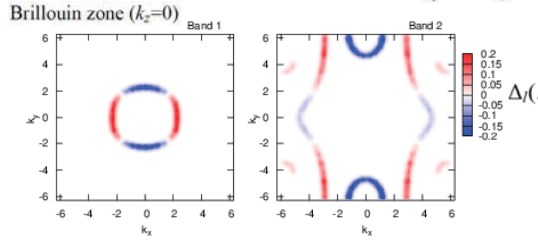


## Model

Band width : $W$=0.5eV

Construct effective tight binding hamiltonian for $t_{1u}$ orbitals

$$\mathcal{H}_0 = \sum_{<i,j>} \sum_{\sigma, mn} t_{mn}(\alpha,\beta,\gamma)\left(c^{\dagger}_{im\sigma} c_{jn\sigma} + h.c.\right)$$

$t_{mn}(\alpha,\beta,\gamma)$ : hopping integral fitted by result of the first principle band calculation

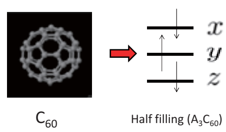


bcc structure

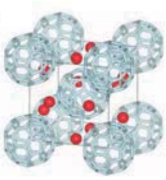

Fermi surface (bcc)

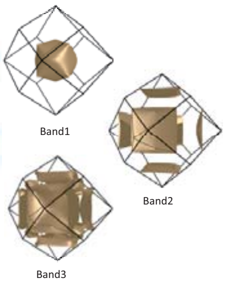


fcc structure

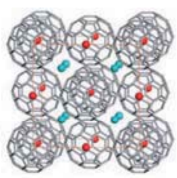

Y. Ganin, *et al.* Nature Mater. **7**, (2008) 367.

Fermi surface (fcc)


Energy band (bcc)


Energy band (fcc)

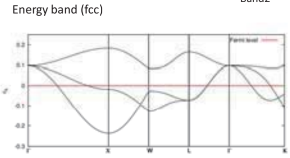

Kohn-Luttinger effective interaction (multi orbital)

W. Kohn and J.M. Luttinger, Phys. Rev. Lett. **15** (1965) 524.

$$V_{mn,m'n'}(k,k') = \left[\hat{U} + \hat{U}\hat{\chi}(k+k')\hat{U}\right]_{mn',m'n}$$

$$U_{mm,mm} = U,\ U_{mn,mn} = U',\ U_{mm,nn} = J,\ U_{mn,nm} = K.$$

Intraorbital, Interorbital, Hund coupling, Pair hopping

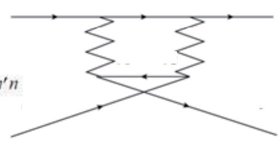

## SC instability

$$T_c \propto \exp(-1/\lambda),\ \lambda > 0$$

$$\lambda\, \Delta_l(\boldsymbol{k}) = -\frac{1}{(2\pi)^3}\sum_{l'}\int_{\epsilon_{\boldsymbol{k}'l'}=\epsilon_F}\frac{dS_{\boldsymbol{k}'l'}}{v_{l'}(\boldsymbol{k}')}V_{ll'}(\boldsymbol{k},\boldsymbol{k}')\Delta_{l'}(\boldsymbol{k}')$$

$$V_{ll'}(\boldsymbol{k},\boldsymbol{k}') = \sum_{mn,m'n'}\bar{A}^{m}_{l}(\boldsymbol{k})\bar{A}^{n}_{l}(-\boldsymbol{k})V_{mn,m'n'}(\boldsymbol{k},\boldsymbol{k}')A^{m'}_{l'}(\boldsymbol{k}')A^{n'}_{l'}(-\boldsymbol{k}').$$

Linear combination of the anisotropic SC state ($O_h$)

M. Sigrist and K. Ueda, Rev. Mod. Phys. **63**, 239 (1991).

$T_{2g}$ symmetry   ω= exp(2πi/3)

| | $\Delta_l(\boldsymbol{k})$ | Degeneracy | Point group (irreducible representation) | |
|---|---|---|---|---|
| Ⅰ | $k_yk_z + \omega k_zk_x + \omega^2 k_xk_y$ | 8 | $D_{3d}(\Gamma_3^+)$ | ⟶ d + id (chiral) |
| Ⅱ | $k_yk_z + k_zk_x + k_xk_y$ | 4 | $D_{3d}(\Gamma_1^+)$ | |
| Ⅲ | $k_yk_z$ | 3 | $D_{4h}(\Gamma_4^+)$ | ⟶ $d_{xy}$ (polar) |
| Ⅳ | $k_yk_z + i\,k_xk_z$ | 6 | $D_{4h}(\Gamma_5^+)$ | |

$E_g$ symmetry

| | $\Delta_l(\boldsymbol{k})$ | Degeneracy | Point group (irreducible representation) |
|---|---|---|---|
| Ⅰ | $k_x^2 - k_y^2$ | 3 | $D_{4h}(\Gamma_3^+)$ |
| Ⅱ | $2k_z^2 - k_x^2 - k_y^2$ | 3 | $D_{4h}(\Gamma_1^+)$ |
| Ⅲ | $k_x^2 + \omega k_y^2 + \omega^2 k_z^2$ | 2 | $O_h(\Gamma_3^+)$ |

Temperature dependence of spin relaxation rate

$$R = \frac{1}{T_1T} = \frac{1}{N}\sum_q |A_q|^2 \frac{\mathrm{Im}[\chi(q,\ \omega_0,\ T)]}{\omega_0}$$

$$\Delta(T) = \Delta_0\sqrt{1-\frac{T}{T_c}} \quad T_c = \Delta_0/1.76 \quad \Delta_0 = 0.01W$$

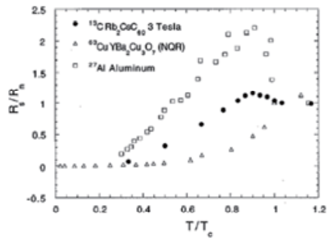


Experimental result

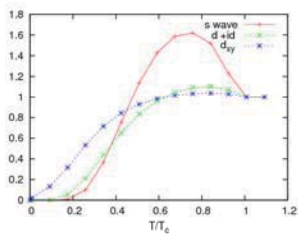


Calculation result (bcc model)

## Conclusion & discussion

- Anisotropic SC state

bcc: $T_g$ 3 fold degeneracy
fcc : $E_g$ 2 fold degeneracy

- Degenerate SC state ⟶ This degeneracy is resolved below $T_c$ .

- Small coherence peak caused by the d + id (chiral) state

(spin relaxation rate in nuclear magnetic resonance experimental)

No.29

# X-ray exposure effect on charge-orbital order in Fe-doped layered manganite $La_{0.5}Sr_{1.5}Mn_{1-x}Fe_xO_4$

Y. Yamaki [A, B], Y. Yamasaki [B], H. Nakao [B], Y. Murakami [B], Y. Kaneko [C, D], Y. Tokura [C, D, E, F]

[A] Department of science, Tohoku University, [B] Condensed Matter Research Center/Photon Factory, KEK, [C] Multiferroics Project, ERATO, [D] Cross-Correlated Materials Research Group, [E] Correlated Electron Research Group, RIKEN, [F] Department of Applied Physics, University of Tokyo

## 1.Introduction

### 1-1. Photo induced phase transition

(1)$Pr_{0.7}Ca_{0.3}MnO_3$ (2)W:$VO_2$

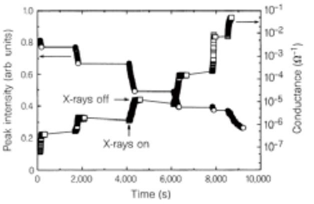

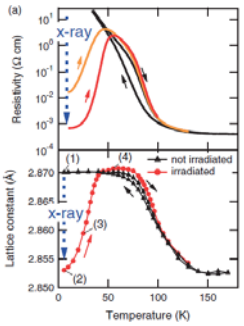

(1) Insulating antiferromagnetic state(charge ordering) → metallic ferromagnetic state
(2)Insulator → metal

### 1-2. Bicritical phase competition & object material

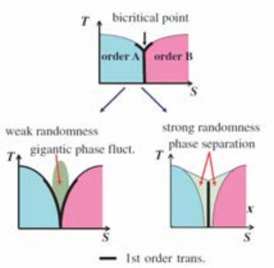

$La_{0.5}Sr_{1.5}MnO_4$

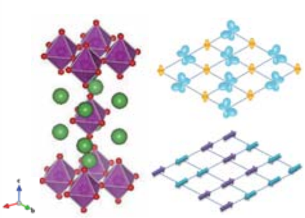

Phase diagram

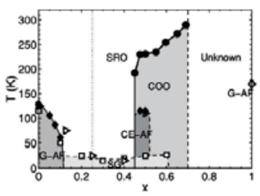

Temperature dependence of order parameter for COO

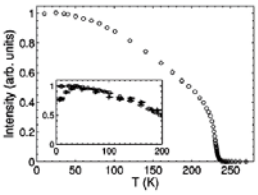

A single layered manganite $La_{0.5}Sr_{1.5}MnO_4$ shows charge-orbital ordering(COO) below T = 240K. We have investigated the impurity effect on COO state in this material and substituted Fe ions for Mn ions. In Fe-doped compound, not only that transition temperature and order parameter of COO decrease but also COO state is strongly suppressed by x-ray irradiation at low temperature. In this paper we report this photo induced phase transition in impurity doped manganite $La_{0.5}Sr_{1.5}Mn_{1-x}Fe_xO_4$.

## 2.Experiments

Experimental configuration

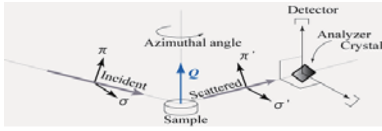

- Resonant and non-resonant x-ray scattering experiment.
- $La_{0.5}Sr_{1.5}Mn_{1-x}Fe_xO_4$ single crystal.
- BL-4C and BL-3A, Photon Factory, KEK.
- Incident x-ray Energy : Mn *K*-edge(~6.55keV) and 6.5keV.
- Polarization analysis : Cu(220).
- Configuration at $E_i // c$ is defined as $\Psi=0$

Spin configurations of Mn ions and Fe ion

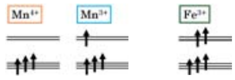

Schematic view of impurity substitution

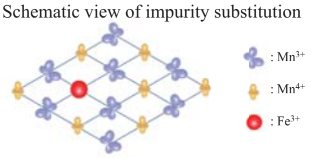

## 3. Results

### 3-1. Temperature dependence of the intensity for Q = (1/4 7/4 0) and the correlation length of COO in $La_{0.5}Sr_{1.5}Mn_{1-x}Fe_xO_4$

(a) Intensities for Q = (1/4 7/4 0)

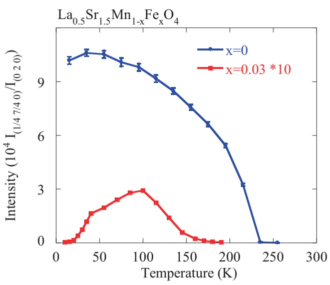

(b) Correlation lengths of COO

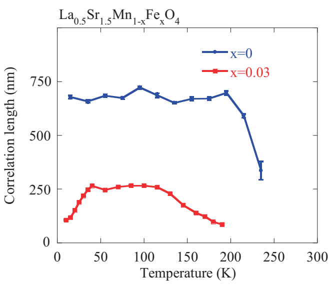

(a)In Fe doped compound, the intensity of Q = (1/4 7/4 0) which reflect lattice distortion accompanied with OO is about 30 times as small as that of pure compound.
(b)The correlation length of COO in Fe doped compound is about 3 times as short as that in pure compound.

**→ COO state is strongly suppressed by substitution of Fe ions.**

### 3-2. Temperature dependence of magnetic property in $La_{0.5}Sr_{1.5}Mn_{1-x}Fe_xO_4$

(a) DC-magnetization

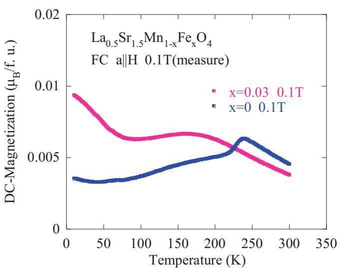

(b) AC-susceptibility

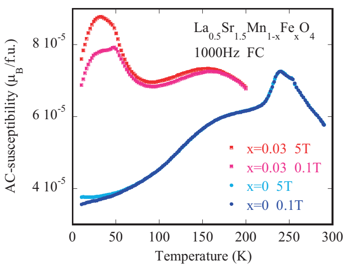

(a)In Fe doped compound, DC-magnetization increases below 90 K.
(b)Temperature dependence of AC-susceptibility in Fe doped compound have peak structure around 40 K and this peak structure grows with increasing of magnetic field in field cooling.

**→ Ferromagnetic component is emerged by substitution of Fe ions.**

### 3-3. X-ray exposure effect on COO in $La_{0.5}Sr_{1.5}Mn_{0.97}Fe_{0.03}O_4$

(a) X-ray exposure time dependence of the intensity for Q = (1/4 7/4 0)

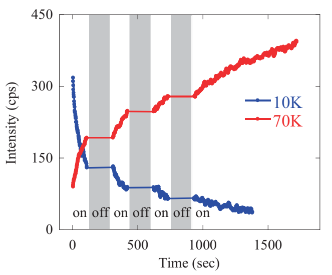

(b) Incident x-ray photon flux dependence of the intensity for Q = (1/4 7/4 0)

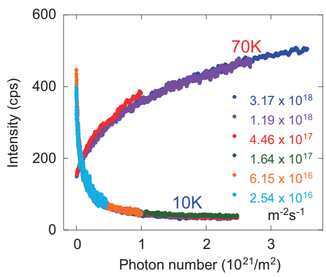

Decreases (in 10 K) or increases (in 70 K) of intensities come about only when a sample is irradiated and changes of the intensities depend on only irradiated photon number.

**→ This phenomenon is induced by x-ray exposure.**

### 3-4. Photon number dependence of the intensity for Q = (1/4 7/4 0) in $La_{0.5}Sr_{1.5}Mn_{0.97}Fe_{0.03}O_4$

(a) Temperature variations in cooling process

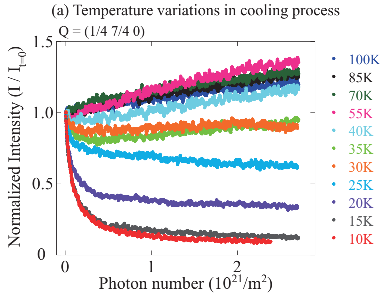

(b) Schematic view of cooling process

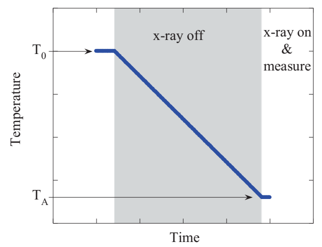

(c) Temperature variations in heating process

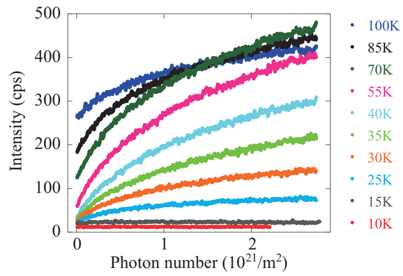

(d) Schematic view of heating process

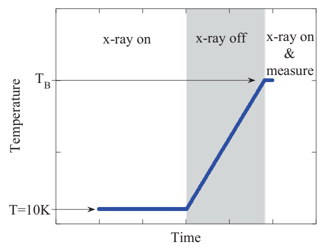

(a)The intensities are normalized by each intensity at t = 0. The intensities decrease below 25 K and increase above 55 K by x-ray exposure.
(c)The intensities all increase between 15 K and 100 K by x-ray exposure.

**→ COO state is suppressed below 25 K and enhanced above 55 K by x-ray exposure.**

## 4. Conclusion

In this study we have investigated photo induced phase transition in impurity doped manganite $La_{0.5}Sr_{1.5}Mn_{1-x}Fe_xO_4$. We assume that this photo induced phase transition would be caused by emerging of phase separation state induced by substitution of Fe ions.

**Cooling process**

| | Intensity |
|---|---|
| 10K - 25K | Monotone decreasing |
| 30K – 40K | Decreasing, then increasing |
| 55K – 100K | Monotone increasing |

**Heating process**

| | Intensity |
|---|---|
| 20K – 100K | Monotone increasing |

**Schematic view of photo induced phase transition in this system**

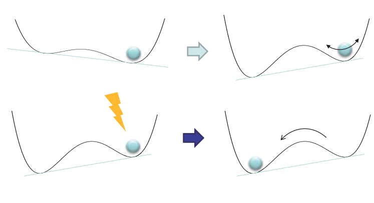

Reference
- Saioa Cobo, Denis Ostrovskii, Sebastian Bonhommeau, Laure Vendier, Gabor Molnar, Lionel Salmon, Koichiro Tanaka, and Azzedine Bousseksou, J. AM. CHEM. SOC. **130**, 9019 (2008).
- V. Kiryukhin, D. Casa, J. P. Keimer, A. Vigliante, Y. Tomioka, and Y. Tokura, Nature 386, 813 (1997).
- K. Shibuya, D. Okuyama, R. Kumai, Y. Yamasaki, H. Nakao, Y. Murakami, Y. Taguchi, T. Arima, M. Kawasaki, and Y. Tokura, Phys. Rev. B **84**, 165108 (2011)
- S. Larochelle, A. Mehta, L. Lu, P. K. Mang, O. P. Vajk, N. Kaneko, J. W. Lynn, L. Zhou, and M. Greven Phys. Rev. B **71**, 024435 (2005)
- Y. Tokura, JPSJ 75, 011001 (2006)

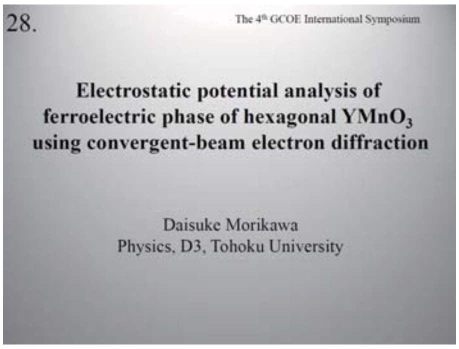


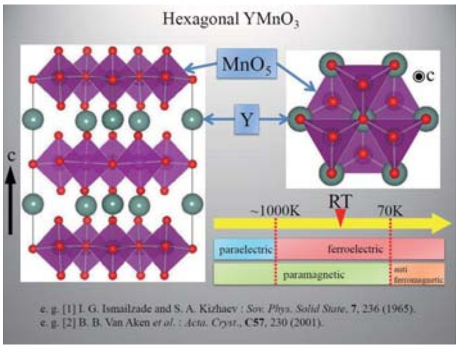


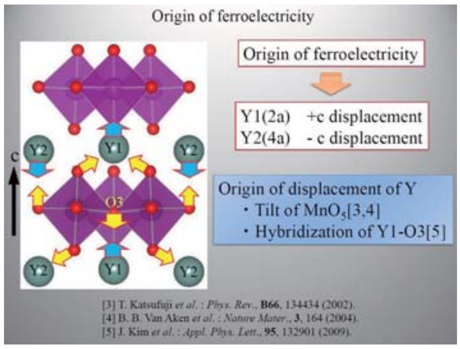


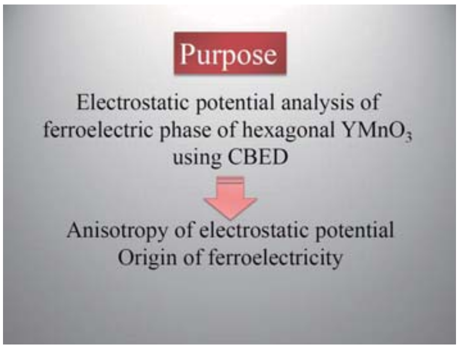


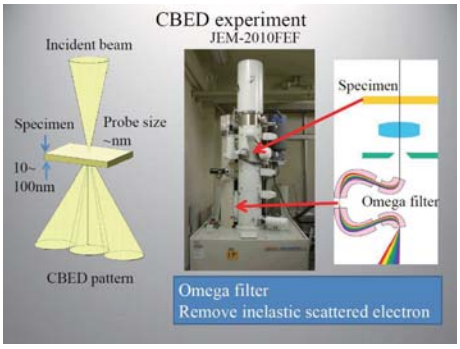


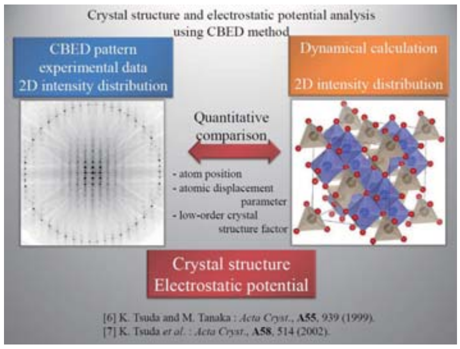


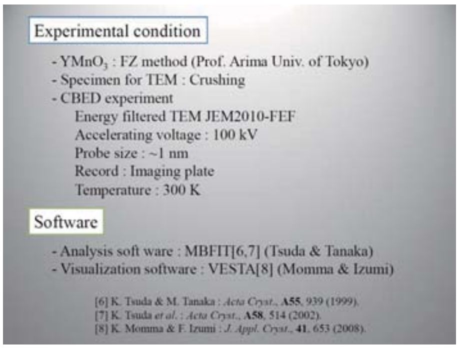


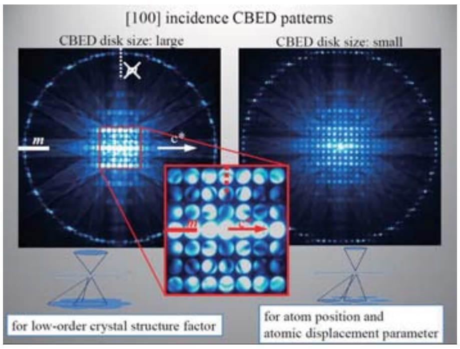


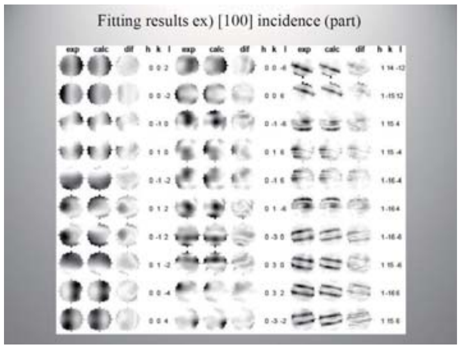


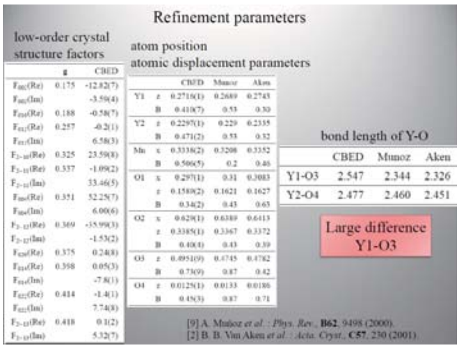


| | g | CBED |
|---|---|---|
| F[illegible](Re) | 0.175 | -12.82(7) |
| F[illegible](Im) | | -3.59(4) |
| F[illegible](Re) | 0.188 | -0.58(7) |
| F[illegible](Re) | 0.257 | -0.2(1) |
| F[illegible](Im) | | 6.58(3) |
| F[illegible](Re) | 0.325 | 23.59(8) |
| F[illegible](Re) | 0.337 | -1.09(2) |
| F[illegible](Im) | | 33.46(5) |
| F[illegible](Re) | 0.351 | 52.25(7) |
| F[illegible](Im) | | 6.00(6) |
| F[illegible](Re) | 0.369 | -35.99(3) |
| F[illegible](Im) | | -1.53(2) |
| F[illegible](Re) | 0.375 | 0.24(8) |
| F[illegible](Re) | 0.398 | 0.05(3) |
| F[illegible](Im) | | -7.8(1) |
| F[illegible](Re) | 0.414 | -1.4(1) |
| F[illegible](Im) | | 7.74(8) |
| F[illegible](Re) | 0.418 | 0.1(2) |
| F[illegible](Im) | | 5.32(7) |

| | | CBED | Munoz | Aken |
|---|---|---|---|---|
| Y1 | z | 0.2718(1) | 0.2689 | 0.2743 |
| | B | 0.410(7) | 0.53 | 0.30 |
| Y2 | z | 0.2297(1) | 0.229 | 0.2335 |
| | B | 0.471(2) | 0.53 | 0.32 |
| Mn | x | 0.3338(2) | 0.3208 | 0.3352 |
| | B | 0.506(5) | 0.2 | 0.46 |
| O1 | x | 0.297(1) | 0.31 | 0.3083 |
| | z | 0.1580(2) | 0.1621 | 0.1627 |
| | B | 0.34(2) | 0.43 | 0.63 |
| O2 | x | 0.629(1) | 0.6389 | 0.6413 |
| | z | 0.3385(1) | 0.3367 | 0.3372 |
| | B | 0.40(4) | 0.43 | 0.39 |
| O3 | z | 0.4951(9) | 0.4745 | 0.4782 |
| | B | 0.73(9) | 0.87 | 0.42 |
| O4 | z | 0.0125(1) | 0.0133 | 0.0186 |
| | B | 0.45(3) | 0.87 | 0.71 |

| | CBED | Munoz | Aken |
|---|---|---|---|
| Y1-O3 | 2.547 | 2.344 | 2.326 |
| Y2-O4 | 2.477 | 2.460 | 2.451 |

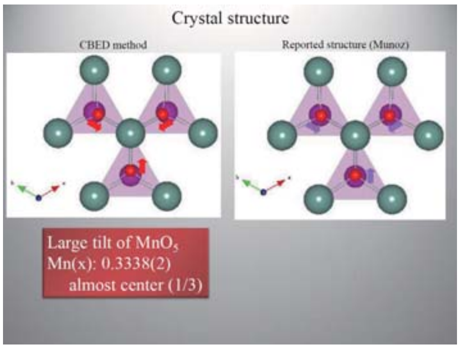


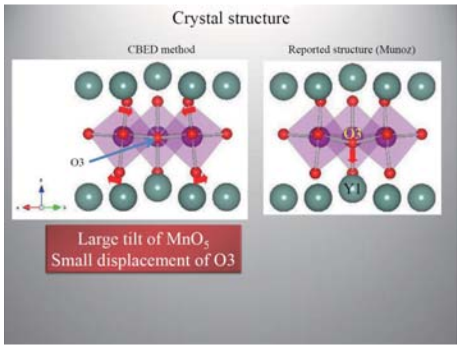


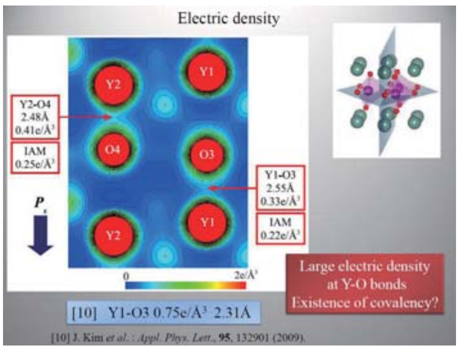


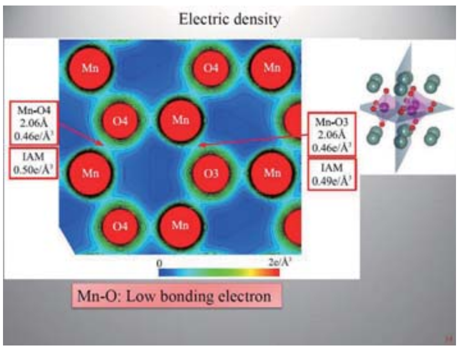


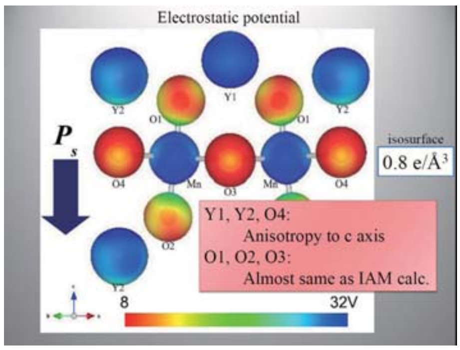


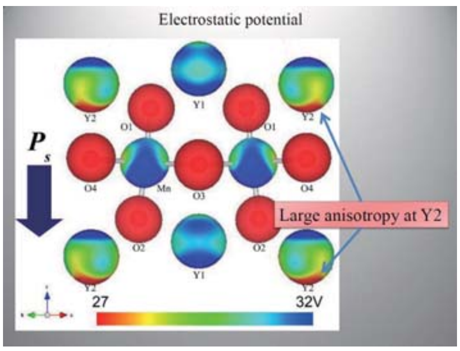


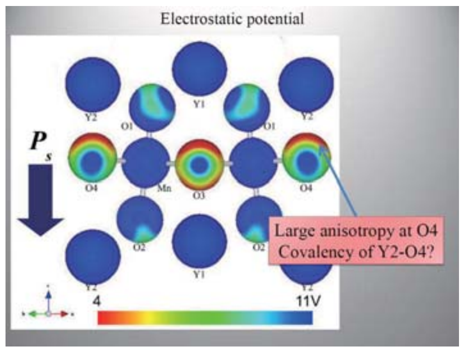


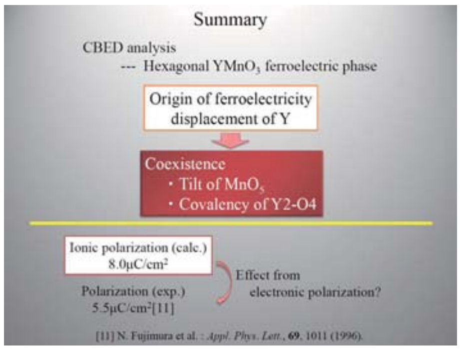

# Analysis of the hypernuclear γ-ray spectroscopy of $^{12}_{\Lambda}C$ and $^{11}_{\Lambda}B$ via the ($\pi^+$, $K^+$) reaction

K. Hosomi for KEK-E566 collaboration, Dept. of Physics, Tohoku Univ.

## Introduction

### ΛN interaction

Study of ΛN interaction is the first step to understand baryon-baryon interactions in a unified way beyond the well-known NN interaction. Instead of difficult ΛN scattering experiments due to a short lifetime of a Λ, it is a realistic and effective way to study ΛN interaction, in particular its spin-dependence, from precise structure of Λ hypernuclei.

### Hypernuclear γ-ray spectroscopy

As shown in Fig. 1, the low-lying level structure of hypernuclei can be understood by combining a Λ in the 0s orbit and the other part called "core". Each state of the core nucleus (with non-zero spin) splits into two states in the hypernucleus. The spacing of a doublet splitting is determined by spin-dependent ΛN interactions and is in the order of a few 100 keV to a few 10 keV. Thus, high resolution γ-ray spectroscopy of hypernucleus with Ge detectors is a unique way to study spin-dependent ΛN interactions.

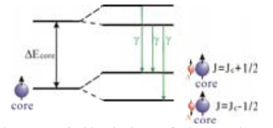

Figure 1: Typical level scheme of Λ hypernucleus.

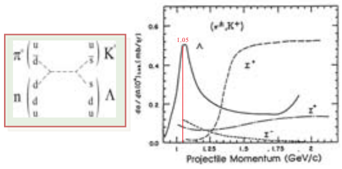

Figure 2: Diagram of n($\pi^+$,$K^+$)Λ and elementary cross section.

### KEK-E566 experiment

The KEK-E566 experiment was performed at KEK-PS K6 beam line in 2005. In this experiment, ($\pi^+$, $K^+$) reaction was used on $^{12}C$ target to produce $^{12}_{\Lambda}C$ and $^{11}_{\Lambda}B$. The beam $\pi^+$ momentum was set to be 1.05 GeV/c because the elementary cross section has a sharp maximum at this energy as shown in Fig. 2. The outgoing $K^+$ had a momentum around 0.75 GeV/c. Fig.3 shows the expected level scheme of this experiment together with the spectrum taken in past experiment(E369).

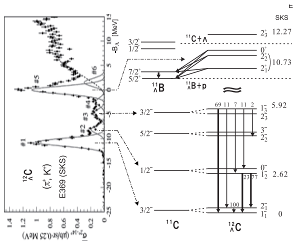

Figure 3: Expected level scheme of $^{12}C(\pi^+,K^+)$ reaction.

## Experimental Setup

### K6 beam line and SKS spectrometer

The primary proton beam is accelerated by KEK 12-GeV PS and irradiated on a production target located at the most upstream of the K6 beam line. The produced secondary pion beam is transported to the experimental target. Fig 4 shows the whole schematic view of the experimental setup.

The pion beam momentum is analyzed by the beam line spectrometer which is consists of QQDQQ magnets, tracking chambers, and timing counters.

The scattered kaons are identified and momentum-analyzed by the SKS spectrometer which consists of SKS magnet, tracking chambers, timing counters, and veto counters for scattered pions and protons.

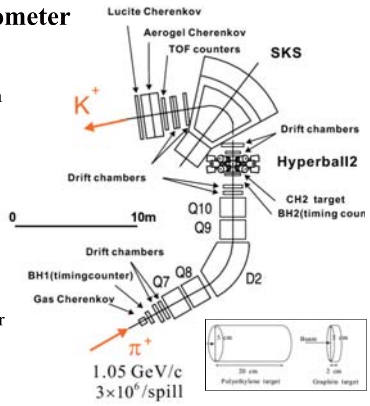

Figure 4: Schematic view of experimental setup.

### Hyperball2

To detect γ-rays emitted form a populated hypernucleus, a Ge detector array called Hyperball2 was installed around the experimental target. As shown in Fig. 5, Hyperball2 has a total of 14 single crystal type Ge detectors and 6 clover-type Ge detectors, each of which is surrounded by BGO counters to suppress the background signal that mainly is caused by Compton scattering.

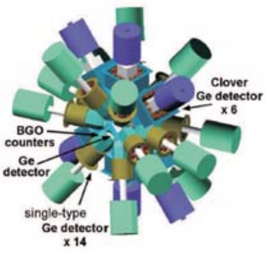

Figure 5: Schematic view of Hyperball2.

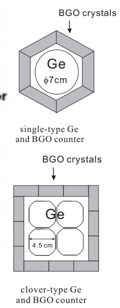


## Missing mass analysis

### Momentum and particle identification

1. Track reconstruction of a set of chambers at the entrance and at the exit of beam line Dipole and SKS magnets, respectively.
2. Momentum reconstruction by the Runge-Kutta method for the scattered particle and the transport matrix for the beam particle.
3. Time of flight determination from the reconstructed track information.
4. Particle identification by mass square for $K^+$ and time of flight for $\pi^+$.

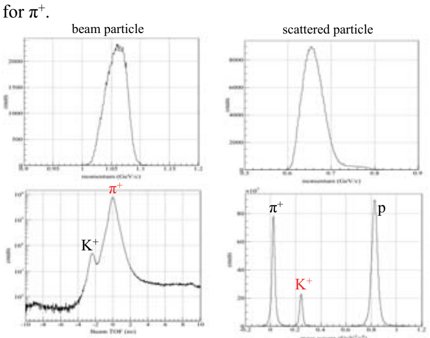


### Reconstruction of the ($\pi^+$,$K^+$) reaction

The vertex position was obtained from the incident $\pi^+$ track and the scattered $K^+$ track. The figures below show z-vertex distribution and xy-vertex distribution. The red line indicates the size of CH2 target.

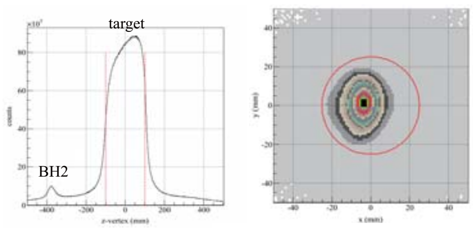


The right figure shows the distribution of the reaction angle for the $^{12}C(\pi^+,K^+)$ events.

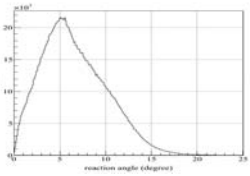

### Calculation of mass spectrum

The binding energy of $\Lambda(B_\Lambda)$ is calculated by

$$-B_\Lambda = M(^{12}_{\Lambda}C) - M_\Lambda - M(^{11}C).$$

The figures below are mass spectra in the scale of $-B_\Lambda$. The graphite target was used for the performance check of spectrometers. The mass resolution is obtained to be 2.8 MeV (FWHM) for the graphite and 6.3 MeV (FWHM) for the CH2 target.

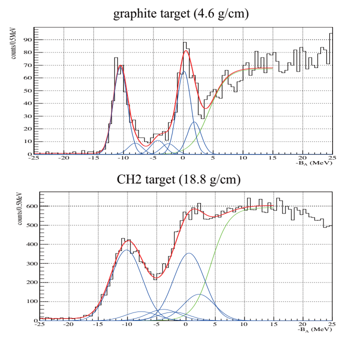


## γ-ray analysis

### Event selection

The hypernuclear γ rays of interest have a typical life time less than 200 ps. Ge detectors time was measured with respect to the beam timing. Because the time resolution of a Ge detector depends on the amplitude of the signal, the time distribution has a correlation with ADC as shown in below.

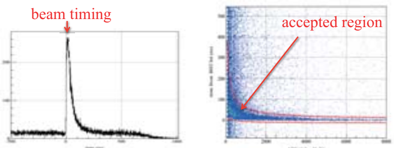


### Energy calibration

A cubic function is used to fit the calibration curve. γ rays used for the calibration and the fitting result are shown below.

| Source | γ-ray energy(keV) |
|---|---|
| $^{152}Eu$ | 121.78 |
| $^{152}Eu$ | 244.70 |
| $^{152}Eu$ | 344.28 |
| $e^+e^-$ | 511.0 |
| $^{152}Eu$ | 778.90 |
| $^{152}Eu$ | 964.06 |
| $^{152}Eu$ | 1085.84 |
| $^{152}Eu$ | 1112.09 |
| $^{60}Co$ | 1173.24 |
| $^{60}Co$ | 1332.50 |
| $^{152}Eu$ | 1408.01 |
| $^{24}Mg$ | 2754.03 |
| $^{16}O$ (DE) | 5101.63 |
| $^{16}O$ ($SE^a$) | 5617.63 |
| $^{16}O$ | 6128.63 |

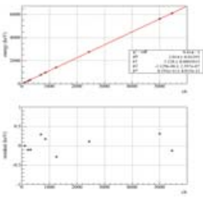

## Summary

- Hypernuclear γ-ray spectroscopy experiment provides a unique way to study the baryon-baryon interactions.
- The KEK-E566 experiment was successfully carried out.
  - $^{12}_{\Lambda}C$ and $^{11}_{\Lambda}B$ was populated via the ($\pi^+$, $K^+$) reaction.
- Data analysis
  - Mass spectrum was reconstructed with a reasonable resolution.
  - Analysis for γ rays detected by Hyperball2 is now in progress.

# Statistical analysis of human written language

Department of Physics , Sho Furuhashi

## Introduction

Sentence length is a quantity showing the writing style. In Japanese, the distribution of sentence length (the number of characters) has some characteristic forms: lognormal distribution[1-3] and Gamma distribution[2].

There is no quantitative study about the features of the distribution of sentence length.

### Purpose

We investigate the features of sentence length distribution by focusing on sentence structure.

A) Lognormal distribution
B) Gamma distribution

## Method and sample

### Dependency tree

Sentence structure can be represented as tree based on dependency grammar between segments.

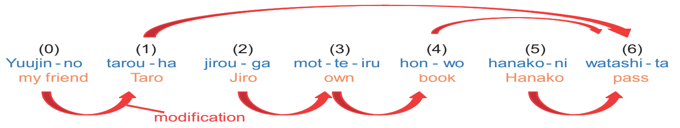


### Sample

Aozora bunko: Online data base that contains public-domain texts.
(Total number of sentences: 116719)
Kyoto university text corpus: A text corpus compiled from the Mainichi Shinbun Newspaper.
(Total number of sentences: 38397 )

## Result A

Multiplicative process $X_n = \prod_{i=0}^{n-1} \alpha_i X_0$ ( $\alpha_i$: positive random variable) is a model of lognormal distribution.

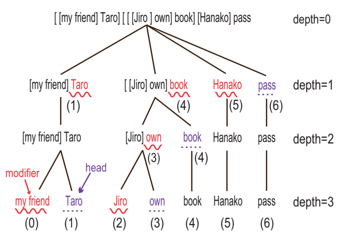


$d_l$ : the depth of leaves

$S_d$ : the number of nodes at depth $d$

$$S_d = l_s(d > d_l)$$

If the branching process is multiplicative process,

$$\langle \ln S_d \rangle \propto d,\ \langle \ln l_s \rangle \propto d_l.$$

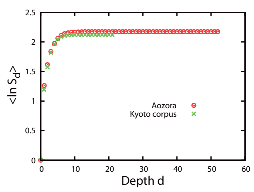


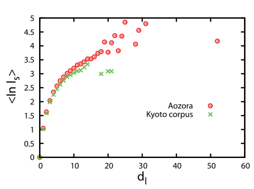


## Conclusion

From the results,

A) multiplicative process does not appear in dependency tree,
B) and, sentence length is sum of exponential distributions.

Sentence length is similar to gamma distribution.

### Reference

1. B. Yasumoto: Mathematical Linguistics No. 4 (1958) 20
2. K. Sasaki: Mathematical Linguistics No. 78 (1976) 13
3. H. Arai: Hitotsubashi University Journal 125 (2001) 205

## Distribution of sentence length

$$R = \sum_{k=k_0}^{k_{max}} |O(k) - E(k)|$$

$O(k)$ : Original data
$E(k)$ : Model distribution

$$f_{LN}(x) = \frac{1}{x\sqrt{2\pi\sigma^2}} \exp\left\{-\frac{(\ln x-\mu)^2}{2\sigma^2}\right\} \qquad f_G(x) = x^{k-1}\frac{e^{-x/\theta}}{\Gamma(k)\theta^k}$$

Sentence length ➡ The number of segments $l_s$

The distributions of $l_s$ ➡ Gamma distribution

$k_0 = 1, k_{max} = 88$
$R = 0.071$ $(E(k) = f_{LN}(k))$,
$R = 0.070$ $(E(k) = f_G(k))$

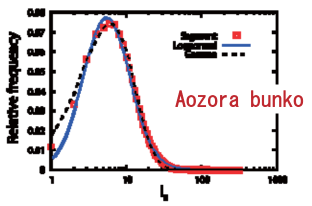


$k_0 = 1, k_{max} = 46$
$R = 0.11$ $(E(k) = f_{LN}(k))$
$R = 0.024$ $(E(k) = f_G(k))$

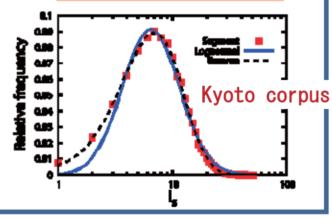


## Result B

The sum of independent exponentially distributed random variables follows gamma distribution.

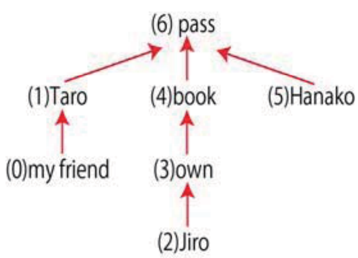


Branches which are connected to the root correspond to phrases.
(subject, modifier)

What forms are the distributions of the size and number of phrases?

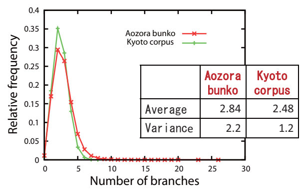


| | Aozora bunko | Kyoto corpus |
|---|---|---|
| Average | 2.84 | 2.48 |
| Variance | 2.2 | 1.2 |

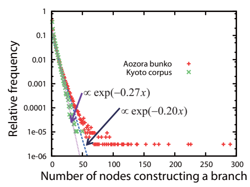

# Study of Λ photoproduction with Neutral Kaon Spectrometer 2

Takao Fujii for NKS2 Collaboration  Department of Physics, Tohoku University

## Introduction

### Physics Motivation

Strangeness photoproduction in the threshold region plays the unique role for the investigation of hadron interactions and their structure. Among the six isospin channels of strangeness photoproduction, most of the experimental data have been obtained for the $K^+$ production channels. On the other hand, the experimental data for the reaction channels with $K^0$ was scarce because of their experimental difficulty (the right figure). So, the investigation of $K^0$ production channels is very important to understand the strangeness photoproduction mechanism.

| Processes | Photon Energy Threshold |
|---|---|
| $\gamma+p\rightarrow K^+ +\Lambda$ | 911.1 MeV |
| $\gamma+p\rightarrow K^+ +\Sigma^0$ | 1046.2 MeV |
| $\gamma+p\rightarrow K^0 +\Sigma^+$ | 1047.5 MeV |
| $\gamma+n\rightarrow K^0 +\Lambda$ | 915.3 MeV |
| $\gamma+n\rightarrow K^0 +\Sigma^0$ | 1050.6 MeV |
| $\gamma+n\rightarrow K^+ +\Sigma^-$ | 1052.1 MeV |

Photon energy threshold of six strangeness photoproduction channels

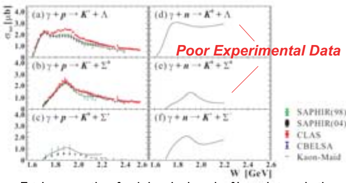

Total cross sections for six isospin channels of kaon photoproduction

#### Major decay mode of $K^0$ and Λ

$K^0\rightarrow K^0_S$ (50%) / $K^0_L$ (50%)

| $K^0_S(c\tau=2.68\,\mathrm{cm})$ | $K^0_L(c\tau=1534\,\mathrm{cm})$ |
|---|---|
| $K^0_S\rightarrow\pi^+\pi^-(69.2\%)$<br>$\rightarrow\pi^0\pi^0$ (30.7%) | $K^0_L\rightarrow\pi^\pm e^\mp\nu_e(40.6\%)$<br>$\rightarrow\pi^\pm\mu^\mp\nu_\mu(27.0\%)$<br>$\rightarrow\pi^0\pi^0\pi^0$ (19.5%)<br>$\rightarrow\pi^+\pi^-\pi^0(12.5\%)$ |

$\Lambda\rightarrow p\pi^-(63.9\%)$ / $n\pi^0(35.8\%)$

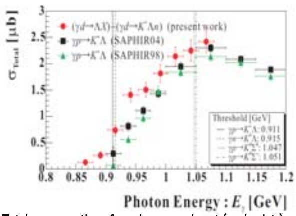

Total cross section of previous experiment ( red point )

### Previous experiment of $\gamma n\rightarrow K^0\Lambda$ reaction

For the measurement of $\gamma n\rightarrow K^0\Lambda$ reaction, we built the Neutral Kaon Spectrometer (NKS) and the NKS2 and have performed the photoproduction experiments with them. In the NKS and NKS2 experiment, the $K^0$ is detected as the $K^0_S$ via its charged decay mode, and the Λ is also. Because no "pure" neutron target exists, the liquid Deuterium is used as the target.

The left figure is the total cross section of this reaction estimated from previous NKS2 experiment. It agree with the toal cross section of $\gamma p\rightarrow K^+\Lambda$ reaction in this energy region ( 0.8<$E_\gamma$<1.1 GeV ).

After this experiment, the central detectors of NKS2 has been upgraded to obtain the high statistical data.

## Neutral Kaon Spectrometer 2 (NKS2)

### Tagged photon beam

The experiment is performed using the real photon beam of the Research Center for Electron Photon Science (ELPH). Electron is accelerated to 1.2 GeV by the LINAC and the electron synchrotron called as STB-Ring. The photon is generated via bremsstrahlung, and scattered electron is tagged by the STB-Tagger system.

- Maximum energy of electron beam : 1.2 GeV
- Radiator : carbon fiber ( $\phi$ 11 $\mu$m)
- Tagger
  - TagF : 50 plastic scintillators
  - TagB : 12 plastic scintillators
  - covered energy range : 6 MeV / 1 TagF counter
- Energy region : 0.8-1.1 GeV (Ee = 1.2 GeV)

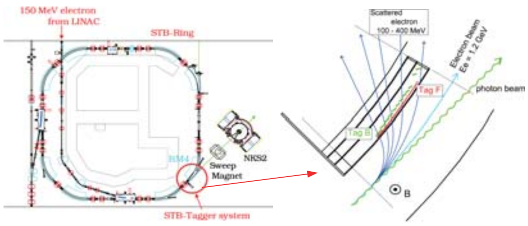

Schematic view of STB-Ring at ELPH and STB-Tagger system

### NKS2

NKS2 is the one of the electromagnetic spectrometer designed for the measurement of $\gamma n\rightarrow K^0\Lambda$ reaction. The Λ and the neutral kaon ($K^0$s) are detected via their charged decay mode( $\Lambda\rightarrow p\pi^-$ , $K^0_S\rightarrow\pi^+\pi^-$ ).

NKS2 consists of a large dipole magnet, two drift chambers, plastic scintillation hodoscopes and electron veto scintillation counters.

Liquid Hydrogen and Deuterium are used as the target.

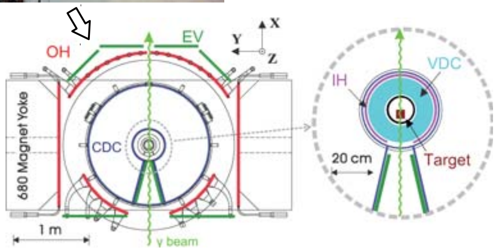

Schematic view of NKS2 & photo from backward of NKS2

- Target
  - Liquid $H_2$ or $D_2$
- Drift chambers
  - Vertex Drift Chamber (VDC)
  - Cylindrical Drift Chamber (CDC)
    - tracking of charged particles
    - momentum
- Hodoscopes
  - Inner Hodoscope (IH)
  - Outer Hodoscope (OH)
    - trigger generation
    - time of flight
- Electron Veto (EV)
  - removal of $e^+e^-$ background

## Experiment & Analysis

### Experiment

The measurement of $K^+$ / $K^0$ and Λ photoproduction cross section with NKS2 has been performed using both of liquid Hydrogen and Deuterium target. The numbers of photons counted by Tagger were $7.7\times10^{11}$ for the Hydrogen target period, and $8.8\times10^{12}$ for the Deuterium target period respectively.

| | Liq. H2 | Liq. D2 |
|---|---|---|
| Number of γ | $7.7\times10^{11}$ | $8.8\times10^{12}$ |

### Calibration of Hodoscopes & Drift Chambers

Before the analysis of experimental data, the calibrations of hodoscopes and drift chambers were carried out. The time standard and the conversion factors ( from TDC channels to time, from ADC channels to energy ) were determined.

In the current analysis status, calibration of hodoscope is not finished completely. So, only forward region of NKS2, IH 1-5 (±54° from beam direction) and OHV1-8 (±59° ), are used in this analysis.

### Vertex distribution

Here shows the vertex distribution of the horizontal plane for each target period. The target region is showed as the red square.

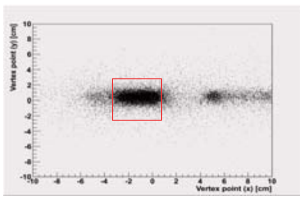

Vertex distribution of $H_2$ target period

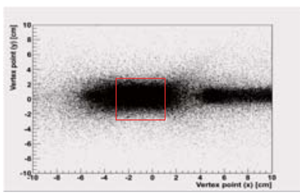

Vertex distribution of $D_2$ target period

### Particle identification (PID)

The particle identification is determined by the mass and the charge of the particle. The mass (m) is calculated by the correlation between the momentum (p) and velocity ( β ) as follows :

$$m^2=p^2\left(\frac{1}{\beta^2}-1\right)$$

The sign of charge is determined by the bending direction in the magnetic field.

- Definition of Pion

$$\beta^{-1}>0.5$$

$$|p|>\frac{0.144}{\beta^{-1}-0.2}-0.08\ \ (0.5\le\beta^{-1}<2.0)$$

$$-0.5<m^2<0.25$$

- Definition of Proton

$$0.5<m^2<1.8\ \ [(\mathrm{GeV}/c^2)^2]$$

- Definition of Deuteron

$$1.8<m^2<5.5\ \ [(\mathrm{GeV}/c^2)^2]$$

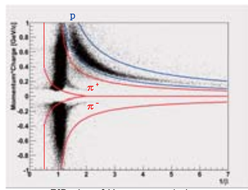

PID plot of $H_2$ target period

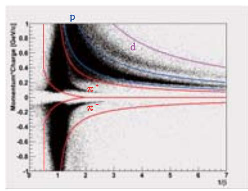

PID plot of $D_2$ target period

## Detection of Λ

The Λ particle is detected as the peak in the $p\pi^-$ invariant mass spectrum. The invariant mass of $p\pi^-$ events is calculated as follows,

$$m_{p\pi^-}{}^2=\left(\sqrt{m_p{}^2+|\boldsymbol{p}_p|^2}+\sqrt{m_{\pi^-}{}^2+|\boldsymbol{p}_{\pi^-}|^2}\right)^2-|\boldsymbol{p}_p+\boldsymbol{p}_{\pi^-}|^2$$

Where $m_p$ and $m_{\pi^-}$ are the masses of the charged pion and proton from the PDG value, and $p_p$ and $p_{\pi^-}$ are the momenta of each particle. Here shows the $p\pi^-$ invariant mass distributions of the hydrogen and deuterium target period. In the $H_2$ data, the enhancement is appeared around 1.115 GeV/c².

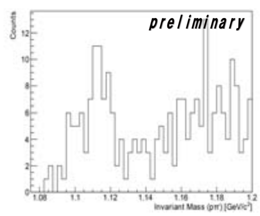

Invariant mass distribution for $H_2$ target

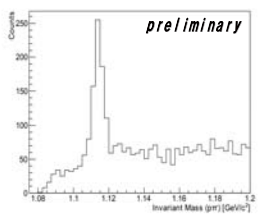

Invariant mass distribution for $D_2$ target

In the $D_2$ data, a clear peak is obtained. The peak position is 1.114 GeV/c², and sigma of peak is 3.6±0.2 MeV/c².

## Summary

- Strangeness photoproduction, especially $\gamma n\rightarrow K^0\Lambda$ reaction, plays the important role for the investigation of hadron interactions and their structure.
- NKS2 is the one of the electromagnetic spectrometer designed for the measurement of this reaction.
- Experiment has been performed using liquid $H_2$ and $D_2$ target.
- Calibration of data is performed, and the Λ particle is detected as the peak in the $p\pi^-$ invariant mass spectrum.
- Analysis for the calculation of the production cross section is being continued.

The 4th GCOE International Symposium (Feb. 20-22, 2012)

# Cosmologically viable gauge mediation

Hiraku Fukushima (Physics, D1)

This work is based on the collaboration with Ryuichiro Kitano and Fuminobu Takahashi (Tohoku Univ.)

## ・Gravitino problem

: tension between

The reheating temperature $T_R$ vs The gravitino abundance $\Omega_{3/2}$

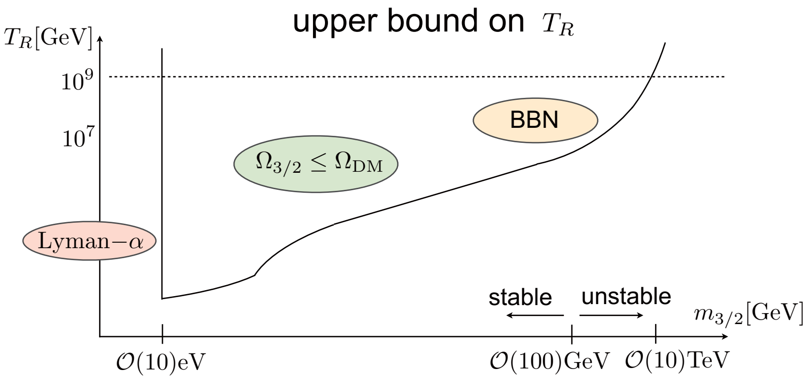


The gravitino abundance is constrained by the Big-Bang Nucleosynthesis (BBN) or observed Dark Matter density, which makes a severe upper bound on the reheating temperature. Gravitino with mass $\mathcal{O}(10)\mathrm{eV} \lesssim m_{3/2} \lesssim \mathcal{O}(10)\mathrm{TeV}$ is forbidden if we require $T_R \gtrsim 10^9\mathrm{GeV}$ .

## ・Constraint on $\Omega_{3/2}$

Gravitinos are produced in a thermal plasma after inflation, and their abundance is proportional to the reheating temperature.

$$\Omega_{3/2} \propto T_R.$$

Their abundance is constrained by

1. BBN (for unstable gravitinos);
   Their decay should not destroy the success of the BBN! Kawasaki, Kohri, Moroi(2005)
2. DM (for stable gravitinos);
   Their abundance should not exceed the observed Dark Matter density today!
   $$\Omega_{3/2} \lesssim \Omega_{\rm DM} \simeq 0.2.$$
   Moroi, Murayama, Yamaguchi(1993)

## ・Why is a high reheating temperature needed?

In order to produce observed amount of baryon asymmetry by thermal loptogenesis, the mass of the right handed (s)neutrino must be larger than $10^9 - 10^{10}\mathrm{GeV}$, which sets an upper bound on the reheating temperature, $T_R \gtrsim 10^9 - 10^{10}\mathrm{GeV}$.

Davidson, Ibarra(2002), Giudice et al.(2004), Buchmuller, Bari, Plumacher(2004)

## ・Our Work

We found a novel scenario of gauge mediation:

- The reheating temperature can be raised as high as $10^{12}\mathrm{GeV}$ with a gravitino mass $m_{3/2} \sim \mathcal{O}(1)\mathrm{GeV}$.
- Observed dark matter density $\Omega_{\rm DM} \simeq 0.2$ is explained by thermally produced gravitino.
- Supersymmetry breaking vacuum is successfully selected as the temperature of the universe drops.

## ・Cosmological evolution of pseudo-moduli

The model:

$$K = f^\dagger f + \bar{f}^\dagger \bar{f} + S^\dagger S - \frac{(S^\dagger S)^2}{\Lambda^2} + \cdots$$
$$W = m^2 S - \lambda S f \bar{f} + c$$

$S$ :SUSY breaking pseudo-moduli field
$f, \bar{f}$ :messenger field
$\Lambda$ :cut-off scale
$m$ :SUSY breaking scale
$c$ :supergravity correction

Scaler potential:

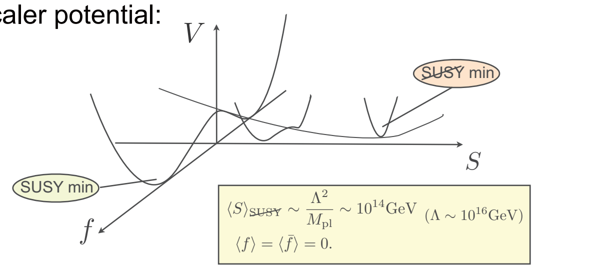


Thermal potential: $V_{\rm thermal} \sim \lambda^2 T^2 |S|^2 + g^2 T^2 |f|^2.$ $g$ :SM gauge coupling

⟶ stabilize $S, f$ at the origin.

For relatively small value of $\lambda$ , $S$ reaches ~~SUSY~~ minimum as the temperature of the universe drops.

Dalianis, Lalak(2011)

## ・Gravitino thermal production

The point:

Thermal production of the gravitino is highly suppressed if the messenger fields are thermalized. K. Choi et al.(1999)

$T_R$ can be raised as high as $10^{12}\mathrm{GeV}$ without the over production of the gravitino!

| | $T < M_{\rm mess}$ | $T > M_{\rm mess}$ |
|---|---|---|
| most effective process | 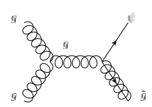 | 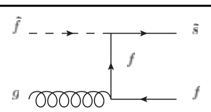 |
| gravitino production rate | $\langle \sigma v_{\rm rel} \rangle n_{\rm rad} \sim \alpha_3 \frac{m_{\tilde{g}}^2}{m_{3/2}^2 M_{\rm pl}^2} T^3$ | $\langle \sigma v_{\rm rel} \rangle n_{\rm rad} \sim \alpha_3 \lambda^2 T$ |

$\Omega_{3/2} \propto \min[T_R, M_{\rm mess}]$ $M_{\rm mess}$ :messenger mass scale

:independent of the reheating temperature for $T_R > M_{\rm mess}$!

(different from the usual estimete $\Omega_{3/2} \propto T_R$ .)

Using this formula, observed dark matter density is explained by thermally produced gravitino for $\lambda \sim 10^{-7}$ and $m_{3/2} \sim \mathcal{O}(1)\mathrm{GeV}$ .

DMRG study of the ground state phase diagram of interacting massless Dirac fermions in graphene under magnetic field

Tatsuya Higashi
Dept. of Physics, Tohoku U.

## Low-energy states of electrons in graphene

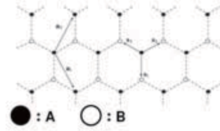


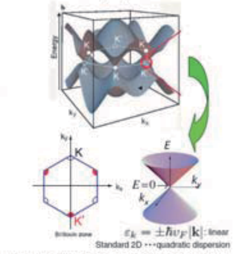


$\mathcal{H}_K = v_F\begin{pmatrix} 0 & p_x - ip_y \\ p_x + ip_y & 0 \end{pmatrix}$ (K,A) (K,B)

$\mathcal{H}_{K'} = v_F\begin{pmatrix} 0 & p_x + ip_y \\ p_x - ip_y & 0 \end{pmatrix}$ (K',A) (K',B)

$\hbar v_F = 3ta/2$ $a$ : Lattice constant, $t$ : Nearest neighbor hopping

Fermi levels are located at the two inequivalent points (K, K'). K,K' (valley) are particular internal degree of freedom of graphene (pseudospin).

Graphene is a new type of 2D electron system. e.g. Unconventional quantization pattern of IQHE

## Electronic states of graphene in magnetic fields

Effects of a magnetic field

$\vec{p} - \vec{\pi} = \vec{p} + e\vec{A}/c$

$a = \frac{l_B}{\sqrt{2}\hbar}(\pi_x - i\pi_y)$ Lowering operator

$a^\dagger = \frac{l_B}{\sqrt{2}\hbar}(\pi_x + i\pi_y)$ Raising operator

$l_B = \sqrt{\frac{\hbar c}{eB}}$ Magnetic length

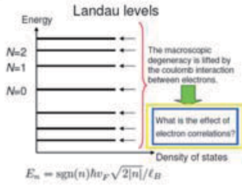


$E_n = \mathrm{sgn}(n)\hbar v_F\sqrt{2|n|}/\ell_B$

Hamiltonian

K : $H_K = \sqrt{2}\frac{\hbar v_F}{l_B}\begin{pmatrix} 0 & a \\ a^\dagger & 0 \end{pmatrix}$ (K,A) (K,B)

K' : $H_{K'} = \sqrt{2}\frac{\hbar v_F}{l_B}\begin{pmatrix} 0 & a^\dagger \\ a & 0 \end{pmatrix}$ (K',A) (K',B)

Eigenfunction ($n \neq 0$)

$\Psi_{Kn} = \frac{1}{\sqrt{2}}\begin{pmatrix} \mathrm{sgn}(n)\phi_{|n|-1} \\ \phi_{|n|} \end{pmatrix}$

$\Psi_{K'n} = \frac{1}{\sqrt{2}}\begin{pmatrix} \phi_{|n|} \\ \mathrm{sgn}(n)\phi_{|n|-1} \end{pmatrix}$

$\phi_n$ : The standard Landau wave function of electrons in the $n$th Landau level.

## CDW ground states of standard 2D electron systems in high Landau levels

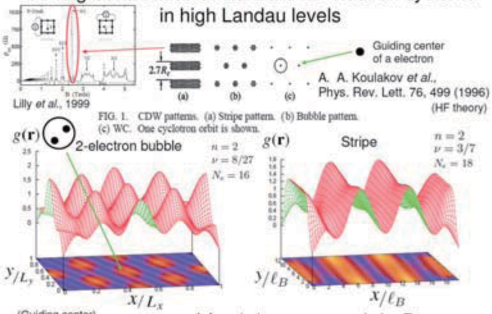


(Guiding center) Pair correlation function : $g(\mathbf{r}) = \frac{L_x L_y}{N_e(N_e-1)}\left\langle \Psi \left| \sum_{i\neq j}\delta(\mathbf{r} + \mathbf{R}_i - \mathbf{R}_j)\right| \Psi \right\rangle$ $\mathbf{R}_i$ : Guiding center coordinate of the $i$th electron

## Effective inter-electron interaction of $N$th Landau level

Standard 2D systems

$H_s = \sum_{i<j}\sum_{\mathbf{q}} e^{-q^2}\left[L_N(q^2/2)\right]^2 V(q) e^{i\mathbf{q}\cdot(\mathbf{R}_i - \mathbf{R}_j)}$ $V_{\rm eff}(r)$

Graphene

$H_g = \sum_{i<j}\sum_{\mathbf{q}} e^{-q^2}\left[F_n(q)\right]^2 V(q) e^{i\mathbf{q}\cdot(\mathbf{R}_i - \mathbf{R}_j)}$ "Mixture" of the nth and n-1th Landau levels of the standard 2D

$F_{n\neq 0}(q) = \frac{1}{2}\left[L_n\left(\frac{q^2}{2}\right) + L_{n-1}\left(\frac{q^2}{2}\right)\right]$

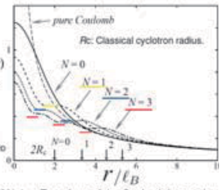


$V(q)$ : Transform of the Coulomb interaction

$\mathbf{R}_i$ : Guiding center coordinate of the $i$th electron

$L_N(x)$ : Laguerre polynomials

The eigenfunction of $n$th Landau level of graphene ($n \neq 0$) $\Psi_{Kn} = \frac{1}{\sqrt{2}}\begin{pmatrix} \mathrm{sgn}(n)\phi_{|n|-1} \\ \phi_{|n|} \end{pmatrix}$

The two effective interactions ($H_s$, $H_g$) are different. What happens to the ground state ?

## Motivation

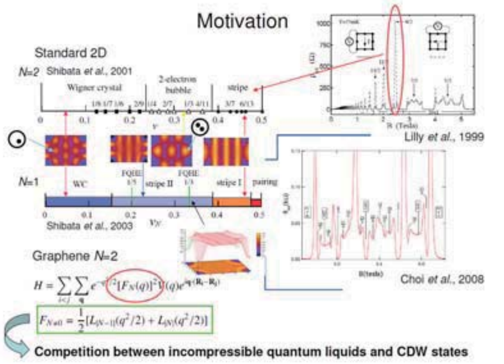


Graphene $N$=2

$H = \sum_{i<j}\sum_{\mathbf{q}} e^{-q^2}\left[F_N(q)\right]^2 V(q) e^{i\mathbf{q}\cdot(\mathbf{R}_i - \mathbf{R}_j)}$

$F_{N\neq 0} = \frac{1}{2}\left[L_{|N|-1}(q^2/2) + L_{|N|}(q^2/2)\right]$

**Competition between incompressible quantum liquids and CDW states**

## Purpose

Previous works

- Hatree-Fock theory (C.-H.Zhang *et al*, PRB 75, 245414 (2007))
  - Charge density waves (CDW) called stripes and bubbles realize in the ground state in high Landau levels of graphene.
  - But, quantum fluctuations are neglected in HF theory.
  - Can the CDW ground states survive under quantum fluctuations?
- Exact diagonalization (ED) (H.Wang *et al*, PRL 100, 116802 (2008))
  - The system size treated by ED is quite small.
  - The filling factor studied is limited.

Because of these limitations, such studies cannot determine the phase diagram of the present system.

**In the present study, we investigate the ground state of graphene in the Landau levels of $N$=2 at various filling factors by the use of the DMRG method, and determine the ground state phase diagram.**

## Model

Periodic boundary condition is imposed both in the x and y directions the period being $L_x$ and $L_y$, respectively. (Torus geometry)

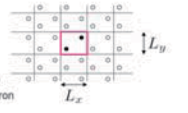


Approximations

- assume spin-polarized ground state
- assume valley-polarized ground state
- neglect Landau level mixing

Relevant energy scales

LL Separation between 0th and 1th Landau level: $\sqrt{2}\hbar v_F/\ell_B \simeq 400\sqrt{B[T]}[K]$

Typical Coulomb energy between electrons: $e^2/\epsilon l_B \simeq 100\sqrt{B[T]}[K]$

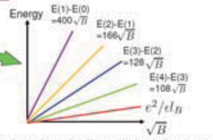


**Solve the inter-electron interaction Hamiltonian for spin and valley-polarized electrons at various filling factors in the $N$=2 Landau level of graphene.**

filling factor : $\nu = 2\pi N_e/L_x L_y = N_e/N_\phi$ $N_\phi$ : Total number of flux quanta in

## DMRG method for quantum 2D electron systems in a high magnetic field

The DMRG method was originally developed for { 1D lattice models. short range interactions.

Map to a 1D model (N. Shibata *et al.* Phys. Rev. Lett. 86, 5755 (2001))

One-particle states of free electrons in 2D under perpendicular magnetic field : $\Psi_{NX}(x, y)$, $X_n = 2\pi\ell^2 n/L_y$

Two quantum numbers { $N$ : Landau level index, $Xn$ : Guiding center ($n$ : integer)

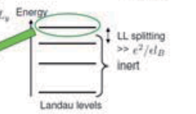


The ground state is determined only by the electrons in top most Landau level.

We can omit the Landau level index, $N$.

The quantum number is only $Xn$, which is a discrete number.

1D lattice model !

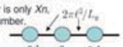


$H = \sum_{n_1}\sum_{n_2}\sum_{n_3}\sum_{n_4} A_{n_1 n_2 n_3 n_4} c^\dagger_{n_1} c^\dagger_{n_2} c_{n_3} c_{n_4}$

[redacted]

$1 \le n_1, n_2, n_3, n_4 \le N_s$ Long-ranged hopping !!

## Ground state phase diagram of $N$=2 Landau level of graphene

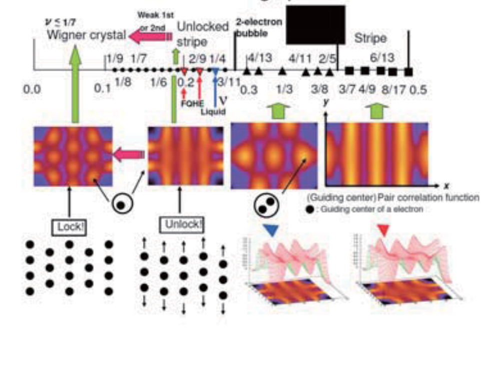


## Ground state at low fillings

$g(\mathbf{r}) = \frac{L_x L_y}{N_e(N_e-1)}\left\langle \Psi \left| \sum_{i\neq j}\delta(\mathbf{r} + \mathbf{R}_i - \mathbf{R}_j)\right| \Psi \right\rangle$

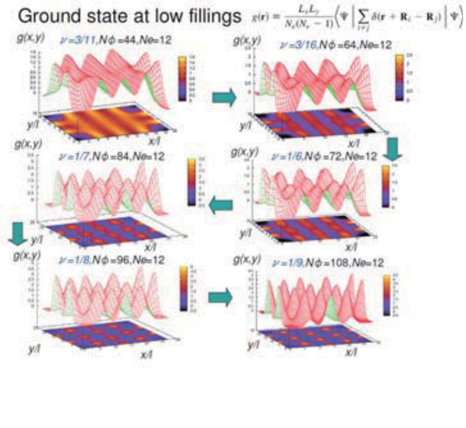


## Ground state at low fillings

$g(\mathbf{r}) = \frac{L_x L_y}{N_e(N_e-1)}\left\langle \Psi \left| \sum_{i\neq j}\delta(\mathbf{r} + \mathbf{R}_i - \mathbf{R}_j)\right| \Psi \right\rangle$

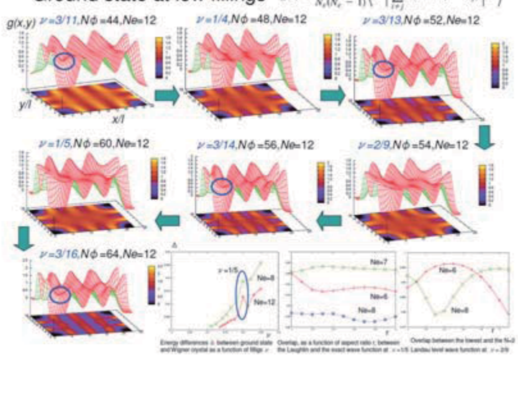


## Comparison with the result of the HF theory

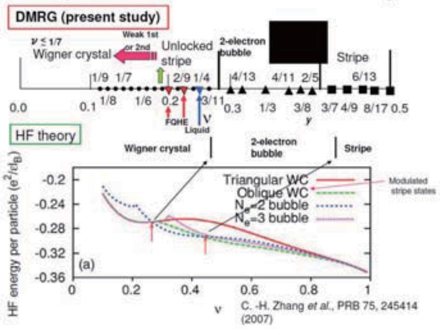


## Comparison with standard 2D systems

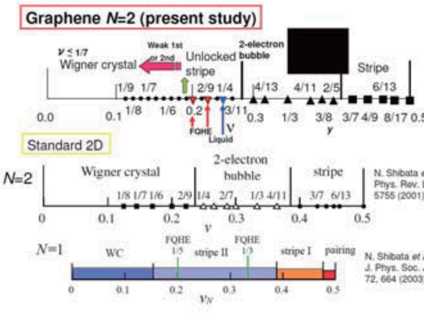


## Summary

- By the use of DMRG method, we determined the ground state of electrons at various fillings of the $N$=2 Landau level of graphene.
- By analyzing the (guiding center) pair correlation function, we obtained the reliable ground state phase diagram.
- Possibility of realizing a unlocked stripe phase
- Possibility of realizing a liquid ground state at $\nu$=1/4
- Possibility of realizing a incompressible quantum liquid state at $\nu$=1/5 and 2/9

# Study of $B^0 \to DK^{*0}(892)$ following by $D \to K^+\pi^-$ at Belle

## 1. Motivation

Lagrangian of charged current weak interaction

$$\mathcal{L}_{int} = -\frac{g}{\sqrt{2}}(\bar{U}_L \gamma_\mu V_{CKM} D_L W_\mu^+) + h.c.$$

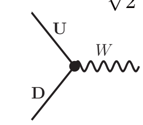


U = (u, c, t)
D = (d, s, b)
$U_L$, $D_L$ : Left handed

CKM(Cabbibo-Kobayashi-Masukawa) matrix

$$V_{CKM} = \begin{pmatrix} V_{ud} & V_{us} & V_{ub} \\ V_{cd} & V_{cs} & V_{cb} \\ V_{td} & V_{ts} & V_{tb} \end{pmatrix}$$

Unitary condition

$$V_{CKM}V_{CKM}^\dagger = 1 \xrightarrow{\text{1 row, 3 column elements}} V_{ud}V_{ub}^* + V_{cd}V_{cb}^* + V_{td}V_{tb}^* = 0$$

Unitary triangle

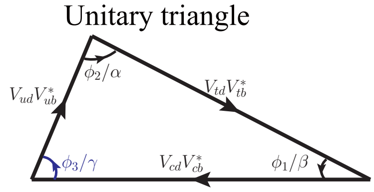


$$\phi_1 = (21.15^{+0.90}_{-0.88})^\circ$$
$$\phi_2 = (89.0^{+4.4}_{-4.2})^\circ$$
$$\phi_3 = (68^{+13}_{-14})^\circ$$

Unitarity triangle is described on complex plane, and represents CP-violation.
To understand CP-violation, the angles of this triangle should be measured precisely.
In the present limits, measurement accuracy of $\phi_3$ is not so good.
Need to study more for $\phi_3$.

## 2. Belle


KEK@Tukuba

- KEKB-factory is a B facility.
- High energy electrons and positrons collide, and annihilate in pairs.
  →The pair annihilation produces a great deal of energy, and B particles are generated from the energy.
- There is the data of 1014 fb$^{-1}$ which is the largest in the world.
  →Good environment for B physics.

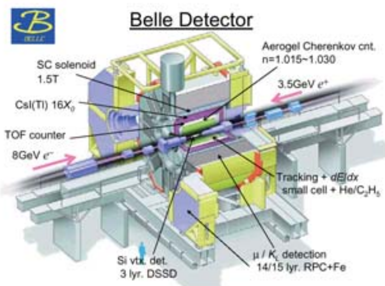


- Belle detector is to search the decays of B particles.
- Belle detector consists of many sub-detectors, and determines the particle type, momentum, charge, and so on.

## 3. Analysis

$$\phi_3 \equiv \arg\left(\frac{V_{ud}V_{ub}^*}{-V_{cd}V_{cb}^*}\right) \sim -\arg(V_{ub})$$

$\phi_3$ is measured with the decay include $b \to u$ transition.
e.c. $B^\pm \to D^{(*)}K^\pm$
Influence of CP violation is expected to appear due to the interference between the two amplitudes of $\bar{D}^0$ and $D^0$ decays into a common final state.

Decay $B^\pm \to DK^\pm$

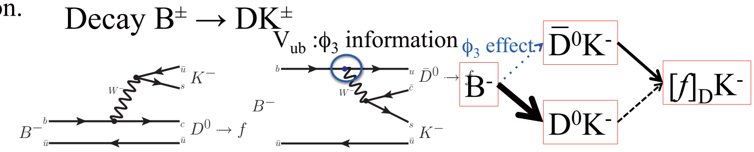


Neutral B Decay $B^0 \to DK^{*0}$

1. More effect of $\phi_3$
2. Less signal events → Large backgrounds

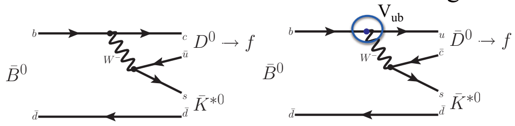


Where, I define $f = K^-\pi^+$.

$$R_{DK^*} \cong \frac{\Gamma(B^0 \to [K^+\pi^-]_D K^{*0}) + \Gamma(\bar{B}^0 \to [K^-\pi^+]_D \bar{K}^{*0})}{\Gamma(B^0 \to [K^-\pi^+]_D K^{*0}) + \Gamma(\bar{B}^0 \to [K^+\pi^-]_D \bar{K}^{*0})}$$
$$= r_S^2 + r_D^2 + 2kr_Sr_D\cos(\delta_S + \delta_D)\cos\phi_3$$

Suppressed mode (numerator)
Favored mode (denominator)

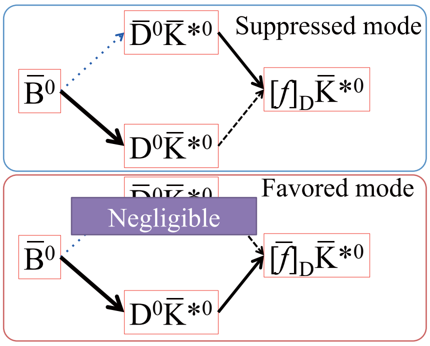


### Background Subtraction

Common used parameter
1. Event topology
2. $\cos\theta_B$

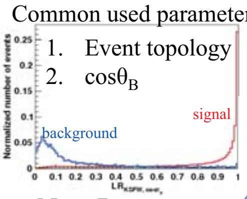


New 7 parameters

More background suppression power

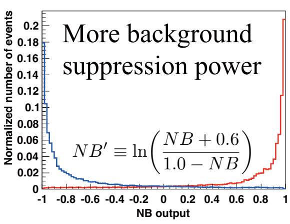


Multivariate analysis is performed using nine variables. In order to optimize an acceptance and rejection, we use the NeuroBayes neural net package.

Since NB has a too peaky distribution to be fitted with simple analytic functions it is transformed to NB' to obtain a smoothed Gaussian like distribution.

### Fit Result

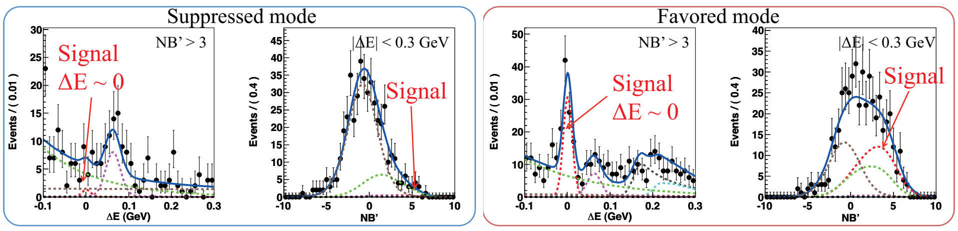


I perform 2D fit for ΔE and NB'.
In suppressed mode, there is no signal.

## 4. Summary & Plan

I obtain $R_{DK^*}$ upper limit.

$$R_{DK^*} = (4.1^{+5.6+2.8}_{-5.0-1.8}) \times 10^{-2}$$
$$< 0.16$$

I update $R_{DK^*}$ upper limit world record.
I'm writing the paper about this result.

Plan

- $B^0 \to [K_S\pi\pi]_D K^{*0}$ Dalitz plot analysis. $\phi_3$ can be extracted with $r_S$, $\delta_S$.
- I try to study about Belle vertex detector.

# Study of light hypernuclei with the Stochastic Variational Method

Y. Nakagawa (Physics, Tohoku Univ.)

Light neutron-rich nuclei ⇔ neutron halo structure of $^6$He, $^{11}$Li  I. Tanihata, J. Phys. G22, 157 (1996)

Λ hypernuclei ⇔ Core shrinkage of $^7_\Lambda$Li  E. Hiyama et al. , PRC59, 2351 (1999) K. Tanida et al. , PRL86, 1982 (2001)

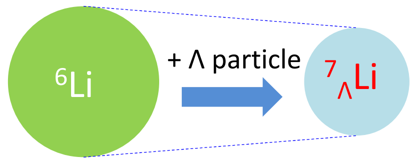


Neutron-rich Λ hypernuclei

✓Halo structure of nucleon＋Λ particle ?

✓Structure of core nucleus ?

## ✓Production of neutron-rich hypernuclei

- $^{10}_\Lambda$Li from KEK experiment  P. K. Saha et al., PRL 94, 052502 (2005)
- $^6_\Lambda$H from FINUDA experiment  M. Agnello et al., PRL 108, 042501 (2012)
- J-PARC experiment  H. Tamura, IJMPA 24, 2101 (2009)

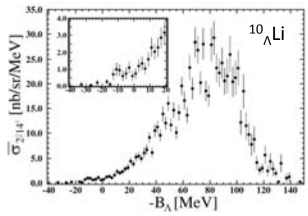


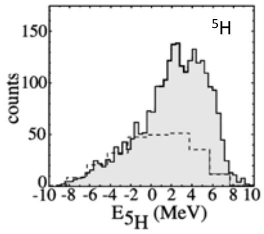


## ✓Resonance state of super heavy hydrogen $^5$H（ N/Z = 4）

(Experiment) A. A. Korsheninnikov et al., PRL 87, 092501 (2001)

E=1.7±0.3 MeV, Γ=1.9±0.4 MeV

(Theory) t+n+n cluster model + Complex Scaling Method  K. Arai, PRC 68, 034303 (2003)

½⁺ state ➔ (L,S) = (0,1/2), (1,1/2), (1,3/2), (2,3/2)

E=1.59MeV, Γ=2.48MeV

## ✓ΛN-ΣN coupling

- s-shell hypernuclei

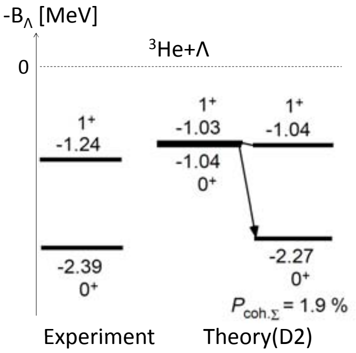


Y. Akaishi et al., PRL 84, 3539 (2000)

- n-rich hypernuclei

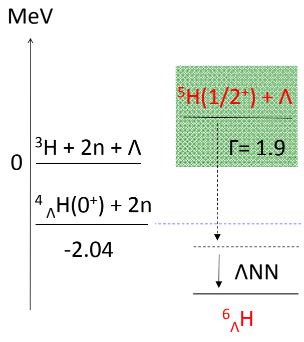


Kin Swe Myint, Y. Akaishi, PTPS 126, 599 (2002)

## ✓Stochastic Variational Method

Y. Suzuki, K. Varga, LNP m54 (Springer, 1998) Y. Suzuki et al., Few Body Syst. 42, 33 (2008)

1. Different $\mathcal{N}$ sets of non-linear variational parameter are generated randomly.
2. By solving the $\mathcal{N}$ eigenvalue problems, the corresponding energies are determined.
3. The parameter set producing the lowest energy is selected for $\mathcal{K}$th parameter set.
4. Increase $\mathcal{K}$ to $\mathcal{K}$+1.
5. Return to 1.

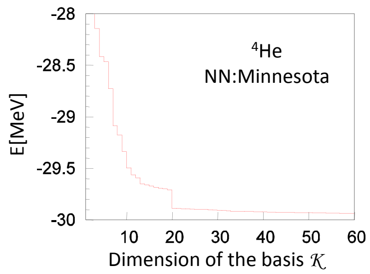


## ✓Variational trial function

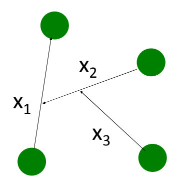


$$\Psi_{JM_JTM_T} = \sum_{k=1}^{\mathcal{K}} c_k \psi_k \qquad \psi_k = \mathcal{A}\left(\left[\phi_L^{space}\phi_S^{spin}\right]_{JM_J}\phi_{TM_T}^{isospin}\right)$$

$$\phi_{LM}^{space} = \exp\left(-\frac{1}{2}\sum_{i,j}^{A-1} A_{ij}\mathbf{x}_i\cdot\mathbf{x}_j\right)\theta_{LM}(\mathbf{x}) \qquad \phi_{SM_S}^{spin} = |[\cdots[[\frac{1}{2},\frac{1}{2}]_{S_{12}},\frac{1}{2}]_{S_{123}},\cdots]_{SM_S}\rangle$$

$$\theta_{LM}(\mathbf{x}) = [\mathcal{Y}_{L_1}(\mathbf{v}_1)\mathcal{Y}_{L_2}(\mathbf{v}_2)]_{LM} \qquad \mathcal{Y}_{LM}(\mathbf{r}) \equiv r^l Y_{LM}(\hat{r}) \qquad \mathbf{v} = \sum_{i=1}^{A-1} u_i\mathbf{x}_i$$

$\mathcal{A}$ : Antisymmetrizer

$c_k$ : Linear variational parameters

$A_{ij}, u_i$ : Non-linear parameters

## ✓Application for s-shell hypernuclei

- Interaction NN ➔ Minnesota, ΛN ➔ Minnesota type

D. R. Thompson et al., NPA 286, 53 (1977)  H. Nemura et al., PTP 103, 929 (2000)

| [MeV] | $^3_\Lambda$H | $^4_\Lambda$H(0⁺) | $^4_\Lambda$H(1⁺) | $^4_\Lambda$He(0⁺) | $^4_\Lambda$He(1⁺) | $^5_\Lambda$He |
|---|---|---|---|---|---|---|
| $B_\Lambda$(cal.) | 0.18 | 2.22 | 1.05 | 2.19 | 1.05 | 4.88 |
| $B_\Lambda$(exp.) | 0.13 | 2.04 | 1.04 | 2.39 | 1.15 | 3.12 |

u=1.5 in $V_{\Lambda N}$

- Parameter "u" dependence in ΛN interaction

$$V = \left(V_R + \frac{1}{2}(1+P_\sigma)V_t + \frac{1}{2}(1-P_\sigma)V_s\right)\left(\frac{u}{2} + \frac{2-u}{2}P_r\right)$$

| u | $^3_\Lambda$H | $^4_\Lambda$H(0⁺) | $^4_\Lambda$H(1⁺) | $^4_\Lambda$He(0⁺) | $^4_\Lambda$He(1⁺) |
|---|---|---|---|---|---|
| 1.5 | 0.18 | 2.22 | 1.05 | 2.19 | 1.05 |
| 2 | 0.20 | 2.28 | 1.14 | 2.24 | 1.12 |
| 2.5 | 0.22 | 2.37 | 1.22 | 2.35 | 1.19 |
| (exp.) | 0.13 | 2.04 | 1.04 | 2.39 | 1.15 |

$E_{cal}(^2H)$=-2.20MeV

$E_{cal}(^3H)$=-8.38MeV

$E_{cal}(^3He)$=-7.71MeV

$E_{cal}(^4He)$=-29.94MeV

PO no. 20

The 4th GCOE International Symposium

# Statics & Dynamics of Wormlike Micellar Systems

Masatoshi Toda
Physics, D3, Tohoku University

February 21, 2012

## Wormlike Micelle ?

Surfactant

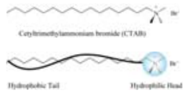


Familiar Example

Hand Soap

Cryo-TEM

T. Shikata *et al.* (1988).

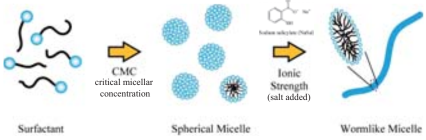


## Linear Viscoelasticity

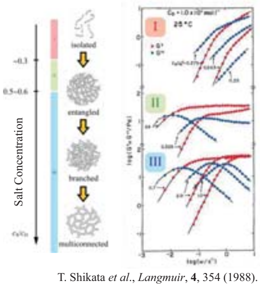


T. Shikata *et al.*, *Langmuir*, **4**, 354 (1988).

Strain ($\gamma_0 \ll 1$)
$\gamma(t) = \mathrm{Re}(\gamma_0 e^{i\omega t})$
Stress
$\sigma_{xy}(t) = \mathrm{Re}(\sigma_0 e^{i\omega t})$
$\sigma_0 = G^*(\omega)\gamma_0$
$G^*(\omega) = G'(\omega) + iG''(\omega)$
Elastic Viscous

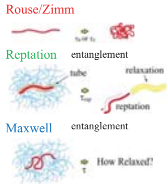


## Nonlinear Viscoelasticity

Simple Shear Flow

Viscosity
$$\eta^+(t,\dot\gamma) = \frac{\sigma_{xy}(t,\dot\gamma)}{\dot\gamma}$$
Shear Stress
Shear Rate

Startup Flow

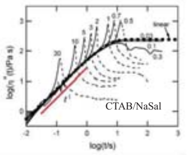


T. Inoue *et al.*, *Langmuir*, **21**, 1201 (2005).
Overshoot & Strain Hardening

Steady Shear Flow ($t = \infty$)

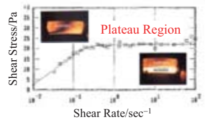


H. Rehage & H. Hoffmann, *Mol. Phys.*, **74**, 933 (1991).
Shear Banding
Shear-Induced Phase Separation

## Purpose of This Study

Micelles ➡ 
Particle
Solvent ➡ Navier-Stokes Eq.
Field
Particle-Field Hybrid Model

Drastic Reduction of Computational Complexity

Few Material Parameters
- Two Elastic Moduli
- Spontaneous Curvature

Helfrich Model

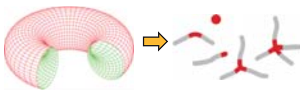

Coarse-Graining of Micellar Energy

Statics and Dynamics of Micellar Systems
Microscopic Origin

## Particle-Field Hybrid Model

Micellar Component

$$\frac{d\mathbf{r}_i}{dt} = \mathbf{v}(\mathbf{r}_i) - \frac{\partial H(\{\mathbf{r}_j\})}{\partial \mathbf{r}_i} + \boldsymbol{\xi}_i$$

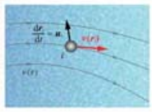

Solvent Component (Incompressible Linearized Navier-Stokes Eq.)

$$\frac{\partial \mathbf{v}}{\partial t} = -\nabla p + \nu\nabla^2\mathbf{v} - \sum_{i=1}^{N}\frac{\partial H(\{\mathbf{r}_j\})}{\partial \mathbf{r}_i}\delta(\mathbf{r}-\mathbf{r}_i) + \boldsymbol{\theta}$$

Fluctuation-Dissipation Theorem

$$\langle\boldsymbol{\theta}(\mathbf{r},t)\boldsymbol{\theta}(\mathbf{r}',t')\rangle = -2\nu T\nabla^2\delta(\mathbf{r}-\mathbf{r}')\delta(t-t')\mathbf{1}$$
$$\langle\boldsymbol{\xi}_i(t)\boldsymbol{\xi}_j(t')\rangle = 2T\delta_{ij}\delta(t-t')\mathbf{1}$$

Y. Oono & K. F. Freed, *J. Chem. Phys.*, **75**, 1009 (1981).

## Coarse-Graining of Micellar Energy

Helfrich Elastic Energy

$$H_{\mathrm{Bending}} = \int d\mathbf{a}\left[2\kappa(c_{\mathrm{m}}(\mathbf{a}) - c_0)^2 + \bar\kappa c_{\mathrm{G}}(\mathbf{a})\right] = H_{\mathrm{m}} + H_{\mathrm{G}}$$

W. Helfrich, *Z. Naturforsch.*, **28c**, 693 (1973).

$c_{\mathrm{m}} = \frac{1}{2}\left(\frac{1}{r_{\min}} + \frac{1}{r_{\max}}\right)$ Mean Curvature

$c_{\mathrm{G}} = \frac{1}{r_{\min}r_{\max}}$ Gaussian Curvature


Three Material Parameters

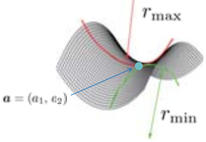


## Mean Curvature Term

$$H_{\mathrm{m}} = \int d\mathbf{a}\, 2\kappa(c_{\mathrm{m}}(\mathbf{a}) - c_0)^2$$

Perfect Torus

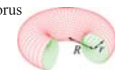

(1) Discretization

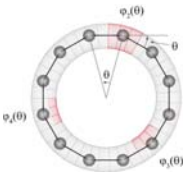

(2) Reconstruction

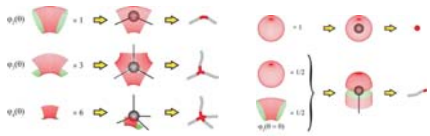

## Gaussian Curvature Term

$n_{\mathrm{c}}$ : # of Disconnected Parts
$n_{\mathrm{h}}$ : # of Holes, *i.e.*, Handles
$\chi$ : Euler characteristics

$$H_{\mathrm{G}} = \int d\mathbf{a}\, \bar\kappa c_{\mathrm{G}}(\mathbf{a}) = 4\pi\bar\kappa(n_{\mathrm{c}} - n_{\mathrm{h}}) = 2\pi\bar\kappa\chi$$

Topological Invariance

Elementary processes (Assumption)

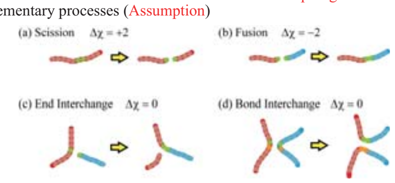


M. Cates, *Macromolecules*, **20**, 2289 (1987).

## Phase Diagram

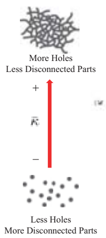


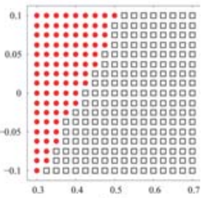

Example of Gel

From Wikipedia

● Gel Solid-Like
□ Sol Fluid-Like

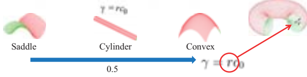


## Internal Structures

Initial State

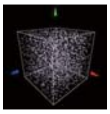

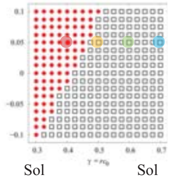

Cryo-TEM

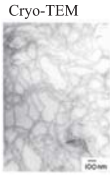

T. Shikata *et al.* (1988).

Gel Sol Sol Sol

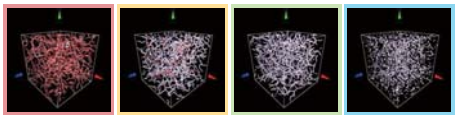

## Topology of Networks

Euler Characteristics

$$\chi = 2(n_{\mathrm{c}} - n_{\mathrm{h}})$$

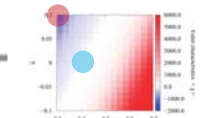

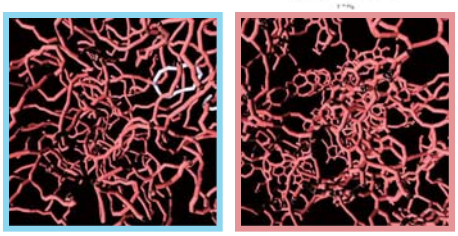

## Comparison with Experiment

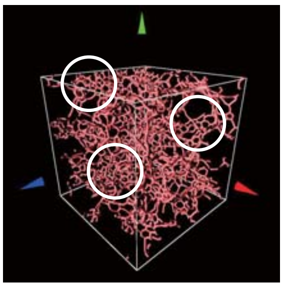

Many Holes
Embedded in Network

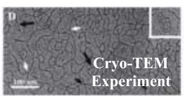


A. Bernheim-Groswasser *et al.*, *J. Phys. Chem. B*, **104**, 12192 (2000).

Material Parameters
$(\kappa, \bar\kappa, c_0)$
⬍
Real Systems

## Startup Flow

Simple Shear Flow

Shear Viscosity
$$\eta^+(t,\dot\gamma) = \frac{\sigma_{xy}(t,\dot\gamma)}{\dot\gamma}$$

Stress Tensor
$$\overleftrightarrow{\sigma} = -\frac{1}{V}\sum_{i=1}^{N}\mathbf{r}_i\mathbf{F}_i$$

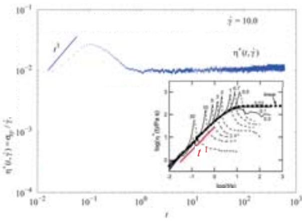

Stress Overshoot Observed

## Origin of Overshoot

Time Evolution of Branch Fraction

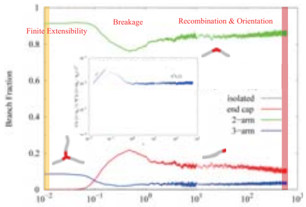


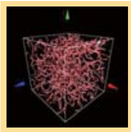

Gel Phase

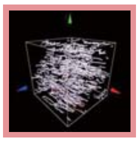

String Phase

Mechanism Different from That of Polymeric Systems

## Conclusions

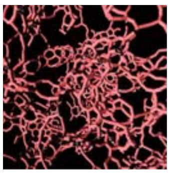

Wormlike Micellar Systems

1. Statics

   $(\kappa, \bar\kappa, c_0)$ ➡ Several Morphology (Sol/Gel)
   Material Parameters

2. Dynamics

   Overshoot ➡ Mechanism Different from That of Polymer

# Boundary state analysis on the equivalence of T-duality and Nahm transformation in superstring theory


Y.Teshima

In collaboration with T. Asakawa , S. Watamura and U. Carow-Watamura



arXiv:1201.0125v2 [hep-th]


## Introduction

### String theory

A theory which regard elementary objects as a string

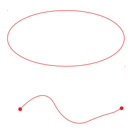

closed string
→ graviton $g_{\mu\nu}$

open string
→ gauge field $A_\mu$

**String theory is a candidate of quantum gravity**
but defined only perturbatively
→ **we want to find the stringy geometry**
(cf. general relativity ◄► Riemannian geometry)
→ This must encode the property of **T-duality**

### T-duality

Spectrum of the closed string

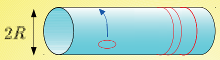


Compact momentum $n$ winding number $w$

$$m^2 = \frac{n^2}{R^2} + \frac{w^2 R^2}{\alpha'^2} + \frac{2}{\alpha'}(N + \tilde{N} - 2)$$

$$\downarrow \quad R \to \tilde{R} = \frac{\alpha'}{R}$$

$$m^2 = \frac{w^2}{\tilde{R}^2} + \frac{n^2 \tilde{R}^2}{\alpha'^2} + \frac{2}{\alpha'}(N + \tilde{N} - 2)$$

Compact Momentum $w$ winding numger $n$

The theory with radius $R$
= The theory with radius $\tilde{R}$
→ **T-duality**

### D-brane

the hypersurface where open strings end.

The direction along the D-brane
→ Neumann condition

The direction perpendicular to the D-brane
→ Dirichlet condition

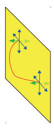

p dimensional D-brane = Dp-brane

The effective theory on N D-branes
= $U(N)$ gauge theory

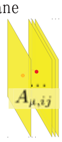


### T-duality and D-brane

Dirichlet and Neumann condition are exchanged under the T-duality

→ { T-dual normal to the D-brane $\mathrm{D}p \to \mathrm{D}(p+1)$
T-dual along the D-brane $\mathrm{D}p \to \mathrm{D}(p-1)$ }

### Bound state of D-branes

Bound state of the D-branes
Correspond to a soliton solution in the effective theory
※ Topological charge
= the number of D-branes

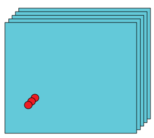

### Various approaches to disscuss T-duality

Buscher rule
Nahm transformation
Boundary state analysis
Hori formula

→ We analyzed the compatibility among them.

## Nahm transformation

### Original Nahm transformation

$U(N)$ Gauge theory $k$ instanton on $T^4$ ⟶ $U(k)$ Gauge theory $N$ instanton on $\tilde{T}^4$

D-brane interpretation

$N\, D4 \,/\, k\, D0$ ⟶ $k\, D4 \,/\, N\, D0$

Consistent with T-duality

### Generalization of Nahm transformation to 2d

We consider the classical solution on $T^2$
=constant magnetic flux

$$U(N)\,,\, C_1 = \int \mathrm{tr}\,\frac{F}{2\pi} = k$$

$$\Longrightarrow A_1 = 0\,,\quad A_2 = \frac{k}{2\pi N R_1 R_2} x_1\,,\quad F_{12} = \frac{k}{2\pi N R_1 R_2}$$

There is a freedom to add constants $\tilde{x}_1, \tilde{x}_2$

$$\to A_1 = \tilde{x}_1\,,\quad A_2 = \frac{k}{2\pi N R_1 R_2} x_1 + \tilde{x}_2$$

$$\tilde{x}_\mu \sim \tilde{x}_\mu + 1/R_\mu$$

$\Longrightarrow$ $\tilde{x}_\mu$ is the coordinate on $\tilde{T}^2$

We will construct the gauge field on $\tilde{T}^2$ by Dirac zero mode ( $\bar{\mathcal{D}}_{\tilde{x}}\psi = 0$ ).

$\bar{\mathcal{D}}_{\tilde{x}}$:The Dirac operator on $T^2 \times \tilde{T}^2$

$$\mathcal{D}_{\tilde{x}} = \gamma^\mu D_{\tilde{x}\mu} = \begin{pmatrix} 0 & \mathcal{D}_{\tilde{x}} \\ \bar{\mathcal{D}}_{\tilde{x}} & 0 \end{pmatrix},\quad \begin{aligned} \mathcal{D}_{\tilde{x}} &= -i(\partial_1 - iA_1 - i\tilde{x}_1) - (\partial_2 - iA_2 - i\tilde{x}_2)\,, \\ \bar{\mathcal{D}}_{\tilde{x}} &= -i(\partial_1 - iA_1 - i\tilde{x}_1) + (\partial_2 - iA_2 - i\tilde{x}_2) \end{aligned}$$

$\bar{\mathcal{D}}_{\tilde{x}}\psi = 0$ has $k$ solutions

→ construct $N \times k$ matrix

$$\to \psi = \underbrace{\left(\psi_1 \cdots \psi_k\right)}_{k}\Big\}\, N$$

The gauge field on $\tilde{T}^2$ is

$$\tilde{A}_\mu(\tilde{x}) = i \int_{T^2} d^2x\, \psi^\dagger \tilde{\partial}_\mu \psi$$

$$\longrightarrow \tilde{A}_1 = 0\,,\quad \tilde{A}_2 = -\frac{N}{2\pi k \tilde{R}_1 \tilde{R}_2}\tilde{x}_2\,,\quad \tilde{F}_{12} = -\frac{N}{2\pi k \tilde{R}_1 \tilde{R}_2}$$

$$\to U(k)\,,\, C_1 = -N$$

**Atiyah-Singer family index theorem**

$$\int_{T^2} \mathrm{ch}(\mathcal{P})\,\mathrm{ch}(E) = \mathrm{ch}(\tilde{E})$$

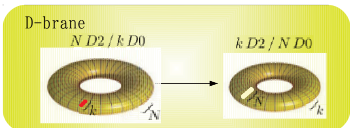


↕ ?

Nahm transformation:
$N\, D2 \,/\, k\, D0 \;\to\; k\, D2 \,/\, N\, \overline{D0}$

## Boundary state on the torus

### Boundary state

partition function of cylinder

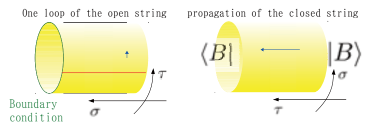


The initial, final state of the closed string associated with
the boundary condition of the open string
‖
D-brane

ex) In case of Dirichlet condition

$$\left.\frac{\partial X^i}{\partial \tau}\right|_{\sigma=0} = 0 \;\longleftrightarrow\; \left.\frac{\partial X^i}{\partial \sigma}\right|_{\tau=0} |B\rangle = 0$$

Calculate the boundary state with the flux associated with $(U(N), C_1 = k)$ on $T^2$

$$|B_F\rangle = \sqrt{(a_1 a_2 N)^2 + k^2}\sum_{\nu\in\mathbb{Z}^2} e^{-i\pi \mathbf{m}^1\mathbf{m}^2 \frac{k}{N}} \times\left[\prod_{n=1}^\infty \exp\left\{-\frac{1}{n}\frac{1}{a_1^2 a_2^2 N^2 + k^2}(\alpha_n^{1\dagger}\alpha_n^{2\dagger})\begin{pmatrix} a_1^2 a_2^2 N^2 - k^2 & 2a_1 a_2 N k \\ -2a_1 a_2 N k & a_1^2 a_2^2 N^2 - k^2 \end{pmatrix}\begin{pmatrix}\tilde{\alpha}_n^{1\dagger} \\ \tilde{\alpha}_n^{2\dagger}\end{pmatrix}\right\}\right] \times \left|\begin{pmatrix} -k\nu_2 \\ k\nu_1 \end{pmatrix}, \begin{pmatrix} N\nu_1 \\ N\nu_2 \end{pmatrix}\right\rangle$$

T-dual transformation
$$\begin{cases} \mathbf{m}^M \longleftrightarrow \mathbf{n}^M \\ \alpha_n^M \longrightarrow \alpha_n^M \\ \tilde{\alpha}_n^M \longrightarrow -\tilde{\alpha}_n^M \end{cases}$$

$$|B_F\rangle_{12} = \sqrt{N^2 + (\tilde{a}_1\tilde{a}_2 k)^2}\sum_{\nu\in\mathbb{Z}^2} e^{-i\pi N k \nu^1 \nu^2} \times\left[\prod_{n=1}^\infty \exp\left\{-\frac{1}{n}\frac{1}{\tilde{a}_1^2 \tilde{a}_2^2 k^2 + N^2}(\alpha_n^{1\dagger}\alpha_n^{2\dagger})\begin{pmatrix} \tilde{a}_1^2 \tilde{a}_2^2 k^2 - N^2 & -2\tilde{a}_1\tilde{a}_2 N k \\ 2\tilde{a}_1\tilde{a}_2 N k & \tilde{a}_1^2 \tilde{a}_2^2 k^2 - N^2 \end{pmatrix}\begin{pmatrix}\tilde{\alpha}_n^{1\dagger} \\ \tilde{\alpha}_n^{2\dagger}\end{pmatrix}\right\}\right] \times \left|\begin{pmatrix} N\nu_2 \\ -N\nu_1 \end{pmatrix}, \begin{pmatrix} k\nu_1 \\ k\nu_2 \end{pmatrix}\right\rangle$$

$$\to U(k)\,,\, C_1 = -N$$

Consistent with the 2d Nahm transformation

## Fermionic Part

NS-NS sector $(\psi_r, \tilde{\psi}_r)$ $\left(r \in \mathbb{Z} + \frac{1}{2}\right)$

R-R sector $(\psi_n, \tilde{\psi}_n)$ $(n \in \mathbb{Z})$

We consider the R-R zeromodes.
(Other modes contribute to the boundary state in the same way to the bosonic sector.)

The state

$$|Dp\rangle = \theta_p^\dagger \theta_{p-1}^\dagger \cdots \theta_0^\dagger \,|[C]\rangle \qquad \theta^\mu = \left(\psi_0^\mu + i\tilde{\psi}_0^\mu\right)/\sqrt{2},\quad \{\theta^\mu, \theta_\nu^\dagger\} = \delta_\mu^\nu$$

$|[C]\rangle$:the vacuum state

satisfies the boundary condition for a Dp brane.

$$\begin{aligned} \theta_\alpha^\dagger\,|Dp\rangle &= 0, \quad (\alpha = 0, \cdots, p)\,, \\ \theta_i\,|Dp\rangle &= 0, \quad (i = p+1, \cdots, 9) \end{aligned}$$

Then the D2/D0 bound state is

$$\begin{aligned} |D2D0\rangle &= N e^{2\pi\alpha' F_{12}\theta^1\theta^2}\,|D2\rangle \\ &= N(1 + F_{12}\theta^1\theta^2)\,|D2\rangle \\ &= N\,|D2\rangle + k\,|D0\rangle \end{aligned}$$

T-duality transformation is represented by an operator:

$$\mathcal{T}_\alpha = \theta^\alpha - \theta^{\alpha\dagger}$$

Then the T-duality of $|D2D0\rangle$ is

$$|D2D0\rangle' = \mathcal{T}_2\mathcal{T}_1\,|D2D0\rangle = k\,|D2\rangle - N\,|D0\rangle$$
$$(N, k) \to (k, -N)$$

RR-charges of D-branes are measured by the coupling to closed-string states of RR-potentials.

RR-state can be defined as

$$\langle \mathcal{A}| = \langle [C]|\,\mathcal{A} = \langle [C]| \sum A_{\mu_1\cdots\mu_q}\theta^{\mu_1\cdots\mu_q}$$

And the T-duality transformation is

$$\begin{aligned} \langle \mathcal{A}|\,\mathcal{T}_1^\dagger\mathcal{T}_2^\dagger &= \langle [C]| \left(\mathcal{A}^{(0)} + \mathcal{A}_1^{(1)}\theta^1 + \mathcal{A}_2^{(1)}\theta^2 + \mathcal{A}_{12}^{(2)}\theta^1\theta^2\right)\mathcal{T}_1^\dagger\mathcal{T}_2^\dagger \\ &= \langle [C]| \left(\mathcal{A}^{(0)}\theta^1\theta^2 - \mathcal{A}_1^{(1)}\theta^2 + \mathcal{A}_2^{(1)}\theta^1 + \mathcal{A}_{12}^{(2)}\right) \end{aligned}$$

Then the T-duality rule for the RR-potentials is

$$\mathcal{A}'^{(0)} = -\mathcal{A}_{12}^{(2)}\,,\quad \mathcal{A}_1'^{(1)} = \mathcal{A}_2^{(1)}\,,\quad \mathcal{A}_2'^{(1)} = -\mathcal{A}_1^{(1)}\,,\quad \mathcal{A}_{12}'^{(2)} = \mathcal{A}^{(0)}$$

The coupling of RR-potentials to D-brane is

$$I_{CS} = \langle \mathcal{A}|\,[GSO]c_0\tilde{c}_0\,|\mathcal{B}\rangle\,.$$

$[GSO]$:GSO projection
$|\mathcal{B}\rangle$ :full boundary state
$c_0, \tilde{c}_0$ :ghost

We can prove that $I_{CS}$ is invariant under T-duality:

$$\begin{aligned} I_{CS} &= \langle \mathcal{A}|\,[GSO]\mathcal{T}^\dagger\mathcal{T}c_0\tilde{c}_0\,|\mathcal{B}\rangle \quad (1 = \mathcal{T}^\dagger\mathcal{T}\,,\ \mathcal{T} = \mathcal{T}_2\mathcal{T}_1) \\ &= \langle \mathcal{A}|\,\mathcal{T}^\dagger[GSO]c_0\tilde{c}_0\mathcal{T}\,|\mathcal{B}\rangle \quad (\text{Since } \mathcal{T} \text{ commutes with } [GSO].) \\ &= \langle \mathcal{A}'|\,[GSO]c_0\tilde{c}_0\,|\mathcal{B}'\rangle \end{aligned}$$

$I_{CS}$ is invariant under T-duality transformation.

### Hori formula

$I_{CS}$ can be written in terms of differential forms as

$$\begin{aligned} I_{CS} &= \mu_2 \int_M \mathcal{A} \wedge \mathrm{Tr}_N\left(e^{2\pi\alpha' F}\right) \\ &= \mu_2 \int_M \left(\mathcal{A}^{(0)} + \ldots + \mathcal{A}_{12}^{(2)}dx^1 \wedge dx^2\right)\left(N + k\,dx^1 \wedge dx^2\right) \\ &= N\mu_2 \int_M \mathcal{A}_{12}^{(2)}dx^1 \wedge dx^2 + k\mu_0 \int_{\mathbb{R}} \mathcal{A}^{(0)} \end{aligned}$$

In terms of differential forms,
T-duality is represented by Hori formula:

$$A' = -\int_{T^2} A e^{dx^i \wedge dy_i}$$

By using this, the Chern-Simons term is transformed as

$$\begin{aligned} &\mu_2 \int_{\tilde{M}} \mathcal{A}' \wedge \mathrm{Tr}_k\left(e^{2\pi\alpha'\tilde{F}}\right) \qquad (\tilde{M} = \mathbb{R} \times \tilde{T}^2) \\ &= \mu_2 \int_{\tilde{M}} \left(\mathcal{A}'^{(0)} + \cdots + \mathcal{A}_{12}'^{(2)}dy^1 \wedge dy^2\right)\left(k - N\,dy^1 \wedge dy^2\right) \\ &= N\mu_2 \int_{\tilde{M}} \mathcal{A}_{12}^{(2)}dy^1 \wedge dy^2 + k\mu_0 \int_{\mathbb{R}} \mathcal{A}^{(0)} \end{aligned}$$

→ invariant under T-duality

## Summary and discussion

- Nahm transformation was extended naively to 2d.
- It consistent with T-duality in string theory.
$(N, k) \to (k, -N)$
∫T2da
- It indicates $\mathbb{Z}_4$-duality nature of T-duality
cf. Fourier transformation $(x, p) \to (p, -x) \to (-x, -p)$
- we introduced the T-duality operator which act both on the boundary state and the RR q-form state.
- We clarified the relationship between T-duality rule at the superstring level and that at the low energy effective theory

# Description of single-Λ hypernuclei with relativistic point coupling model

Department of Physics, Nuclear Theory group
Yusuke Tanimura

## Hypernuclear physics

Normal nuclei consist of protons and neutrons.
Nuclei containing baryons with strangeness (hyperons) are called hypernuclei

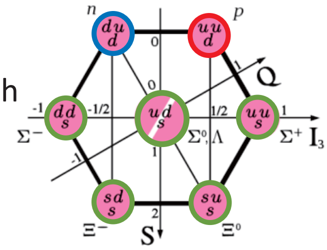


Λ particle may change properties of normal nuclei (*impurity effect*) such as

- Shape and radius
- Cluster structure
- Collective excitations
- …

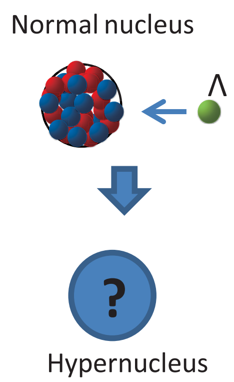


Response of nuclei to an addition of a Λ
→Structure information which cannot be seen with normal probes

## Relativistic mean field (RMF) calculations for hypernuclei

NN and NΛ interactions are described as meson exchanges

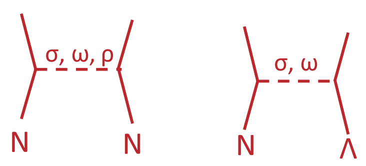


No relativistic 3-D mesh calculation has been realized because of "variational collapse",
Y. Zhang, et al, Int. J. Mod. Phys. E**19** 55 (2010)
K. Hagino and Y. T., PRC**82**, 057301 (2010)

→RMF is not developed as much as non-relativistic mean field calc., in which 3-D calculations are performed using zero range interactions.

→Relativistic zero range NΛ interaction may be useful in future relativistic calculation for hypernuclei

## Model Lagrangian

We have proposed a new nucleon-Λ interaction:

Relativistic point coupling (RPC) model

$$\mathcal{L}^{N\Lambda}_{\rm int} = \mathcal{L}^{N\Lambda}_{\rm 4f} + \mathcal{L}^{N\Lambda}_{\rm der} + \mathcal{L}^{N\Lambda}_{\rm ten}$$

$$\mathcal{L}^{N\Lambda}_{\rm 4f} = -\alpha_S^{(N\Lambda)}(\bar\psi_N\psi_N)(\bar\psi_\Lambda\psi_\Lambda) - \alpha_V^{(N\Lambda)}(\bar\psi_N\gamma_\mu\psi_N)(\bar\psi_\Lambda\gamma^\mu\psi_\Lambda)$$

$$\mathcal{L}^{N\Lambda}_{\rm der} = -\delta_S^{(N\Lambda)}(\partial_\mu\bar\psi_N\psi_N)(\partial^\mu\bar\psi_\Lambda\psi_\Lambda) - \delta_V^{(N\Lambda)}(\partial_\mu\bar\psi_N\gamma_\nu\psi_N)(\partial^\mu\bar\psi_\Lambda\gamma^\nu\psi_\Lambda)$$

$$\mathcal{L}^{N\Lambda}_{\rm ten} = -\alpha_T^{(N\Lambda)}(\bar\psi_\Lambda\sigma^{\mu\nu}\psi_\Lambda)(\partial_\mu\bar\psi_N\gamma_\nu\psi_N)$$

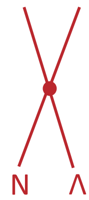


- An extension of RPC for NN interaction (Buervenich et al., PRC65, 044308('02))
- Finite range meson exchange is simulated by contact couplings between the fermions
- Zero range is numerically easy to handle

## Results

5 parameters are fitted to the experimental data of Λ binding energies of
$^{16}_{\Lambda}$O, $^{40}_{\Lambda}$Ca, $^{51}_{\Lambda}$V, $^{89}_{\Lambda}$Y, $^{138}_{\Lambda}$La, $^{208}_{\Lambda}$Pb.

Comparison between theoretical and experimental Λ binding energies
(Y. T. and K. Hagino, Phys. Rev. C**85**, 014306 (2012))

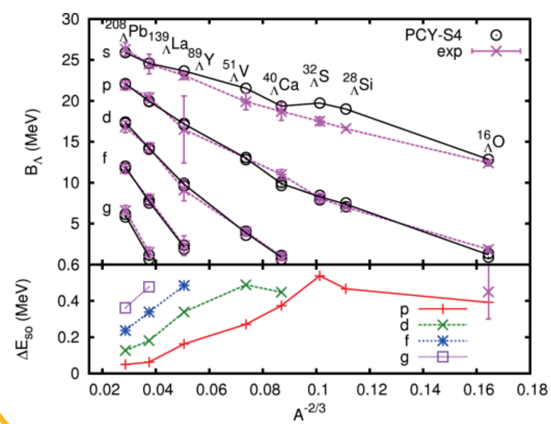


- Well reproduces the experimental data ($\chi^2_{\rm dof} = 0.92$)
- Suitable for 3D calculations or beyond-mean-field methods because of its numerical simplicity

# "Study of $B^{\pm}\to DK^{\pm}$, $D\to K_SK^{\pm}\pi^{\mp}$ for the measurement of CP-violating angle $\phi_3$, and $D^{*\pm}\to D\pi^{\pm}$, $D\to K_SK^{\pm}\pi^{\mp}$ for the modeling of $D\to K_SK^{\pm}\pi^{\mp}$ Dalitz plane

## 1.Motivation & Theory

CKM (Cabibbo-Kobayashi-Maskawa) Matrix

$$V = \begin{pmatrix} V_{ud} & V_{us} & V_{ub} \\ V_{cd} & V_{cs} & V_{cb} \\ V_{td} & V_{ts} & V_{tb} \end{pmatrix} = \begin{pmatrix} 1-\frac{\lambda^2}{2} & \lambda & A\lambda^3(\rho - i\eta) \\ -\lambda & 1-\frac{\lambda^2}{2} & A\lambda^2 \\ A\lambda^3(1-\rho-i\eta) & -A\lambda^2 & 1 \end{pmatrix} + \mathcal{O}(\lambda^4)$$

Complex terms

$\lambda = \sin\theta_c \sim 0.22$

Unitarity $VV^{\dagger} = 1$

Unitarity triangle

$V_{ud}V_{ub}^* + V_{cd}V_{cb}^* + V_{td}V_{tb}^* = 0$

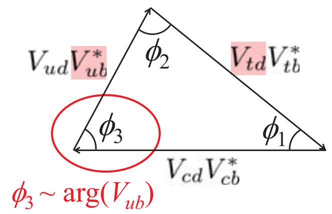


Unitarity triangle is described on complex plane, and represents CP-violation. To understand CP-violation, the angles of this triangle should be measured precisely.

Present limits for each angle

$\phi_1 = 21.15^\circ\ ^{+0.90^\circ}_{-0.88^\circ}$

$\phi_2 = 89.0^\circ\ ^{+4.4^\circ}_{-4.2^\circ}$

$\phi_3 = 68^\circ\ ^{+13^\circ}_{-14^\circ}$

The measurement accuracy of $\phi_3$ is not so good, and should be improved.

$\phi_3$ can be measured by examining the asymmetry between $B^-\to DK^-$ and $B^+\to DK^+$ decays. Among the various $B^{\pm}$ decays, $B^{\pm}$ meson which decays to neutral $D$ meson ($D^0$ or $\bar{D}^0$) and $K^{\pm}$ meson is used for $\phi_3$ measurement.

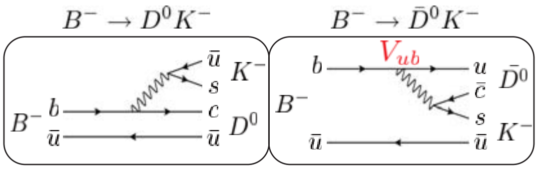


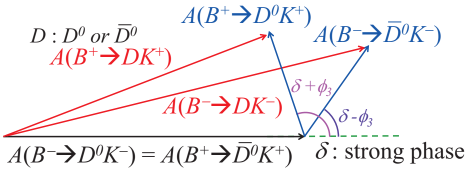


$D^0$ and $\bar{D}^0$ can decay to the same final states. Therefore $B^-\to D^0K^-$ and $B^-\to \bar{D}^0K^-$ decay amplitudes interfere each other. The interfering between $D^0$ and $\bar{D}^0$ is used to measure $\phi_3$.

## 2.Facility

### KEKB-factory & Belle Detector


KEK@Tukuba

- KEKB-factory is a facility to make $B$ particles.
- High energy electrons and positrons collide, and annihilate in pairs.
- From the pair annihilation, heavy $B$ mesons are generated.

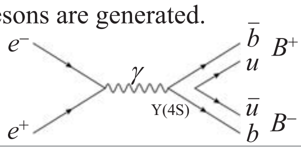


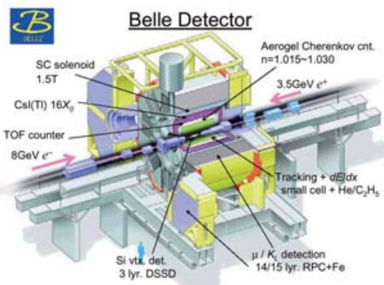


- Belle detector is to search the decays of $B$ particles.
- Belle detector consists of many sub-detectors, and determines the particle type, momentum, charge, and so on.
- The mother particles are reconstructed from detected particles.
- We have recorded the world largest data of 1014 $fb^{-1}$.

## 3.Analysis

- Neutral $D$ particles decay to various particles. In this study, $D\to[K_S K^{\pm}\pi^{\mp}]$ decay is searched.
- There are 2 modes in $D\to K_S K^{\pm}\pi^{\mp}$ decays : $D^0\to K_S K^-\pi^+$ , $D^0\to K_S K^+\pi^-$ and their charge conjugate mode, beause both $D^0$ and $\bar{D}^0$ can decay into $K_S K^-\pi^+$ and $K_S K^+\pi^-$.
- $D$ decays into $K_S K \pi$ via many intermediate processes (e.g. $D\to[K_S\pi^+]_{K^{*+}} K^-$, $D\to[K^-\pi^+]_{K^{*0}} K_S$ , … etc.).
- These processes should be separated because strong phases differ. The Dalitz plot analysis is needed.
- $D^0\to K_S K^-\pi^+$ cannot be distinguished from $\bar{D}^0\to K_S K^-\pi^+$ in $B^{\pm}\to DK^{\pm}$, however, the information of each Dalitz plene is needed to fit $B^{\pm}\to DK^{\pm}$, $D\to K_S K^{\pm}\pi^{\mp}$ Dalitz plane.
- Therefore, $D^{*\pm}\to D\pi^{\pm}$, $D\to K_S K^{\pm}\pi^{\mp}$ decay which has large statistics and can be distinguished between $D^0$ and $\bar{D}^0$ using the charge of $D^{*\pm}$ is studied to model the Dalitz distribution of $D\to K_S K^{\pm}\pi^{\mp}$ decay.

### $D^{*\pm}\to D\pi^{\pm}$, $D\to K_S K^{\pm}\pi^{\mp}$ : Dalitz analysis

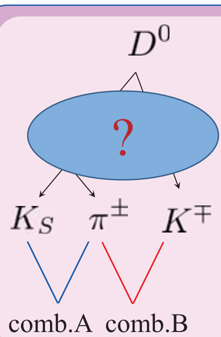


When $D$ decays into 2 particles, and one of them decays furthermore into 2 particles, the reconstructed mass of the correct pair combination yields a mass of a certain particle.

Therefore to verify intermediate states, the plot of combination A versus combination B is used. This is the so called Dalitz plot which is used to extract the value of $\phi_3$.

Dalitz Plot

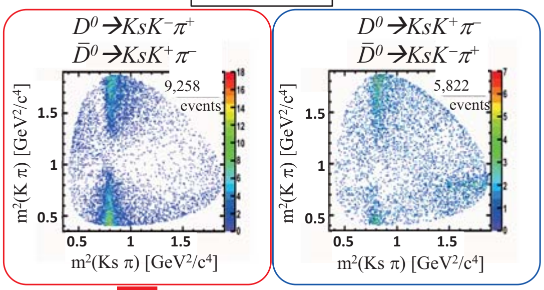


141 $fb^{-1}$

The Dalitz plot of B→DK is fitted using the fit result of these Dalitz plots.

2 dimensional fit

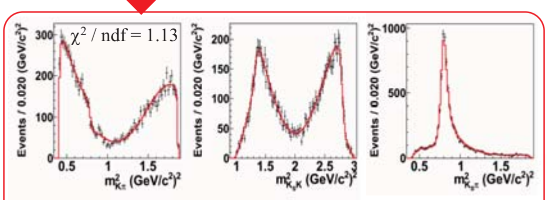


Black dots : data , Red line : fitted function

$D^0\to K_SK^-\pi^+$ and charge conjugate mode are fitted using 141 $fb^{-1}$ data sample. The another mode is being prepared to fit.

## 4.Summary and Plan

- The precise measurement for $\phi_3$ is important in terms of verification for CP-violation.
- $B\to DK$ decay is used for the measurement of $\phi_3$.
- Among the various $D$ decays, we use $D\to K_SK^{\pm}\pi^{\mp}$ with Dalitz plot.
- To make the model of $D\to K_SK^{\pm}\pi^{\mp}$ decay, $D^{*\pm}\to D\pi^{\pm}$, $D\to K_SK^{\pm}\pi^{\mp}$ is analyzing. $D^0\to K_SK^-\pi^+$ have been fitted.
- Of course, the final purpose is the measurement of $\phi_3$ using $B^{\pm}\to DK^{\pm}$, $D\to K_SK^{\pm}\pi^{\mp}$.

# New geometric interpretation of D-branes and DBI action


Particle Theory and Cosmology Group, Department of Physics

Shuhei Sasa (D1)

In collaboration with Tsuguhiko Asakawa, Satoshi Watamura.


## 1. Introduction

### Symmetries of string theory:

There are various symmetries in string theory. In this poster, we will focus mainly on diffeomorphisms, B-field gauge transformations and T-duality.

T-duality

- Simplest example: $S^1$ compactification

Radius of $S^1$ : $R \longrightarrow \frac{1}{R}$ (T-duality)

Kaluza-Klein mode (cotangent vector) ⟷ exchange ⟷ Winding mode (tangent vector)

- General background with U(1) isometry:
  for NS-NS flux: a metric g
  a Kalb-Ramond 2-form B (called B-field)
  a dilaton $\phi$

→ T-duality in these background is known as the Buscher rule.

What is a T-duality invariant formulation of SUGRA?
→ Candidate: Generalized Geometry

(There is another candidate; the doubled field theory which is locally same.)

## 2. Quick review of generalized geomtery

### A basic object of generalized geometry

Let M be a D-dimensional smooth manifold (for the target space).
The generalized tangent bundle over M,

$$\mathbb{T}M = TM \oplus T^*M$$

is endowed with

- a fiberwise symmetric non-degenerate bilinear form
$$\langle X+\xi, Y+\eta\rangle = \frac{1}{2}(\imath_X\eta + \imath_Y\xi) = \frac{1}{2}\begin{pmatrix}X^i\\ \xi^i\end{pmatrix}^T\begin{pmatrix}0 & 1\\ 1 & 0\end{pmatrix}\begin{pmatrix}Y^i\\ \eta^i\end{pmatrix}$$
- the Dorfman bracket
$$[X+\xi, Y+\eta] = [X,Y] + \mathcal{L}_X\eta - \imath_Y d\xi$$

for $X+\xi,\ \ Y+\eta\ \in \Gamma(TM\oplus T^*M)$ .
$\imath_X$ : a interior product by X

### Symmetries of the symmetric bilinear form $\langle,\rangle$

In particular, we will focus on two types of symmetries as follows:

- Diffeomorphisms:
  For a diffeomorphism $f: M\to M$,
  $$f_*\oplus f^{*-1}: TM\oplus T^*M \to TM\oplus T^*M$$
  is induced. This is called generalized pushforward
- B-transformations:
  For a 2-form $B\in\Omega^2(M)$,
  $$e^B: \mathbb{T}M\to\mathbb{T}M,\quad X+\xi\mapsto X+\xi+\imath_X B$$
  For an exact 2-form $B = dA\in\Omega^2_{ex}(M)$, this provides a B-field gauge transformation.

The symmetries of $\langle,\rangle$ form a O(D,D) symmetry group.
(There are still other transformations.)

### Generalized Geometry

- treats gauge transformations for a Kalb-Ramond 2-form B (called B-field) the same as diffeomorphisms.
- The infinitesimal generators of these transformations are
  - tangent vector fields for diffeomorphisms
  - differential 1-forms for B-field gauge transformations
  
  ➔ The sections of $TM\oplus T^*M$ act on itself.
- We define generalized Lie derivatives under these transformations as
$$\mathcal{L}_{X+\xi}(Y+\eta) = \mathcal{L}_X(Y+\eta) - \imath_Y d\xi$$
  ($\mathcal{L}_X(Y+\eta)$: Usual Lie derivative for a diffeomorphism; $\imath_Y d\xi$: Corresponding to a B-field gauge transformation)

### Generalized metric structure (target space)

- We define a generalized metric as a maximal positive-definite subbundle $C_+\subset\mathbb{T}M$ , i.e. for $^\forall a,b\in\Gamma(C_+)\setminus$ zero section,
$$\langle a,b\rangle > 0$$
and $C_+$ has the rank D.
Decompose : $\mathbb{T}M = C_+\oplus C_-$
$C_- = C_+^\perp$ is an orthogonal component of $C_+$ and has a negative-definite value for $\langle,\rangle$ .
- The structure group O(D,D) of $\mathbb{T}M$ is reduced to O(D)×O(D) by specifying the generalized metric $C_+$ .
- Since the intersection $TM\cap C_+ = \{0\}$ , we can describe the generalized metric as a graph of $E = g+B: TM\to T^*M$ :
$$V_+ = v^M(\partial_M + (g+B)_{MN}dx^N)\in\Gamma(C_+)$$

- Another definition of the generalized metric is an self-adjoint orthogonal endmorphism $G:\mathbb{T}M\to\mathbb{T}M$ such that
$$\langle a, Ga\rangle > 0 \quad \text{for } ^\forall a,b\in\Gamma(C_+)\setminus \text{zero section}$$
$$G^2 = G^TG = 1 \ \Longrightarrow\ \text{Eigenvalues : } G = \pm 1 \ \Longrightarrow\ C_\pm = \mathrm{Ker}(1\mp G)$$

The generalized metric $G$ is given by
$$G = \begin{pmatrix} -Bg^{-1} & g^{-1}\\ g-Bg^{-1}B & g^{-1}B\end{pmatrix}$$

Restriction of the Generalized metric to TM gives a modified Riemannian metric $g - Bg^{-1}B$ .

### Dilaton structure (target space)

We redefine a dilaton $\phi$ as a new O(d,d) invariant dilaton $d$ such that
$$e^{-2d} = e^{-2\phi}\sqrt{\det g}$$
Strictly speaking, the measure $e^{-2d}dx^0\wedge\cdots\wedge dx^{D-1}$ is O(d,d) invariant.

Then under T-duality,
$$\phi\to\phi - \frac{1}{2}\ln\det E_{ij}$$

## 3. D-brane in the framework of generalized geometry

### Dp-brane

- is defined as a (p+1)-dimensional hypersurface $S\subset M$ on which open strings can end. Zero modes of a open string living on the D-brane worldvolume $S$ include a gauge field $A_a$, (D-p) scalar fields $\Phi^i$ describing the transverse fluctuations and their superpartners.
- is topologically expressed by $(S,\varphi,V)$ for the condensed background fields $A_a$ and $\Phi^i$ .

  $\varphi: S\hookrightarrow M$ is a p-dimensional embedding of submanifold.
  $V\to M$ is a complex vector bundle with a connection $A_a$ (a so-called Chan-Paton bundle). The rank of $V$ equals the number of coincident D-branes.
  
  (We consider only Abelian gauge theory.)

### Questions:

1. Dirac-Born-Infeld (DBI) action gives the low-energy effective theory of a D-brane. It can be derived by calculating a partition function in string theory. However it is not obvious why DBI action appears.
2. By T-duality, the gauge field is replaced with the scalar field and vice versa. However geometrical meaning of these fields are different. Can we treat these fields alike in the framework of geometry?
3. The scalar fields appear as NG boson for broken translational symmetry. How about the gauge field?

### Embedding of a Dp-brane worldvolume and a static gauge

Let
$\sigma^\alpha$ : coordinates on a D-brane S $\quad(\alpha = 0,\cdots,p)$
$x^M = (x^a, x^i)$ : coordinates on a target space M
$(a = 0,\cdots,p,\quad i = p+1,\cdots,D)$

**Physical gauge**

Using a diffeomorphism on the D-brane worldvolume S, we choose a static gauge $\sigma^\alpha = x^a$ .

The coordinates on S : $(x^a, \Phi^i(x^a))$ — $\Phi^i(x^a)$: Transverse displacements of the D-brane

Embedding $\varphi: S\hookrightarrow M$ induce the pushforward $\varphi_*: TS\to TM$ ,
$$\varphi_*\left(v^\alpha(\sigma)\partial_\alpha^{(\sigma)}\right) = v^a(x^a,\Phi^i(x^a))(\partial_a^{(x)} + \partial_a\Phi^i\partial_i^{(x)})$$

These vector fields can be described by using a diffeomorphism of the target space M such that
$$e^\Phi: S_0\to S,\quad (x^a,0)\mapsto(x^a,\Phi^i(x^a))$$
and its pushforward
$$(e^\Phi)_*: TS_0\to TS$$
$$v^a(x^a,0)\partial_a\mapsto v^a(x^a,\Phi^i(x^a))(\partial_a + \partial_a\Phi^i\partial_i)$$

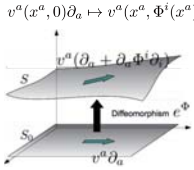


### A D-brane in the framework of generalized geometry

Dirac structure:
A subbundle $L\subset\mathbb{T}M = TM\oplus T^*M$ over a submanifold $S\subset M$ with the rank D such that

Isotropic: $L = L^\perp$ i.e. $\langle a,b\rangle = 0$ for $^\forall a,b\in\Gamma(L)$
Integrability: $[a,b]\in\Gamma(L)$

### Strategy for constructing DBI action

1. We choose a "standard" Dirac structure $L_0 = TS_0\oplus N^*S_0$ $\subset\mathbb{T}M$ over S given by sections of the form
$$V_0 = v^a(x^a,0)\partial_a + \xi_i(x^a,0)dx^i\in\Gamma(L_0)$$
2. We define a Dirac structure $L = e^F(e^\Phi)_*L_0\subset\mathbb{T}M$ where $F = dA$ is a two-form field strength.
$$V_L = v^a(x^a,\Phi^i(x^a))(\partial_a + \partial_a\Phi^i\partial_i + F_{ab}dx^b) + \xi_i(x^a,\Phi^i(x^a))(dx^i - \partial_a\Phi^i dx^a)\in\Gamma(L)$$
3. Generalized metric structure

   When viewed from the Dirac structure $L_0$ , since $L_0$ is isotropic and the intersection $L_0\cap C_+ = \{0\}$, the generalized metric can also be written as a graph of $t = s+a: L_0\to L_0^*$ ,
$$V_+ = v^a(\partial_a + t_a{}^j\partial_j + t_{ab}dx^b) + \xi_i(dx^i + t^i{}_b dx^b + t^{ij}\partial_j)\in\Gamma(C_+)$$
   We find the relation
$$t_{ab} = E_{ab} - E_{ai}E^{ij}E_{jb},\quad t_a{}^j = -E_{ak}E^{kj}$$
$$t^i{}_b = E^{ik}E_{kb},\quad t^{ij} = E^{ij}$$
   These relations are similar to the Buscher rule since T-duality exchanges vector fields and 1-forms.
   (But this is not T-duality.)

   Restriction of the generalized metric $G$ to $L$ gives a modified metric $s - (a+\mathcal{F})s^{-1}(a+\mathcal{F})$ .
   [ abbreviation: for example, D×D matrix $s = \begin{pmatrix} s_{ab} & s_a{}^j\\ s^i{}_b & s^{ij}\end{pmatrix}$ ]
   
   Here,
$$\mathcal{F} = \begin{pmatrix} F_{ab} & \partial_a\Phi^i\\ -\partial_a\Phi^i & 0\end{pmatrix}$$
   We have
$$\det{}^{\frac{1}{4}}(s - (a+\mathcal{F})s^{-1}(a+\mathcal{F}))_{MN} = \det{}^{-\frac{1}{4}}s_{MN}\ \det{}^{\frac{1}{2}}(s+a+\mathcal{F})_{MN}$$
4. Dilaton structure

   We can rewrite the dilaton structure in terms of the symmetric tensor $s_{MN}$.
$$e^{-d} = e^{-\phi}\det{}^{\frac{1}{4}}s_{MN}\ \det{}^{\frac{1}{2}}E_{ij}$$
5. DBI action

   Combining the result of 4 and 5 , we get
$$S_{\mathrm{DBI}} = \int_S e^{-\phi}\sqrt{\det E_{ij}}\sqrt{\det(s+a+\mathcal{F})_{MN}}dx^0\wedge\cdots\wedge dx^p$$
$$= \int_S e^{-\phi}\sqrt{\det(\varphi^*(g+B)+F)_{ab}}dx^0\wedge\cdots\wedge dx^p$$

## 4. Non-linear realization

### Non-linear realization

- Consider infinitesimal transformation with generators
$$\epsilon = \epsilon_\parallel + \epsilon_\perp = \epsilon^a\partial_a + \epsilon^i\partial_i$$
$$\Lambda = \Lambda_\parallel + \Lambda_\perp = \Lambda_a dx^a + \Lambda_i dx^i$$
- By computation of the generalized Lie derivative $\mathcal{L}_{\epsilon+\Lambda}V_+$ , we can read that

$$\delta t_{ab} = -\epsilon^c\partial_c t_{ab} - \partial_a\epsilon^c t_{cb} - t_{ac}\partial_b\epsilon^c - \partial_a\Lambda_i t^i{}_b - t_a{}^j\partial_b\Lambda_j + \partial_{[a}\Lambda_{b]}$$
$$\delta t_a{}^j = -\epsilon^c\partial_c t_a{}^j - \partial_a\epsilon^c t_c{}^j - \partial_a\Lambda_i t^{ij} + \partial_a\epsilon^j$$
$$\delta t^i{}_b = -\epsilon^c\partial_c t^i{}_b - t^i{}_c\partial_b\epsilon^c - t^{ij}\partial_b\Lambda_j - \partial_b\epsilon^i$$
$$\delta t^{ij} = -\epsilon^c\partial_c t^{ij}$$

$$\delta\Phi^i = \epsilon^i - \epsilon^a\partial_a\Phi^i$$
$$\delta A_a = \Lambda_a - \epsilon^b\partial_b A_a - \partial_a\epsilon^b A_b - \Phi^i\partial_a\Lambda_i$$

→ We need these terms for non-linear realization of broken symmetries.

Put x, y:
$$S_{\mathrm{DBI}} = \int_S e^{-2xd}\det{}^y\{s - (a+\mathcal{F})s^{-1}(a+\mathcal{F})\}_{MN}dx^0\wedge\cdots\wedge dx^p$$
$$= \int_S e^{-2x\phi}\det{}^{\frac{x}{2}-y}s_{MN}\det{}^x E_{ij}\det{}^{2y}(s+a+\mathcal{F})_{MN}dx^0\wedge\cdots\wedge dx^p$$

Diffeomorphism invariance: $\frac{x}{2} + y = \frac{1}{2}$
Vanishing $\det^{\frac{x}{2}-y}s_{MN}$ for non-linear realization: $\frac{x}{2} - y = 0$

We get $x = \frac{1}{2},\quad y = \frac{1}{4}$

P-15

# Electron microscopy and spectroscopy studies of organic molecules inside SWCNT

Md. Mahbubul Haque, Yohei Sato, Masami Terauchi, Tomonari Wakabayashi[A] , Kazu Suenaga[B]

Date: 2012-Feb-20

IMRAM, Tohoku University, Sendai, Japan
[A]Kinki University, Higashi Osaka , Japan
[B]Nanotube Research Center, AIST, Tsukuba, Japan

The 4th GCOE International Symposium on "Weaving Science Web beyond Particle-Matter Hierarchy" Feb 20-22, 2012

## Introduction

**What are polyynes?**

1. Polyynes are one-dimensional linear chain of C atoms having alternate single and triple bonds.
2. They are pure sp-hybridized molecules.
3. The terminals of polyynes may contain atoms or group of atoms
4. The simplest form of polyynes contain H atoms at both the terminals.
5. The general formula of simplest polyynes car be written as

**General formula**
$-(C\equiv C)_n-$

An example of polyyne molecule ($C_8H_2$)

**Basic properties**
-Unstable in air or even in liquid at high concentration
-Very stable inside SWCNT

**Why polyynes are interesting?**

At least three different aspects:

1. Physics: We can observe directly the physical properties of such usually rare one-dimensional material
2. Chemistry: Longer polyynes may be possible to obtain by connecting smaller polyynes hence their chemical properties can be observed.
3. Application: It is expected that polyynes could be the smallest semiconducting molecular nano-wire.

## Synthesis of polyynes

Polyynes can be found naturally as interstellar objects.
In laboratory, synthesis of polyynes can be carried out using several methods.

Laser ablation of graphite particle in n-hexane
(or other organic solvents)

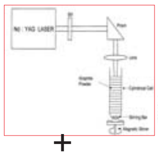


+

HPLC (High Performance Liquid Chromatography)
coupled with UV multichannel and VIS spectrometer

UV-vis absorption spectra of polyynes in n-hexane

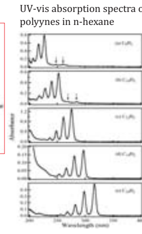


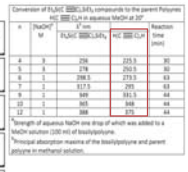

R. Eastmond, T.R. Johnson, D.R.M.Walton, Tetrahedron 28 (1972) 4601.

H. Tabata et al. Carbon 44, 3168-3176, 2006

## Synthesis of hybrid system (polyynes@SWCNT)

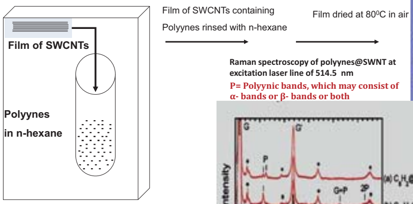


Air and Humidity free condition
80⁰C for 24 hrs

Raman spectroscopy of polyynes@SWNT at excitation laser line of 514.5 nm
P= Polyynic bands, which may consist of α- bands or β- bands or both

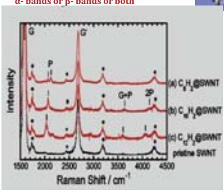


Nishide et al. J. Phys. Chem. C Vol. 111, No. 13, 2007

The encapsulation of polyynes inside SWCNT has been confirmed by Raman Spectroscopy because CC triple bond stretching phonon frequency is about 2000 cm⁻¹

## Our Motivation

We would like to carry out-

**Microscopic studies for polyynes@SWCNT to obtain-**
HRTEM images of polyyne to understand their encapsulation, distribution, orientation etc. inside SWCNT

And

**Spectroscopic studies -**
EELS (electron energy loss spectra) of polyyne@SWNT-
to understand their electronic properties.
We would like to compare EELS data with Raman excitation profile of polyynes trapped inside nanotube

Raman Excitation Profile of Polyynes@SWNT

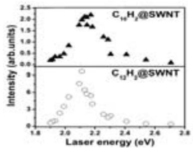


L. M. Malard et al. PRB 76, 233412, 2007

## Our Motivation...

Coronene Molecule

Intermolecular spacing is 3.5 ± 0.3 A⁰


Coronene Molecules inside SWCNT

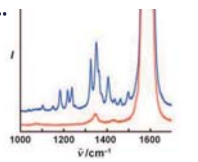


Toshiya Okazaki et al. Angew. Chem. Int. Ed. 2011, 50, 4853-4857

Raman spectra of coronenes@SWCNT (blue)
Raman spectra of SWCNT (red)

**We would like to get Electron diffraction and EELS of coronene@SWCNT in order to study structural and electronic properties of molecular coronenes inside SWCNT.**

## Experimental Condition

**Specimen ($C_{10}H_2$@SWCNT)is collected from T. Wakabayashi lab at Kinki University**

Before the experiments, specimen was heated up until 250 degree for 2 hours in vacuum.

**Instrument**
TEM equipped with monochromator

**HRTEM (Mono OFF)**
60kV at room Temperature
EXP.time: 5 sec
Detector: CCD camera
and negative films

**EELS (Mono ON)**
Accelerating voltage :60kV
at Room Temperature
Probe size: ~1.5 nmϕ
Beam current: 2pA
ΔE=~65meV
EXP.time: 18-28sec
Detector: Imaging Plate (IP)

## Instrument

**Monochromator TEM**
Electron source : FEG
Monochromator : Wien-filter
TEM colmun : JEM-2010FEF
Analyzer : Ω-filter
Detector : Imaging Plate

**Condition of EELS**
HT : 60kV
Probe size : 1.5nmϕ
Temperature : 100K (LiqN$_2$ holder)
ΔE : 61 meV-0.15 eV
Exp.time : 6s (Low-loss)
256 s (Core-loss)

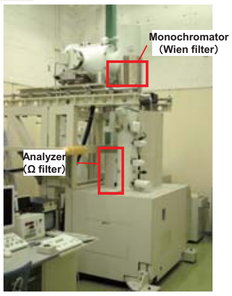


## Some of our results -of polyynes

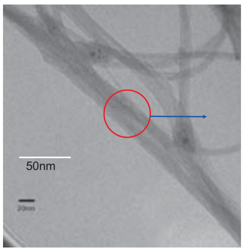


EELS Measurements of Bundles of SWCNTs

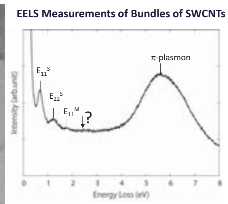


Existence of polyynes inside the bundle of SWCNTs is not clear from this EELS data

HRTEM images of polyynes inside SWCNT

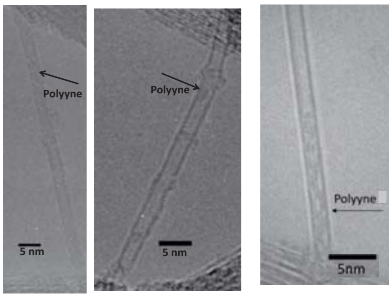


The region marked by arrows contains polyynes

## Kataura Plot

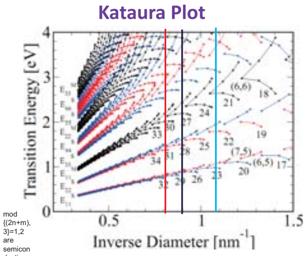


Fig. Downloaded from R. Saito Lab's website

The numbers on the Kataura plot refer to the family of carbon nanotubes which have the similar electronic properties

The black dots represent metallic while red and blue dots refer to semiconducting, type I and type II respectively, carbon nanotubes

**The vertical bars of three different colors on the plot are used here to assign $E_{ii}$ energies of three EELS measurents**

(1) EELS Measurements of Isolated SWCNT encapsulating Polyynes

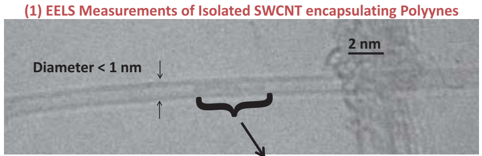


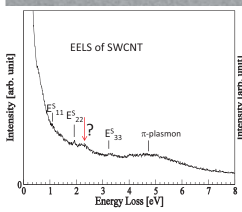


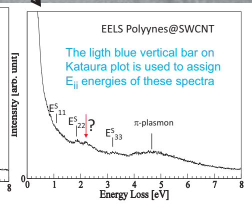


The ligth blue vertical bar on Kataura plot is used to assign $E_{ii}$ energies of these spectra

(2) EELS Measurements of Isolated SWCNT encapsulating Polyynes

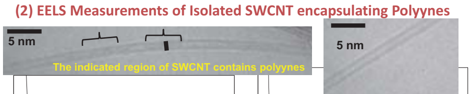


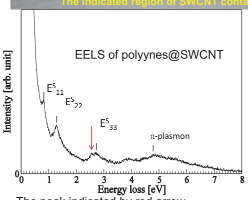


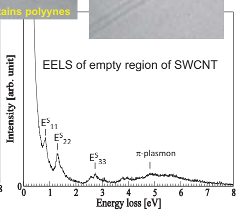


The peak indicated by red arrow should be due to polyynes.

The diameter of the nanotube is about 1.2 nm
The electron energy loss due to polyynes is ~2.55 eV

The dark blue vertical bar on Kataura plot is used to assign $E_{ii}$ energies of these spectra

(3) EELS Measurements of Isolated SWCNT encapsulating Polyynes

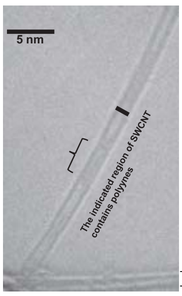


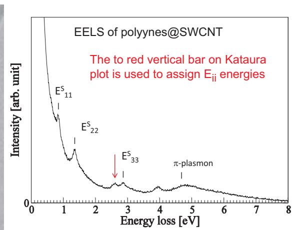


The to red vertical bar on Kataura plot is used to assign $E_{ii}$ energies

The peak indicated by red arrow should be due to polyynes.

The diameter of the nanotube is about 1.3 nm
The electron energy loss due to polyynes is ~2.62 eV

## Some of our results – ED of coronenes@SWCNTs

HRTEM image of bundle of SWCNTs containing coronenes

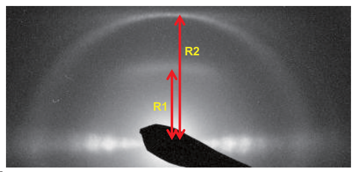


Intensity comes from 11$\bar{2}$0 graphitic plane of CNT
Intensity comes from 10$\bar{1}$0 graphitic plane of CNT
Intensity comes molecular planes of coronenes

Calculation of intermolecular spacing ($d_2$) of coronenes:
$d_2 = (R_1/R_2)\ d_1$ where d1 is the spacing between 10$\bar{1}$0 planes = 2.13 A⁰
$d_2$ = 3.2 A⁰

## Some of our results -EELS of coronenes@SWCNTs

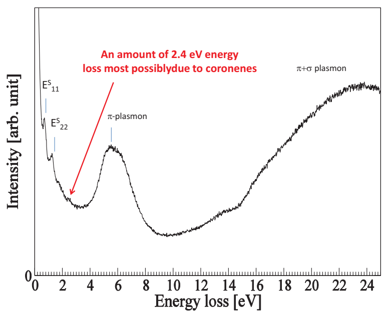


## Summary and Future Plan

- The encapsulation of polyynes by SWCNT has been confirmed by HRTEM images.
- The distribution of polyynes inside nanotube is not uniform.
- The orientation of polyynes seems bending inside large-diameter nanotube.
- The EELS measurements seems that the electron energy loss due to polyynes depends on diameter of nanotube.

| EELS measurement | Diameter of SWCNT in nm (appox.) | Electron loss energy of Polyynes (eV) |
|---|---|---|
| 1 | 0.9 | 2.3 |
| 2 | 1.1 | 2.55 |
| 3 | 1.2 | 2.62 |

- **The encapsulation of coronenes by SWCNT is confirmed by electron diffraction from bundle of SWCNT.**

*The 4th GCOE international symposium, Tohoku Univ. , 20-22/Feb/2012*

# Medium heavy Λ hyper nuclear spectroscopic experiment by the $(e,e'K^+)$ reaction

Graduate school of science, Tohoku University
Toshiyuki Gogami for HES-HKS collaboration

## 1.Introduction

Figure.1 : HES-HKS group photo in the experimental hall C in JLab (2009).

We have been performing Λ hypernuclear spectroscopic experiment by the $(e,e'K^+)$ reaction since 2000 at Thomas Jefferson National Accelerator Facility (JLab). The $(e,e'K^+)$ can achieve 100 keV (FWHM) energy resolution compared to a few MeV (FWHM) by the $(K^-,\pi^-)$ and $(\pi^+,K^+)$ experiments (Table.1). Therefore, more precise Λ hypernuclear structures can be investigated by the $(e,e'K^+)$ experiment. $^{7}_{\Lambda}He$, $^{9}_{\Lambda}Li$, $^{10}_{\Lambda}Be$, $^{12}_{\Lambda}B$, $^{28}_{\Lambda}Al$ and $^{52}_{\Lambda}V$ were measured in the experiment at JLab Hall C. In addition, $^{9}_{\Lambda}Li$, $^{12}_{\Lambda}B$, $^{16}_{\Lambda}N$ were measured in the experiment at JLab Hall A.

Table.1 : The features of $(e,e'K^+)$ reaction comparing to $(\pi^+,K^+)$ and $(K^-,\pi^-)$ reactions.

| | $(e,e'K^+)$ | $(\pi^+,K^+)$ | $(K^-,\pi^-)$ |
|---|---|---|---|
| Reaction | $e + p \to e + K^+ + \Lambda$ | $\pi^+ + n \to K^+ + \Lambda$ | $K^- + n \to \pi^- + \Lambda$ |
| Momentum transfer (Typical ) | ~300 [MeV/c] | ~300 [MeV/c] | ~100 [MeV/c] |
| | Λ can be bounded in deeper orbit | | |
| Λ's Spin At forward angle | flip ≈ non-flip<br>Spin dependent structure | non-flip | non-flip |
| Λ's from | proton<br>Mirror lambda hypernuclei | neutron | neutron |
| Beam | primary<br>High quality , high intensity | secondary | secondary |
| Target | Thin (~100 mg/cm²)<br>(Isotopically enriched) | Thick(> a few [g/cm²] ) | Thick(> a few [g/cm²] ) |
| Energy resolution (FWHM) | ≤ 500 [keV]<br>Fine structure | 1 – 3 [MeV] | 1 – 3 [MeV] |

## 2.Experimental Setup (JLab E05-115)

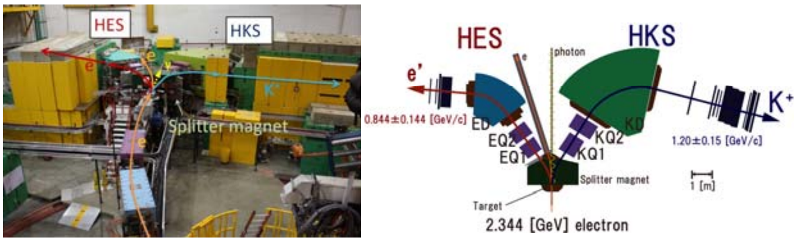


Figure.2 : The experimental setup of JLab E05-115 (2009)

Missing Mass : $M^2_{HY} = (E_e + M_T - E_{K+} - E_{e'})^2 - (\mathbf{p}_e - \mathbf{p}_{K+} - \mathbf{p}_{e'})^2$ ➡
- Λ binding energy
- Cross section

Measure with spectrometers

The $(e,e'K^+)$ experiment is a coincidence experiment between scattered electron and generated kaon. The cross section of $(e,e'K^+)$ are larger at forward scattered angles of these two particles. Therefore, both of these two particles need to be detected at forward angles at the same time. To do so, a dipole magnet (splitter magnet) was set just after the target to separate scattered electron and kaon into different directions.
Figure.1 shows the experimental setup of JLab E05-115. There are HES (High resolution Electron Spectrometer) and HKS (High resolution Kaon Spectrometer) to measure momenta of scattered electron and kaon associated with $(e,e'K^+)$ reaction, respectively. Both HES and HKS consist of QQD magnets.

| | HES | HKS |
|---|---|---|
| Δp/p | ~2 × $10^{-4}$ | ~2 × $10^{-4}$ |
| Momentum [GeV/c] | 0.844 ± 0.144 | 1.20± 0.15 |
| Angle [degree] | 3.0 – 9.0 | 1.0 – 13.0 |
| Beam energy [GeV] | 2.344 | |
| Target (Hypernuclei) | $^{7}Li$ , $^{9}Be$ , $^{10}B$ , $^{12}C$ , $^{52}Cr$ (,$CH_2$,$H_2O$) | ($^{7}_{\Lambda}He$, $^{9}_{\Lambda}Li$, $^{10}_{\Lambda}Be$, $^{12}_{\Lambda}B$, $^{52}_{\Lambda}V$) (,Λ,Λ) |

## 3.Particle identification

Figure.3 : Picture of HKS detector package

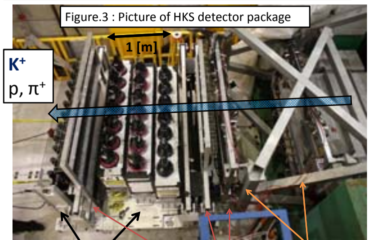


Cherenkov detectors -AC,WC-
- Aerogel (n=1.05)
- Water (n=1.33)

TOF walls -2X,1Y,1X- (Plastic scintillators)
TOF σ ≈ 170 [ps]

Drift chambers -KDC1,KDC2-
σ ≈ 250 [μm]

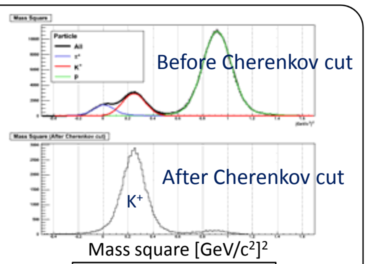


Figure.4 : Mass square distribution

**There is not only kaon in HKS but also proton and pion as background particles. To measure kaon efficiently, HKS has two drift chambers(KDC1,KDC2) for tracking, three scintillator walls(KTOF1X,1Y,2X) for TOF measurement and two type of Cherenkov detectors(WC1,WC2,AC1,AC2,AC3) for proton and pion rejection in the stages of trigger and offline analysis (Fig.3).**
**Figure.4 shows mass square distribution which can be calculated by the following equation :**

$$m^2 = p^2\left(\frac{1}{\beta^2} - 1\right)$$

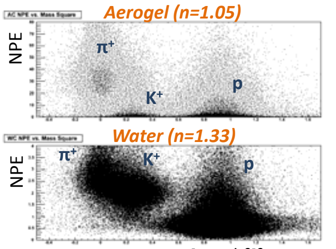


Figure.5 : NPE of Cherenkov detector vs. mass square

**where, $p$ is a momentum reconstructed by a transfer matrix of HKS, and $\beta$ (= $v/c$) is derived by TOF measurement. Figure.5 is showing NPE of Cherenkov detectors vs. mass square. We can distinguish pion, kaon and proton with mass square and Cherenkov detector information as you can see in the figure. When the Cherenkov and mass square cut are applied to survive ~90% kaon in the total event, <2% proton and <1% pion are contaminated in the kaon.**

## 4.New tracking code for high multiplicity data

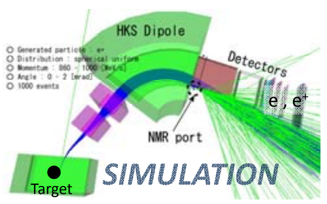


Figure.6 : Background simulation of HKS

It is getting harder to perform the $(e,e'K^+)$ experiment as the proton number of the target, $Z_{tar}$ is larger. This is because that the background events which are caused by electromagnetic processes roughly proportional to $Z^2_{tar}$. Mainly, the electron arm suffers from these backgrounds. However, the hadron arm (HKS) also suffers from them which are not on the HKS optics . A positron generated in the target by pair creation process hit the vacuum chamber which is just after the HKS dipole magnet, and generate background events such as positron and electron in the HKS detectors (Fig.6). These background events make the singles rate of HKS be higher ( ~30MHz/plane, 8μA beam on $^{52}Cr$ target).

We used two planar-type drift chambers which have 6-layers (uu'xx'vv') in each chamber for HKS tracking. Figure.7 shows the multiplicity of the typical layer of the drift cambers. The multiplicity for $^{52}Cr$ target (~5) is much higher than that for $CH_2$ target (~2) as you can see the figure. The conventional tracking code that we used in JLab hall C cannot handle high multiplicity data efficiently. Therefore, we lose events for high multiplicity data in the tracking stage. To deal with the high multiplicity data, a new tracking code need to be developed.

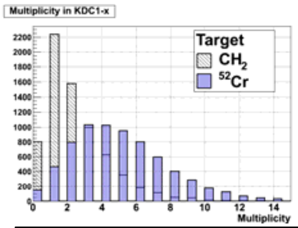


Figure.7 : Multiplicity of the typical layer of HKS drift chambers.

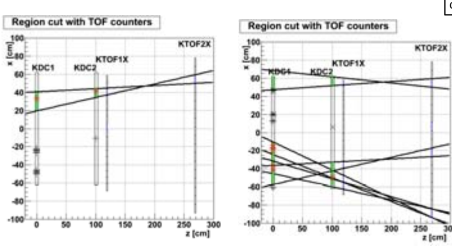


Figure.8 : Event display of the developed hit-wire selection for tracking. Blue squares represent hit TOF segments, green regions are selective regions determined by the TOF combinations, red markers are selected hit-wires for tracking and black markers are hit-wires which are not used for tracking.

A new event selection routine is developed and implemented to increase the tracking efficiency for the high multiplicity data. Before the pattern recognition which is in the first stage of the tracking, hit-wires to use for tracking are selected by the combination of the TOF detectors considering HKS optics (Fig.8).

After this development, the number of kaons is increased by ~130%, and also the analysis time is decreased by ~30% for $^{52}Cr$ target.

## 5.Energy scale calibration

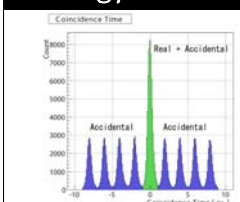


Figure.9 : Coincidence time between HES and HKS.

One of the large advantages of the $(e,e'K^+)$ reaction is that the absolute energy calibration can be done with data of Λ and $\Sigma^0$ converted from a proton target such as $CH_2$ and $H_2O$ target. We measure both positions and angles of electron and kaon at the reference planes. Then, those information are converted to momentum vectors at the target by transfer matrices to calculate the missing mass. Therefore, the tuning of the transfer matrices is a heart part to measure hypernuclei with better energy resolution.

**Figure.9 shows a coincidence time between HES and HKS after the kaon selection. It is calculated by the following equation :**

$$T_{coin} = T_{HES} - T_{HKS}$$

**where, $T_{HKS}$ and $T_{HES}$ are the times at the target which are simply calculated by path length from the focal planes to the target and β of the particles. In the figure, the beam structure of the CEBAF ( ~2ns bunch structure) can be seen, and a peak on the center is a bunch which includes real coincidence events.**

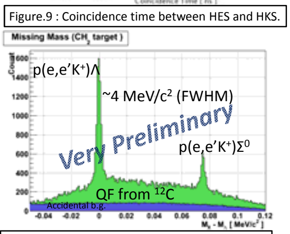


Figure.10 : Missing mass spectrum of $CH_2$ target

Figure.10 shows a missing mass spectrum of $CH_2$ target. When the real coincidence events are chosen, peaks of Λ and $\Sigma^0$ clearly can be seen on the Quasi-free Λ events which come from $^{12}C$ and accidental background events. These peaks are used for the energy scale calibration. Also, thick tungsten alloy sieve slits which are set just before the Q-magnet of each spectrometer are used for calibration of angular component.

## 6.Summary

- We performed the $(e,e'K^+)$ experiment at JLab Hall-C in 2009 (JLab E05-115), and successfully took data of $^{7}_{\Lambda}He$, $^{9}_{\Lambda}Li$, $^{10}_{\Lambda}Be$, $^{12}_{\Lambda}B$ and $^{52}_{\Lambda}V$.
- Kaon identification
  - When the cut applied to survive ~90%, <2% proton and <1% pion contaminate in the kaon.
- New tracking code for high multiplicity data ( $^{52}Cr$ , $H_2O$ target )
  - The number of kaon is increased by ~130%
  - The analysis time is decreased by ~30%
- Energy scale calibration is in progress.

# Coherent double pion photoproduction on the deuteron

C. Kimura   Department of Physics, Tohoku University

## Introduction

• **Double pion photoproduction**

• Investigation of double pion photoproduction from the deuteron is useful in understanding the interaction between photon and bound nucleon.

•Since the deuteron consists of loosely bounded two nuclei, the quasi-free process is considered to dominate the photo-absorption process.

•The impact approximation works well in the meson photoproduction process on the deuteron, that is, the photon interacts mainly with each nucleon in the deuteron (quasi-free process).

• **Non quasi-free process**

• In the previous study, the cross-section of the double pion photoproduction using NKS(ref.1).

• The reaction through the quasi-free process on the deuteron was found to be smaller than that on the proton. And double delta production was observed and the cross section was obtained (Fig. 1).

• These results suggested the contribution of the non quasi-free process is not small for the photoabsorption on the bound nucleon.

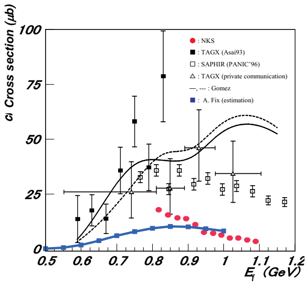


Figure1: Experimental data and theoretical calculation of total cross section of $\gamma d \to \Delta^{++}\Delta^{-}$.

• **Coherent production**

• The process without deuteron breakup is called coherent process(ref.2).

• In the NKS experiment, deuteron was detected in final state. It seems that the contribution of this process to photoabsorption is not small.

• This process was studied by a few theoretical approach and a few experiments (Fig.2) .

• We expect to know detailed mechanism of this process using NKS2.

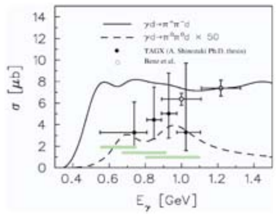


Figure2: Predicted cross section of coherent production and experimental data.

• **The aim of this study**

• The effect from the binding of the proton and the neutron can be studied in this reaction.

1. Investigation of the mechanism of photoabsorption on a bound nucleon using deuteron target and GeV region photon beam.
2. Obtaining the cross section and its energy dependence in a wide energy region of photon.
3. Investigating the role of coherent photoproduction process ($\gamma d \to \pi^+\pi^- d$) in photoabsorption.

## Experiment

**Photon beam**

• The experiment was carried out at Research Center for Electron Photon Science (ELPH), using a photon beam.

• A photon beam is created by bremsstrahlung from an electron beam, and tagged by tagging counters.

• The photon energy range : $0.8 < E_\gamma < 1.1$ GeV (Energy width~6 MeV)

**Neutral Kaon Spectrometer 2** (Fig. 3)

• The charged particles in the final state were detected using the Neutral Kaon Spectrometer 2 (NKS2)

- Dipole magnet (B ~ 0.42 T at the center)
- Drift chambers :Vertex Drift Chamber (VDC), Cylindrical Drift Chamber (CDC)
- TOF counters : Inner Hodoscope (IH), Outer Hodoscope (OH)
- Electron Veto
- Trigger: Detection of more than two charged particles
- Target: Liquid deuterium :located at the center of NKS2

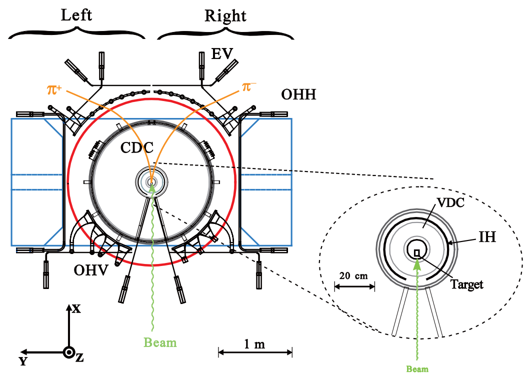


Figure 3 Schematic view of NKS2

## Analysis

### Event Selection

1. Selecting good event using some criteria, hodoscopes timing, tracking $\chi^2$, vertex distribution , etc.
2. Selecting events which include the three charged particle.
3. Check the momentum conservation between photon energy and total momentum of three particles .
4. Particle identification (Fig.4)
   - Mass of particles
     - Drift Chamber: Reconstructed track
       –> Curvature
       –> Momentum
     - Hodoscope: Time of flight
       –>Velocity of particles

$m^2 = (1/\beta^2 - 1)p^2$

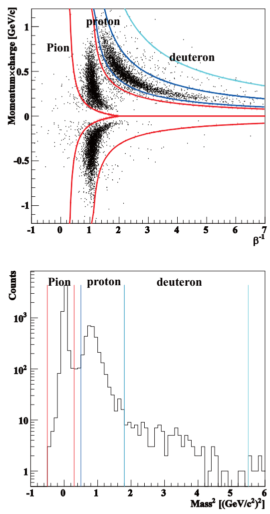


Figure 4: Upper figure is distribution of momentum and inverse velocity of charged particles . Lower figure shows mass square distribution.

4. Check the evidence of $\gamma d \to \pi^+\pi^- d$ reaction as follows (fig.5):
   - Missing mass distribution $\gamma d \to \pi^+\pi^- X$.
   - Energy deposit at IH.

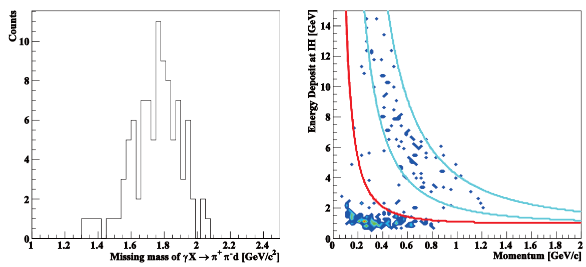


Figure 5: Left is missing mass distribution of $\gamma d \to \pi^+\pi^- X$. There is a peak at around deuteron mass (1.88 GeV/c$^2$).

Right shows the distribution of energy deposit at IH. The distribution between two sky bleu line which obtained from Bethe-Bloch formula are deuteron. Under the red line are pion.

## Summary

• The coherent photoproduction on the deuteron is useful for understanding the mechanism of photoabsorption on a bound nucleon in the GeV region.

• The experiments were carried out in the energy range 0.8-1.1 GeV at ELPH with NKS2.

• The event which include deuteron are detected in our data, and checked these event are $\gamma d \to \pi^+\pi^- d$ event.

## Further outlook

• Improvement of the analysis method to derive the target reaction.

• Improvement the statics and extend the photon energy region.

• Estimation of the detection efficiencies to obtain the cross section and its energy dependence.

• Discussion the mechanism of this reaction and the effect to photoabsorption.

Reference

.[1] K. Hirose et al.: Phys. Lett. B674 (2009)

[2] A. Fix and H. Arenhoevel : Eur. Phys.J. A25 115-135(2005)

The 4th GCOE Internal Symposium

# The analysis of Lambda hypernuclear spectroscopic experiment via (e,e'K+) reaction at JLab Hall-C

D.Kawama
for JLab E05-115 Collaboration
Department of Physics, Tohoku Univ.

## JLab E05-115 experiment : 2009 Aug to Nov at JLab Hall-C

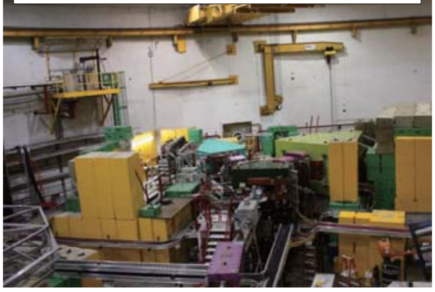

## Data Summary

| Target | hypernucleus | Target Thickness [mg/cm²] | Average beam current [μA] | Total Charge [C] |
|---|---|---|---|---|
| $CH_2$ | Λ, $\Sigma^0$ | 450.8 | 2.0 | 0.28 |
| $H_2O$ | Λ, $\Sigma^0$ | ~500 | 2.7 | 0.20 |
| $^7$Li | $^7_\Lambda$He | 184.0 | 32.0 | 4.84 |
| $^9$Be | $^9_\Lambda$Li | 188.1 | 38.3 | 5.33 |
| $^{10}$B | $^{10}_\Lambda$Be | 56.1 | 38.7 | 6.25 |
| $^{12}$C | $^{12}_\Lambda$B | 112.5 | 26.8 | 5.90 |
| $^{52}$Cr | $^{52}_\Lambda$V | 134.0<br>154.0 | 7.6 | 0.83<br>5.53 |

- $CH_2$, $H_2O$ … for the momentum calibration used as proton target
- $^{12}_\Lambda$B … Study of the structure, linearity check using ground state
- $^7_\Lambda$He, $^9_\Lambda$Li, $^{10}_\Lambda$Be … Study for light hypernuclei
  - Charge Symmetry Breaking (CSB) effect, Λ-$\Sigma^0$ coupling effect
- $^{52}_\Lambda$V … Study for medium hypernuclei
  - Fine structure study, Λ single particle energy

## Experimental Setup –magnets–

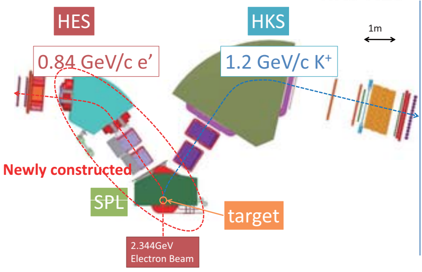


## Experimental Setup –detectors–

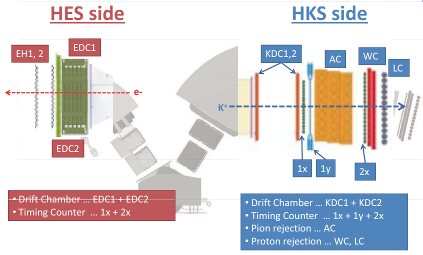


## HES-HKS Spec & Expected energy resolution

**High resolution & Wide acceptance spectrometers**

| | HES | HKS |
|---|---|---|
| Configuration | Q-Q-D (50deg) | Q-Q-D (70deg) |
| e'/K+ Central Momentum | 0.84 GeV/c | 1.2 GeV/c |
| e'/K+ Momentum Acceptance | ±0.15 GeV/c | ±0.15 GeV/c |
| e'/K+ Solid Angle | ~7msr | ~8.5msr |
| Mom. Resolution (FWHM) [MeV/c] | 2.0 × 10-4 | 2.0 × 10-4 |
| Ang. Resolution (FWHM) [mrad] | 3 | 2 |

$dE_{Beam}$=190keV, $dE_{HKS}$=220keV, $dE_{HES}$=190keV

**Total Energy Resolution = 350keV (FWHM, design value)**

## Tracking and kaon PID

**Tracking** … Performed with enough resolution & efficiencies on both HKS and HES (at least in the low rate data)

**Kaon PID**
AC … $\pi^+$, $e^+$ rejection
WC … p rejection
$m^2$ cut … clean $K^+$ selection

Kaon could be selected with ~95% cut efficiency ($^{12}$C target)

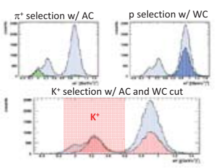


## Coin Time Analysis

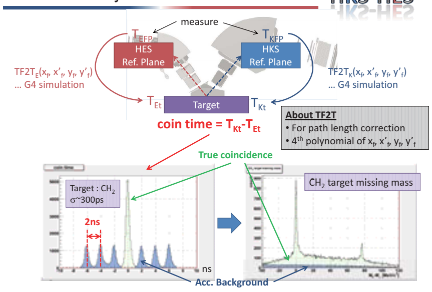


## Coincidence time

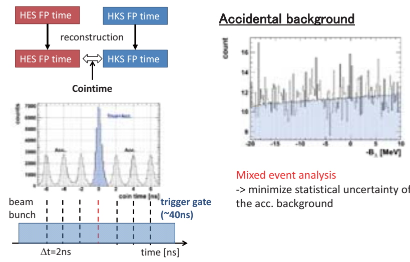


Mixed event analysis
-> minimize statistical uncertainty of the acc. background

## Direct calibration of the F2T function

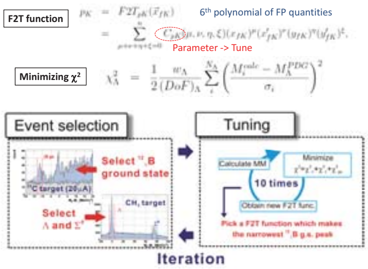


## Magnetic field improvement

Modified
- Shape of Q1 magnetic field
- Magnitudes of every magnet fields

so as to improve SS pattern and Λ, $\Sigma^0$ peak position

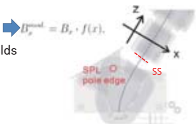


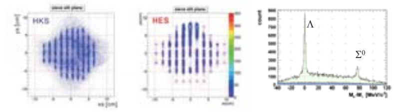


## $CH_2$ spectrum

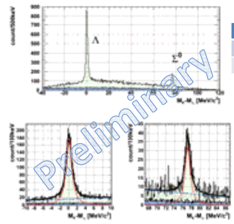


**Fitting result**

| | Λ | $\Sigma^0$ |
|---|---|---|
| mean [MeV/c²] | 0.05 | 0.07 |
| FWHM [MeV/c²] | 1.51 | 1.43 |

Estimation of the momentum resolution

## Estimation of momentum resolution

$dMM^2 = c_0(\text{Beam } dp/p)^2 + c_1(\text{HKS } dp/p)^2 + c_2(\text{HES } dp/p)^2 + c_3(\text{HKS angle})^2 + c_4(\text{HES angle})^2 + c_5 \text{Eloss}^2$

Fitting result, Accelerator, Sieve Slit analysis, Simulation

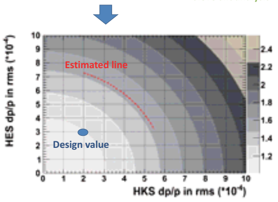


ex.)
$dp_K/p \sim 4*10^{-4}$
$dp_e/p \sim 6*10^{-4}$

Need further calibration

## $^{12}_\Lambda$B –spectrum–

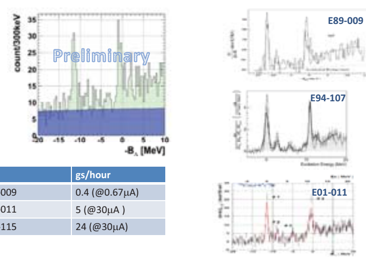


| | gs/hour |
|---|---|
| E89-009 | 0.4 (@0.67μA) |
| E01-011 | 5 (@30μA ) |
| E05-115 | 24 (@30μA) |

## $^{12}_\Lambda$B –fitting results–

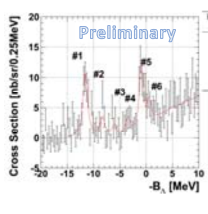


**Binding energy and excitation energy**

| Peak No. | $-B_\Lambda$ [MeV] ±(stat.)±(sys.) | Ex [MeV] ±(stat.)±(sys.) | FWHM [MeV] |
|---|---|---|---|
| #1 | −11.50 ± 0.10 ± 0.2 | 0 | 1.1 |
| #2 | −8.37 ± 0.19 ± 0.2 | 19.86 ± 0.45 ± 0.2 | 1.1 (fixed) |
| #3 | −6.14 ± 0.30 ± 0.2 | 17.63 ± 0.55 ± 0.2 | 1.1 (fixed) |
| #4 | −3.86 ± 0.26 ± 0.2 | 15.36 ± 0.52 ± 0.2 | 1.1 (fixed) |
| #5 | −0.82 ± 0.13 ± 0.2 | 12.31 ± 0.38 ± 0.2 | 1.3 |
| #6 | 1.14 ± 0.62 ± 0.2 | 10.35 ± 0.80 ± 0.2 | 1.1 (fixed) |

**Differential cross section**

| Peak No. | $(d\sigma/d\Omega)$ [nb/sr] ±(stat.)±(sys.) | σ [nb] ±(stat.)±(sys.) |
|---|---|---|
| #1 | 62 ± 17 ± 7 | 0.53 ± 0.15 ± 0.06 |
| #2 | 16 ± 6 ± 2 | 0.14 ± 0.05 ± 0.02 |
| #3 | 8 ± 6 ± 1 | 0.07 ± 0.05 ± 0.01 |
| #4 | 13 ± 6 ± 2 | 0.11 ± 0.05 ± 0.01 |
| #5 | 72 ± 23 ± 9 | 0.62 ± 0.19 ± 0.07 |
| #6 | 15 ± 9 ± 2 | 0.13 ± 0.07 ± 0.02 |

## Summary

**JLab E05-115 Experiment 2009 Aug–Nov carried out successfully**

- Now we are finalizing the data analysis
- Resolution study from the $CH_2$ spectrum
  - Need further calibration, but the basic way of the calibration was established
- $^{12}_\Lambda$B spectrum was consistent with the other data

**To do**
- Tracking analysis for higher rate data
- F2T func. parameter optimization
  - Calibration of the acceptance edge
  - Improvement of the magnetic field

## GCOE Poster 11

# Shot noise measurements for a Kondo-correlated quantum dot in the unitary limit

Yuma Okazaki

1

## The Kondo effect in a quantum dot

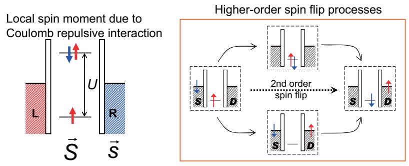


Antiferromagnetic interaction — Kondo Hamiltonian ($J$>0)

$$H_K = J\vec{s}\cdot\vec{S}$$

A formation of the Kondo singlet (many-body spin singlet)

Kondo temperature: $k_B T_K \approx \frac{\sqrt{\Gamma U}}{2}\exp\left(-\frac{\pi U}{4\Gamma}\right)$

2

## Transport properties of the Kondo quantum dot

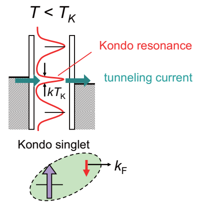


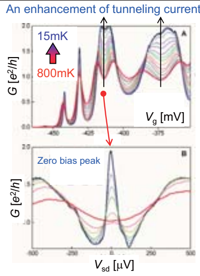


The QD structure allow us to investigate its non equilibrium properties.
We investigate non equilibrium properties of this effect via shot noise.

W. G. van der Wiel et al. Science (2000)

3

## Current noise measurements


FFT power spectral density
$S$ (A²/Hz)

**White spectrum ($f$ ~ MHz)**

Thermal noise : Thermal agitation of electrons
$S = 4k_B TG$

Shot noise : Particle fluctuation reflecting the discrete nature of electrons
$S = 2e^*\langle I \rangle$

4

## The Kondo effect out of equilibrium

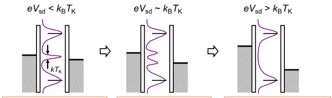


| | Fermi liquid | Crossover | Sequential tunneling |
|---|---|---|---|
| | Quasi-particle flowing through the Kondo resonance carries the current | Splitting of the Kondo resonance (NCA theory) | The Kondo resonance is completely suppressed |
| DC conductance | Transport parameters determined by the Fermi liquid theory was confirmed. M. Grobis et al. PRL (2008) | The splitting of the Kondo resonance was demonstrated in the three-terminal quantum dot. R. Leturcq et al. PRL (2005) | |
| Current noise | Enhancement of current noise due to the Kondo correlation. Theory: E. Sela et al. PRL (2006), A. Golub PRB (2006), A. O. Gogolin et al. PRL (2006). Experiments: O. Zarchin et al. PRBR (2008), Y. Yamauchi et al. PRL (2011) | Unreported logarithmic temperature dependence of the Fano factor | |

**Our study**
( crossover from the Kondo to sequential tunneling)

5

## Setup for measuring current noise

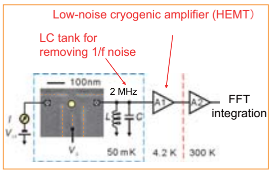


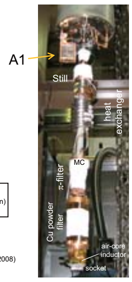


2DEG
GaAs/AlGaAs quantum well structure
(50 nm below the surface)
$n$ = 6.74 x 10¹¹ [cm⁻²]
$\mu$ = 4 x 10⁵ [cm²/Vs]

Gain
A1 ~ 1 V/V (impedance conversion)
A2 ~ 200 V/V

L. Dicarlo et al. Rev.Sci Instrum. (2006)
M. Hashisaka et al. Rev. Sci. Instrum. (2008)

6

## The Kondo effect in the unitary limit

Temperature dependence of the Coulomb oscillation

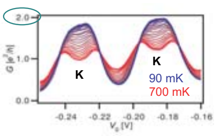


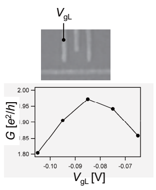


A careful control of the barrier symmetry evolved the Kondo state to the unitary limit, in which uninterested shot noise induced by non-Kondo process can be completely suppressed.

7

## Temperature scaling and Kondo temperature

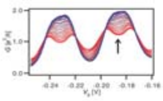

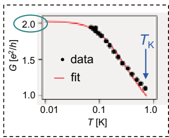


Kondo temperature $G(T_K) = G_0/2$

Empirical form

$$G(T) = G_0\left[1+(2^{1/s}-1)\left(\frac{T}{T_K}\right)^2\right]^{-s}$$

Scaling parameter : $s$ = 0.21

D. Goldhaber-Gordon *et al.* PRL (1998).
T. A. Costi *et al.* J. Phys. Cond. Matt. (1994).

8

## Temperature scaling in the Anderson model

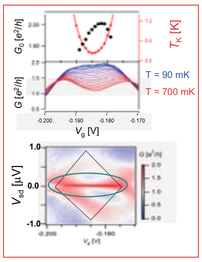


Friedel sum rule

$$G_0 = \frac{2e^2}{h}\frac{4\Gamma_L\Gamma_R}{(\Gamma_L+\Gamma_R)^2}\sin^2\left(\frac{\pi}{2}\langle N\rangle\right)$$

$G_0$ reflects the number of electrons in the dot and the symmetry of the dot-lead coupling

Temperature scaling of asymmetrical Anderson model

$$k_B T_K = \frac{4\sqrt{\Gamma U}}{\pi}\exp\left(-\frac{\pi\varepsilon_0(\varepsilon_0+U)}{2U\Gamma}\right)$$

F. D. M. Haldane PRL (1978)

$U$ = 743 μeV, Γ = 159 μeV

The quantum dot shows characteristic properties of the Anderson model

9

## Backscattering current and shot noise

Partitioning for a tunnel junction ($D$ << 1)
$I_t \propto D$
$S_I = 2eI_t$
Transmission coefficient : $D$

Kondo regime ($D$ ~ 1) : opposite limit
$I_{bs} \propto 1-D$
$S_I = 2eI_{bs}$

Estimation of Backscattering current

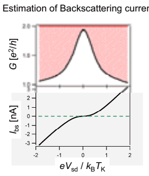


Subtracting thermal noise
$S_I = S - 4k_B TG$

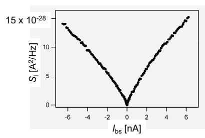


10

## Shot noise measurements and the Fano factor

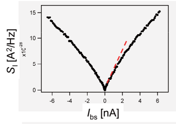


Fano factor gradient of plot: $F_b = \frac{\Delta S_I}{2e\Delta I_{bs}}$

$F_b$ > 1 (super-Poissonian)
$F_b$ = 1 (Poissonian noise)
$F_b$ < 1 (sub-Poissonian)

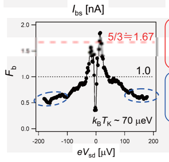


An enhancement of Fano factor is observed for a small source-drain bias regime. The observed value of the Fano factor agrees with the theoretical prediction 5/3.

At a large $V_{sd}$, the Fano factor reaches $F_b$ = 0.5, which corresponds to the predicted Fano factor for sequential tunneling events with symmetrical dot-lead barriers.

Crossover from Kondo regime to sequential transport determined via shot noise

11

## Out of particle hole symmetry

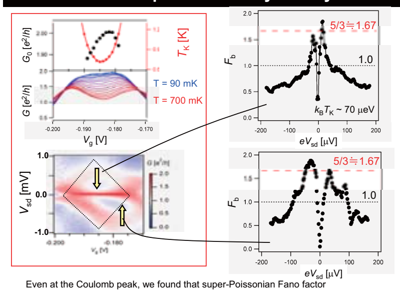


Even at the Coulomb peak, we found that super-Poissonian Fano factor

12

## Temperature dependence of the Fano factor

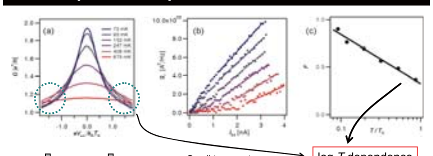


log $T$ dependence

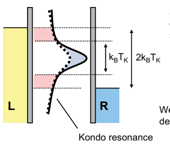


Small temperature dependence in a large source-drain bias

Current change due to expanding transport window
+ Deformation of the Kondo resonance

We found that unexpected logarithmic temperature dependence of the Fano factor for the crossover regime

13

## Summary

**Shot noise properties of a Kondo correlated quantum dot in the unitary limit**

- For a small $V_{sd}$, the predicted super-Poissonian Fano factor was observed.
- A crossover from Kondo regime to sequential tunneling regime determined via shot noise.
- Super-Poissonian Fano factor was observed even near a Coulomb peak.
- The temperature dependence of the Fano factor in the crossover regime shows unexpected logarithmic temperature dependence.

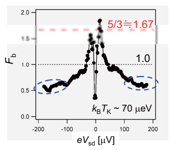


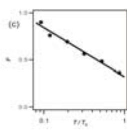


14

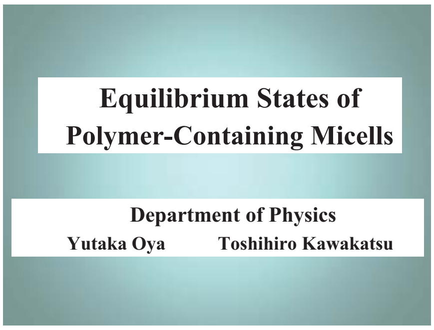
Equilibrium States of
Polymer-Containing Micells
Department of Physics
Yutaka Oya Toshihiro Kawakatsu

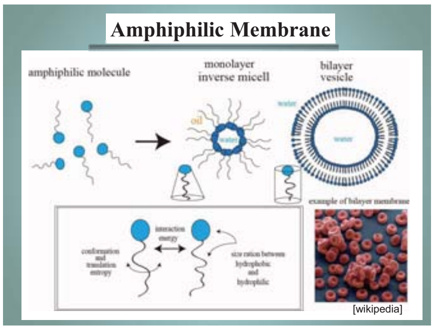
Amphiphilic Membrane
amphiphilic molecule
monolayer
inverse micell
bilayer
vesicle
water
oil
example of bilayer membrane
[wikipedia]

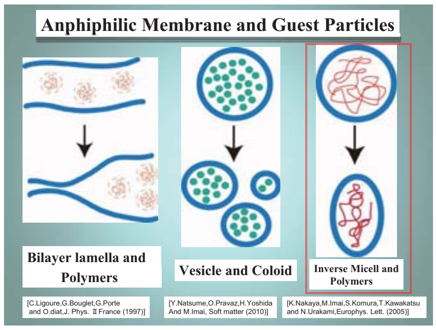
Anphiphilic Membrane and Guest Particles
Bilayer lamella and Polymers
Vesicle and Coloid
Inverse Micell and Polymers
[C.Ligoure,G.Bouglet,G.Porte and O.diat,J. Phys. Ⅱ France (1997)]
[Y.Natsume,O.Pravaz,H.Yoshida And M.Imai, Soft matter (2010)]
[K.Nakaya,M.Imai,S.Komura,T.Kawakatsu and N.Urakami,Europhys. Lett. (2005)]

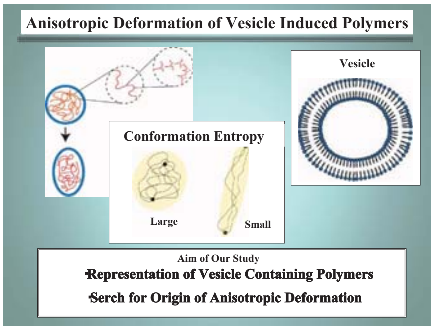
Anisotropic Deformation of Vesicle Induced Polymers
Vesicle
Conformation Entropy
Large
Small
Aim of Our Study
Representation of Vesicle Containing Polymers
Serch for Origin of Anisotropic Deformation

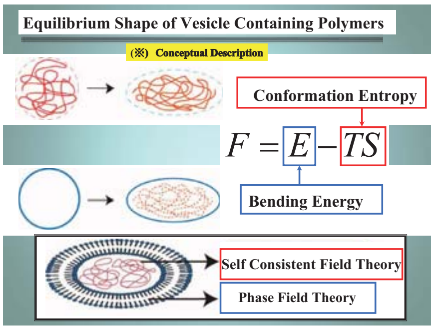
Equilibrium Shape of Vesicle Containing Polymers
(※) Conceptual Description
Conformation Entropy
$F = E - TS$
Bending Energy
Self Consistent Field Theory
Phase Field Theory

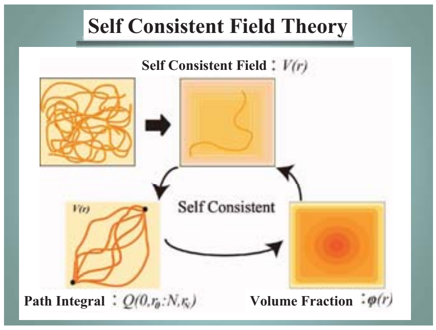
Self Consistent Field Theory
Self Consistent Field : $V(r)$
Self Consistent
Path Integral : $Q(0,r_0;N,r_N)$
Volume Fraction : $\varphi(r)$

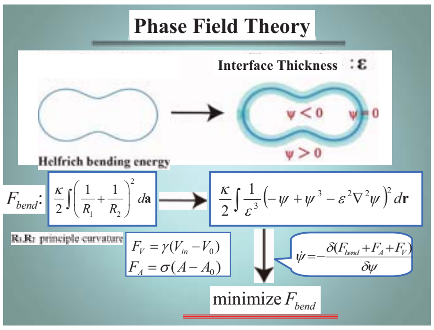
Phase Field Theory
Interface Thickness : $\varepsilon$
$\psi < 0$
$\psi = 0$
$\psi > 0$
Helfrich bending energy
$F_{bend}: \frac{\kappa}{2}\int\left(\frac{1}{R_1}+\frac{1}{R_2}\right)^2 da$
$\frac{\kappa}{2}\int\frac{1}{\varepsilon^3}\left(-\psi+\psi^3-\varepsilon^2\nabla^2\psi\right)^2 d\mathbf{r}$
$R_1, R_2$ principle curvature
$F_V = \gamma(V_{in} - V_0)$
$F_A = \sigma(A - A_0)$
$\dot{\psi} = -\frac{\delta(F_{bend}+F_A+F_V)}{\delta\psi}$
minimize $F_{bend}$

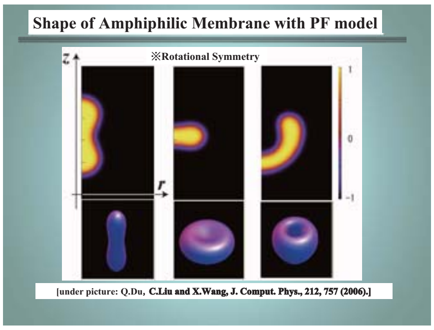
Shape of Amphiphilic Membrane with PF model
※Rotational Symmetry
[under picture: Q.Du, C.Liu and X.Wang, J. Comput. Phys., 212, 757 (2006).]

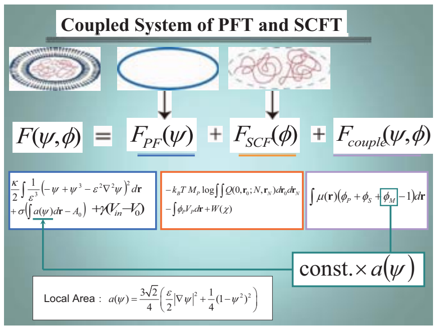
Coupled System of PFT and SCFT
$F(\psi,\phi) = F_{PF}(\psi) + F_{SCF}(\phi) + F_{couple}(\psi,\phi)$
const. $\times\, a(\psi)$
Local Area : $a(\psi) = \frac{3\sqrt{2}}{4}\left(\frac{\varepsilon}{2}|\nabla\psi|^2 + \frac{1}{4}(1-\psi^2)^2\right)$

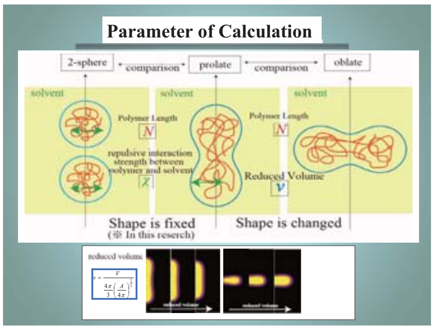
Parameter of Calculation
2-sphere
comparison
prolate
comparison
oblate
solvent
Polymer Length
N
repulsive interaction strength between polymer and solvent
χ
Reduced Volume
v
Shape is fixed
(※ In this reserch)
Shape is changed
reduced volume

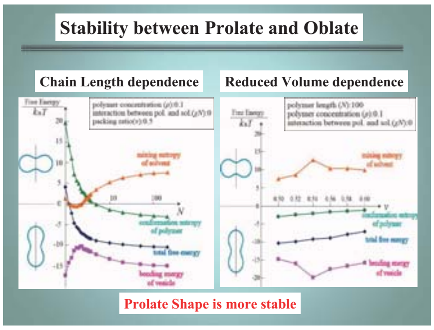
Stability between Prolate and Oblate
Chain Length dependence
Reduced Volume dependence
mixing entropy of solvent
conformation entropy of polymer
total free energy
bending energy of vesicle
Prolate Shape is more stable

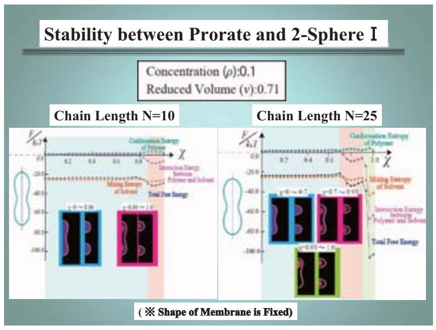
Stability between Prorate and 2-Sphere Ⅰ
Concentration (ρ):0.1
Reduced Volume (v):0.71
Chain Length N=10
Chain Length N=25
Total Free Energy
(※ Shape of Membrane is Fixed)

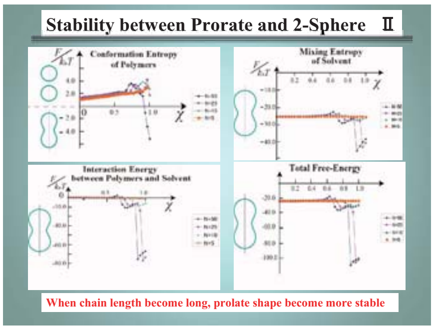
Stability between Prorate and 2-Sphere Ⅱ
Conformation Entropy of Polymers
Mixing Entropy of Solvent
Interaction Energy between Polymers and Solvent
Total Free-Energy
When chain length become long, prolate shape become more stable

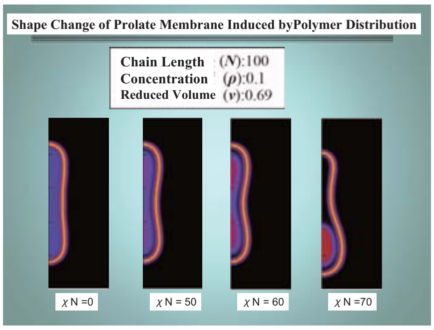
Shape Change of Prolate Membrane Induced byPolymer Distribution
Chain Length (N):100
Concentration (ρ):0.1
Reduced Volume (v):0.69
χN =0
χN = 50
χN = 60
χN =70

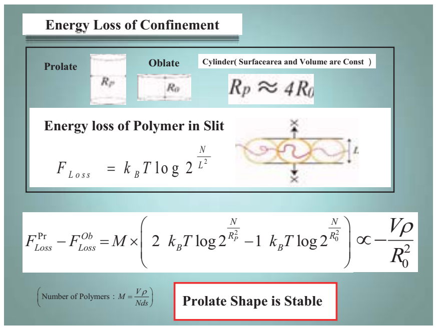
Energy Loss of Confinement
Prolate
Oblate
Cylinder( Surfacearea and Volume are Const )
$R_P \approx 4R_O$
Energy loss of Polymer in Slit
$F_{Loss} = k_B T \log 2^{\frac{N}{L^2}}$
$F_{Loss}^{Pr} - F_{Loss}^{Ob} = M \times \left(2\ k_B T \log 2^{\frac{N}{R_P^2}} - 1\ k_B T \log 2^{\frac{N}{R_O^2}}\right) \propto -\frac{V\rho}{R_O^2}$
Number of Polymers : $M = \frac{V\rho}{Nds}$
Prolate Shape is Stable

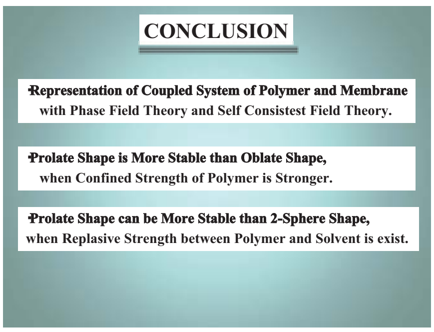
CONCLUSION
Representation of Coupled System of Polymer and Membrane with Phase Field Theory and Self Consistest Field Theory.
Prolate Shape is More Stable than Oblate Shape, when Confined Strength of Polymer is Stronger.
Prolate Shape can be More Stable than 2-Sphere Shape, when Replasive Strength between Polymer and Solvent is exist.

# "Properties of proton-rich unstable nuclei and two-proton radioactivity"

Tomohiro Oishi[A], Kouichi Hagino[A], Takahito Maruyama[A], Hiroyuki Sagawa[B]

[A] Department of Physics, Tohoku University, [B] Center for Mathematical Sciences, University of Aizu

## I. Unstable Nuclei

Nuclei that (1) decay with a quite short lifetime, (2) have a large proton- or neutron-excessiveness, are called "unstable nuclei".

They have some exotic physical properties which are not present in stable nuclei.

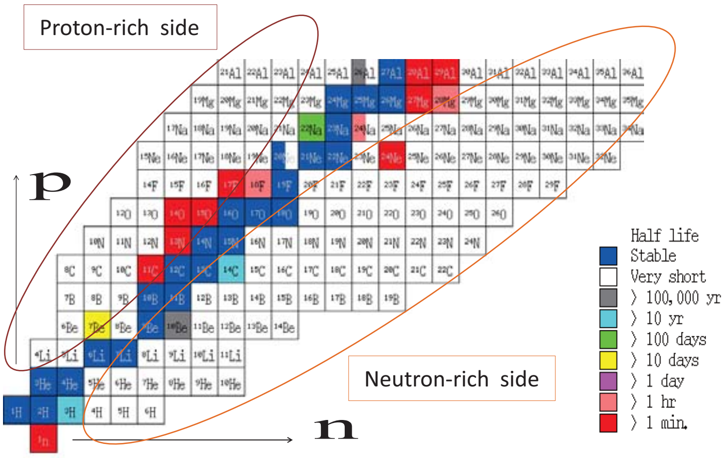


## II. Effect of Coulomb Force (EoC)

For the proton-rich unstable nuclei, Coulomb force (repulsive) is also indispensable besides the nuclear force (attractive).

### II(a). EoC for "di-nucleon correlation"

di-nucleon correlation; the spatial localization of two neutrons or protons in nuclei.

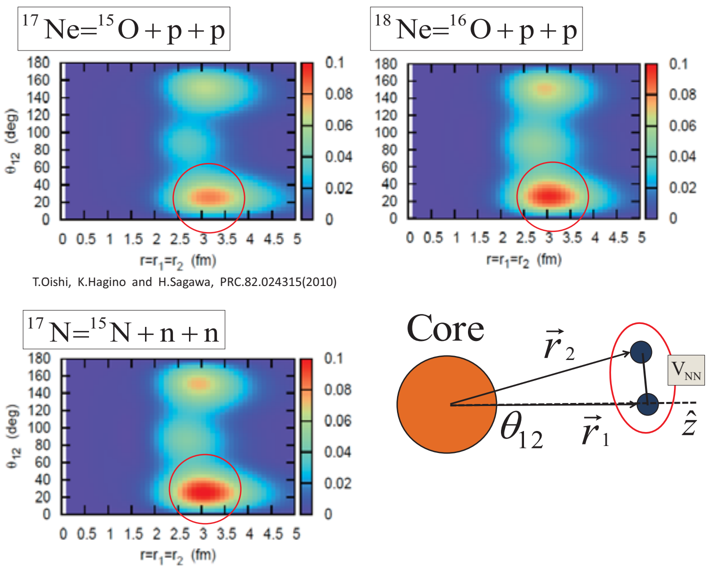


T.Oishi, K.Hagino and H.Sagawa, PRC.82.024315(2010)

| | $^{18}Ne$ | $^{17}Ne$ | $^{17}N$ |
|---|---|---|---|
| $\langle V_{NN,Nucl.}\rangle$ (MeV) | -4.22 | -4.01 | -3.60 |
| $\langle V_{NN,Coul.}\rangle$ (MeV) | 0.53 | 0.51 | - |
| $S_{2N}$ (MeV) | -4.57 | (-0.94) | 9.05 |
| $S_{2N,exp}$ (MeV) | -4.52 | -0.94 | 8.37 |

### II(b). EoC for "soft dipole excitation"

soft dipole excitation; the excitation at low energy of weakly bound nuclei.

$$B_{E1} = \sum_{\mu} \left| \langle 1,\mu,- | \hat{O}_{E1} | 0,0,+ \rangle \right|^2$$

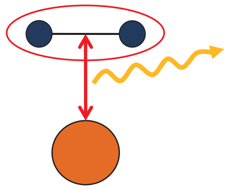

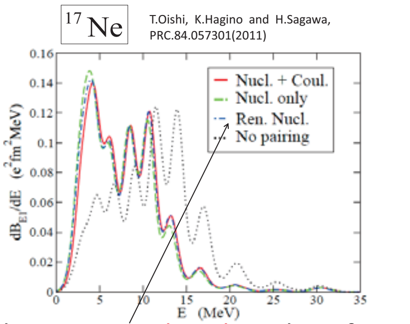


EoC is well reproduced by a 10%-reduced nuclear force.

## III. Two-proton Radioactivity

One of the most important physics of proton-rich nuclei is "two-proton- (2p-) decay or radioactivity".

*e.g.* $^6Be \rightarrow ^4He + 2p$

### Analysis with a schematic 1D-3body-model

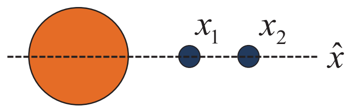


$\Rightarrow \Psi_{pp}(t, x_1, x_2)$

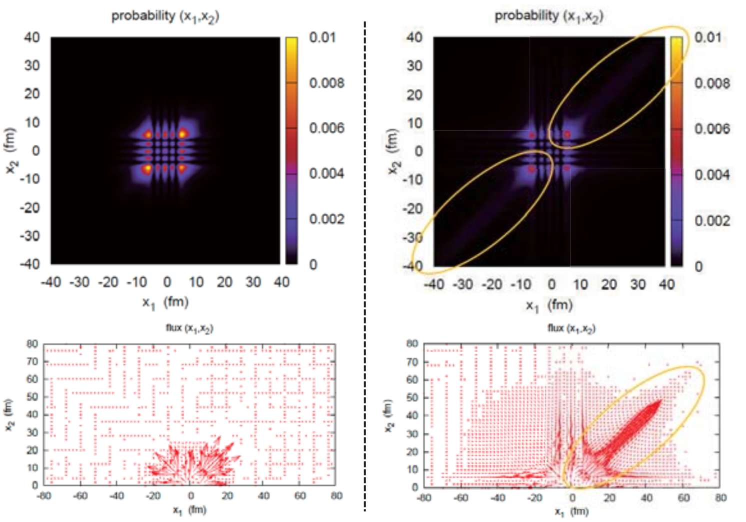


T.Maruyama, T.Oishi and K.Hagino, now in preparation

"(ellipse)" indicates emitted 2p.

## IV. Summary

1) EoC to the di-nucleon correlation or the soft dipole excitation is investigated. → Coulomb repulsion reduces the pairing interaction by about 10%.
2) The time-dependent method is applied to the 2p-decay in a schematic 1D-model. → Time evolution of many-particle-system is well described.

Future work;
realistic 3D-time-dependent analysis of 2p-radioactivity.

# Oscillatory Instability of Slow Crack Propagation in Rubbers under Large Deformation

Daiki Endo

Department of Physics, Tohoku University

## Introduction

When a rubber balloon is ruptured, oscillatory crack patterns on a macroscopic scale are observed quite consistently. This oscillating mechanism is still not understood due to the difficulty in measuring rapid crack propagation and treating rapid crack dynamics with significant inertia.

Hence, if we could perform an experiment in which the crack propagation speed is significantly reduced, it may be possible to develop an alternative approach that overcomes those problems.

## Experiments of Slow Fracture

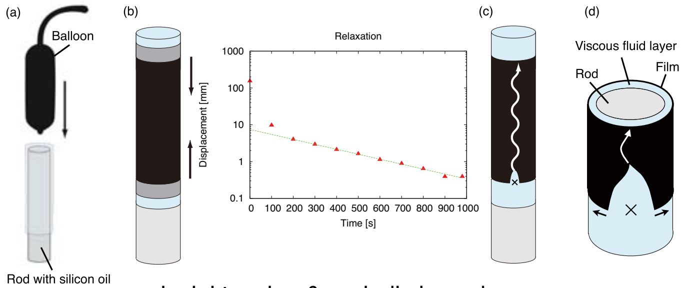


uniaxial tension & periodic boundary

| Sample: Qualatex 260Q made by Pioneer Balloon Company | |
|---|---|
| Material | Natural rubber |
| Thickness | 0.31mm |
| Circumferential length | 20mm |

| | |
|---|---|
| Kinematic viscosity of silicon oils | 1,000 ～ 10,000cSt |
| Diameter of rods | 15 ～ 35mm |

The above figure shows schematic illustrations of experimental procedure. (a) Oil-coated cylinder is covered by an inflated balloon. By this process, we prepare the rubber film which is stretched on the viscous fluid layer around the cylinder. (b) Relaxation to pure uniaxial tension. (c) Crack initiation. (d) Cross-section of experimental system. The high-viscosity oil between the film and the cylinder significantly reduces the sliding speed of the film with respect to the substrate.

crack speed $v$ $\quad 1\ \mathrm{mm/s} \sim 1\ \mathrm{m/s}$

strain $\varepsilon$ $\quad 1 \sim 5$

$$\rho \ddot{u}_i = \frac{\partial \sigma_{ik}}{\partial x_k} \Rightarrow \gamma \dot{u}_i = \frac{\partial \sigma_{ik}}{\partial x_k}$$

- Oscillatory and straight patterns are observed.
- The oscillatory instability is observed at strong nonlinear elastic region.
- Shapes of oscillatory patterns are dependent on the applied strain and the relaxation time.

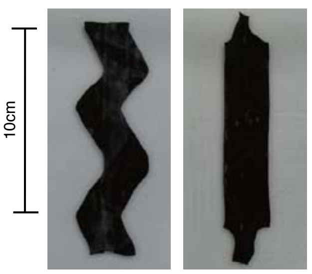


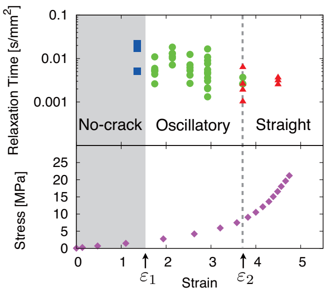


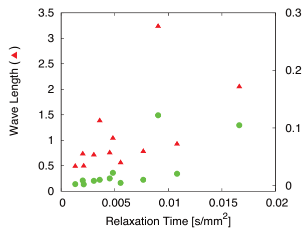


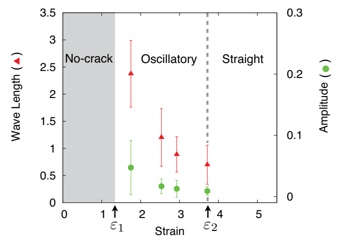


## Summary

- Oscillatory and straight crack patterns are observed in our slow fracture experiments of rubbers.
- The oscillatory instability is observed at strong nonlinear elastic region of rubbers.
- Oscillatory and straight crack patterns are obtained in neo-Hookean model.
- In linear elastic model, oscillatory patterns are not obtained.

The nonlinear elasticity plays an important role in the oscillatory crack pattern formation.

## Numerical Simulations

The experimental system is approximated by 2-D system consists of triangle continuum elements

which have
- •nonlinear elasticity
- •viscous resistance

with
- •uniaxial tensile
- •periodic
- •initial crack

boundary condition

with appropriate fracture criterion.

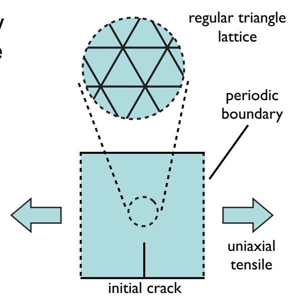


energy density function

$$F = S \cdot f \begin{cases} \text{Linear Elasticity (Reference)} \\ f = \frac{1}{2}\lambda \varepsilon_{ii}\varepsilon_{jj} + \mu \varepsilon_{ij}\varepsilon_{ij} \qquad \lambda = 4\,,\ \mu = 2 \\ \text{Neo-Hookean} \\ f = \frac{1}{2}\mu\left(\lambda_1^2 + \lambda_2^2 + \lambda_3^2 - 3\right) \quad \mu = 2\,,\ \lambda_1\lambda_2\lambda_3 = 1 \end{cases}$$

dissipation function of viscous resistance

$$G = \frac{1}{2}\eta \int \left(\frac{d\boldsymbol{x}}{dt}\right)^2 dS$$

equation of motion

$$\frac{\partial}{\partial q_j}\left(\sum_i F_i\right) + \frac{\partial}{\partial \dot{q}_j}\left(\sum_i G_i\right) = 0$$

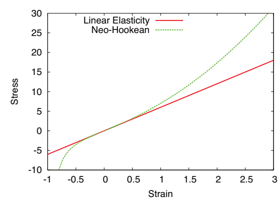


If a strain energy density of $i$-th element exceeds critical value $f_c$, the element is removed irreversibly

- Oscillatory and straight patterns are obtained in neo-Hookean model. Shapes of the oscillation patterns have a similar strain dependency to the experimental result.
- In linear elastic model, oscillatory patterns are not obtained.

$f_c = 10 \quad N = 128 \times 256$

(a) $\varepsilon = 0.5$ (b) $\varepsilon = 1.5$ (c) $\varepsilon = 0.5$

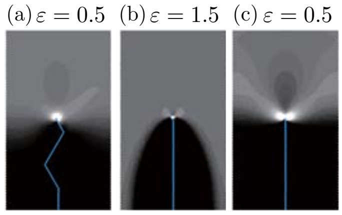

Neo-Hookean Linear

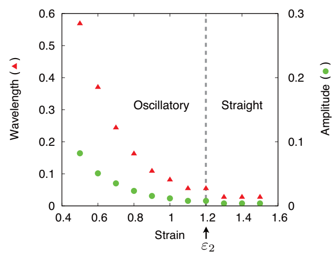

# Structure of Neutron-rich Nucleus $^{31}$Ne Deduced from Nuclear Reactions

Yasuko Urata, Kouichi Hagino  Department of Physics, Tohoku University

## ① Halo nucleus

**Neutron-rich nuclei**

- are not stable against $\beta$ decays and do not exist in nature.
- recent experimental techniques enable to synthesize and study such nuclei
- have interesting features, such as halo structure

Nuclear chart

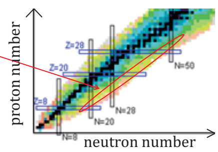


**Halo nuclei**

Spatially extended density distribution of the weakly bound valence neutron(s): ➤ $^{11}$Li, $^{11}$Be, $^{6}$He, $^{19}$C, ...

Halo structure is constructed by a s- or p- orbit, for which the centrifugal barrier is small.

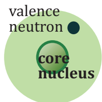


## Mean Field Picture

Nucleons are independent particles which are moving in some average potential created by all the nucleons in the nucleus.

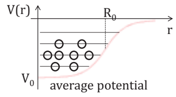


Naive spherical shell model
→ $1f_{7/2}$ configuration for the valence neutron of $^{31}$Ne

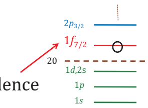


➤ **Single particle motion in a deformed potential**

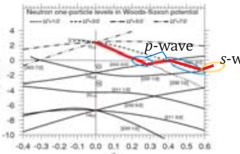


**Nilsson diagram** (I.Hamamoto, Phy.Rev.C 81, 021304(R) (2010))

➤ $\beta$ ~ 0.2-0.3 : [330 1/2]
$\beta$ ~ 0.4-0.6 : [321 3/2] } p-wave halo
( $\beta$ ≳ 0.6 : [200 1/2] → s-wave halo )

## Recent Experiment for $^{31}$Ne

- Large Coulomb breakup cross section for $^{31}$Ne (T.Nakamura, et al., Phys. Rev. Lett.103,262501(2009))
  → soft E1 (electric dipole) excitation
- Large reaction cross section for $^{31}$Ne (M.Takechi et al., Nucl.Phys.A 834, 412c (2010))
  → large radius

➤ **$^{31}$Ne is a halo nucleus**

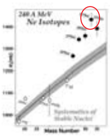

reaction cross section

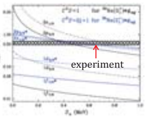


Coulomb breakup cross section

## ② Motivation

In the Nilsson model, the rotational excitation energy of the core nucleus is neglected.
**In reality, however,** $^{30}$Ne has the first 2$^+$ excited state at 0.801 MeV.

- Inclusion of the excitation energy of the core nucleus with a particle-rotor model
- Calculation of Coulomb breakup cross sections and reaction cross sections

➤ **The effect of finite excitation energy**
➤ **Ground state properties of $^{31}$Ne**

## ③ Particle-rotor Model

- $^{31}$Ne : (deformed core $^{30}$Ne) + $n$
- Axial quadrupole deformation of the core
- The core nucleus has a rotational band.

→ $H = H_{\text{spherical}} + H_{\text{deformed}} + H_{\text{rotation}}$

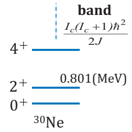


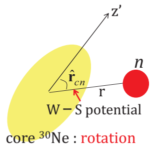


$$\Psi_{IM} = \sum_{I_c jl} \alpha_{jlI_c} \left( {}^{31}\text{Ne} \right)^{(IM)} \quad \text{For example,} \quad = f_{7/2}\,0^+ + p_{3/2}\,2^+ + p_{3/2}\,4^+ + \cdots$$

## PRM and Nilsson Diagram

$H_{\text{rotation}} = 0$
→ Nilsson diagram ($\varepsilon_K$)

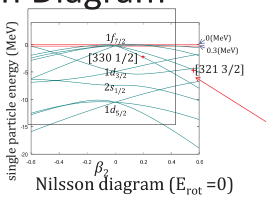


Nilsson diagram ($E_{\text{rot}}$ =0)

➤ **The effect of $E_{\text{rot}} \neq 0$**

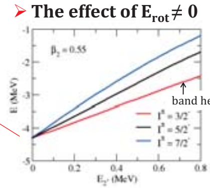


## Coulomb breakup

The projectile $^{31}$Ne is excited by the electromagnetic field made by the Pb target.
→ Breakup into $^{30}$Ne+n
→ Dominant E1 excitation

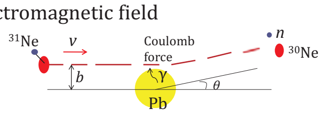


$$B(E1; i \to f) = \frac{1}{2I_i + 1} \left| \langle f \| \hat{D} \| i \rangle \right|^2$$ Dipole operator is $\hat{D}_\mu = eZ_{eff} r Y_{1\mu}(\hat{\mathbf{r}}_n), Z_{eff} = -\frac{Z}{A+1}$

Total cross section is $\sigma(E1) = \sum_f \frac{16\pi^3}{9\hbar c} N_{E1}(E_f - E_i) B(E1; i \to f)$  $N_{E1}$ : virtual photon number

## Reaction Cross Section

Reaction cross section ($\sigma_r$) is the total cross section except for the elastic scattering.

$$\sigma_r = \int d\mathbf{b} \frac{1}{2I+1} \sum_M \langle \Psi_{IM} | (1 - |S|^2) | \Psi_{IM} \rangle$$ $|\Psi_{IM}\rangle$ : initial state wave function (ground state)

S : scattering matrix → $|S|^2$ is the probability that the projectile remains in the elastic channel after the collision with the target.

## ④ Result: Coulomb Breakup

Y. Urata, K. Hagino, and H. Sagawa Phys. Rev. C 83, 041303(R) (2011)

Total Cross Section

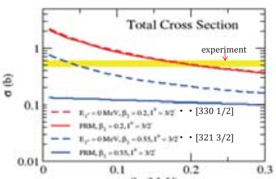


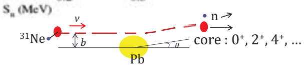


➤ **The effect of rotational excitation of core nucleus**
$I^\pi$=3/2$^-$ configuration at $\beta_2$=0.55 cannot reproduce the experimental cross section.

➤ **$I^\pi$=3/2$^-$ configuration at $\beta_2$= 0.2 is a candidate for the ground state of $^{31}$Ne**

Cross section with 0$^+$ core  ● $\beta_2$=0.2 , $I^\pi$=3/2$^-$

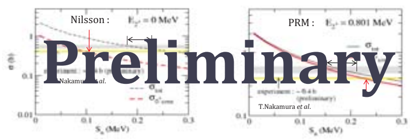


**Nilsson model calculation**
➤ does not reproduce the two kinds of data simultaneously.

**PRM calculation**
➤ reproduces both the data consistently.

## ⑤ Result: Reaction Cross Section

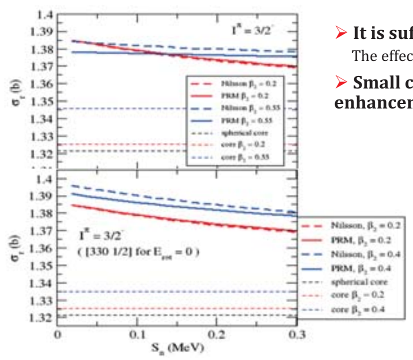


➤ **It is sufficient to calculate with Nilsson model for the reaction cross section.**
The effect of rotational excitation of core is small.

➤ **Small contribution of the last neutron with $I^\pi$=3/2$^-$ at $\beta_2$=0.55 to the enhancement of the reaction cross section for $^{31}$Ne**

➤ **In the Nilsson Model, the effect of core deformation changes the cross section only by about 0.01 b,**
while there is the effect of last neutron configuration due to the deformation of potential in the weakly bound region with PRM calculation.

Component ($S_n$ = 0.2 MeV)

| | $0^+\otimes p_{3/2}$ | $2^+\otimes p_{3/2}$ | Total $p_{3/2}$ |
|---|---|---|---|
| $\beta_2$ = 0.2 | | | |
| Nilsson | 24.1% | 24.1% | 48.2% |
| PRM | 48.5% | 8.4% | |
| $\beta_2$ = 0.4 | | | |
| Nilsson | 26.9% | 26.9% | 53.8% |
| PRM | 45.6% | 13.6% | |

Rms Radii

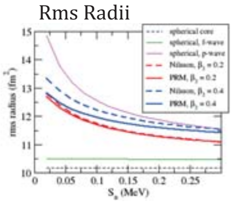


➤ **The behaviors of reaction cross sections are similar to that of rms radii,**
➤ **and can be understood from the amount of p-wave component in their configurations.**

## ⑥ Summary

◆ **Ground state properties of $^{31}$Ne** → particle-rotor model
※ rotational excitation energy of the core nucleus

Coulomb breakup cross section

◆ **The effect of excitation energy of the core nucleus**
→ $I^\pi$ = 3/2$^-$ configuration at $\beta_2$ = 0.55 is excluded.

◆ **Total and 0$^+$ cross sections of the Coulomb breakup**
→ $I^\pi$ = 3/2$^-$ configuration at $\beta_2$ = 0.2 reproduces the data consistently.

Reaction cross section

◆ **Nilsson model works reasonably well.**

◆ **Reaction cross sections and rms radii**
→ can be interpreted from neutron configurations.

◆ **Study of $\beta_2$ dependence**

# Investigating of the topological order in the quantum Hall effect

Toru Ito
Department of Physics, Tohoku University

## Fractional quantum Hall effect

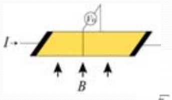

$R = \frac{V_L}{I}$

$R_H = \frac{V_H}{I} = \frac{h}{ne^2}$

$\nu = \frac{n}{n_\phi} = \frac{nhc}{eB} = 1,2,3,\cdots$

$\frac{h}{e^2} = 25812.807572\ \mathrm{W}$

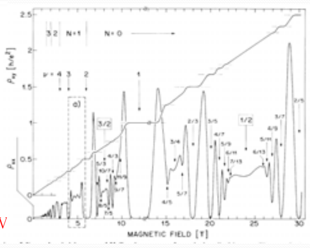


## Laughlin's wavefunction

$$\psi_{Lf} = \prod_{i<j}(z_i - z_j)^m e^{\sum_i \frac{-|z_i|^2}{4\ell^2}}$$

$z = x - iy$ : Complex coordinate

$\ell = \sqrt{\hbar / eB}$ : Magnetic length

$m$ : Odd integer determined by filling faraction

Numerically, Laughlin's state have over **99%** overlap (very good model of the ground state wavefunction)

---

$\vec{r}_{ij} = z_i - z_j$ : Polar coordinate

$$\prod_{i<j}(z_i - z_j)^m = \prod_{i<j}|r_{ij}|^m e^{im\theta_{ij}}$$

This factor represent **m** magnetic fluxes

AB effect of quantized magnetic flux

$$\frac{e}{\hbar}\oint \vec{A}d\vec{s} = 2\pi \longleftrightarrow e^{i(m-1)(2\pi)}$$

$$\vec{B} = \begin{pmatrix} 0 \\ 0 \\ \delta(\vec{r})\frac{h}{e} \end{pmatrix} \quad \vec{A} = \begin{pmatrix} A_r \\ A_\theta \end{pmatrix} = \begin{pmatrix} 0 \\ \frac{\hbar}{e|r|} \end{pmatrix}$$

---

ν=1/m Laughlin's state in 1-hole torus geometry has **m**-fold degeneracy

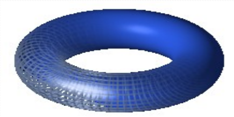

In g-hole geometry (g-genus Riemann surface), Laughlin's state has $m^g$-fold degeneracy

This degeneracy called topological degeneracy

## Kinds of Quantum Numbers

- Quantum numbers related to symmetry
  - Example: angular momentum ⇔ rotational symmetry
  - Degeneracy from the algebra of the group generators
- Quantum numbers determined by topology
  - Examples:
    - Quantized circulation in superfluid He
    - Magnetic flux quantization in superconductors
  - Related to the winding number of a condensate wave function
  - Survive for adding relatively strong perturbation

Hall conductance of FQH is quantum number of this kind

## Classification of states (X.G.Wen)

orders
- Symmetry-breaking orders
- Non-symmetry-breaking orders
  - Quantum phenomena
    - Gapped
      - Topological-orders — FQH state is here
    - Non-gapped
      - Other systems
  - Classical systems

## How confirm realization of topological orders?

A new approach is proposed.
This approach use the entanglement entropy of the two divided systems

Definition of the entanglement entropy (EE) of two sub systems

Density matrix of total system : $\rho_{tot} = |\psi\rangle\langle\psi|$

Density matrix of Sub system A : $\rho_A = tr_B \rho_{tot}$

EE of sub system A : $S_A = -tr_A \rho_A \ln \rho_A$

EE represents quantum entanglement of two systems.

---

Example of EE: spin-1/2 system composed of two particles

(i) $|\Psi\rangle = \frac{1}{2}\left[|\uparrow\rangle_A + |\downarrow\rangle_A\right]\otimes\left[|\uparrow\rangle_B + |\downarrow\rangle_B\right]$

Not Entangled

$S_A = 0$

(ii) $|\Psi\rangle = \left[|\uparrow\rangle_A \otimes |\downarrow\rangle_B + |\downarrow\rangle_A \otimes |\uparrow\rangle_B\right]/\sqrt{2}$

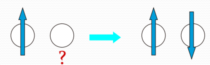

Entangled

$S_A = \log 2$

## The scaling law of entanglement entropy

Gapped systems have finite correlation length, then the EE is proportional to the boundary length L of two divided systems

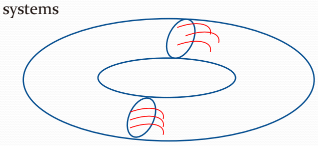

$$S_A \propto \alpha L + O(\frac{1}{L})$$

---

In topologically ordered systems, the scaling low of the EE has universal correction γ

$$S_A = \alpha L - \gamma + O(\frac{1}{L})$$

γ is called topological entanglement entropy (TEE)

---

Topological entanglement entropy reflect topological character of the ground state

m=3 Laughlin state: $-\gamma = -n\ln\sqrt{3} = -0.54n$

m=5 Laughlin state: $-\gamma = -n\ln\sqrt{5} = -0.805n$

n =(number of boundaries)

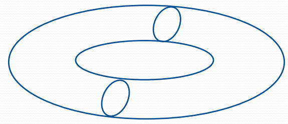

1-hole torus :n=2

---

Numerical calculation of EE(spherical geometry)

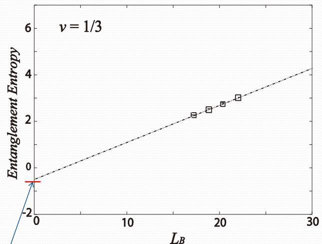


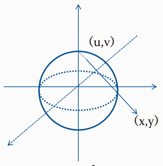


n=1

Numerically obtained TEE is very close to the theoretical prediction

## Summary

- Topologically system is characterized by non-symmetry breaking order
- Such order called topological order
- One of a way of numerically confinement of the topological order is calculating of the topological entanglement entoropy

# *Autonomous decision-making and informed consent*

Haruka Hikasa

(Philosophy, Tohoku University)

## *1.Introduction*

In a time of technical progress, medical technology has made particular progress. Decision making is required in the use of technology. In years gone by, doctors would make the choices regarding the best medical treatment options for the patient. Now, generally the patients themselves make the choice of whether to undergo certain medical treatments, and may even refuse medical treatment at the cost of their life. This is based on a principle of "respect for autonomy"; the acceptance that a person should make decisions according to his/her own values and beliefs. In order to protect that principle, the informed consent of the patient for his/her medical treatment is thought to be indispensable.

However, the relation between autonomy and informed consent is not immediately clear, and various arguments exist concerning it. Therefore, I would like to consider the prerequisites of "respect for autonomy" in decision-making, and the way in which informed consent ought to be practiced. This problem is important to a considered understanding of human life in an age of science and technology.

## *2.Principle of "Respect for autonomy" in bioethics*

In bioethics, the respect for autonomy is one of the most important principles. According to this principle, the healthcare providers have the duty to respect a patient's autonomy, and the providers has the duty to support autonomous choice so that a patient can attain to their own purpose. In other words, healthcare providers disclose relevant information to a patient, and a patient makes a decision having understood the situation. And generally it is thought that informed consent is required in order to apply a principle of respecting patient's autonomy at the place of practice.

## *3.Compromising a person's autonomy*

According to Taylor, however, respect for autonomy cannot serve as the foundation for securing informed consent. "Compromise of a person's autonomy" is diminution of autonomy by being forced by others in decision-making regarding action and choice. Moreover, the autonomy declines with a person being deceived, or acting without information. Whether autonomy is a diminution of autonomy depends upon whether a person is **intentionally** directed to the point of determinations and acts. In other words, whether autonomy is compromised depends on whether a person is under the control of others. The others, here, are those who are intentionally going to govern his/her decisions and acts. From a viewpoint of medical advice of healthcare providers, if a patient is operated upon or deceived by them and makes a decision unconsciously which they intend, a patient's autonomy will have been diminished with regard to his/her medical decision-making.

## *4. No compromising a person's autonomy*

If the intentional control by others is not imposed, the autonomy of the person is not compromised. The person still directs their own decisions and acts and can be fully autonomous with regard to them. In that case, the degree of achievement of his/her purpose need not concern us, and it can be said that he/she is autonomous.

## *5. "Instrumental value of autonomy" is the ethical foundation of informed consent*

When a person is not controlled intentionally, and when his/her aims are not achieved by lack of knowledge, **the autonomy itself** of the person was not compromised and only **the instrumental value of autonomy** of the person is compromised. As for the autonomy of the patient with regard to the treatment decision, it will not be compromised even if healthcare providers failed to secure the informed consent of the patient as a result of having non-intentionally or carelessly neglected to disclose relevant information.

## *6. Achievement of value and the purpose -Securing of "instrumental value of autonomy"*

In this way, respect for autonomy will not be the only theoretical basis for securing informed consent. It can, nonetheless, be fair grounds to secure informed consent if we think achieving respect for autonomy secures the instrumental value of the autonomy. As we argued in the beginning, healthcare providers should support patients in such a way that patients can achieve their purposes in medical care. All we need for this is dialog and participation of patients and healthcare providers.

## *7. Shared decision making for patient's best interests*

In order to respect a patient's autonomous choice and for a patient to make the final choices, healthcare providers need to know a patient's purposes and values and to offer information required for medical treatment choices. For that purpose, healthcare providers should give patients information required for choice; patients should reflect on their purposes and values, and both should have a mutual dialog for the purpose of knowledge acquisition regarding the medical treatment. That is to say, in order to secure suitable informed consent, the dialog, it is indispensable to have a sufficient communication about medical treatment between healthcare providers and patients for achieving agreement and selection, and participation of both in decision-making. The patients can, in this way, make autonomous decision that will satisfy their own purposes and values.

***REFERENCES***

James Stacey Taylor, *Practical Autonomy and Bioethics*, New York, Routledge, 2010.

Dan W. Brock, *Life and Death: Philosophical Essays in Biomedical Ethics*, New York, Cambridge University Press , 1993.

Beauchamp, Tom L., and Childress, James F., *Principles of Biomedical Ethics*. 5th ed., New York, Oxford University Press, 2001.

Jonsen, Albert R. and Siegler, Mark and Winslade, William J., *CLINICAL ETHICS:A Practical Approach to Ethical Decisions in Clinical Medicine.* 5th ed. , McGraw-Hill Medical Publishing, New York, 2002.

# The concept of objectification in life philosophy and natural science

Marika Hirama

Department of Philosophy, Tohoku University

***Introduction***

In this presentation, I will focus on two German philosophers , who dealt with problems of human life and attempted to establish a rigorous method equivalent to that of natural science. My aim here is to elucidate the differences and similarities in the meaning of the term *'objectification'* as used in life philosophy and natural science.

## *1. Life philosophy and Heidegger's early thought*

During the time of his early studies in Freiburg (1919-23), Martin Heidegger analyzed human life in a philosophical way. In that period, *Life philosophy* still held a strong influence in Continental philosophy. At that time, with the prosperity of natural science, application of positivistic approaches to humanity had become popular. Against such currents, life philosophy generally attempted to illuminate human life in a different way to experimental psychology or biology. This movement of thought, which reflected the situation of the period, inspired the young Heidegger's ideas.

Heidegger appreciated the effort and consciousness of problems in life philosophy. He often mentioned it in his early lectures. Wilhelm Dilthey had an especially profound influence on Heidegger in forming a perspective from which to approach human life. Heidegger shared the motivation of Dilthey to search for life's strict expression in terms other than those of natural science.

## *2. Differences in attitude toward scientific objectification between Heidegger and Dilthey*

The two philosophers take contrasting attitudes, however, toward the objectification of natural science. Dilthey, especially in the autumn of his life, wrestled with life's objective expression. He tried to express the inner structure of life objectively in the relation to the historical world. His final aim was to make a science of human life which bears comparison with natural science.

For the purpose of research into human life he avoided the metaphysical route and focused somewhat on evaluation of the empirical method. This was because it was important for him not to transcend but to base his thinking on each actual experience. So he appreciated the own value of natural science and adopted the criterion of scientific objectification, which is formed by generalization.

On the contrary, Heidegger rejected scientific objectification radically. He thought that human life is never expressed in its own structure in such a way. So he tried to generate the original method with which to approach human life not relying on the scientific objectification.

## *3.Dilthey's project of human studies*

Dilthey is known as a founder of human studies (*Geisteswissenshaften*) as a domain independent of natural science. According to him, human beings are both natural and historical beings. And the object of human studies is historical human life, which is never grasped by the scientific *explanation.* The historical human life is only approached by *understanding.* Understanding never aims to build universal principles like natural science. It aims rather to describe the individual, which always takes its own position in each historical context.

At the same time Dilthey attempted to make a bridge between a human individual life and objective spirit. He thought that every individual life is comprehended in a common historical world. Furthermore, each individual receives each meaning of presence from this world. He also thought that a finite individual life can express and understand itself objectively or universally in a similar way to natural science by way of human studies. So according to him natural science and human studies are concerned with two different realms of life, but both are equally strict sciences.

In this way, although he clearly distinguished the methods of natural science and human studies, eventually he relied on scientific objectivity, namely, universal and valid objectivity, to secure the academic rigor of human studies.

Here we can find the great difference between Dilthey and Heidegger.

## *4. The genesis of the scientific objectification*

More radically than Dilthey, Heidegger thought that human lives can never be expressed *objectively* in the meaning of natural science. Because he thought that by the process of such objectification life is separated from itself *(Entlebung)*. He thought the genesis of the scientific objectification as figured below.

*Life's daily region*

*instability
*under the control of the accidental event or each individual tendency
*continual deficiency and complacence
*uncertainty

→

*Tendency to stabilize and get the possibility of prediction

↓

*Tendency to generalize and objectify tendency to build universal principals

↓

*Readiness for the occurrence of each science

According to Heidegger, life 's realm is always exposed to instability and uncertainty. It's instance is for example unforeseen accident and especially each person's death. He thought that such unstable characteristic of life made ready for scientific attitudes of objectification. However, he thought that life itself would never be understood in this way like other particular sciences, which begin with the tendency to stabilize. Life itself is essentially uncertain and instable. Heidegger called the tendency to stabilize *the fall (Ruinanz)*. And in order to trace back to the origin which doesn't suffer the tendency to objectify, philosophy of life must proceed against this tendency.

## *5. Objectification to which philosophy should aim*

But on the other hand, philosophy as one science (*als Wissenschaft*) can never be completely separated from *objectification.* It needs a strict formation of concepts. So Heidegger attempted to form concepts without injuring the activity or historicity of life. Heidegger didn't reject the objectification itself. He tried, however, to regenerate the meaning of objectification which never depends on scientific meaning.

For Dilthey, the main problem of human studies was describing the individual. Therefore each individual needs to overcome its finiteness of individuality in order to express and understand itself not arbitrary but objectively. For that purpose the existence of the human history, community, or culture that incorporates the individual were very important. Understanding the individual experience can be accomplished sufficiently only through the historical world which is common and open for all the human spirit.

On the contrary, Heidegger thought that the finiteness of life can never be overcome and rather philosophy should go along with this finiteness. He became conscious of a deficiency in describing the individual life as Dilthey had done. Expression by describing has always a tendency to separate from the finite life and to tend toward the infinite.

According to Heidegger, philosophical objectivity means "*not being apart from the acting life*". Philosophical approaches to human life should always be coordinated with each irreplaceable acting life. The meaning or criterion of objectivity in philosophy is never fixed and rather it should be constantly renewed. For that purpose the objectification he aimed to has always a characteristic of incompleteness.

In his early lectures, Heidegger mainly tried to disclose the wrong application of objectification to human life. So in his descriptions negative expressions appeared frequently. He was in that time on the way to discover his own philosophical attitude different from the methods of natural science and also different from that of Dilthey. And eventually in "Being and time"(1927), he presented first his own systematical construction of concepts. Then his target of consideration diverted from life to *being.* His research into strict methodologies led him to investigate the meaning of *being.* This transition of the theme occurred through his attitude toward philosophical objectification, which continually requires renewal to be along with acting life.

**References:**

Heidegger, M., *Grundprobleme der Phänomenologie* ; *Gesamtausgabe Band*58 : Vittorio Klostermann, Frankfurt am Main, 1993

···*Phänomenologische Interpretation zu Aristoteles / Einführung in die phänomenologische Forschung* ; *Gesamtausgabe Band*61 : Vittorio Klostermann,Frankfurt am Main, 1985

Dilthey, W., *Der Aufbau der Geschichtlichen Welt in den Geisteswissenshaften* ; *Gesammelte Schriften Band* Ⅶ : B.G.Teubner Stuttgart , 1926

Makkreel, A, R., *Dilthey- Philosopher of the Human Studies* ; Princeton University Press, 1975

# On the Myth-Making Function in Bergson

Koki Tamura (Department of Philosophy, Tohoku University)

## Introduction

### Purpose

To show clearly the originality of 'the myth-making function' (la fonction fabulatrice) in Henri Bergson through a comparison with 'the creative imagination' (l'imagination créatrice) in Théodule Ribot

### Background

- According to Bergson, the myth-making function is the virtual instinct in human being that restrains intelligence from excessive reflection.
- Several studies on the myth-making function have focused on the relation between instinct and intelligence.
- Bergson also insists that the myth-making function is a sort of imagination, but yet there is a difference between the function and psychological imagination.

## Methods & Materials

### Methods

- To concentrate on following issues:
  **1. imagination and intelligence in Bergson and Ribot**
  **2. imagination and emotion in Bergson and Ribot**
- To analyze both descriptions about the relation between imagination and intelligence, and also imagination and emotion

### Materials

- Intelligence is guided in fact by present perceptions or by that more or less vivid residue of perception called recollection (MR, 126).
- it [a virtuality of instinct, the residue of instinct] cannot exercise direct action, but, since intelligence works on representations, it will call up ''imaginary'' ones, which will hold their own against the representation of reality and will succeed, through the agency of intelligence itself, in counteracting the work of intelligence (MR, 124).
- the emotion felt by a man in the presence of nature certainly counts for something in the origin of religion. But, we repeat, religion is less a fear than a reaction against fear, and it is not, in its beginnings, a belief in deities (MR, 160).
- this demand [a fundamental demand of life] has called into being the myth-making faculty; the myth-making function is thus to be deduced from the conditions of existence of the human species (MR, 207).

- the creative imagination has the faculty of *thinking analogically* […] as an essential and fundamental element in the order of intelligence (IC, 22).
- The imagination in the order of intelligence is equivalent to the will in the order of action (IC, 6).
- the creative imagination implicates affective elements [, and] all inventions presuppose a demand, a desire, a tendency, an impulse (IC, 27).
- All the creations are useful practically and a demand for life has produced them (IC, 38).

## Conclusion

### Conclusion

The myth-making function is

(1)the creative function that makes representations; therefore the myth-making function can take the place of intelligence. However, the same thing may be said of the creative imagination.

(2)the function that is made by *the emotion*, in other words, the demand of life makes the myth-making function. On the other hand, the creative imagination is not made by any emotions, but only may be affected by emotions.

### Future Discussions

Why can the human will to live outwits *the nature* that made insects, animals, human beings and so on, by means of the myth-making function or intelligence?

## Results & Discussions

### Results & Discussions

- Both the myth-making function and the creative imagination make representations that look just like present perceptions to disturb excessive intellection, being affected with emotions (for example, fear, pity, joy and so on).
- Bergson divides the emotions into two groups:
  **(1) infra-intellectual emotion**
  **(2) supra-intellectual emotion**
- In Bergson's view, in fact, there are some emotions that are excited by perception and representation. Generally speaking, psychologists discuss these emotions**(1)**.
- However, there is also the emotion as the demand of life that forms the basis of all the creation and stimulates the myth-making function to make representations, images, mythology, religious ceremonies, literatures, etc**(2)**.
- The myth-making function and the creative imagination are more or less similar, but Bergson clarifies not only the source of imaginative creations but also the source of imagination(the myth-making function). In this sense, the myth-making function is distinct from the creative imagination.

### References


- Bergson, Henri, *Les deux sources de la morale et de la religion*, PUF, 1932/2008. (MR)
- Deleuze, Gilles, *Le bergsonisme*, PUF, 1966/1968.
- Jankélévitch, Vladimir, *Henri Bergson*, PUF, 1959/2008.
- Ribot, Théodule, *Essai sur l'imagination créatrice*, Félix Alcan, 1900/1921. (IC)
- -------------------, *La logique des sentiments*, Félix Alcan, 1905.
- Violette, René, *La spiritualité de Bergson*, Edouard Privat, 1968.
- Worms, Frédéric, *Bergson ou les deux sens de la vie*, PUF, 2004.

# ‘Prolegomena’ Revisited

Touhoku University, Depertment of Philosophy, Masatoshi Echigo

## Introduction

Husserl presented the structure of sciences as systems of right knowledge in the ‘Prolegomena’ in his *Logical Investigations*. That is what he calls “pure logic”. Sciences have the character of a system of knowledge precisely because they contain pure logic in themselves. To defend pure logic, in ‘Prolegomena’ Husserl denies psychological interpretations of logic, relativistic arguments to truth, or the skepticism to right knowledge. The essential argument among these arguments is the criticism of Protagorean skepticism; Husserl thinks that every relativism or skepticism has the Protagorean view in common.

## Protagorean skepticism and Husserl’s criticism of it

Protagorean skepticism claims that the individual man is the measure of all things. “For each man that is true which seems to *him* true, one thing to one man and the opposite to another, if that is how he sees it”(LI). Thus “all truth (and knowledge) is relative - relative to the contingently judging subject”. Hence Protagorean skepticism denies general truth or truth in itself. Husserl refutes Protagorean skepticism “in an objectively valid manner”: “laws such as the law of contradiction have their roots in the mere meaning of truth”, and “from these it follows that talk of subjective truth, that is one thing for one man and the opposite for another, must count as the purest nonsence”. This is also because “in setting up his theory he (the skeptic) is making a claim to be convincing to others, a claim presupposing that very objectivity of truth which his thesis denies”.

## The first problem of the criticism

Husserl's criticism is relevant to a kind of Protagorean skepticism. In this kind of skepticism the skeptic himself knows what so called truth is or what right knowledge is. Otherwise he could not refute the other theories in general and set his own theory as true.
Can Husserl’s criticism eliminate all kinds of skepticisms? Could not there remain any kind of skepticism? It seems that a skepticism which can avoid this criticism remains. That is Pyrrhonian skepticism. What I call here Pyrrhonian skepticism is a theory which claims that “if people who hold beliefs posit as real the things they hold beliefs about, while Skeptics(Pyrrhonian skeptics) utter their own phrases in such a way that they are implicitly cancelled by themselves, then they cannot be said to hold beliefs in uttering them”(OP), and hence that “in uttering these phrases they(Pyrrhonian skeptics) say what is apparent to themselves and report their own feelings without holding opinions”. This skepticism implicitly shows that it is insufficient to draw a mere figure positing ego and objects or contents. The very functions of various assessments (doubtful, sure and so on) of objects or contents by ego must be considered. Then truth or knowledge cannot be defended unless Pyrrhonian skepticism, which does not decide whether or not truth in itself exists is refuted. Thus the task of refuting this type of skepticism still remains. This is the first problem which Husserl’s criticism involves.

## The second problem of the criticism

It follows that Husserl so to speak naively posits being-in-itself, such as truth in itself because he doesn’t focus on acts which assess ontological entities of objects in the “Prolegomena”; this is the second problem of Husserl’s criticism. When skepticism is given right consideration, it reveals various acts of comprehending objects by ego. Indeed, skepticism denies truth and knowledge. Therefore it is essential to affirm general truth in itself to defend sciences and knowledge. But is it not until skeptical problems are addressed rightly that we are able to identify and approach general, epistemological problems about subject and its acts?
In this sense, it is interesting that Husserl consistently and naively posits being-in-itself, such as truth in itself in *Logical Investigations*. It is true that the way that how being-in-itself exist is clearly distinguished from how real things exist, but when someone asks "so, where and how is that being-in-itself", there is no choice but to answer "somewhere and somehow" as far as *Logical Investigations* goes. Another detailed consideration about ontological entities of being-in-itself is necessary.
This does not necessarily mean that the arguments about epistemology in *Logical Investigation* are naive. As we know, Husserl addressed epistemological problems including how we acquire the general and what intentionality is in “Investigation II”, “Investigation V”, and “Investigation VI”. Though these investigations are thorough; being-in-itself remains ambiguous. This is partly because Husserl did not focus on elements of ego in considerations of the “Prolegomena”. This is a pity, though it is all the better for frequent criticisms of Husserl’s theory about being-in-itself. If Husserl had already contemplated various assessments of objects by ego in *Logical Investigations*, the arguments about ontological entities of being-in-itself would be more interesting.

## Conclusion

In summary, Husserl's criticism of skepticism can be summarized as follows: Husserl posits truth in itself because he claims all theories about logic presuppose truth or knowledge and he also defends them, but there is room for doubt that truth in itself exists in a rigorous sense because his argument in the ‘Prolegomena’ does not consider Pyrrhonian skepticism. On top of that being-in-itself is left ambiguous because Husserl overlooked the problem of assessment acts by ego. It might possibly seem that the way in which he addresses the problems from the ‘Prolegomena’ is non sense, but we must not evaluate his arguments such a way. This is because they are meaningful when they are considered in the course of the development of Husserl’s thought. In fact we should contemplate even obvious faults in his arguments by contrast with Husserl’s later thought. This task is left to contemporary researchers.

Bibliography
Empiricus, Sextus, edited by Annas, Julia and Barnes, Jonathan. Outlines of Scepticism. Cambridge: Cambridge University Press, 2000. (quoted as OP)
Husserl, Edmund. *Logische Untersuchungen*(Husserliana XIII), den Haag: Martinus Nijhoff, 1975.
——, translated by Findlay, J. N. *Logical Investigations*. Volume I, London and New York: Routledge, 2001. (quoted as LI)

- The problem of the relationship between individuality and universality in Hegel`s philosophy


- Yuusuke Minegishi
- Department of Literature, Tohoku University


- Introduction

- One of the most important motives in Hegel`s philosophy is that of the subjectivity. This motif is derived from the argument over the relationship between individuality and universality in the medieval times. ―It is further formed by Hegel`s attempt to respond to the problem of the character and status of cognition, which has been one of the matters of concern for Modern philosophy since Descartes.

- 1.

- It is characteristic of Hegel, that the problem of individuality and universality receives treatment as " -logical- " in Hegel`s sense of the word, that is to say it is treated as a -metaphysical problem-. The common sense and common place understanding of "individuality"is that it is a word that signifies this or that particular one who recognizes or thinks. Hegel`s understanding however is different. According to his theory, individuality and universality are not different from each other originally.
- His thought is based on the notion, that the universality is a movement which develops itself. Universality has, unlike Aristotelian substance (ουσια), not stationary attributes. It forms itself however into one conclusive process by determining itself through its ownself, that is, by particularizing itself.― In this way the character of the universality as subjectivity consists in developing a process. Hegel recognizes the individuality as the subjectivity in the one process, for this is the conclusion which is drawn from the nature of the subjectivity.

- 2.

- It is significant that the aim and end of the process is nothing other than this subjectivity itself. The subjectivity arrives back upon itself through the movement of determination and particularization. This movement is called "Reflexion". ―The notion of arriving back implies that the subjectivity, which goes through the process, is by nature that, which it has been. ―But "by nature" means by no means that it has been so before attributes have been predicated in the case of substance. ―"That what it has been by nature" however reveals itself with the principle "to know"―; and it is nothing else but "to know".
- Therefore this self-developing-process of subjectivity functions as a bringing out of the internal structure of self-consciousness, which is the most important motif in Modern philosophy.
- We are apt to delude ourselves into believing that the self-consciousness is self-evident to anyone. it is not easy, however, to state what it is in its essence. To solve this difficulty, Hegel provides an answer with his theory of the self-development of subjectivity as arriving back upon itself. ―This is also expressed as "the Concept is the personality". The term "concept" is the key-word not only for his "logic", but for his whole system of philosophy, permates his notion of subjectivity which itself contains universality, individuality and particularity as its element.

- 3.

- The notion "personality" as a philosophical term has been formed by degrees through efforts to understand the meaning of the Holy Trinity (Father, Son and the Holy Spirit) in Christian theology. ―St. Augustine of Hippo(354~430) for example, explains the notion of " ―one essence and three persons― " by means of triplicity of the mind ( memory, intelligence and volition ).―
- Nicholas of Cusa ( 1401~1464 ) is the one who opens the way for Hegels theory of subjectivity. ―In the one of his chief works " ―On no other― ", Nicholas develops his theory of self-determination of the universality (―i.e. God ) with the notion of the " ―no other―". ―Everything that exists is, so far as it exists, determined. The cognition, which recognizes it is also determined. For existence and cognition the "―no other― " is their principle and therefore not differs from themselves. ―From this viewpoint Nicholas understands the individuality and universality as a unity.
- In the foundation of Hegel`s subjectivity theory Nicholas`s thought plays an important role in establishing the notion that the universality is a movement which develops itself. As the background of Nicolas`s " no other " plays the theological motif creation. It is however not to disregard that Nicholas would show the creator and the creature not as two quite different things but they are in unity. Creation is unlike this or that act which is done commonly, by no means any particular performance at this or that point in time. It means to bring the creature into that what it has been. Nicholas learns this thought by the Latin commentaries of the Bible written by Meister Eckhart.
- We should not indeed forget that Nicholas and Eckhart`s thought have a theological origin. We must however on the other hand take their incomparable and so profound thought in order to understand Hegel`s subjectivity and personality of the concept more deeply and radically. And we can gain an wider perspective for the subjectivity, which is one of the most important motives of Modern philosophy and metaphysic in general. The problem of subjectivity is a problem of metaphysics which requires furtherexamination from more far-reaching perspective.

- Bibliography


- G.W.F. Hegel, Wissenschaft der Logik, Das Sein (1812), Hamburg,1999
- G.W.F. Hegel, Wissenschaft der Logik, Die Lehre vom Wesen (1813), Hamburg, 1999
- G.W.F. Hegel, Wissenschaft der Logik,Die Lehre vom Begriff (1816), Hamburg, 2003
- ニコラス・クザーヌス『観察者の指針、すなわち非他なるものについて』松山康國訳、塩路憲一訳註、ドイツ神秘主義叢書7、創文社、一九九二年
- アウグスティヌス、『三位一体』泉治典訳、アウグスティヌス著作集28、教文館、二〇〇四年
- エックハルト、『創世記比喩解』中山善樹訳、エックハルトラテン語著作集1、知泉書館、二〇〇五年
- エックハルト、『知恵の書註解』中山善樹訳、エックハルトラテン語著作種2、知泉書館、二〇〇四年

# Hume on Logic and Demonstration

SUGAWARA Hiromichi (Philosophy, D3)
Graduate School of Arts and Letters, Tohoku University

**Introduction**

*As is commonly known, the 18th century Scottish philosopher David Hume presented seven philosophical relations in his Treatise. Later these were divided into two subjects as all objects of human reasoning or inquiry in his Enquiry; 'relations of ideas' and 'matters of fact'. The former are objects of our knowledge and certainty. These were resemblance, contrariety, degrees in quality, and proportions in quantity and number. According to him, these relations are intuitively certain, except equality or any exact proportion in the relations of proportions in quantity or number. Equality or any exact proportion is demonstrably certain. Besides the question of what intuition might be as an operation of our minds, demonstrations relating to intuition in Hume's arguments are significant. Because Hume was primarily concerned with revealing faculties or operations of our mind: human understanding. On the other hand, he definitely stated in his Abstract that 'the author[Hume himself, in fact] has finished what regards logic[in Book I of Treatise]', impersonating a book reviewer of it. However his arguments on human understanding doesn't surely seem to be engaged in logic at least in our time – modern formal logic. Thus Hume's logic must be considered as different mode of logic from our logic or Aristotelian school logic.*

## 1. The Early Stage of Hume's Logic

### (1) Traditional Logic in School


From Wikipedia

Aristotle's *Organon* was a core text of European universities during the 14th and 15th centuries. None the less, his *Topics*, and the like, works that take up the ways or laws by which we practically reason in various situations was rarely included in university curricula of that time. Though unlike Russell said so, Aristotle himself by no means thought little of inductive reasoning, medieval logicians, philosophers, and theologians placed high value exclusively on deductive arguments that were constructed from categorical propositions.

*Comment:
According to Gaukroger, the period between the beginning of 16th century and the publication of Boole's *Mathematical Analysis of Logic* (1847) is regarded as 'the interregnum in the history of logic'(Gaukroger intro 1).

### (2) The Heuristic Methodology

The flourishing of natural philosophy in early-modern times originates from Copernicus, and is chiefly due to the adoption of experimental methods by practitioners of natural philosophy outside the universities. This method in their inquiry depended not on deductive arguments but on inductive reasoning, or reasoning from cause to effect, as a principle of thinking. For *new* natural philosophers, unlike neo-Aristotelian natural philosophers, who had set the notions of *generalized* experiences, had to appeal to the particular experiences of natural phenomena for seeking out *new* phenomena of nature.


From Wikipedia

### (3) The Bridge between Natural Philosophy and Hume


From Wikipedia

For Francis Bacon, whom Hume considered as 'the father of experimental physics', induction is logic itself and also scientific method. He said, "we reject proof by syllogism". The reason Hume appreciated him, however, was related I think to Bacon's approach to the way our reasoning or thought should be considered together with faculties or operations of our mind. Thus Bacon is an originator, who began "to put the science of man on a new footing". Later Hume attempted to establish 'the science of man' of his own, with 'the experimental method of reasoning' from Newton's 'Rules for the study of natural philosophy' in *Principia - inductive reasoning, or reasoning from cause to effect*.

## 2. The Naturalistic View of Logic

Leibnitz's Indication of the Common Systems of Logic toward the Copiousness in Explaining the Operations of the Understanding (ATHN 4)

### (1) Hume's View of Logic

So, what does logic mean for Hume? I think that to answer that question, we should pay attention to Hume's criticism on existing logic that was taught at schools in those days. Though Hume restrainedly related the criticism in a footnote to the *Treatise*, it is significant to an understanding of his view of logic.

"This error consists in the vulgar division of the acts of the understanding, into *conception*, *judgment*, and *reasoning*, and in the definitions we give of them. […] But these distinctions and definitions are faulty in very considerable articles. […] What we may in general affirm concerning these three acts of the understanding is, that taking them in a proper light, they all resolve themselves into the first, and are nothing but particular ways of conceiving our objects. […] the act of the mind exceeds not a simple conception". (THN 1.3.7.5.n2)

### (2) Arnauld & Nicoles' View of Logic

There is a text book of logic, A. Arnauld & P. Nicole's *La Logique ou l'Art de Penser,* that Hume surely read, and which he would apparently (though partly) see as a target of his criticism on school logic. According to this book, "logic is the art of conducting reason well in knowing things, as much to instruct ourselves about them as to instruct others", and the art consists in *reflections*, which are made four operations of our mind: *concevoir*, *juger*, *raisonner*, and *ordonner* (Arnauld & Nicole 23).

However, there are plausible reasons for Arnauld & Nicole to have enumerated the operations of our mind. They aimed at educational effectiveness in presenting their material to those, who had not studied any rules or disciplines of logic. Moreover they thought that operations of our mind in reasoning are done naturally (ibid.).

## 3. A Different View of the Same Object

Hume's Criticism of a Long System of Rules and Precept by Scholastic Headpieces & Logicians (THN 1.3.15.3)

### (1) Two Definitions of Cause

Hume presented famous two definitions of cause in his *Treatise* and *Enquiry*. It is commonly said that, one is from the point of philosophical relation; the other is from the view of natural relation (THN 1.3.14.30; EHU 7.2.4).

**D1**: "An object precedent and contiguous to another, and where all the objects resembling the former are plas'd in like relations of precedency and contiguity to those objects, that resemble the latter".
**D2**: "A CAUSE is an object precedent and contiguous to another, and so united with it, that the idea of the one determines the mind to form the idea of the other, and the impression of the one to form a more lively idea of the other".
↓
In these definitions, it is essential to count them as drawn from the objects whether foreign to cause or domestic to cause. The former is independent of faculties or operations of our mind, while the latter depends on faculties or operations of our mind, that is, on the principle of '*associations of ideas*', in spite of our perceiving the same objects.

### (2) General Rules by which to Judge of Cause & Effect

On the other side, Hume presented "general rules, by which we may know when they [cause & effect] really are so". From first to third rules are articulated about 'contiguity of time and space of cause and effect', 'precedence of cause', and 'constant conjunction of cause and effect', fourth rule confirms the principle of uniformity of nature , and so on.
↓
After fixing these rules provisionally, he claimed that "here is all the Logic I think proper to employ in my reasoning". Moreover he commented on them as that "perhaps even this was not very necessary, but might have been supply'd by the natural principles of our understanding" (THN 1.3.15.3).

## Conclusion

(1) For Hume, logic is a set of provisional and elaborate rules to deal with unexperienced particular object, with the method of inductive reasoning or reasoning from cause to effect, to be aimed for a higher level of assurance, which could be strengthened by the evidences of repeated experiences and general or historical confirmations. Demonstration is simply our discovering the relations of ideas.
(2) If this is ever appropriate understanding for Hume's argument of logic, he could be practically on a par with the claim that all the reasoning we employ would result in probable reasoning, without appealing to a certain exemplar model, including proportions in number in philosophical relation.
(3) Historically speaking, he argued against the traditional scholastic doctrines of logic that had made unreflectingly or dogmatically represent *terminus* something ambiguous as materials of logic.

## 4. Hume on Demonstration as a Philosophical Relation

Let's see what Hume calls demonstration. We should notice that these four relations, including latter three relations, are presented as philosophical relation, which is applied for "particular circumstance, in which, even upon the arbitrary union of two ideas in the fancy, we may think proper to compare them" (THN 1.1.5.1).

As I said earlier, only in cases of equality or any exact proportion in the relations of proportions in quantity or number, we can determine their relations without any error. For when we do so, we are possessed of a precise standard (i.e. a unit) to judge them. But unfortunately Hume didn't exhibit an clear example of demonstrative reasoning. D. C. Stove (or Broughton, Mackie, Beauchamp & Rosenberg), for example, claimed that what Hume meant by demonstrative arguments was strictly deductively valid arguments with necessarily true or a priori true premises (Stove 35-36). It would be one of reasons that skepticism about induction and logical necessity about deduction are like two sides of the same coin in interpretation on Hume. On the other hand, D. Owen (or Beebee) interprets Hume's original form in philosophical relation of demonstration as follows (Owen 94-96).

**An Example of Demonstration of the Equality of "$5^3 + 12 = 137$"**

① We begin with intuiting that the idea of $5^2$ and the idea of 25 stand in the relation of equality each other.
② At the same time, we intuit the proposition of $5 \times 5 = 25$.
③ Then we intuit the proposition of $5^2 \times 5 = 125$.
④ And then we intuit the proposition of $5^3 + 12 = 12 + 125$.
⑤ Finally we intuit the proposition of $5^3 + 12 = 137$.

**Comment:
At least, the term 'deduction' was not used for limited expression of deductively valid arguments with necessarily true or a priori true premises in that days (Yolton 92-93; Owen 117, et al.). Hume actually used the word 'deduction' as exclusively 'reasoning' or 'argument'.

I agree basically with Owen. To be sure, he never rejected demonstrations *in itself* as the laws of thinking. But that derivation was not the principal interest of Hume. Because he gave a thought to this problem as follows.

"Truth is of two kinds, consisting either in the discovery of the proportions of ideas, consider'd as such, or in the conformity of our ideas of objects to their real existence".(THN 2.3.10.2)

**References**

ATHN: Hume, David. [1740], *An Abstract of a Book lately Published; Entitled, A Treatise of Human Nature*, in THN.
EHU: -------- [1748], *An Enquiry concerning Human Understanding*, in *Enquiries concerning Human Understanding and the Principles of Morals*, edited by L.A.Selby-Bigge, revised by P.H.Nidditch.
THN: -------- [1739-40], *A Treatise of Human Nature*, edited by L.A.Selby-Bigge, revised by P.H.Nidditch.
Arnauld, Antoine. And Nicole, Pierre. [1662], *La Logique ou l'Art de Penser: Contenant, outré les Regles communes, plusieurs observations nouvelles propres à former le iugement*.
Bacon, Francis. [1620], *The Oxford Francis Bacon: The Instauratio Magna Part II: Novum Organum and Associated Texts*, edited translated by G. Rees & M. Wakely.
Beauchamp, T. L., and Rosenberg, Alexander. [1981], *Hume and the Problem of Causation* (pp.42-45).
Beebee, Helen. [2006], *Hume on Causation* (pp.14-35).
Broughton, Janet. [1983], 'Hume's Skepticism about Causal Inferences', Pacific Philosophical Quarterly, Volume 64, (pp.3-18).
Descartes, René. [1637] *Œvres de Descartes*, Tome V et VI, publiées par C. Adam et P. Tannery.
Gaukroger, Stephen. [1989], *Cartesian Logic: an Essay on Descartes's Conception of Inference*.
Groarke, Louis. [2009], *An Aristotelian Account of Induction: Creating Something from Nothing* (pp.95-155).
Harrison, Jonathan. [1976], *Hume's Moral Epistemology*.
Jones, Peter. [1982], *Hume's Sentiments: their Ciceronian and French Context*.
Locke, John. [1689], *An Essay concerning Human Understanding*, edited by P. H. Nidditch.
Mackie, J. L. [1979], 'A Defence of Induction', in *Perception and Identity Essays Presented to a A. J. Ayer with his Replies to them*, edited by G. Macdonald (pp.115-116).
Moody, E. A. [1966], 'The Medieval Contribution to Logic', in Studies in Medieval Philosophy, Science, and Logic.
Owen, David. [1999], *Hume's Reason*.
Serjeantson, R. C. [2005], 'Hume's General Rule and the 'Chief Business of Philosophers'', in *Impressions on Hume*, edited by M. Frasca-Spada and P. J. E. Kail (pp.187-212).
Stove, D. C. [1965], 'Hume, Probability, and Induction', in *David Hume: Critical Assessments* Volume 2, edited by Stanley Tweyman.
Yolton, John. [1970], Locke and the Compass of Human Understanding.
Zabeeh, Farhang. [1960], 'Hume's Scepticism with regard to Deductive Reason', in *David Hume: Critical Assessments* Volume 1, edited by Stanley Tweyman.

Tohoku University Scienceweb GCOE
"Weaving Science Web beyond Particle-matter Hierarchy"
The 4th GCOE International Symposium

# The rationality of the Precautionary principle: making the precautionary principle more applicable

FUJIO Yasuhiko
Graduate School of Arts and Letters, Tohoku University

## Introduction

### Scientific uncertainty

We must make decisions in circumstances in which insufficient knowledge of possible high risk events compromises the reliability of scientific analysis.

### The rationality of the Precautionary principle

The Precautionary Principle (PP) requires us to adopt approaches in order to protect human health and the environment despite a lack of sufficient scientific certainty.

Some doubt the applicability of PP, claiming that it lacks a rational basis and may thus lead to irrational conclusions.

This might suggest that we cannot make public policy decisions by means of the precautionary principle alone.

**I would like to examine the notion of "rationality" and to emphasize the implications of "deliberative democracy" with regard to the better application of PP.**

## Risk analysis and management

### Risk-Cost-Benefit Analysis

There exists an important question: introducing the new technology, can we make profits commensurate with costs and risks?

We need "risk-cost-benefit analysis(RCBA)": the method of calculating cost of the introduction of new technology and predicting risks and benefits.

### Problems of risk management

**RCBA (risk-cost-benefit analysis)**: Such procedures embody uncertainties; models used in RCBA are not always perfectly sophisticated models of real events.

In principle, we never entirely know what happened, happens and will happen in the real world, which makes us more modest about our actions that might pose harm to human health or the environment.

## Scientific Uncertainty

### The limits of our knowledge and science

As science is the process for exploring veiled realms, in cutting-edge research scientific knowledge is constantly renewed by new scientific discoveries.

There are, however, some cases where we cannot elucidate the causal mechanism of complex phenomena at the present time due to the complexity of phenomena (ex. global warming)

Thus, scientific uncertainty is due to the plasticity or limits of our knowledge.

### Attitudes towards scientific uncertainty

In regulating or prohibiting a certain product or procedure, it seems to be necessary to prove the causal relationship between products and the possible harmful effect.

As we know, since scientific knowledge might be renewed, we must not have too much confidence in science.

**Therefore, we, especially policy-makers, must keep in mind that science has limitations.**

## Precautionary Principle

### The Emergence of PP

PP has been adopted in the legislation for protection of human health or environment.

The most prominent and frequently cited version of PP is probably the 1992 *Rio declaration*:

> **" In order to protect the environment, the precautionary approach shall be widely applied by States according to their capabilities. Where there are threats of serious or irreversible damage, lack of full scientific certainty shall not be used as a reason for postponing cost-effective measures to prevent environmental degradation. "**

One of the most remarkable characteristics of PP is that even if there exist no full scientific evidences it is possible and legitimate to regulate or prohibit products or procedures which might pose serious and irreversible damage to human health or the environment.

### The defects of PP

Opponents characterize the definition of PP as too vague to serve as a regulatory standard.

Because of its vagueness PP might lack rational foundation as the principle for action.

### Is PP rational?

Perhaps its vagueness let us use PP arbitrarily; the government use PP in order to defend the domestic market from imported goods.

It might be impossible that we lead to rational consequences by means of PP alone.

Therefore, we have to consider the implication of PP as a norm in the context of society.

## The future generations

### Effects on the future generations

In the era of modern science and technology there exist threats to health or the environment of the future generation(ex. nuclear waste, greenhouse gas effects etc.)

Must we pay homage to the rights of the future generation which doesn't exist at present?

### Moral obligations to the future generations

Intergenerational ethics: requires us to keep in mind the benefits of the future generations.

We have to preserve the living conditions of the future so as not to damage their welfare.

## Deliberative Democracy

### Social justice and democratic legitimacy

There is an ideal that all participants in public decision making should be well informed and in dialogue with each other voluntarily.

This ideal is based on the belief that reasonable consensus should be derived from dialogues.

### Deliberative democracy and PP

Precautionary measures are fundamental elements of the ideal democratic decision making of risks imposed on the future generations by the present generation.

We must pay homage to the future's ability to make decisions in order for them to be informed well and in dialogue voluntarily.

## Conclusions

- **We must perform risk management on the grounds that there might be scientific uncertainty.**
- **Without support of social consensus, the PP would not function well.**
- **We must maintain conditions of living by which the future generations can live, as well as our own conditions.**
- **In deliberative democracy we can take precautionary measures to make sustainable developments possible.**

## Reference

・松王政浩、「予防原則に合理的根拠はあるのか」、21世紀倫理創成研究 = Journal of Innovative Ethics（1）、神戸大学倫理創成プロジェクト、2008年
・Johnson, G.F., *Deliberative Democracy for the Future: The Case of Nuclear Waste Management in Canada*, University of Toronto Press, 2008
・Sandin, P., "Common-sense precaution and varieties of precautionary principle", In *Risk: Philosophical Perspectives*, ed. Lewens, T., Routledge,2007
・World Commission on the Ethics of Scientific Knowledge and Technology, *The Precautionary Principle*, the United Nations Educational, Scientific and Cultural Organization, 2005

# Viscosity solutions on a Riemannian manifold

**Abdullah Kizilay**
Mathematical Institute
Tohoku University
*sa9m39@math.tohoku.ac.jp*

## Preliminaries

### Level Set:

For an almost everywhere differentiable function $u : \mathbb{R}^N \times [0,T) \to \mathbb{R}$ ($\nabla u \neq 0$ a.e.), define level set at time $t$ as,

$$\Gamma_t = \Big\{x \in \mathbb{R}^N : \ u(t,x) = 0\Big\},$$

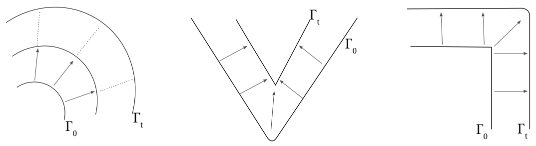


**Figure 1.** Evolving surfaces with their unit normal vectors.

### Surface Evolution Equation, In general

$\boxed{V = G(t, x, \mathbf{n}, \nabla \mathbf{n})} \cdots\cdots \to$

using level set representation

$$u_t + F(t, x, u, \nabla u, \nabla^2 u) = 0$$

where,
$F : (0,T) \times \Omega \times \mathbb{R} \times \mathbb{R}^n \times \mathcal{S}^n \to \mathbb{R}$
$\mathcal{S}^n$, space of symmetric matrices.

for $t > 0$, and $x \in \Gamma_t$
$V$ : normal velocity $\left( := \frac{u_t}{|\nabla u|}\right)$
$\mathbf{n}$ : unit normal vector $\left( := \frac{\nabla u}{|\nabla u|}\right)$

### Example:

**1.** $V = H$ (Mean curvature flow) $\Longrightarrow u_t + |\nabla u| \mathrm{div}\left(\frac{\nabla u}{|\nabla u|}\right) = 0$
**2.** $V = K$ (Gaussian curvature flow)

### Semijets:

*Let $f : (0,T) \times M \to \mathbb{R}$ be a lower semicontinuous function (upper semicontinuous function). Define a parabolic second order* ***subjet*** *(**superjet**) of $f$ at a point $(t_0, x_0) \in (0,T) \times M$ by*

$$\mathcal{P}^{2,-} f(t_0,x_0) (\mathcal{P}^{2,+} f) := \left\{ \begin{array}{c} \big(D_t\varphi(t_0,x_0), D_x\varphi(t_0,x_0), D_x^2\varphi(t_0,x_0)\big) : \varphi \in C^{1,2}((0,T)\times M) \\ \text{and } f - \varphi \text{ attains a local minimum (max.) at } (t_0,x_0) \end{array} \right\}$$

*where, by $\varphi \in C^{1,2}((0,T) \times M)$, we mean that $\varphi$ is once continuously differentiable in $t \in (0,T)$, and twice continuously differentiable in $x \in M$.*

Here, $\mathcal{P}^{2,-} f(t,x)$, and $\mathcal{P}^{2,+} f(t,x)$ are subsets of $\mathbb{R} \times T_xM^* \times \mathcal{L}_s^2(T_xM)$, where $T_xM^*$ is the cotangent space at $x \in M$, and $\mathcal{L}_s^2(T_xM)$ denote the space of bilinear forms on $T_xM$, and $\varphi$ is defined in a neighbourhood of $(t_0, x_0)$.

### Cauchy-Dirichlet problem:

We consider the following Cauchy-Dirichlet problem of the form:

$$[CDP] := \begin{cases} u_t + F(t, x, u, Du, D^2u) = 0 \text{ in } (0,T) \times \Omega \\ u(t,x) = h(t,x), (t,x) \in [0,T) \times \partial\Omega, \\ u(0,x) = \psi(x), x \in \overline{\Omega}, \end{cases}$$

where $u$ is the function of $(t,x) : [0,T) \times M \to \mathbb{R}$ and $M$ is a finite-dimensional complete Riemannian manifold, $Du, D^2u$ mean $D_xu(t,x), D_x^2u(t,x)$, $\Omega$ is open and bounded in $M$, $T > 0$, $h \in C^{1,2}\big([0,T) \times \overline{\Omega}\big)$ and $\psi \in C^2(\overline{\Omega})$.

## Definition(Viscosity solution)

*Let $M$ be a Riemannian manifold, and $F \in C(\mathcal{X}, \mathbb{R})$. We say that an upper semicontinuous function (lower semicontinuous function) $u : [0,T) \times \overline{\Omega} \subset M \to \mathbb{R}$ is a* ***viscosity subsolution*** *(**viscosity supersolution**) of* [CDP] *on $[0,T) \times \overline{\Omega}$, if*

$$\begin{cases} u(t,x) \leq (\geq) h(t,x), (t,x) \in [0,T) \times \partial\Omega, \\ u(0,x) \leq (\geq) \psi(x), x \in \overline{\Omega}, \end{cases}$$

*hold for all $(t,x) \in (0,T) \times \Omega$, and for $(p, \zeta, A) \in \mathcal{P}^{2,+}u(t,x) (\in \mathcal{P}^{2,-}u(t,x))$,*

$$p + F(t, x, u(t,x), \zeta, A) \leq 0 \ (\geq 0)\ ,$$

*hold.*
*If $u$ is both a viscosity subsolution and a viscosity supersolution of* [CDP], *we say that $u$ is a* ***viscosity solution*** *of* [CDP].

Here,

$$\mathcal{X} := \Big\{(t, x, r, \zeta, A) : t \in [0,T], x \in M, r \in \mathbb{R}, \zeta \in T_xM^*, A \in \mathcal{L}_s^2(T_xM)\Big\}.$$

## Key Tools

### Properness of $F$:

*We will say that a function $F : \mathcal{X} \to \mathbb{R}$ is* ***proper*** *if satisfies;*
*(i) $F$ is degenerate elliptic provided that*

$$P \leq Q \Longrightarrow F(x, r, \zeta, Q) \leq F(x, r, \zeta, P),$$

*(ii) $F$ is nondecreasing in the variable $r$.*

### Exponential map:

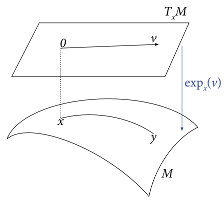


### Jacobi field:

Let $\gamma : [0,l] \to M$ be geodesic, and
$\alpha(t,s) : [0,l] \times [-\varepsilon, \varepsilon] \to M$ variation through geodesics $\alpha(t,s) = \gamma(t)$. Any vector field satisfying the Jacobi equation

$$\left(\frac{\nabla}{dt}\right)^2 V = R\big(\gamma'(t), V(t)\big)\gamma'(t)$$

along a geodesic is called a **Jacobi field**.

### Proposition:

*For the function $\varphi(x,y) = d(x,y)^2$ on $M \times M$,*
*(1) If $M$ has nonnegative sectional curvature then*

$$\Big\langle D^2\varphi(x,y)(v, L_{xy}v), (v, L_{xy}v)\Big\rangle \leq 0.$$

*(2) If $M$ has nonpositive sectional curvature then*

$$\Big\langle D^2\varphi(x,y)(v, L_{xy}v), (v, L_{xy}v)\Big\rangle \geq 0.$$

Here, we denote by $L_{xy}$ the parallel transport along the unique minimizing geodesic connecting $x$ to $y$

## Theorem(Comparison Principle)

*Let $\Omega$ be a bounded open subset of a complete finite-dimensional Riemannian manifold $M$ with nonnegative sectional curvature, and $F : \mathcal{X} \to \mathbb{R}$ be proper for each fixed $t \in (0,T)$ and intrinsically uniformly continuous with respect to $x$, uniformly in $t$. Let $u \in USC([0,T) \times \overline{\Omega})$ be a subsolution and $v \in LSC([0,T) \times \overline{\Omega})$ a supersolution of* [CDP]. *Then $u \leq v$ on $[0,T) \times \Omega$.*

$M$ has nonnegative sectional curvature
⇓ implies
$P \leq L_{yx}(Q)$ and degenerate ellipticity
⇓ implies

$$F(t, y, r, L_{xy}\zeta, Q) - F(t, x, r, \zeta, L_{yx}Q) \leq w\big(\alpha d(x,y)^2 + d(x,y)\big).$$

⇓ means
$F$ is intrinsically uniformly continuous.

## References

[1] M.G. Crandall, H. Ishii, P.-L. Lions, *User's guide to viscosity solutions of second order partial differential equations*, Bull. Amer. Math. Soc. 27 (1992), 1-67.

[2] D. Azagra, J. Ferrera, B. Sanz, *Viscosity solutions to second order partial differential equations on Riemannian manifolds*, Journal of Differential Equations, Vol. 245(2008), 307-336.

[3] Y. Giga, *Surface evolution equations. A level set approach*, Monographs in Mathematics, 99. Birkhauser Verlag, Basel, 2006.

# Smoothness of densities of generalized locally non-degenerate Wiener functionals

Nobuaki NAGANUMA
Mathematical Institute, Tohoku University

## 1 Introduction

Several criteria for existence of smooth densities of Wiener functionals are known in the framework of Malliavin calculus. In this presentation, we introduce the notion of generalized locally non-degenerate Wiener functionals, and prove that they possess smooth densities. The result presented here unifies earlier works by Shigekawa [3] and Florit-Nualart [2]. Using the criteria, we investigate existence of smooth densities for the functionals which fail the following properties:

1. Functionals themselves have higher order derivatives,
2. Determinants of the Malliavin covariance matrices have higher order negative moments.

## 2 Framework and Main Result

**Definition 1** (Classical Wiener space)**.** Let $N \in \mathbf{N}$.

$$\begin{aligned} W &:= \{x : [0,1] \to \mathbf{R}^N, \text{continuous}, x(0) = 0\}, \\ \|x\|_W &:= \max_{s\in[0,1]} |x(s)|_{\mathbf{R}^N}, \quad x \in W, \\ \mathcal{H} &:= \{h = (h^1, \ldots, h^N) \in W; \\ &\qquad h_j \text{ is absolutely continuous w.r.t. Lebesgue measure} \\ &\qquad \text{and } \dot{h}_j \text{ is square integrable}\}, \\ (h,k)_{\mathcal{H}} &:= \int_0^1 (\dot{h}(s), \dot{k}(s))_{\mathbf{R}^N}\, ds, \quad h,k \in \mathcal{H}, \\ P &: \text{Wiener measure.} \end{aligned}$$

Under the measure $P$, the coordinate process $B_t(x) := x(t)$ defines the $N$-dimensional Brownian motion starting from the origin.

**Definition 2** ($\mathcal{H}$-derivative)**.** The directional derivative of Wiener functional $F : W \to \mathbf{R}^d$ along to $h \in \mathcal{H}$ is defined by

$$(DF(x), h)_{\mathcal{H}} := \frac{d}{d\varepsilon} F(x + \varepsilon h)\Big|_{\varepsilon=0}.$$

**Definition 3** (Sobolev space on Wiener space)**.** Let $n \in \mathbf{N}$ and $1 < p < \infty$.

$$\begin{aligned} \|F\|_{\mathcal{D}^{n,p}(W;\mathbf{R}^d)} &:= \sum_{k=0}^{n} \|D^k F\|_{\mathcal{L}^p(W;\mathscr{H}^k(\mathcal{H};\mathbf{R}^d))}, \\ \mathcal{D}^{n,p}(W;\mathbf{R}^d) &:= \overline{\mathscr{P}(W;\mathbf{R}^d)}^{\|\cdot\|_{\mathcal{D}^{n,p}(W;\mathbf{R}^d)}}. \end{aligned}$$

Here, we introduce the notion of generalized locally non-degenerate Wiener functionals and state the main result.

**Definition 4** ($(A,n,q)$-locally non-degenerate)**.** Let $A \subset \mathbf{R}^d$ be an open set, $n \in \mathbf{N}$ and $1 < p, q < \infty$. A functional $F \in \mathcal{D}^{1,p}(W;\mathbf{R}^d)$ is said to be $(A,n,q)$-*locally non-degenerate* if there exist $1 < q_1, \ldots, q_n < \infty$ and some $\mathcal{H}^d$-valued functional $U = (U^1, \ldots, U^d)$ such that

(LND1) $1/q_1 + \cdots + 1/q_n = 1/q$,

(LND2) $U \in \mathcal{D}^{m,q_m}(W;\mathcal{H}^d)$ for any $1 \le m \le n$,

(LND3) $1_{\{F\in A\}}[(DF^j, U^k)_{\mathcal{H}} - \delta_{jk}] = 0$ $\mu$-a.s. for any $1 \le j,k \le d$.

Here, $\delta_{jk}$ denotes Kronecker's delta.

**Theorem 5.** *Let $1 < p, q < \infty$ satisfy $1/p + 1/q \le 1$ and suppose $q > d$. If a functional $F \in \mathcal{D}^{1,p}(W;\mathbf{R}^d)$ is $(A,n,q)$-locally non-degenerate, then it possesses a density $\rho \in C^{n-1}(A;\mathbf{R})$ on $A$ with respect to Lebesgue measure.*

## 3 Proof of the Main Result

A key lemma to prove the main result is the following integration by parts formula:

**Lemma 6.** *Let $1 < p,q,r < \infty$ satisfy $1/p + 1/q \le 1$ and suppose that a functional $F \in \mathcal{D}^{1,p}(W;\mathbf{R}^d)$ is $(A,n,q)$-locally non-degenerate. Then, for any multi-index $\alpha$ with length $1 \le m \le n$, there exists $G^\alpha \in \mathcal{D}^{n-m,s_m}(W;\mathbf{R})$ such that*

$$\int_W \partial^\alpha \varphi \circ F\, dP = \int_W (\varphi \circ F) G^\alpha\, dP \quad \textit{for all } \varphi \in C^n_{\mathrm{cpt};A}(\mathbf{R}^d;\mathbf{R}).$$

*Here, $\{s_m\}_{m=1}^n$ is a decreasing sequence defined inductively by*

$$\frac{1}{s_m} := \begin{cases} \dfrac{1}{q_n} + \dfrac{1}{r}, & m = 1, \\ \dfrac{1}{q_{n-(m-1)}} + \dfrac{1}{s_{m-1}}, & 2 \le m \le n. \end{cases}$$

From this lemma, we see that there exists $g^\alpha \in \mathcal{L}^q(\mathbf{R}^d, \nu; \mathbf{R})$ such that

$$\int_{\mathbf{R}^d} \partial^\alpha \varphi\, d\nu = \int_{\mathbf{R}^d} \varphi g^\alpha\, d\nu \quad \text{for all } \varphi \in C^n_{\mathrm{cpt};A}(\mathbf{R}^d;\mathbf{R}),$$

where $\nu = P \circ F^{-1}$. This equation and the Sobolev embedding theorem help us to obtain Theorem 5.

## 4 Application

We study existence of smooth density of $\delta$-dimensional Bessel process $r$, which is defined by

$$r_t = r_0 + \int_0^t \frac{\delta - 1}{2r_s}\, ds + B_t,$$

where $r_0 > 0$ and $B$ is one-dimensional Brownian motion. The drift coefficient in this stochastic differential equation has 'singularity" at the origin, especially it is not Lipschitz continuous. Thus we have little hope of differentiability of $r$ in general, however, we see:

**Proposition 7** ([1])**.** *Let $\delta \ge 2$. We have $r_t \in \mathcal{D}^{1,p}(W;\mathbf{R})$ for any $p > 1$ and*

$$Dr_t = \int_0^{\cdot} \mathbf{1}_{[0,t]}(s) \exp\left(-\int_s^t \frac{\delta - 1}{2r_u^2}\, du\right) ds.$$

**Theorem 8.** *Let $\delta > 8$ and $1 < q < \delta/6$. Then $r_t$ is $(\mathbf{R}, 1, q)$-locally non-degenerate and has a continuous density on $\mathbf{R}$.*

To prove non-degeneracy, we choose $U \in \mathcal{D}^{1,q}(W;\mathcal{H})$ as

$$U := \left(1 - \exp\left(-\int_0^t \frac{\delta - 1}{2r_s^2}\, ds\right)\right)^{-1} \int_0^{\cdot} \mathbf{1}_{[0,t]}(s) \frac{\delta - 1}{2r_s^2}\, ds.$$

Using Theorem 5, we obtain the desired result.

## References

[1] Elisa Alòs and Christian-Oliver Ewald. Malliavin differentiability of the Heston volatility and applications to option pricing. *Adv. in Appl. Probab.*, 40(1):144–162, 2008.

[2] Carme Florit and David Nualart. A local criterion for smoothness of densities and application to the supremum of the Brownian sheet. *Statist. Probab. Lett.*, 22(1):25–31, 1995.

[3] Ichiro Shigekawa. *Stochastic analysis*, volume 224 of *Translations of Mathematical Monographs*. American Mathematical Society, Providence, RI, 2004.

# Relative Randomness for Martin-Löf random Sets

NingNing Peng (D2)
Mathematical Institute, Tohoku University

## Abstract

Let $\Gamma$ be a set of functions on the natural numbers. We introduce a new randomness notion called semi $\Gamma$-randomness, which is associating with a $\Gamma$-indexed test. We prove that weak n-randomness is strictly stronger than semi $\Delta^0_n$-randomness. Other new results are shown, we investigate the characterization of randomness notions. Moreover, we investigate the relationships between various definitions of randomness. (This is a joint work with Kojiro Higuchi, Takeshi Yamazaki, Kazuyuki Tanaka).

## What is random?

Suppose we are given two infinite binary sequences, say

- A sequence of 1's: **1111111111111** $\cdots$
- A sequence obtained by fair coin tosses: **01001110110110** $\cdots$

Most people will agree that the sequence of coin tosses appear to be more random than the sequence of 1's.

- This is due to the fact that the sequence of 1's follows a simple "Law" which we can describe easily.
- The sequence of coin tosses is rather chaotic.

## Definition (Martin-Löf, 1966)

- A Martin-Löf test, or ML-test is a uniformly c.e. sequence $(G_m)_{m\in\mathbb{N}}$ of open sets such that $\forall m \in \mathbb{N}\ \mu G_m \leq 2^{-m}$.
- A sequence $Z \subseteq \mathbb{N}$ fails the test if $Z \in \bigcap_m G_m$, otherwise $Z$ passes the test.
- $Z$ is ML-random if it passes every Martin-Löf test.

## Definitions (Kurtz, 1981)

- A generalized ML-test is a uniformly c.e. sequence $(G_m)_{m\in\mathbb{N}}$ of open sets such that $\mu(\bigcap_m G_m) = 0$.
- $Z$ is weakly 2-random if it passes every generalized ML-test.
- ML-random is also called 1-random. $Z$ is 2-random if it is 1-random relative to $\emptyset'$.

## Facts

- 2-random $\Rightarrow$ weakly 2-random $\Rightarrow$ ML-random.
- The reverse implications fail (Kurtz, Kautz).

## Motivation

- This is concerned with the algorithmic notion of randomness such as originally introduced by P. Martin-Löf in 1966.
- One approach is to generalize the Martin-Löf-test by giving the $m$-th component (a c.e. set of measure at most $2^{-m}$) via a function in some function class $\Gamma$.
- The main purpose of this post is to give a general framework for such randomness notions.
- To do this, we introduce the notion of semi $\Gamma$-randomness.

## Definition (Peng, 2011)

A set $Z$ is $\Gamma$-random if $Z$ is ML-random relative to $A$ for all $A \in \Gamma$. In particular, $\Gamma$-randomness is called $\mathbb{L}$-randomness if $\Gamma$ is the set of low sets.

In fact, it turned out that $\mathbb{L}$-randomness is equivalent to $\emptyset'$-Schnorr randomness.

## Theorem (Yu, 2012)

*For every $\emptyset'$-Schnorr test $\{U^{\emptyset}_e\}_{e\in\mathbb{N}}$, there is a real $z$ with $z' \leq_T \emptyset'$ such that there is z-Martin-Löf-test $\{V^z_e\}_{e\in\mathbb{N}}$ so that $\bigcap_{e\in\mathbb{N}} V^z_e \supseteq \bigcap_{e\in\mathbb{N}} U^{\emptyset'}_e$.*

We would like to introduce another characterization of $\mathbb{L}$-randomness. Then, the next lemma is useful.

## Lemma

*Let $\Gamma, \Gamma' \subset \mathbb{N}^{\mathbb{N}}$ such that for any $f \in \Gamma$ there is a function $g \in \Gamma \cap \Gamma'$ with $f \leq_{LR} g$. Then, $\Gamma$ randomness is equivalent to $\Gamma \cap \Gamma'$ randomness.*

## Proposition

*The following are equivalent:*

- *$X$ is $\mathbb{L}$ randomness,*
- *$X$ is $\mathbb{L} \cap \mathbb{G}$ randomness,*
- *$X$ is $\mathbb{L} \cap$ **PA** randomness.*

Let **MLR** denote the class of ML-random reals.

## Theorem

*For every $\emptyset'$-Schnorr test $\{U^{\emptyset}_e\}_{e\in\mathbb{N}}$ and every $\Pi^0_1$ class $P \subset$ **MLR**, there is a low real $z \in P$ such that there is z-Martin-Löf-test $\{V^z_e\}_{e\in\mathbb{N}}$ so that $\bigcap_{e\in\mathbb{N}} V^z_e \supseteq \bigcap_{e\in\mathbb{N}} U^{\emptyset'}_e$.*

## Definition

- Let $\Gamma \subseteq \mathbb{N}^{\mathbb{N}}$. We say that a sequence $\{G_n\}_{n\in\mathbb{N}}$ of c.e open sets is a $\Gamma$-indexed test if and only if there exists $f \in \Gamma$ such that $G_n = W_{f(n)}$ for all $n \in \mathbb{N}$ and $\mu(G_n) \leq 2^{-n}$.
- A set $Z \subseteq \mathbb{N}$ fails the test if $Z \in \bigcap_n G_n$, otherwise $Z$ passes the test.
- $A$ is semi $\Gamma$-random if it passes every $\Gamma$-indexed test.

The following lemma is for separation between weak randomness and semi $\Gamma$-randomness.

## Lemma

*For any $\Gamma, \Gamma' \subset \mathbb{N}^{\mathbb{N}}$ such that $\Gamma$ randomness is not equivalent to Martin-Löf randomness and $\Gamma'$ is countable, there exists a semi $\Gamma'$ random real which is not $\Gamma$ random.*

## Main Theorem

*If $n > 2$, then weakly $n$ randomness is strictly stronger than semi $\Delta^0_n$-randomness.*

Finally, we consider the case around $n = 2$.

## Lemma

*There exists a $\Pi^0_1(\emptyset')$ null set $P$ containing a semi $\mathbb{L}$ random element.*

## Theorem

*Weakly 2 randomness is strictly stronger than semi $\mathbb{L}$-randomness*

## Future Study

- Study other supper classes of $\mathbb{L}$-randomness.
- Is the a characterization of $\emptyset'$-computable randomness via ML randomness?

## References

- NingNing Peng, Takeshi Yamazaki, Kazuyuki Tanaka and ChenGuang Liu, "A Lemma on K-random Extension", The 3rd IEEE International Conference on Computer and Electrical Engineering, vol. 3, 2010.
- NingNing Peng. "The notions between Martin-Löf randomness and 2-randomness," RIMS Workshop on "Formal Systems and Computability Theory", Kyoto University, Sep 2010.
- Liang Yu. Characterizing strong randomness via Martin-Löf randomness. Annals of Pure and Applied Logic, vol. 163, no. 3, pp. 214-224. 2012.

 sa8m42@math.tohoku.ac.jp

# Lower bounds of the canonical heights on certain elliptic curves

Tadahisa Nara (Mathematical Institute, Tohoku University)

**Elliptic curves and rational points** We denote the set of rational numbers by $\mathbb{Q}$. An *elliptic curve* $E$ over $\mathbb{Q}$ is a nonsingular curve defined by the equation $y^2 = x^3 + Ax + B$ $(A, B \in \mathbb{Q})$. Then by $E(\mathbb{Q})$, we denote the set of rational points of $E$ with the point at infinity $O$ ( $=(\infty, \infty)$ ). One of the main problems about elliptic curves is to determine $E(\mathbb{Q})$, that is, the rational solution of the above equation. The Mordell–Weil theorem is a basic result about this problem, which states that $E(\mathbb{Q})$ is a finitely generated abelian group. We denote the rank of the abelian group by $\mathrm{rank}E(\mathbb{Q})$.

**The canonical height and its computations** Heights of a point represent arithmetic complexity of the point. The *canonical height* is one of the heights which is useful to consider $E(\mathbb{Q})$.

**Definition 1** *For $P = (x, y) \in E(\mathbb{Q})$ we write $x = a/c$ with $\gcd(a, c) = 1$. We define $h(P) = \log\max\{|a|, |c|\}$. We define $\hat{h}(P) = \lim_{n\to\infty} \frac{1}{4^n} h([2^n]P)$, which is called the canonical height of $P$ on $E(\mathbb{Q})$, where $[2^n]P$ means the multiple of $P$ by $2^n$ in the abelian group $E(\mathbb{Q})$.*

A remarkable property of the canonical height is the equality $\hat{h}([m]P) = m^2\hat{h}(P)$. This means that the canonical heights of points in a basis of $E(\mathbb{Q})$ are relatively small.

The above definition, which is usually used, is brief but not suitable for practical computaions. Néron and Tate showed that there is a function $\lambda_p$ such that $\hat{h}(P) = \sum_{p:prime,\infty} \lambda_p(P)$, which is called the Néron local height function. By computing $\lambda_p(P)$ for some $p$ prime number (and $\infty$), we can estimate the value of the canonical height of $P$.

We computed a lower bound of the canonical height independent of points.

**Theorem 1** *Let $E/\mathbb{Q}$ be an elliptic curve defined by $y^2 = x^3 + a_2x^2 + a_4x + a_6$ $(a_2, a_4, a_6 \in \mathbb{Z})$ with the discriminant $\Delta$. Let $D$ be a square-free integer and $E_D/\mathbb{Q}$ the elliptic curve $y^2 = x^3 + a_2Dx^2 + a_4D^2x + a_6D^3$. Assume that $\Delta$ is sixth-power-free. Then for $P \in E_D(\mathbb{Q}) \setminus E_D(\mathbb{Q})[2]$,*

$$\hat{h}(P) > \frac{1}{4}\log|D| + \frac{1}{16}\log\frac{(1-|q|)^8}{|q|} + \frac{1}{4}\log\left|\frac{\omega}{2\pi}\right| - \frac{7}{16}\sum_{p|\Delta, p\neq 2}\log p - \frac{5}{12}\log 2,$$

*where $\omega_1$ and $\omega_2$ are periods of $E$ such that $\omega_1 > 0$, $\mathrm{Im}(\omega_2) > 0$ and $\mathrm{Re}(\omega_2/\omega_1) = 0$ or $-1/2$, $q = \exp(2\pi i\omega_2/\omega_1)$ and*

$$\omega = \begin{cases} \omega_1 & (D > 0) \\ \mathrm{Im}(\omega_2) & (D < 0, \Delta > 0) \\ 2\mathrm{Im}(\omega_2) & (D < 0, \Delta < 0) \end{cases}.$$

Estimates of the canonical height as the above theorem can give an information of the arithmetic of elliptic curves. As an application of it, we can show the following theorem.

**Theorem 2** *Let $t \in \mathbb{Z}$, $D(t) = t^6 + 4t^4 + 30t^3 + 5t^2 + 54t + 245$, $E_D$ the elliptic curve defined by $y^2 = x^3 + 2D(t)x^2 + 163D(t)^2x + 2205D(t)^3$ and $P$ the point $(D(t)(t^4 + 2t^2 + 12t), D(t)^2(t^3 + t + 3))$ on $E_D$. We assume that $D(t)$ is square-free. Then $P$ is a primitive if $|t| \geq 2216$. In particular $E_D(\mathbb{Q}) \simeq \langle P\rangle$ if $\mathrm{rank}\, E_D(\mathbb{Q}) = 1$.*